PHYSICAL REVIEW D **86,** 014022 (2012)

Measurement of inclusive jet and dijet production in pp collisions at $\sqrt{s} = 7$ TeV using the ATLAS detector

G. Aad *et al.**
(ATLAS Collaboration)

(Received 29 December 2011; published 24 July 2012)

Inclusive jet and dijet cross sections have been measured in proton-proton collisions at a center-of-mass energy of 7 TeV using the ATLAS detector at the Large Hadron Collider. The cross sections were measured using jets clustered with the anti-k_t algorithm with parameters $R = 0.4$ and $R = 0.6$. These measurements are based on the 2010 data sample, consisting of a total integrated luminosity of 37 pb^{-1}. Inclusive jet double-differential cross sections are presented as a function of jet transverse momentum, in bins of jet rapidity. Dijet double-differential cross sections are studied as a function of the dijet invariant mass, in bins of half the rapidity separation of the two leading jets. The measurements are performed in the jet rapidity range $|y| < 4.4$, covering jet transverse momenta from 20 GeV to 1.5 TeV and dijet invariant masses from 70 GeV to 5 TeV. The data are compared to expectations based on next-to-leading-order QCD calculations corrected for nonperturbative effects, as well as to next-to-leading-order Monte Carlo predictions. In addition to a test of the theory in a new kinematic regime, the data also provide sensitivity to parton distribution functions in a region where they are currently not well-constrained.

DOI: 10.1103/PhysRevD.86.014022 PACS numbers: 12.38.Qk, 13.87.Ce

I. INTRODUCTION

At the Large Hadron Collider (LHC), jet production is the dominant high transverse-momentum (p_T) process. Jet cross sections serve as one of the main observables in high-energy particle physics, providing precise information on the structure of the proton. They are an important tool for understanding the strong interaction and searching for physics beyond the standard model (see, for example, Refs. [1–20]).

The ATLAS Collaboration has published a first measurement of inclusive jet and dijet production at $\sqrt{s} = 7$ TeV, using an integrated luminosity of 17 nb^{-1} [21]. This measurement considered only jets with transverse momentum larger than 60 GeV and in a rapidity interval $|y| < 2.8$.[1]

The analysis presented here extends the previous measurement using the 2010 data sample of (37.3 ± 1.2) pb^{-1}, an integrated luminosity more than 2000 times larger than that of the previous study. This more than doubles the kinematic reach at high jet transverse momentum and large dijet invariant mass. There are strong physics reasons to extend the measurement to jets of lower transverse momentum and larger rapidity as well. Jets at lower p_T are more sensitive to nonperturbative effects from hadronization and the underlying event, and forward jets may be sensitive to different dynamics in QCD than central jets. Moreover, LHC experiments have much wider rapidity coverage than those at the Tevatron, so forward jet measurements at the LHC cover a phase space region that has not been explored before.

The kinematic reach of this analysis is compared to that of the previous ATLAS study in Fig. 1. This data sample extends the existing inclusive jet p_T measurement from 700 GeV to 1.5 TeV and the existing dijet mass measurement from 1.8 TeV to 5 TeV. Thus this analysis probes next-to-leading-order (NLO) perturbative QCD (pQCD) and parton distribution functions (PDFs) in a new kinematic regime. The results span approximately $7 \times 10^{-5} < x < 0.9$ in x, the fraction of the proton momentum carried by each of the partons involved in the hard interaction.

II. THE ATLAS DETECTOR

The ATLAS detector is described in detail in Ref. [22]. In this analysis, the tracking detectors are used to define candidate collision events by constructing vertices from tracks, and the calorimeters are used to reconstruct jets.

*Full author list given at the end of the article.

[1]ATLAS uses a right-handed coordinate system with its origin at the nominal interaction point in the center of the detector and the z-axis along the beam pipe. The x-axis points from the interaction point to the center of the LHC ring, and the y axis points upward. Cylindrical coordinates (r, ϕ) are used in the transverse plane, ϕ being the azimuthal angle around the beam pipe, referred to the x-axis. The pseudorapidity is defined in terms of the polar angle θ with respect to the beamline as $\eta = -\ln \tan(\theta/2)$. When dealing with massive jets and particles, the rapidity $y = \frac{1}{2} \ln(\frac{E+p_z}{E-p_z})$ is used, where E is the jet energy and p_z is the z-component of the jet momentum.

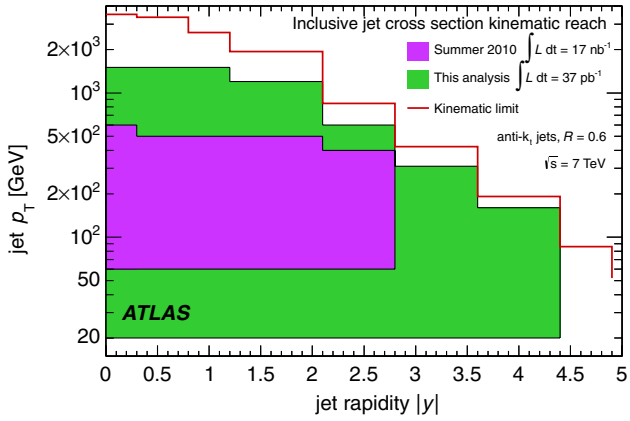

FIG. 1 (color online). Kinematic reach of the inclusive jet cross section measured in this analysis compared to that of the previous study [21] for jets identified using the anti-k_t algorithm with $R = 0.6$. The kinematic limit for the center-of-mass energy of 7 TeV is also shown.

The inner detector used for tracking and particle identification has complete azimuthal coverage and spans the region $|\eta| < 2.5$. It consists of layers of silicon pixel detectors, silicon microstrip detectors, and transition radiation tracking detectors, surrounded by a solenoid magnet that provides a uniform field of 2 T.

The electromagnetic calorimetry is provided by the liquid argon (LAr) calorimeters that are split into three regions: the barrel ($|\eta| < 1.475$), the endcap ($1.375 < |\eta| < 3.2$) and the forward (FCal: $3.1 < |\eta| < 4.9$) regions. The hadronic calorimeter is divided into four distinct regions: the barrel ($|\eta| < 0.8$), the extended barrel ($0.8 < |\eta| < 1.7$), both of which are scintillator/steel sampling calorimeters, the hadronic endcap (HEC; $1.5 < |\eta| < 3.2$), which has LAr/Cu calorimeter modules, and the hadronic FCal (same η-range as for the EM-FCal) which uses LAr/W modules. The total calorimeter coverage is $|\eta| < 4.9$.

III. CROSS SECTION DEFINITION

Jet cross sections are defined using the anti-k_t jet algorithm [23] implemented in the FASTJET [24] package. Two different values are used for the clustering parameter R (0.4 and 0.6), which can be seen intuitively as the radius of a circular jet in the plane (ϕ, y) of azimuthal angle and rapidity. The jet cross section measurements are corrected for all experimental effects, and thus are defined for the "particle-level" final state of a proton-proton collision [25]. Particle-level jets in the Monte Carlo simulation are identified using the anti-k_t algorithm and are built from stable particles, which are defined as those with a proper lifetime longer than 10 ps. This definition includes muons and neutrinos from decaying hadrons.

Inclusive jet double-differential cross sections are measured as a function of jet p_T in bins of y, in the region $p_T > 20$ GeV, $|y| < 4.4$. The term "inclusive jets" is used in this paper to indicate that all jets in each event are considered in the cross section measurement. Dijet double-differential cross sections are measured as a function of the invariant mass of the two leading (highest p_T) jets, which is given as $m_{12} = \sqrt{(E_1 + E_2)^2 - (\vec{p}_1 + \vec{p}_2)^2}$, where $E_{1,2}$ and $\vec{p}_{1,2}$ are the energies and momenta of the two leading jets. The cross sections are binned in the variable y^*, defined as half the rapidity difference of the two leading jets, $y^* = |y_1 - y_2|/2$. The quantity y^* is the rapidity in the two-parton center-of-mass frame (in the massless particle limit), where it is determined by the polar scattering angle with respect to the beamline, θ^*

$$y^* = \frac{1}{2} \ln\left(\frac{1 + |\cos\theta^*|}{1 - |\cos\theta^*|}\right) \quad (1)$$

For the dijet measurement, the two leading jets are selected to lie in the $|y| < 4.4$ region, where the leading jet is required to have $p_T > 30$ GeV and the subleading jet $p_T > 20$ GeV. Restricting the leading jet to higher p_T improves the stability of the NLO calculation [26].

Theory calculations are used in the same kinematic range as the measurement.

IV. MONTE CARLO SAMPLES

The PYTHIA 6.423 generator [27] with the MRST LO* PDF set [28] was used to simulate jet events in proton-proton collisions at a center-of-mass energy of $\sqrt{s} = 7$ TeV and to correct for detector effects. This generator utilizes leading-order perturbative QCD matrix elements (ME) for $2 \to 2$ processes, along with a leading-logarithmic, p_T-ordered parton shower (PS), an underlying event simulation with multiple parton interactions, and the Lund string model for hadronization. Samples were generated using the ATLAS Minimum-Bias Tune 1 (AMBT1) set of parameters [29], in which the model of nondiffractive scattering has been tuned to ATLAS measurements of charged particle production at $\sqrt{s} = 900$ GeV and $\sqrt{s} = 7$ TeV.

The particle four-vectors from these generators were passed through a full simulation [30] of the ATLAS detector and trigger that is based on GEANT4 [31]. Finally, the simulated events were reconstructed and jets were calibrated using the same reconstruction chain as the data.

V. THEORETICAL PREDICTIONS

A. Fixed-order calculations

1. NLO predictions

The measured jet cross sections are compared to fixed-order NLO pQCD predictions, with corrections for nonperturbative effects applied. For the hard scattering, both the NLOJET++ 4.1.2 [32] package and the POWHEG generator [33,34] were used, the latter in a specific configuration

where the parton shower was switched off and calculations were performed using NLO matrix elements. The two programs have been used with the CT10 [35] NLO parton distribution functions, and the same value of renormalization and factorization scale, corresponding to the transverse momentum of the leading jet, $p_{\mathrm{T}}^{\mathrm{max}}$:

$$\mu = \mu_{\mathrm{R}} = \mu_{\mathrm{F}} = p_{\mathrm{T}}^{\mathrm{max}} \tag{2}$$

For POWHEG, $p_{\mathrm{T}}^{\mathrm{max}}$ is evaluated at leading-order and is denoted $p_{\mathrm{T}}^{\mathrm{Born}}$. Using this scale choice, the cross section results of the two NLO codes are compatible at the few percent level for inclusive jets over the whole rapidity region. They are also consistent for dijet events where both jets are in the central region, while they differ substantially when the two leading jets are widely separated in rapidity ($y^* \gtrsim 3$). In these regions, NLOJET++ gives an unstable and much smaller cross section than POWHEG that is even negative for some rapidity separations. POWHEG remains positive over the whole region of phase space. It should be noted that the forward dijet cross section predicted by NLOJET++ in this region has a very strong scale dependence, which however is much reduced for larger values of scale than that of Eq. (2).

The forward dijet cross section for NLOJET++ is much more stable if instead of a scale fixed entirely by p_{T}, a scale that depends on the rapidity separation between the two jets is used. The values chosen for each y^*-bin follow the formula

$$\mu = \mu_{\mathrm{R}} = \mu_{\mathrm{F}} = p_{\mathrm{T}} e^{0.3y^*} \tag{3}$$

and are indicated by the histogram in Fig. 2. These values are motivated by the formula (shown by the dot-dashed curve)

$$\mu = \mu_{\mathrm{R}} = \mu_{\mathrm{F}} = \frac{m_{12}}{2\cosh(0.7y^*)} \tag{4}$$

that is suggested in Ref. [36], and are in a region where the cross section predictions are more stable as a function of scale (they reach a "plateau"). At small y^*, the scale in Eq. (3) reduces to the leading jet p_{T} (dotted line), which is used for the inclusive jet predictions. With this scale choice, NLOJET++ is again in reasonable agreement with POWHEG, which uses the scale from Eq. (2). The NLOJET++ predictions are used as a baseline for both inclusive jet and dijet calculations, with the scale choice from Eq. (2) for the former and that from Eq. (3) for the latter. The POWHEG scale used for both inclusive jets and dijets, $p_{\mathrm{T}}^{\mathrm{Born}}$, is given by Eq. (2) but evaluated at leading-order. Despite using different scale choices, the dijet theory predictions from NLOJET++ and POWHEG are stable with respect to relatively small scale variations and give consistent results.

The results are also compared with predictions obtained using the MSTW 2008 [37], NNPDF 2.1 (100) [38,39] and HERAPDF 1.5 [40] PDF sets.

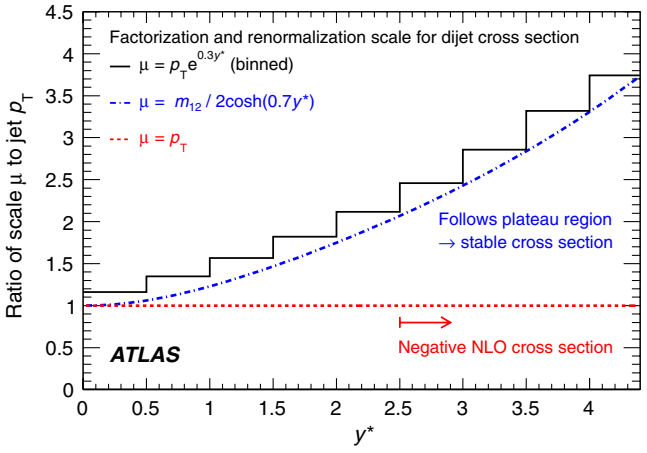

FIG. 2 (color online). The histogram indicates the values of the renormalization and factorization scales (denoted by $\mu = \mu_R = \mu_F$) used for the dijet predictions obtained using NLOJET++, as a function of y^*, half the rapidity separation between the two leading jets. This is motivated by the scale choice suggested in Ref. [36] (dot-dashed line), and is also compared to the scale choice used for the inclusive jet predictions (dotted line).

The main uncertainties on the NLO prediction come from the uncertainties on the PDFs, the choice of factorization and renormalization scales, and the uncertainty on the value of the strong coupling constant α_s. To allow for fast and flexible evaluation of PDF and scale uncertainties, the APPLGRID [41] software was interfaced with NLOJET++ in order to calculate the perturbative coefficients once and store them in a look-up table. The PDF uncertainties are defined at 68% confidence level and evaluated following the prescriptions given for each PDF set. They account for the data uncertainties, tension between input data sets, parametrization uncertainties, and various theoretical uncertainties related to PDF determination.

To estimate the uncertainty on the NLO prediction due to neglected higher-order terms, each observable was recalculated while varying the renormalization scale by a factor of 2 with respect to the default choice. Similarly, to estimate the sensitivity to the choice of scale where the PDF evolution is separated from the matrix element, the factorization scale was separately varied by a factor of 2. Cases where the two scales are simultaneously varied by a factor 2 in opposite directions were not considered due to the presence of logarithmic factors in the theory calculation that become large in these configurations. The envelope of the variation of the observables was taken as a systematic uncertainty. The effect of the uncertainty on the value of the strong coupling constant, α_s, is evaluated following the recommendation of the CTEQ group [42], in particular, by using different PDF sets that were derived using the positive and negative variations of the coupling from its best estimate.

Electroweak corrections were not included in the theory predictions and may be non-negligible [43].

2. Nonperturbative corrections

The fixed-order NLO calculations predict parton-level cross sections, which must be corrected for nonperturbative effects to be compared with data. This is done by using leading-logarithmic parton shower generators. The corrections are derived by using PYTHIA 6.425 with the AUET2B CTEQ6L1 tune [44] to evaluate the binwise ratio of cross sections with and without hadronization and the underlying event. Each bin of the parton-level cross section is then multiplied by the corresponding correction. The uncertainty is estimated as the maximum spread of the correction factors obtained from PYTHIA 6.425 using the AUET2B LO**, AUET2 LO**, AMBT2B CTEQ6L1, AMBT1, Perugia 2010, and Perugia 2011 tunes (PYTUNE_350), and the PYTHIA 8.150 tune 4*C* [44–47], as well as those obtained from the HERWIG++ 2.5.1 [48] tune UE7000-2 [44]. The AMBT2B CTEQ6L1 and AMBT1 tunes, which are based on observables sensitive to the modeling of minimum-bias interactions, are included to provide a systematically different estimate of the underlying event activity.

The corrections depend strongly on the jet size; therefore separate sets of corrections and uncertainties were derived for jets with $R = 0.4$ and $R = 0.6$. The correction factors and their uncertainties depend on the interplay of the hadronization and the underlying event for the different jet sizes, and they have a significant influence at low p_{T} and low dijet mass. For $R = 0.4$, the correction factors are dominated by the effect of hadronization and are approximately 0.95 at jet $p_{\mathrm{T}} = 20$ GeV, increasing closer to unity at higher p_{T}. For $R = 0.6$, the correction factors are dominated by the underlying event and are approximately 1.6 at jet $p_{\mathrm{T}} = 20$ GeV, decreasing to between 1.0–1.1 for jets above $p_{\mathrm{T}} = 100$ GeV. Figure 3 shows the nonperturbative corrections for inclusive jets with rapidity in the interval $|y| < 0.3$, for jet clustering parameters $R = 0.4$ and $R = 0.6$. The correction factors for the other rapidity bins become closer to unity as the jet rapidity increases, as can be seen in Fig. 20 in Appendix A.

Nonperturbative corrections have been evaluated for the dijet measurement as well, as a function of the dijet mass and the rapidity interval y^*, for each of the two jet sizes. These follow a similar behavior to those for inclusive jets, with the corrections becoming smaller for large invariant masses and rapidity differences.

B. NLO Matrix Element + Parton Shower

The measured jet cross sections are also compared to POWHEG [49], an NLO parton shower Monte Carlo generator that has only recently become available for inclusive jet and dijet production. POWHEG uses the POWHEG BOX package [50–52] and allows one to use either PYTHIA or HERWIG [53] + JIMMY [54] to shower the partons, hadronize them, and model the underlying event. The ATLAS underlying event tunes, AUET2B for PYTHIA and AUET2

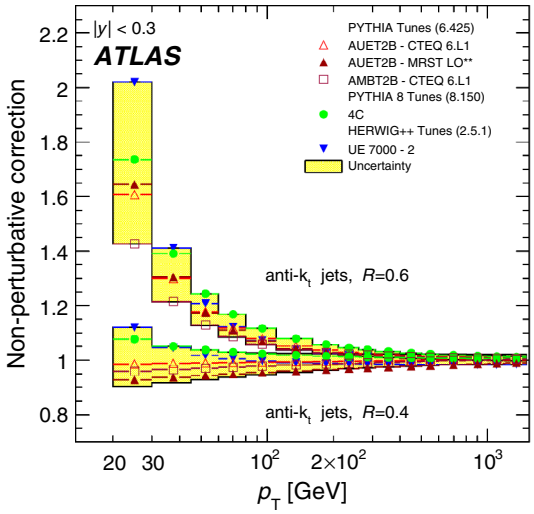

FIG. 3 (color online). Nonperturbative correction factors for inclusive jets identified using the anti-k_t algorithm with clustering parameters $R = 0.4$ and $R = 0.6$ in the rapidity region $|y| < 0.3$, derived using various Monte Carlo generators. The correction derived using PYTHIA 6.425 with the AUET2B CTEQ6L1 tune is used for the fixed-order NLO calculations presented in this analysis.

[55] for HERWIG, are derived from the standalone versions of these event generators, with no optimization for the POWHEG predictions. The showering portion of POWHEG uses the PDFs from PYTHIA or HERWIG as part of the specific tune chosen.

In the POWHEG algorithm, each event is built by first producing a QCD $2 \rightarrow 2$ partonic scattering. The renormalization and factorization scales are set to be equal to the transverse momentum of the outgoing partons, $p_{\mathrm{T}}^{\mathrm{Born}}$, before proceeding to generate the hardest partonic emission in the event.[2] The CT10 NLO PDF set is used in this step of the simulation. Then the event is evolved to the hadron level using a parton shower event generator, where the radiative emissions in the parton showers are required to be softer than the hardest partonic emission generated by POWHEG.

The coherent simulation of the parton showering, hadronization, and the underlying event with the NLO

[2]Technical details of the POWHEG generation parameters, which are discussed below, are given in Refs. [33,34]. The folding parameters used are 5-10-2. A number of different weighting parameters are used to allow coverage of the complete phase space investigated: 25 GeV, 250 GeV and 400 GeV. The minimum Born p_{T} is 5 GeV. For all the samples, the leading jet transverse momentum is required to be no more than 7 times greater than the leading parton's momentum. The p_{T} of any additional partonic interactions arising from the underlying event is required to be lower than that of the hard scatter generated by POWHEG. The parameters used in the input file for the event generation are `bornktmin` = 5 GeV, `bornsuppfact` = 25, 250, 400 GeV, `foldcsi` = 5, `foldy` = 10, and `foldphi` = 2.

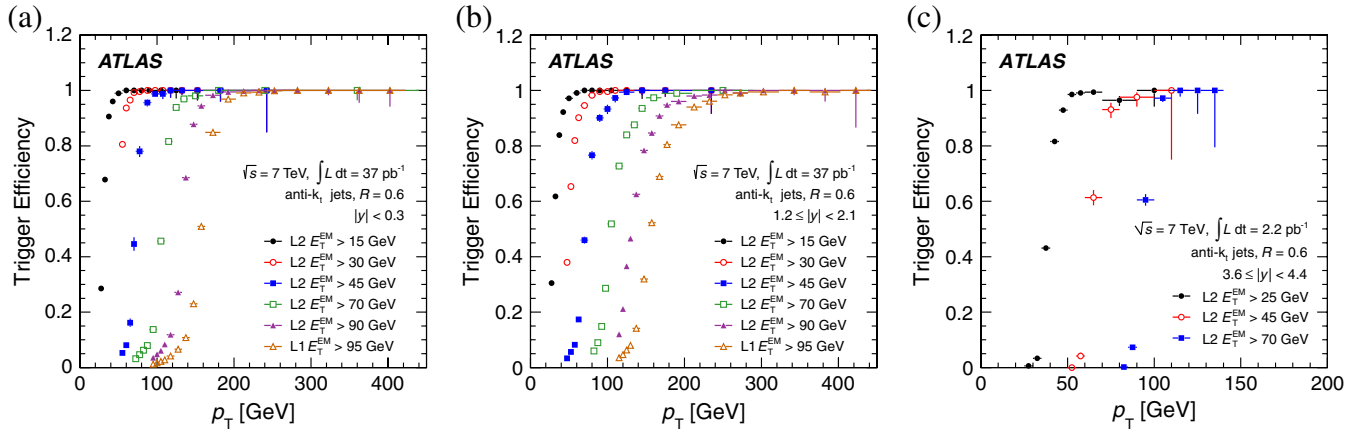

FIG. 4 (color online). Combined L1 + L2 jet trigger efficiency as a function of reconstructed jet p_T for anti-k_t jets with $R = 0.6$ in the central region $|y| < 0.3$ (a), the barrel-endcap transition region $1.2 \leq |y| < 2.1$ (b) and the FCal region $3.6 \leq |y| < 4.4$ (c) for the different L2 trigger thresholds used in the analysis. The trigger thresholds are at the electromagnetic scale, while the jet p_T is at the calibrated scale (see Sec. VI C). The highest trigger chain used for $|y| < 2.8$ does not apply a threshold at L2, so its L1 threshold is listed. The efficiency in the $|y| > 3.2$ rapidity range is not expected to reach 100% due to the presence of a dead FCal trigger tower that spans 0.9% of the (η, ϕ)-acceptance. This inefficiency is assigned as a systematic uncertainty on the trigger efficiency in the measurement.

matrix element is expected to produce a more accurate theoretical prediction. In particular, the nonperturbative effects are modeled in the NLO parton shower simulation itself, rather than being derived separately using a LO parton shower Monte Carlo generator as described in Sec. V A 2.

VI. DATA SELECTION AND CALIBRATION

A. Data set

The inclusive jet and dijet cross section measurements use the full ATLAS 2010 data sample from proton-proton collisions at $\sqrt{s} = 7$ TeV.

For low-p_T jets, only the first 17 nb^{-1} of data taken are considered since the instantaneous luminosity of the accelerator was low enough that a large data sample triggered with a minimum-bias trigger (see Sec. VI B) could be recorded. This provides an unbiased sample for reconstructing jets with p_T between 20–60 GeV, below the lowest jet trigger threshold. In addition, during this period there were negligible contributions from "pileup" events, in which there are multiple proton-proton interactions during the same or neighboring bunch crossings. Thus this period provides a well-measured sample of low-p_T jets. The first data-taking period was not used for forward jets with $|y| > 2.8$ and $p_T > 60$ GeV because the forward jet trigger was not yet commissioned.

For all events considered in this analysis, good operation status was required for the first-level trigger, the solenoid magnet, the inner detector, the calorimeters and the luminosity detectors, as well as for tracking and jet reconstruction. In addition, stable operation was required for the high-level trigger during the periods when this system was used for event rejection.

B. Trigger

Three different triggers have been used in this measurement: the minimum-bias trigger scintillators (MBTS); the central jet trigger, covering $|\eta| < 3.2$; and the forward jet trigger, spanning $3.1 < |\eta| < 4.9$. The MBTS trigger requires at least one hit in the minimum-bias scintillators located in front of the endcap cryostats, covering $2.09 < |\eta| < 3.84$, and is the primary trigger used to select minimum-bias events in ATLAS. It has been demonstrated to have negligible inefficiency for the events of interest for this analysis [56] and is used to select events with jets having transverse momenta in the range 20–60 GeV. The central and forward jet triggers are composed of three consecutive levels: Level 1 (L1), Level 2 (L2) and event filter. In 2010, only L1 information was used to select events in the first 3 pb^{-1} of data taken, while both the L1 and L2 stages were used for the rest of the data sample. The jet trigger did not reject events at the event-filter stage in 2010.

The central and forward jet triggers independently select data using several thresholds for the jet transverse energy ($E_T \equiv E \sin\theta$), each of which requires the presence of a jet with sufficient E_T at the electromagnetic (EM) scale.[3] For each L1 threshold, there is a corresponding L2 threshold that is generally 15 GeV above the L1 value. Each such L1 + L2 combination is referred to as an L2 trigger chain. Figure 4 shows the efficiency for L2 jet trigger chains with

[3]The electromagnetic scale is the basic calorimeter signal scale for the ATLAS calorimeters. It has been established using test-beam measurements for electrons and muons to give the correct response for the energy deposited in electromagnetic showers, while it does not correct for the lower response of the calorimeter to hadrons.

various thresholds as a function of the reconstructed jet p_T for anti-k_t jets with $R = 0.6$ for both the central and forward jet triggers. Similar efficiencies are found for jets with $R = 0.4$, such that the same correspondence between transverse-momentum regions and trigger chains can be used for the two jet sizes. The highest trigger chain does not apply a threshold at L2, so its L1 threshold is listed.

As the instantaneous luminosity increased throughout 2010, it was necessary to prescale triggers with lower E_T thresholds, while the central jet trigger with the highest E_T threshold remained unprescaled. As a result, the vast majority of the events where the leading jet has transverse momentum smaller than about 100 GeV have been taken in the first period of data-taking, under conditions with a low amount of pileup, while the majority of the high-p_T events have been taken during the second data-taking period, with an average of 2–3 interactions per bunch crossing. For each p_T-bin considered in this analysis, a dedicated trigger chain is chosen that is fully efficient ($> 99\%$) while having as small a prescale factor as possible. For inclusive jets fully contained in the central or in the forward trigger region, only events taken by this fully efficient trigger are considered. For inclusive jets in the HEC-FCal transition region $2.8 \leq |y| < 3.6$, neither the central nor the forward trigger is fully efficient. Instead, the logical OR of the triggers is used, which is fully efficient at sufficiently high jet p_T (see Fig. 5).

A specific strategy is used to account for the various prescale combinations for inclusive jets in the HEC-FCal transition region, which can be accepted either by the central jet trigger only, by the forward jet trigger only, or by both. A similar strategy is used for dijet events in a given (m_{12}, y^*)-bin, which can be accepted by several jet triggers depending on the transverse momenta and pseudorapidities of the two leading jets. Events that can be accepted by more than one trigger chain have been divided into several categories according to the trigger combination that could have accepted the events. For inclusive jets in the transition region, these correspond to central and forward triggers with a similar threshold; for dijets the trigger combination depends on the position and transverse momenta of the two leading jets, each of which is "matched" to a trigger object using angular criteria. Corrections are applied for any trigger inefficiencies, which are generally below 1%. The equivalent luminosity of each of the categories of events is computed based on the prescale values of these triggers throughout the data-taking periods, and all results from the various trigger combinations are combined together according to the prescription given in Ref. [57].

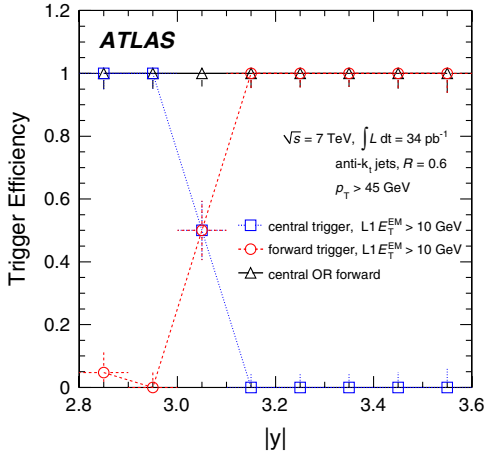

FIG. 5 (color online). Efficiencies for the central and forward jet triggers with a L1 E_T threshold of 10 GeV, and for their logical OR, as a function of the rapidity y of the reconstructed jet in the transition region between the two trigger systems. The logical OR is used for the inclusive jet measurement to collect data in the $2.8 \leq |y| < 3.6$ rapidity slice.

C. Jet reconstruction and calibration

Jets are reconstructed at the electromagnetic scale using the anti-k_t algorithm. The input objects to the jet algorithm are three-dimensional topological clusters [58] built from calorimeter cells. The four-momentum of the uncalibrated, EM-scale jet is defined as the sum of the four-momenta of its constituent calorimeter energy clusters. Additional energy due to multiple proton-proton interactions within the same bunch crossing ("pileup") is subtracted by applying a correction derived as a function of the number of reconstructed vertices in the event using minimum-bias data. The energy and the position of the jet are next corrected for instrumental effects such as dead material and noncompensation. This jet energy scale (JES) correction is calculated using isolated jets[4] in the Monte Carlo simulation as a function of energy and pseudorapidity of the reconstructed jet. The JES correction factor ranges from about 2.1 for low-energy jets with $p_T = 20$ GeV in the central region $|y| < 0.3$ to less than 1.2 for high-energy jets in the most forward region $3.6 \leq |y| < 4.4$. The corrections are cross-checked using *in situ* techniques in collision data (see below) [59].

D. Uncertainties in jet calibration

The uncertainty on the jet energy scale is the dominant uncertainty for the inclusive jet and dijet cross section measurements. Compared to the previous analysis [21], this uncertainty has been reduced by up to a factor of 2, primarily due to the improved calibration of the calorimeter electromagnetic energy scale obtained from $Z \rightarrow ee$ events [60], as well as an improved determination of the single particle energy measurement uncertainties from *in situ* and test-beam measurements [61]. This improvement is confirmed by independent measurements,

[4]An isolated jet is defined as a jet that has no other jet within $\Delta R = 2.5R$, where R is the clustering parameter of the jet algorithm.

including studies of the momenta of tracks associated with jets, as well as the momentum balance observed in γ + jet, dijet, and multijet events [59].

In the central barrel region ($|\eta| < 0.8$), the dominant source of the JES uncertainty is the knowledge of the calorimeter response to hadrons. This uncertainty is obtained by measuring the response to single hadrons using proton-proton and test-beam data, and propagating the uncertainties to the response for jets. Additional uncertainties are evaluated by studying the impact on the calorimeter response from varying settings for the parton shower, hadronization, and the underlying event in the Monte Carlo simulation. The estimate of the uncertainty is extended from the central calorimeter region to the endcap and forward regions, the latter of which lies outside the tracking acceptance, by exploiting the transverse-momentum balance between a central and a forward jet in events where only two jets are produced.

In the central region ($|\eta| < 0.8$), the uncertainty is lower than 4.6% for all jets with $p_T > 20$ GeV, which decreases to less than 2.5% uncertainty for jet transverse momenta between 60 and 800 GeV. The JES uncertainty is the largest for low-p_T (~ 20 GeV) jets in the most forward region $|\eta| > 3.6$, where it is about 11–12%. Details of the JES determination and its uncertainty are given in Ref. [59].

E. Offline selection

1. Event selection

To reject events due to cosmic-ray muons and other noncollision backgrounds, events are required to have at least one primary vertex that is consistent with the beam-spot position and that has at least five tracks associated with it. The efficiency for collision events to pass these vertex requirements, as measured in a sample of events passing all selections of this analysis, is well over 99%.

2. Jet selection

For the inclusive jet measurements, jets are required to have $p_T > 20$ GeV and to be within $|y| < 4.4$. They must also pass the specific fully efficient trigger for each p_T-and $|y|$-bin, as detailed in Sec. VI B. For the dijet measurements, events are selected if they have at least one jet with $p_T > 30$ GeV and another jet with $p_T > 20$ GeV, both within $|y| < 4.4$. Corrections are applied for inefficiencies in jet reconstruction, which are generally less than a few percent.

Jet quality criteria first established with early collision data are applied to reject jets reconstructed from calorimeter signals that do not originate from a proton-proton collision, such as those due to noisy calorimeter cells [59]. For this analysis, various improvements to the jet quality selection have been made due to increased experience with a larger data set and evolving beam conditions, including the introduction of new criteria for the forward region.

The main sources of fake jets were found to be: noise bursts in the hadronic endcap calorimeter electronics; coherent noise from the electromagnetic calorimeter; cosmic rays; and beam-related backgrounds.

Quality selection criteria were developed for each of these categories by studying jet samples classified as real or fake energy depositions. This classification was performed by applying criteria on the magnitude and direction of the missing transverse momentum, $\vec{E}_T^{\text{miss}}$. Following this, about a dozen events with $|\vec{E}_T^{\text{miss}}| > 500$ GeV were found that pass the standard analysis selection. These events were visually scanned and were generally found to be collision events with mostly low p_T jets and a muon escaping at low scattering angle.

The efficiency for identifying real jets was measured using a tag-and-probe method. A "probe jet" sample was selected by requiring the presence of a "tag jet" that is within $|\eta| < 2.0$, fulfills the jet quality criteria, and is back-to-back ($\Delta\phi > 2.6$) and well-balanced with a probe jet ($|p_{T1} - p_{T2}|/p_T^{\text{avg}} < 0.4$, with $p_T^{\text{avg}} = (p_{T1} + p_{T2})/2$ and where $p_{T1,2}$ are the transverse momenta of the tag and probe jets). The jet quality criteria were then applied to the probe jet, measuring as a function of its $|\eta|$ and p_T the fraction of jets that are not rejected.

The efficiency to select a jet is shown in Fig. 6 for an example rapidity region, along with the systematic uncertainty on this efficiency.

The jet quality selection efficiency is greater than 96% for jets with $p_T = 20$ GeV and quickly increases with jet p_T. The efficiency is above 99% for jet $p_T > 60$ GeV in all rapidity regions. The inclusive jet and dijet cross sections are corrected for these inefficiencies in regions where the

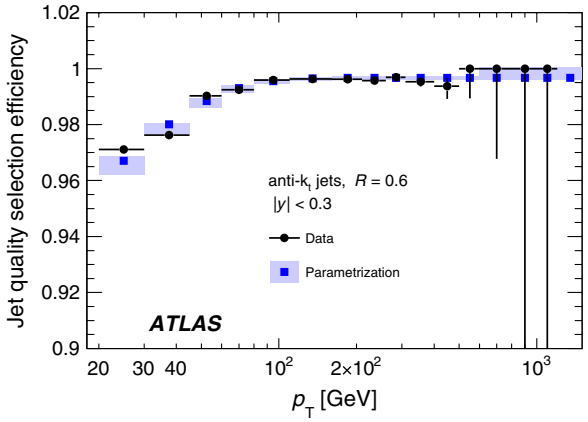

FIG. 6 (color online). Efficiency ϵ for jet quality selection as a function of p_T for anti-k_t jets with $R = 0.6$ in the rapidity region $|y| < 0.3$. The black circles indicate the efficiency measured *in-situ* using a tag-probe method. The blue squares indicate the fit to the parametrization $\epsilon(p_T) = A - e^{-(Bp_T - C)}$ used in this analysis, where A, B, and C are fitted constants, and the shaded band indicates the systematic uncertainty on the efficiency obtained by varying the tag jet selection. The turn-on is due to more stringent jet quality selection at low jet p_T.

efficiency is less than 99%. The systematic uncertainty on the efficiency is taken as a systematic uncertainty on the cross section.

F. Background, vertex position, and pileup

Background contributions from sources other than proton-proton collisions were evaluated using events from cosmic-ray runs, as well as unpaired proton bunches in the accelerator, in which no real collision candidates are expected. Based on the duration of the cosmic-ray runs and the fact that only one event satisfied the selection criteria, the noncollision background rates across the entire data period are considered to be negligible.

The primary vertices span the luminous region around the nominal beamspot. To determine the systematic uncertainty due to possibly incorrect modeling of the event vertex position, the jet p_{T} spectrum was studied as a function of the $|z|$ position of the primary vertex with the largest $\sum p_{\mathrm{T}}^2$ of associated tracks. The fraction of events with $|z| > 200$ mm is 0.06%, and the difference in the p_{T} spectrum compared to events with $|z| < 100$ mm is small. Consequently, the uncertainty from mismodeling of the vertex position was taken to be negligible.

The p_{T} of each jet is corrected for additional energy from soft pileup interactions in the event (see Sec. VI C). An uncertainty associated with this pileup offset correction is assigned that is dependent on the number of reconstructed primary vertices, as described in Sec. VIII A. The jet measurements are then compared to the Monte Carlo simulation without pileup.

G. Luminosity

The integrated luminosity is calculated by measuring interaction rates using several ATLAS devices, where the absolute calibration is derived using van der Meer scans [62]. The uncertainty on the luminosity is 3.4% [63]. The calculation of the effective luminosity for each bin of the observable for inclusive jets follows the trigger scheme described in Sec. VI B. The integrated luminosity for each individual trigger is derived using separate prescale factors for each luminosity block (an interval of luminosity with homogeneous data-taking conditions, which is typically two minutes). For dijets, each bin receives contributions from several trigger combinations, for which the luminosity is calculated independently. The luminosity that would be obtained without correction for trigger prescale is (37.3 ± 1.2) pb^{-1}. Since the central jet trigger with the largest transverse-momentum threshold was always unprescaled, this is the effective luminosity taken for jets with transverse momentum above about 220 GeV.

VII. UNFOLDING

A. Technique used

Aside from the jet energy scale correction, all other corrections for detector inefficiencies and resolutions are performed using an iterative unfolding, based on a transfer matrix that relates the particle-level and reconstruction-level observable, with the same binning as the final distribution. The unfolding is performed separately for each bin in rapidity since the migrations across rapidity bins are negligible compared to those across jet p_{T} (dijet mass) bins. A similar procedure is applied for inclusive jets and dijets, with the following description applying specifically to the inclusive jet case.

The Monte Carlo simulation described in Sec. IV is used to derive the unfolding matrices. Particle-level and reconstructed jets are matched together based on geometrical criteria and are used to derive a transfer matrix. This matrix contains the expected number of jets within each bin of particle-level and reconstructed jet p_{T}. A folding matrix is constructed from the transfer matrix by normalizing row-by-row so that the sum of the elements corresponding to a given particle-level jet p_{T} is unity. Similarly, an unfolding matrix is constructed by normalizing column-by-column so that the sum of the elements corresponding to a specific reconstructed jet p_{T} is unity. Thus each element of the unfolding matrix reflects the probability for a reconstructed jet in a particular p_{T}-bin to originate from a specific particle-level p_{T}-bin, given the assumed input particle-level jet p_{T} spectrum. The spectra of unmatched particle-level and reconstructed jets are also derived from the simulated sample. The ratio between the number of matched jets and the total number of jets provides the matching efficiency both for particle-level jets, $\epsilon^{\mathrm{ptcl},i}$, and for reconstructed jets, $\epsilon_{\mathrm{reco},j}$.

The data are unfolded to particle level using a three-step procedure, with the final results being given by the equation:

$$N^{\mathrm{ptcl},i} = \sum_j N_{\mathrm{reco},j} \times \epsilon_{\mathrm{reco},j} A^{\mathrm{ptcl},i}_{\mathrm{reco},j} / \epsilon^{\mathrm{ptcl},i}, \tag{5}$$

where i and j are the particle-level and reconstructed bin indices, respectively, and $A^{\mathrm{ptcl},i}_{\mathrm{reco},j}$ is an unfolding matrix refined through iteration, as discussed below.

The first step is to multiply the reconstructed jet spectrum in data by the matching efficiency $\epsilon_{\mathrm{reco},j}$, such that it can be compared to the matched reconstructed spectrum from the Monte Carlo simulation. In the second step, the iterated unfolding matrix $A^{\mathrm{ptcl},i}_{\mathrm{reco},j}$ is determined using the iterative, dynamically stabilized (IDS) method [64]. This procedure improves the transfer matrix through a series of iterations, where the particle-level distribution is reweighted to the shape of the corrected data spectrum, while leaving the folding matrix unchanged. The main difference with respect to previous iterative unfolding techniques [65] is that, when performing the corrections, regularization is provided by the use of the significance of the data-MC differences in each bin. The third step is to divide the spectrum obtained after the iterative unfolding by the matching efficiency at particle level, thus correcting for the jet reconstruction inefficiency.

The statistical uncertainties on the spectrum are propagated through the unfolding by performing pseudoexperiments. An ensemble of pseudoexperiments is created in which each bin of the transfer matrix is varied according to its statistical uncertainty. A separate set of pseudoexperiments is performed where the data spectrum is varied while respecting correlations between jets produced in the same event. The unfolding is then applied to each pseudoexperiment, and the resulting ensembles are used to calculate the covariance matrix of the corrected spectrum.

As a cross-check, the results obtained from the iterative unfolding have been compared to those using a simpler bin-by-bin correction procedure, as well as the "singular value decomposition" (SVD) method implemented in TSVDUNFOLD [66,67]. These methods use different regularization procedures and rely to different degrees on the Monte Carlo simulation modeling of the shape of the spectrum. The unfolding techniques have been tested using a data-driven closure test [64]. In this test the particle-level spectrum in the Monte Carlo simulation is reweighted and convolved through the folding matrix such that a significantly improved agreement between the data and the reconstructed spectrum from the Monte Carlo simulation is attained. The reweighted, reconstructed spectrum in the Monte Carlo simulation is then unfolded using the same procedure as for the data. The comparison of the result with the reweighted particle-level spectrum from the Monte Carlo simulation provides the estimation of the bias.

The bin-by-bin method gives results consistent with those obtained using the IDS technique, but requires the application of an explicit correction for the NLO k-factor to obtain good agreement. A somewhat larger bias is observed for the SVD method.

B. Cross-check with jet shapes

The use of Monte Carlo simulation to derive the transfer matrix in the unfolding procedure requires that the simulation models the jet properties well. The modeling of the energy flow around the jet core provides a useful test of this. The energy and momentum flow within a jet can be expressed in terms of the differential jet shape, defined for a jet with radius parameter R, as the fraction $\rho(r) = \frac{1}{\Delta r}\frac{p_{\mathrm{T}}^{r}}{p_{\mathrm{T}}^{R}}$, where p_{T}^{R} is the transverse momentum within a radius R of the jet center, and p_{T}^{r} is the transverse momentum contained within a ring of thickness $\Delta r = 0.1$ at a radius $r = \sqrt{(\Delta y)^2 + (\Delta\phi)^2}$ from the jet center.

Jet shape measurements using calorimeter energy clusters and tracks were performed with 3 pb^{-1} of data [68], and show good agreement with the PYTHIA and HERWIG + JIMMY Monte Carlo simulations in the kinematic region 30 GeV $< p_{\mathrm{T}} <$ 600 GeV and rapidity $|y| < 2.8$. Using the same technique, the uncorrected jet shapes in the forward rapidity region $2.8 \leq |y| < 4.4$ have been studied in the context of the present analysis. As an example, the results for the HEC-FCal transition region $2.8 \leq |y| < 3.6$, the most difficult detector region to model, are shown in Fig. 7. The maximum disagreement in shape between data and the Monte Carlo simulation is approximately 20%, demonstrating that the distribution of energy within the jets is reasonably well-modeled even in this worst case. Any bias from mismodeling of the jet shape is included in the unfolding uncertainties described below, so this jet shape study serves only as a cross-check.

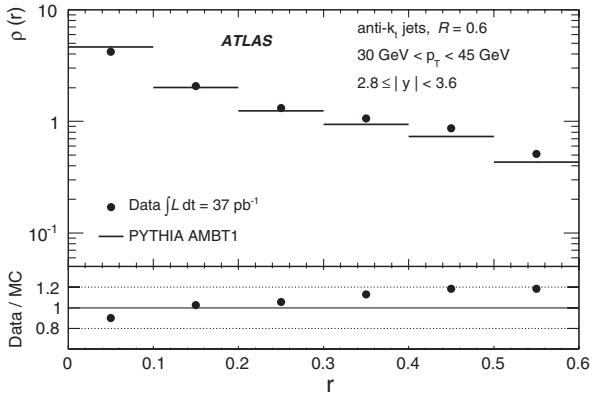

FIG. 7. The jet shape $\rho(r)$ measured using calorimeter energy clusters for anti-k_t jets with $R = 0.6$ in the rapidity interval $2.8 \leq |y| < 3.6$, compared to PYTHIA with tune AMBT1 (used for unfolding), and for jets with transverse momenta in the range $30 < p_{\mathrm{T}} < 45$ GeV. The statistical error bars are smaller than the size of the markers, while systematic errors are not shown.

VIII. SYSTEMATIC UNCERTAINTIES AND CORRELATIONS

A. Uncertainty sources from jet reconstruction and calibration

The uncertainty on the jet reconstruction efficiency for $|y| < 2.1$ (within the tracking acceptance) is evaluated using track jets, which are used to play the role of "truth jets." In this paper, truth jets are defined to be jets at the particle level, but excluding muons and neutrinos. The efficiency to reconstruct a calorimeter jet given a track jet nearby is studied in both data and the MC simulation. The data versus MC comparison of this efficiency is used to infer the degree to which the calorimeter jet reconstruction efficiency may be mismodeled in the Monte Carlo simulation. The disagreement was found to be 2% for calorimeter jets with p_{T} of 20 GeV and less than 1% for those with $p_{\mathrm{T}} > 30$ GeV. The disagreement for jets with $|y| < 2.1$ is taken as a systematic uncertainty for all jets in the rapidity range $|y| < 4.4$. This is expected to be a conservative estimate in the forward region where the jets have higher energy for a given p_{T}.

The JES uncertainty was evaluated as described in Sec. VI D and in Ref. [59]. The jet energy and angular resolutions are estimated from the Monte Carlo simulation using truth jets that have each been matched to a reconstructed calorimeter jet. The jet energy resolution (JER) in

the Monte Carlo simulation is compared to that obtained in data using two *in situ* techniques, one based on dijet balance and the other using a bisector method [69]. In general the two resolutions agree within 14%, and the full difference is taken as a contribution to the uncertainty on the unfolding corrections, which propagates to a systematic uncertainty on the measured cross section as described in Sec. VIII B. The angular resolution is estimated from the angle between each calorimeter jet and its matched truth-level jet. The associated systematic uncertainty is assessed by varying the requirement that the jet is isolated.

The JES uncertainty due to pileup is proportional to $(N_{\mathrm{PV}} - 1)/p_{\mathrm{T}}$, where N_{PV} is the number of reconstructed vertices. The total pileup uncertainty for a given (p_{T}, y)-bin is calculated as the average of the uncertainties for each value of N_{PV} weighted by the relative frequency of that number of reconstructed vertices in the bin.

B. Uncertainty propagation

The uncertainty of the measured cross section due to jet energy scale and jet energy and angular resolutions has been estimated using the Monte Carlo simulation by repeating the analysis after systematically varying these effects. The jet energy scale applied to the reconstructed jets in MC is varied separately for each JES uncertainty source both up and down by 1 standard deviation. The resulting p_{T} spectra are unfolded using the nominal unfolding matrix, and the relative shifts with respect to the nominal unfolded spectra are taken as uncertainties on the cross section. The effects of the jet energy and angular resolutions are studied by smearing the reconstructed jets such that these resolutions are increased by 1 standard deviation of their respective uncertainties (see Sec. VIII A). For each such variation, a new transfer matrix is constructed, which is used to unfold the reconstructed jet spectrum of the nominal MC sample. The relative shift of this spectrum with respect to the nominal unfolded spectra is taken as the uncertainty on the cross section.

The impact of possible mismodeling of the cross section shape in the Monte Carlo simulation is assessed by shape variations of the particle-level jet spectra introduced to produce reconstructed-level spectra in agreement with data as discussed in Sec. VII.

The total uncertainty on the unfolding corrections is defined as the sum in quadrature of the uncertainties on the jet energy resolution, jet angular resolution, and the simulated shape. It is approximately 4–5% at low and high p_{T} (except for the lowest p_{T}-bin at 20 GeV, where it reaches 20%), and is smaller at intermediate p_{T} values. This uncertainty is dominated by the component from the jet energy resolution.

C. Summary of the magnitude of the systematic uncertainties

The largest systematic uncertainty for this measurement arises from the jet energy scale. Even with the higher precision achieved recently as described in Sec. VI D, the very steeply falling jet p_{T} spectrum, especially for large rapidities, translates even relatively modest uncertainties on the transverse momentum into large changes for the measured cross section.

As described in Sec. VI G, the luminosity uncertainty is 3.4%. The detector unfolding uncertainties have been discussed in the previous subsection. Various other sources of systematic uncertainties were considered and were found to have a small impact on the results. The jet energy and angular resolutions, as well as the jet reconstruction efficiency, also contribute to the total uncertainty through the unfolding corrections.

The dominant systematic uncertainties for the measurement of the inclusive jet p_{T} spectrum in representative p_{T} and y regions for anti-k_t jets with $R = 0.6$ are shown in Table I. Similarly, the largest systematic uncertainties for the dijet mass measurement are given for a few representative m_{12} and y^* regions in Table II.

An example of the breakdown of the systematic uncertainties as a function of the jet transverse momentum for the various rapidity bins used in the inclusive jet measurement is shown in Fig. 8.

D. Correlations

The behavior of various sources of systematic uncertainty in different parts of the detector has been studied in detail in order to understand their correlations across various p_{T}, m_{12} and rapidity bins. As shown in Tables III and IV, 22 independent sources of systematic uncertainty have been identified, including luminosity, jet energy scale and resolution, and theory effects such as the uncertainty of the modeling of the underlying event and the QCD showering. For example, the sources labeled "JES 7–13" in these tables correspond to the calorimeter response to hadrons, which dominates the JES uncertainty

TABLE I. The effect of the dominant systematic uncertainty sources on the inclusive jet cross section measurement, for representative p_{T} and y regions for anti-k_t jets with $R = 0.6$.

p_{T} [GeV]	$\lvert y\rvert$	JES	JER	Trigger	Jet rec.
20–30	2.1–2.8	$^{+35\%}_{-30\%}$	17%	1%	2%
20–30	3.6–4.4	$^{+65\%}_{-50\%}$	13%	1%	2%
80–110	<0.3	10%	1%	1%	1%

TABLE II. The effect of the dominant systematic uncertainty sources on the dijet cross section measurement, for representative m_{12} and y^* regions for anti-k_t jets with $R = 0.6$.

m_{12} [TeV]	y^*	JES	JER	Trigger	Jet rec.
0.37–0.44	2.0–2.5	$^{+46\%}_{-27\%}$	7%	1%	2%
2.55–3.04	4.0–4.4	$^{+110\%}_{-50\%}$	8%	2%	2%
0.21–0.26	<0.5	10%	1%	1%	2%

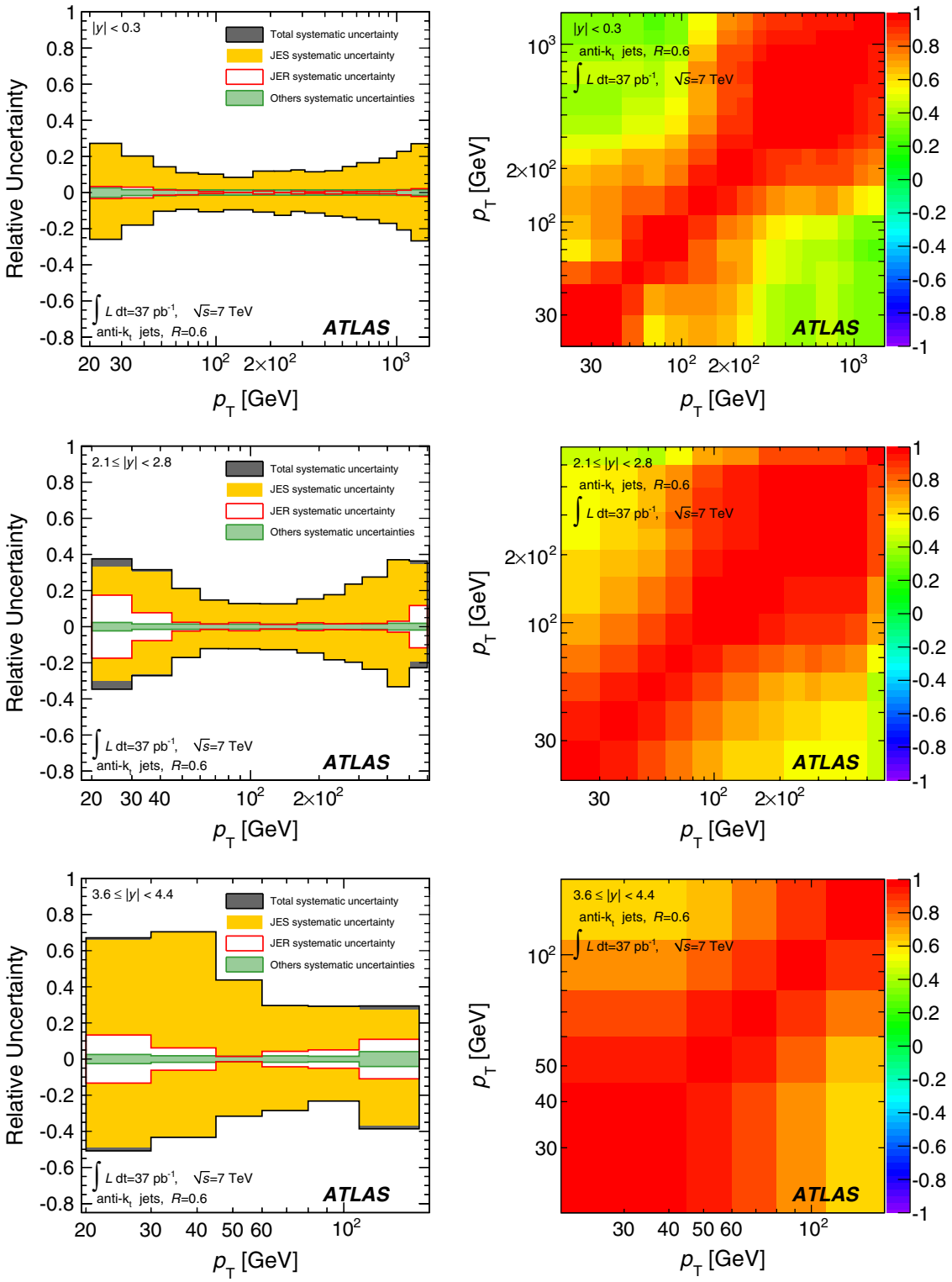

FIG. 8 (color online). The magnitude (left) and correlation between p_T-bins (right) of the total systematic uncertainty on the inclusive jet cross section measurement for anti-k_t jets with $R = 0.6$ in three representative $|y|$-bins. The magnitudes of the uncertainties from the JES, the JER, and other sources are shown separately. The correlation matrix is calculated after symmetrizing the uncertainties. The statistical uncertainty and the 3.4% uncertainty of the integrated luminosity are not shown here.

TABLE III. Description of bin-to-bin uncertainty correlation for the inclusive jet measurement. Each number corresponds to a nuisance parameter for which the corresponding uncertainty is fully correlated versus p_T. Bins with the same nuisance parameter are treated as fully correlated, while bins with different nuisance parameters are uncorrelated. The sources indicated by the letter "u" are uncorrelated both between p_T- and $|y|$-bins. The 1-standard-deviation amplitude of the systematic effect associated with each nuisance parameter is detailed in Tables V–XVIII in Appendix B2. The JES uncertainties for jets with $|y| \geq 0.8$ are determined relative to the JES of jets with $|y| < 0.8$. As a consequence, several of the uncertainties that are determined using jets with $|y| < 0.8$ are also propagated to the more forward rapidities (such as the E/p uncertainties). Descriptions of the JES uncertainty sources can be found in Refs. [59,70]. All tables are available on HEPDATA [71].

	$\|y\|$-bins						
Uncertainty Source	0–0.3	0.3–0.8	0.8–1.2	1.2–2.1	2.1–2.8	2.8–3.6	3.6–4.4
JES 1: Noise threshold	1	1	2	3	4	5	6
JES 2: Theory UE	7	7	8	9	10	11	12
JES 3: Theory showering	13	13	14	15	16	17	18
JES 4: Nonclosure	19	19	20	21	22	23	24
JES 5: Dead material	25	25	26	27	28	29	30
JES 6: Forward JES	31	31	31	31	31	31	31
JES 7: E/p response	32	32	33	34	35	36	37
JES 8: E/p selection	38	38	39	40	41	42	43
JES 9: EM + neutrals	44	44	45	46	47	48	49
JES 10: HAD E-scale	50	50	51	52	53	54	55
JES 11: High p_T	56	56	57	58	59	60	61
JES 12: E/p bias	62	62	63	64	65	66	67
JES 13: Test-beam bias	68	68	69	70	71	72	73
Unfolding	74	74	74	74	74	74	74
Jet matching	75	75	75	75	75	75	75
Jet energy resolution	76	76	77	78	79	80	81
y-resolution	82	82	82	82	82	82	82
Jet reconstruction eff.	83	83	83	83	84	85	86
Luminosity	87	87	87	87	87	87	87
JES 14: Pileup (u_1)	u	u	u	u	u	u	u
Trigger (u_2)	u	u	u	u	u	u	u
Jet identification (u_3)	u	u	u	u	u	u	u

in the central region. After examining the rapidity dependence of all 22 sources, it was found that 87 independent nuisance parameters are necessary to describe the correlations over the whole phase space. The systematic effect on the cross section measurement associated with each nuisance parameter in its range of use is completely correlated in p_T and y (dijet mass and y^*). These parameters represent correlations between the uncertainties of the various bins. Since many of the systematic effects are not symmetric, it is not possible to provide a covariance matrix containing the full information. For symmetric uncertainties corresponding to independent sources, the total covariance matrix is given by

$$\mathrm{cov}\,(i,j) = \sum_{\lambda} \Gamma_{\lambda i}\Gamma_{\lambda j}, \tag{6}$$

where λ is an index running over the nuisance parameters, and $\Gamma_{\lambda i}$ is the 1-standard-deviation amplitude of the systematic effect due to source λ in bin i. The full list of relative uncertainties, γ_λ, where each uncertainty may be asymmetric, is given for all sources λ and bins of this analysis in Tables V–XXXVI. Figure 8 shows the magnitude and approximate bin-to-bin correlations of the total systematic uncertainty of the inclusive jet cross section measurement. The correlation matrix is here converted from the covariance matrix, which is obtained using Eq. (6), after symmetrizing the uncertainties: $\Gamma_{\lambda i} = (\Gamma^+_{\lambda i} + \Gamma^-_{\lambda i})/2$. The inclusive jet and dijet data should not be used simultaneously for PDF fits due to significant correlations between the two measurements.

IX. RESULTS AND DISCUSSION

A. Inclusive jet cross sections

The inclusive jet double-differential cross section is shown in Figs. 9 and 10 and Tables V–XVIII in Appendix B for jets reconstructed with the anti-k_t algorithm with $R = 0.4$ and $R = 0.6$. The measurement extends from jet transverse momentum of 20 GeV to almost 1.5 TeV, spanning 2 orders of magnitude in p_T and 10 orders of magnitude in the value of the cross section. The measured cross sections have been corrected for all detector effects using the unfolding procedure described in Sec. VII. The results are compared to NLOJET++ predictions (using the CT10 PDF set) corrected for nonperturbative effects, where the theoretical uncertainties from scale

TABLE IV. Description of bin-to-bin uncertainty correlation for the dijet measurement. Each number corresponds to a nuisance parameter for which the corresponding uncertainty is fully correlated versus dijet mass, m_{12}. Bins with the same nuisance parameter are treated as fully correlated, while bins with different nuisance parameters are uncorrelated. The sources indicated by the letter "u" are uncorrelated both between m_{12}- and y^*-bins. The 1-standard-deviation amplitude of the systematic effect associated with each nuisance parameter is detailed in Tables XIX–XXXVI in Appendix C. Descriptions of the JES uncertainty sources can be found in Refs. [59,70]. All tables are available on HEPDATA [71].

	y^*-bins								
Uncertainty Source	0.0–0.5	0.5–1.0	1.0–1.5	1.5–2.0	2.0–2.5	2.5–3.0	3.0–3.5	3.5–4.0	4.0–4.4
JES 1: Noise threshold	1	1	2	3	4	4	5	6	6
JES 2: Theory UE	7	7	8	9	10	10	11	12	12
JES 3: Theory showering	13	13	14	15	16	16	17	18	18
JES 4: Nonclosure	19	19	20	21	22	22	23	24	24
JES 5: Dead material	25	25	26	27	28	28	29	30	30
JES 6: Forward JES	31	31	31	31	31	31	31	31	31
JES 7: E/p response	32	32	33	34	35	35	36	37	37
JES 8: E/p selection	38	38	39	40	41	41	42	43	43
JES 9: EM + neutrals	44	44	45	46	47	47	48	49	49
JES 10: HAD E-scale	50	50	51	52	53	53	54	55	55
JES 11: High p_{T}	56	56	57	58	59	59	60	61	61
JES 12: E/p bias	62	62	63	64	65	65	66	67	67
JES 13: Test-beam bias	68	68	69	70	71	71	72	73	73
Unfolding	74	74	74	74	74	74	74	74	74
Jet matching	75	75	75	75	75	75	75	75	75
Jet energy resolution	76	76	77	78	79	79	80	81	81
y-resolution	82	82	82	82	82	82	82	82	82
Jet reconstruction eff.	83	83	83	83	84	84	85	86	86
Luminosity	87	87	87	87	87	87	87	87	87
JES 14: Pileup (u_1)	u	u	u	u	u	u	u	u	u
Trigger (u_2)	u	u	u	u	u	u	u	u	u
Jet identification (u_3)	u	u	u	u	u	u	u	u	u

variations, parton distribution functions, and nonperturbative corrections have been accounted for.

In Figs. 11–13, the inclusive jet results are presented in terms of the ratio with respect to the NLOJET++ predictions using the CT10 PDF set. Figure 11 compares the current results to the previous measurements published by ATLAS [21], for jets reconstructed with the anti-k_t algorithm with parameter $R = 0.6$. This figure is limited to the central region, but similar conclusions can be drawn in all rapidity bins. In particular the two measurements are in good agreement, although the new results cover a much larger kinematic range with much reduced statistical and systematic uncertainties.

Figure 12 shows the ratio of the measured cross sections to the NLOJET++ theoretical predictions for various PDF sets. Predictions obtained using CT10, MTSW 2008, NNPDF 2.1, and HERAPDF 1.5, including uncertainty bands, are compared to the measured cross sections, where data and theoretical predictions are normalized to the prediction from the CT10 PDF set. The data show a marginally smaller cross section than the predictions from each of the PDF sets. This trend is more pronounced for the measurements corresponding to the anti-k_t algorithm with parameter $R = 0.4$, compared to $R = 0.6$.

The description becomes worse for large jet transverse momenta and rapidities, where the MSTW 2008 PDF set follows the measured trend better. However, the differences between the measured cross section and the prediction of each PDF set are of the same order as the total systematic uncertainty on the measurement, including both experimental and theoretical uncertainty sources. A χ^2 test of the compatibility between data and the PDF curves, accounting for correlations between bins, provides reasonable probabilities for all sets, with nonsignificant differences between them.[5]

The comparison of the data with the POWHEG prediction, using the CT10 NLO PDF set, is shown for anti-k_t jets with $R = 0.4$ and $R = 0.6$ in different rapidity regions in Fig. 13. The data are compared with four theory curves, all of which are normalized to the same common denominator of the NLOJET++ prediction corrected for nonperturbative effects: POWHEG showered with PYTHIA with the default AUET2B tune; the same with the Perugia 2011 tune; POWHEG showered with HERWIG; and POWHEG run in "pure NLO" mode (fixed-order calculation), without matching to parton shower, after application of nonperturbative corrections calculated

[5]Comparisons to HERAPDF 1.0, CTEQ 6.6, and NNPDF 2.0 were also performed, but they are not shown as they are very similar to those for HERAPDF 1.5, CT10, and NNPDF 2.1, respectively.

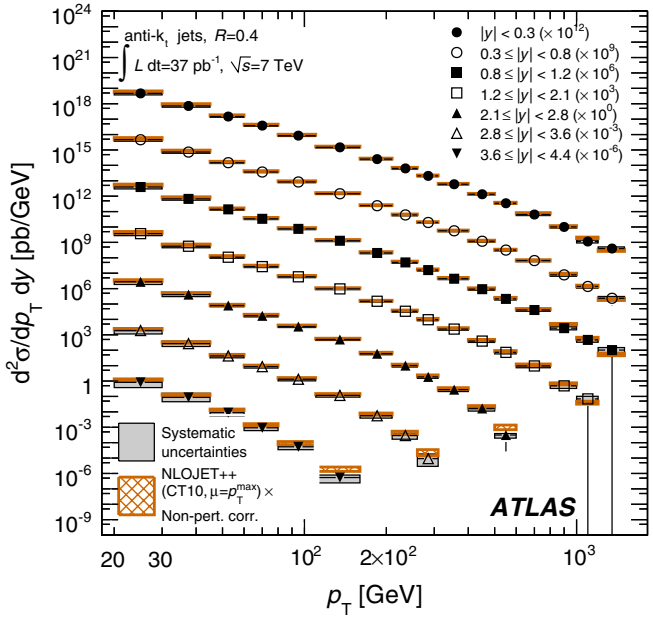

FIG. 9 (color online). Inclusive jet double-differential cross section as a function of jet p_T in different regions of $|y|$ for jets identified using the anti-k_t algorithm with $R = 0.4$. For convenience, the cross sections are multiplied by the factors indicated in the legend. The data are compared to NLO pQCD calculations using NLOJET++ to which nonperturbative corrections have been applied. The error bars, which are usually smaller than the symbols, indicate the statistical uncertainty on the measurement. The dark-shaded band indicates the quadratic sum of the experimental systematic uncertainties, dominated by the jet energy scale uncertainty. There is an additional overall uncertainty of 3.4% due to the luminosity measurement that is not shown. The theory uncertainty, shown as the light, hatched band, is the quadratic sum of uncertainties from the choice of the renormalization and factorization scales, parton distribution functions, $\alpha_s(M_Z)$, and the modeling of nonperturbative effects, as described in the text.

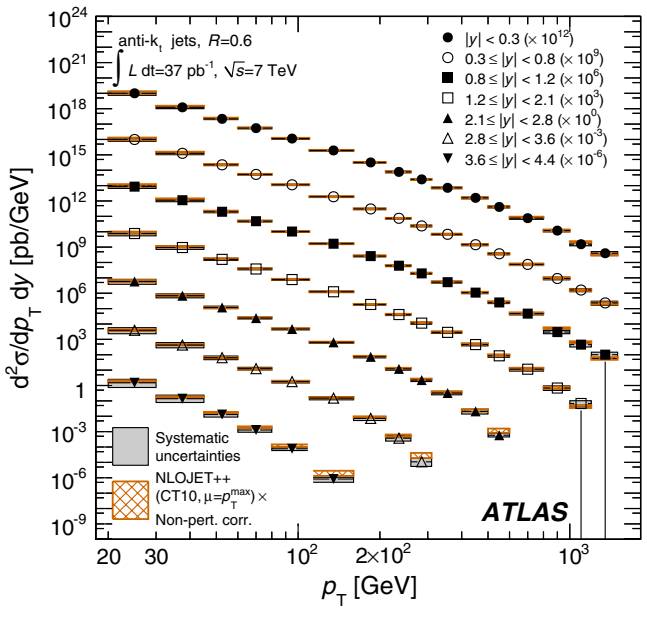

FIG. 10 (color online). Inclusive jet double-differential cross section as a function of jet p_T in different regions of $|y|$ for jets identified using the anti-k_t algorithm with $R = 0.6$. For convenience, the cross sections are multiplied by the factors indicated in the legend. The data are compared to NLO pQCD calculations using NLOJET++ to which nonperturbative corrections have been applied. The theoretical and experimental uncertainties indicated are calculated as described in Fig. 9.

using PYTHIA and the AUET2B tune. Scale uncertainties are not shown for the POWHEG curves, but they have been found to be similar to those obtained with NLOJET++.

Good agreement at the level of a few percent is observed between NLO fixed-order calculations based on NLOJET++ and POWHEG, as described in Sec. VA 1. However, significant differences reaching $O(30\%)$ are observed if POWHEG is interfaced to different showering and soft physics models, particularly at low p_T and forward rapidity, but also at high p_T. These differences exceed the uncertainties on the nonperturbative corrections, which are not larger than 10% for the inclusive jet measurements with $R = 0.4$, thus indicating a significant impact of the parton shower. The Perugia 2011 tune tends to produce a consistently larger cross section than the standard AUET2B tune over the full rapidity range. The technique of correcting fixed-order calculations for nonperturbative effects remains the convention to define the baseline theory prediction until NLO parton shower generators become sufficiently mature to describe data well. The corrected NLO result predicts a consistently

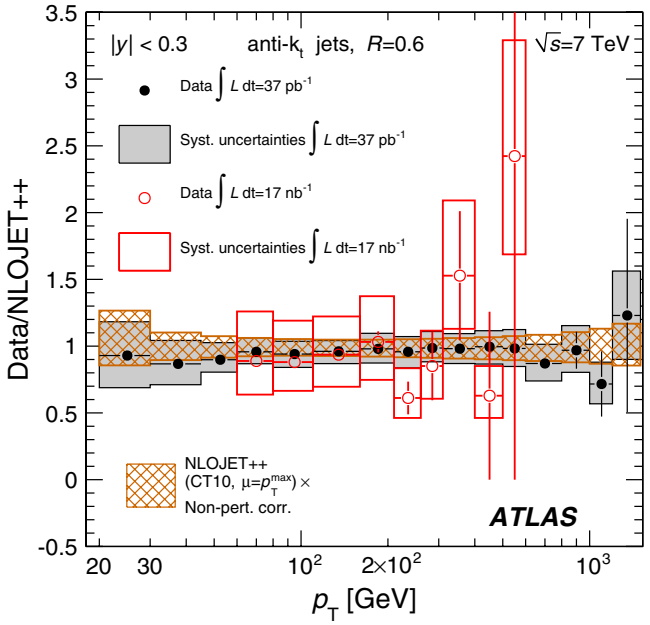

FIG. 11 (color online). Ratio of inclusive jet cross section to the theoretical prediction obtained using NLOJET++ with the CT10 PDF set. The ratio is shown as a function of jet p_T in the rapidity region $|y| < 0.3$, for jets identified using the anti-k_t algorithm with $R = 0.6$. The current result is compared to that published in Ref. [21].

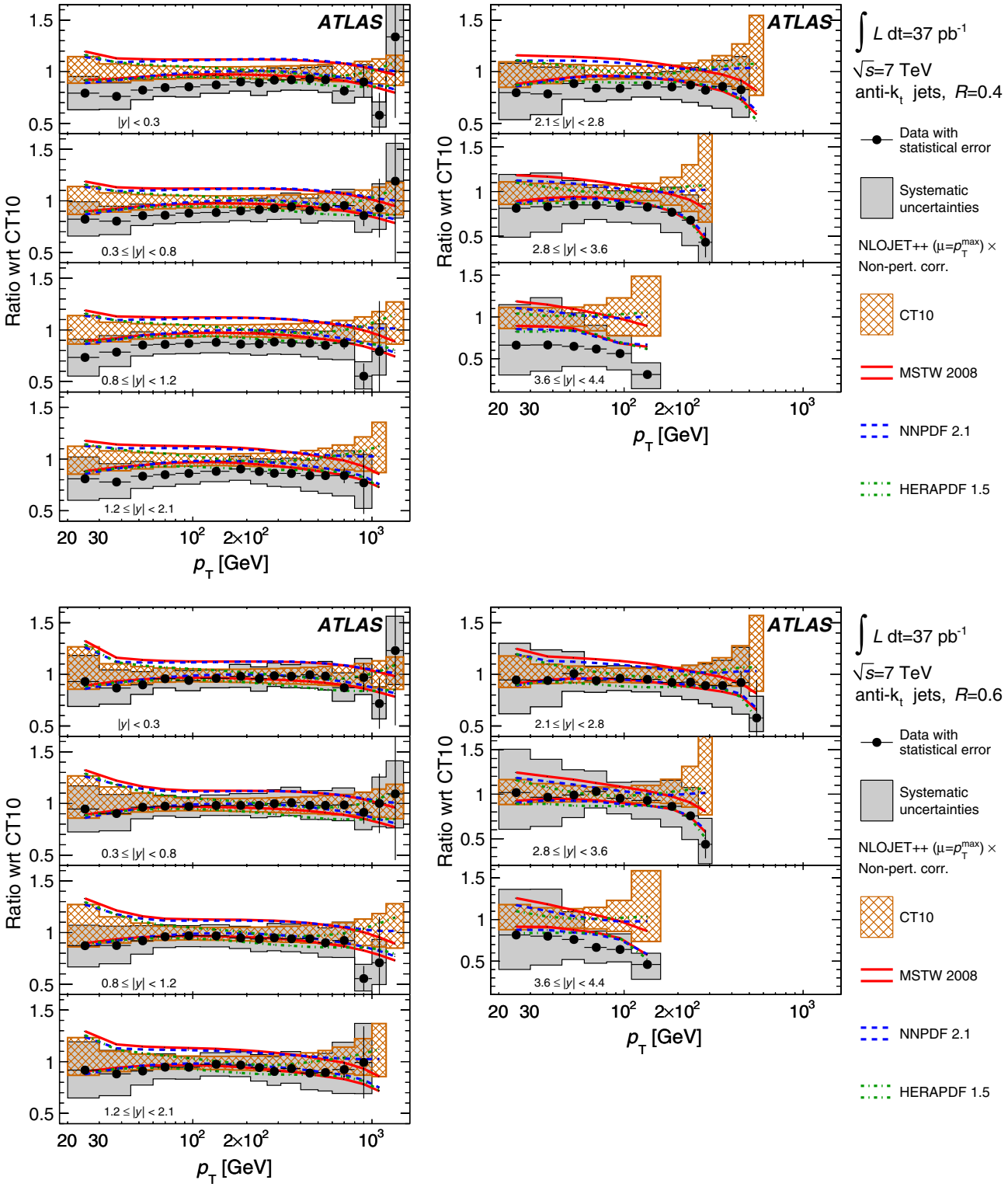

FIG. 12 (color online). Ratios of inclutive jet double-differential cross section to the theoretical prediction obtained using NLOJET++ with the CT10 PDF set. The ratios are shown as a function of jet p_T in different regions of $|y|$ for jets identified using the anti-k_t algorithm with $R = 0.4$ (upper plots) and $R = 0.6$ (lower plots). The theoretical error bands obtained by using NLOJET++ with different PDF sets (CT10, MSTW 2008, NNPDF 2.1, HERAPDF 1.5) are shown. Statistically insignificant data points at large p_T are omitted in the ratio.

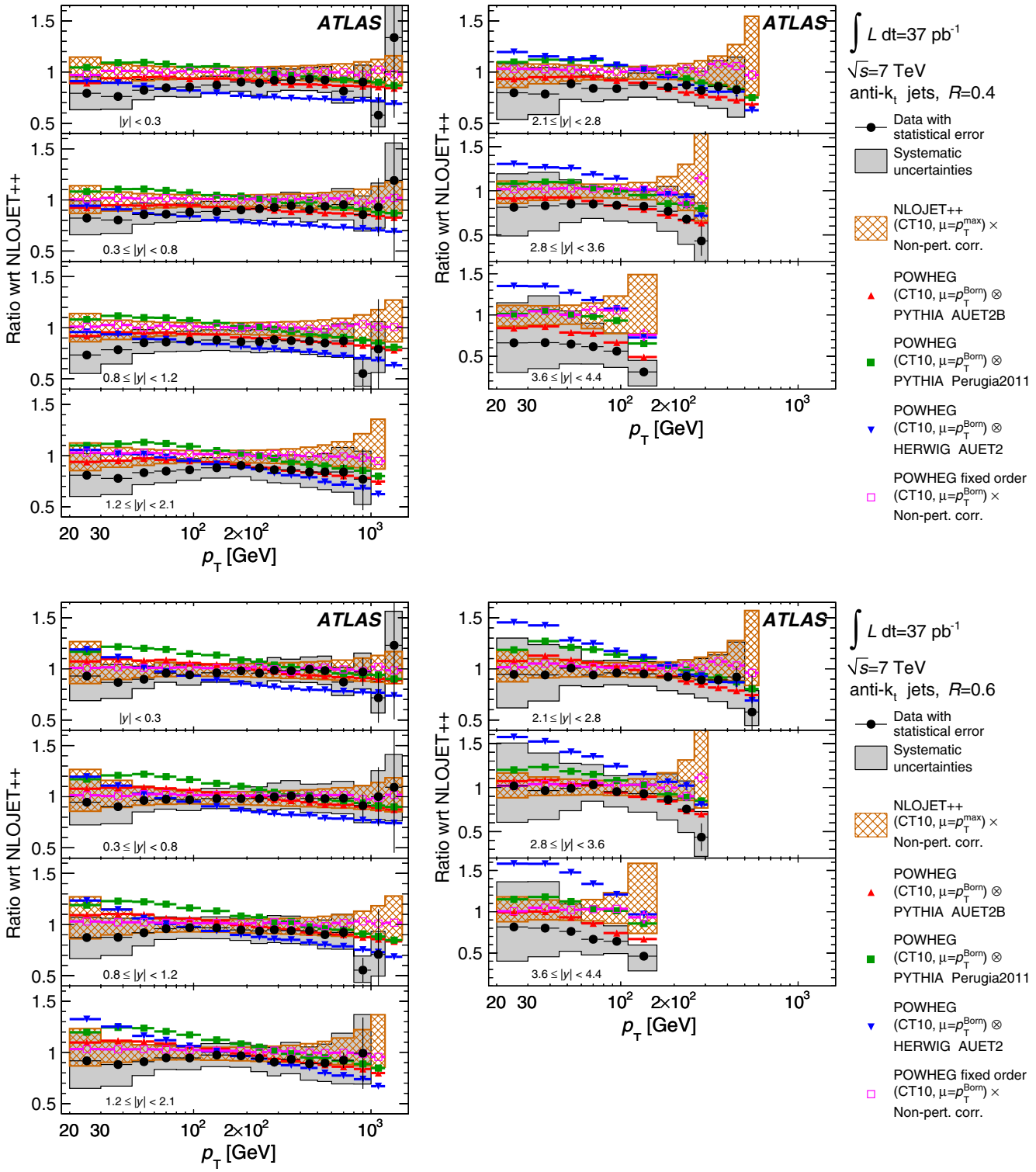

FIG. 13 (color online). Ratios of inclusive jet double-differential cross section to the theoretical prediction obtained using NLOJET++ with the CT10 PDF set. The ratios are shown as a function of jet p_T in different regions of $|y|$ for jets identified using the anti-k_t algorithm with $R = 0.4$ (upper plots) and $R = 0.6$ (lower plots). The ratios of POWHEG predictions showered using either PYTHIA or HERWIG to the NLOJET++ predictions corrected for nonperturbative effects are shown and can be compared to the corresponding ratios for data. Only the statistical uncertainty on the POWHEG predictions is shown. The total systematic uncertainties on the theory and the measurement are indicated. The NLOJET++ prediction and the POWHEG ME calculations use the CT10 PDF set. Statistically insignificant data points at large p_T are omitted in the ratio.

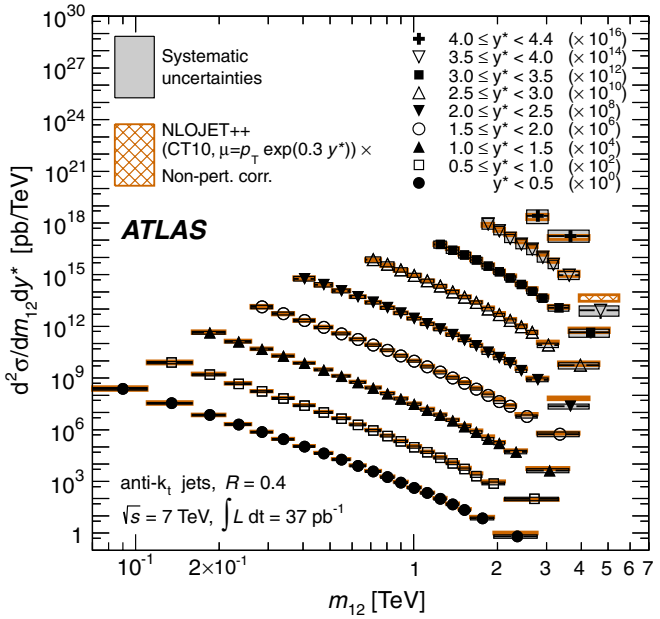

FIG. 14 (color online). Dijet double-differential cross section as a function of dijet mass, binned in half the rapidity separation between the two leading jets, $y^* = |y_1 - y_2|/2$. The results are shown for jets identified using the anti-k_t algorithm with $R = 0.4$. For convenience, the cross sections are multiplied by the factors indicated in the legend. The data are compared to NLO pQCD calculations using NLOJET++ to which nonperturbative corrections have been applied. The error bars, which are usually smaller than the symbols, indicate the statistical uncertainty on the measurement. The dark-shaded band indicates the quadratic sum of the experimental systematic uncertainties, dominated by the jet energy scale uncertainty. There is an additional overall uncertainty of 3.4% due to the luminosity measurement that is not shown. The theory uncertainty, shown as the light, hatched band, is the quadratic sum of uncertainties from the choice of the renormalization and factorization scales, parton distribution functions, $\alpha_s(M_Z)$, and the modeling of nonperturbative effects, as described in the text.

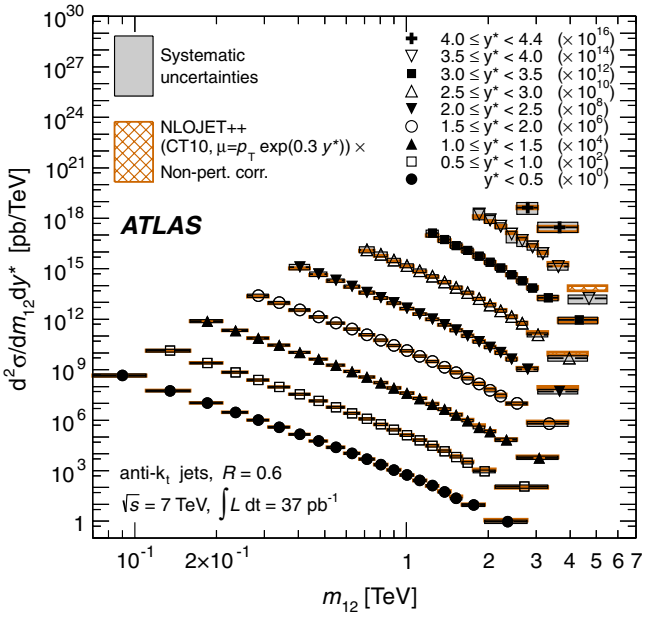

FIG. 15 (color online). Dijet double-differential cross section as a function of dijet mass, binned in half the rapidity separation between the two leading jets, $y^* = |y_1 - y_2|/2$. The results are shown for jets identified using the anti-k_t algorithm with $R = 0.6$. For convenience, the cross sections are multiplied by the factors indicated in the legend. The data are compared to NLO pQCD calculations using NLOJET++ to which nonperturbative corrections have been applied. The theoretical and experimental uncertainties indicated are calculated as described in Fig. 14.

larger cross section than that seen in the data. Good agreement in normalization is found between the data and the prediction from POWHEG showered with the default tune of PYTHIA. These results are confirmed by a χ^2 test of the compatibility of the POWHEG results with the data, where the curve obtained using the HERWIG shower results in a much worse χ^2 after all error correlations have been accounted for.

B. Dijet cross sections

The dijet double-differential cross section has been measured as a function of the dijet invariant mass for various bins of the variable y^*, which is the rapidity in the two-parton center-of-mass frame. The quantity y^* is calculated as half the absolute value of the rapidity difference of the two leading jets, ranging from 0 to 4.4. The results are shown in Figs. 14 and 15 and Tables XIX–XXXVI in Appendix C for anti-k_t jets with $R = 0.4$ and $R = 0.6$. The cross section measurements extend from dijet masses of 70 GeV to almost 5 TeV, covering 2 orders of magnitude in invariant mass and 9 orders of magnitude in the cross section. The dijet measurements are fully corrected for detector effects and are compared to NLOJET++ predictions calculated using the scale defined in Eq. (3) (see Sec. V A 1) and the CT10 PDF set, with nonperturbative corrections applied to the theory prediction. The theoretical uncertainties have been assessed as described for the inclusive jet measurements in Sec. IX A.

The dijet data are also compared with NLOJET++ predictions obtained using the MSTW 2008, NNPDF 2.1, and HERAPDF 1.5 PDF sets. Figures 16 and 17 show the dijet mass spectra for anti-k_t jets with $R = 0.4$ and $R = 0.6$ respectively, where both the data and the predictions from the above-mentioned PDF sets have been normalized to the CT10 prediction. The data for $R = 0.6$ exhibit a slight falling slope with respect to the CT10 prediction and appear to be described better by other PDF sets, a similar behavior to that observed in the inclusive jet data. However, in all cases, the differences between the data and each PDF set lie well within the systematic and theory uncertainties, indicating a reasonable agreement with the dijet data, particularly in the kinematic region at low y^*.

The data are also compared with POWHEG predictions produced using the CT10 PDF set and showered with different tunes of the PYTHIA or HERWIG generator. These comparisons are shown for $R = 0.4$ and $R = 0.6$

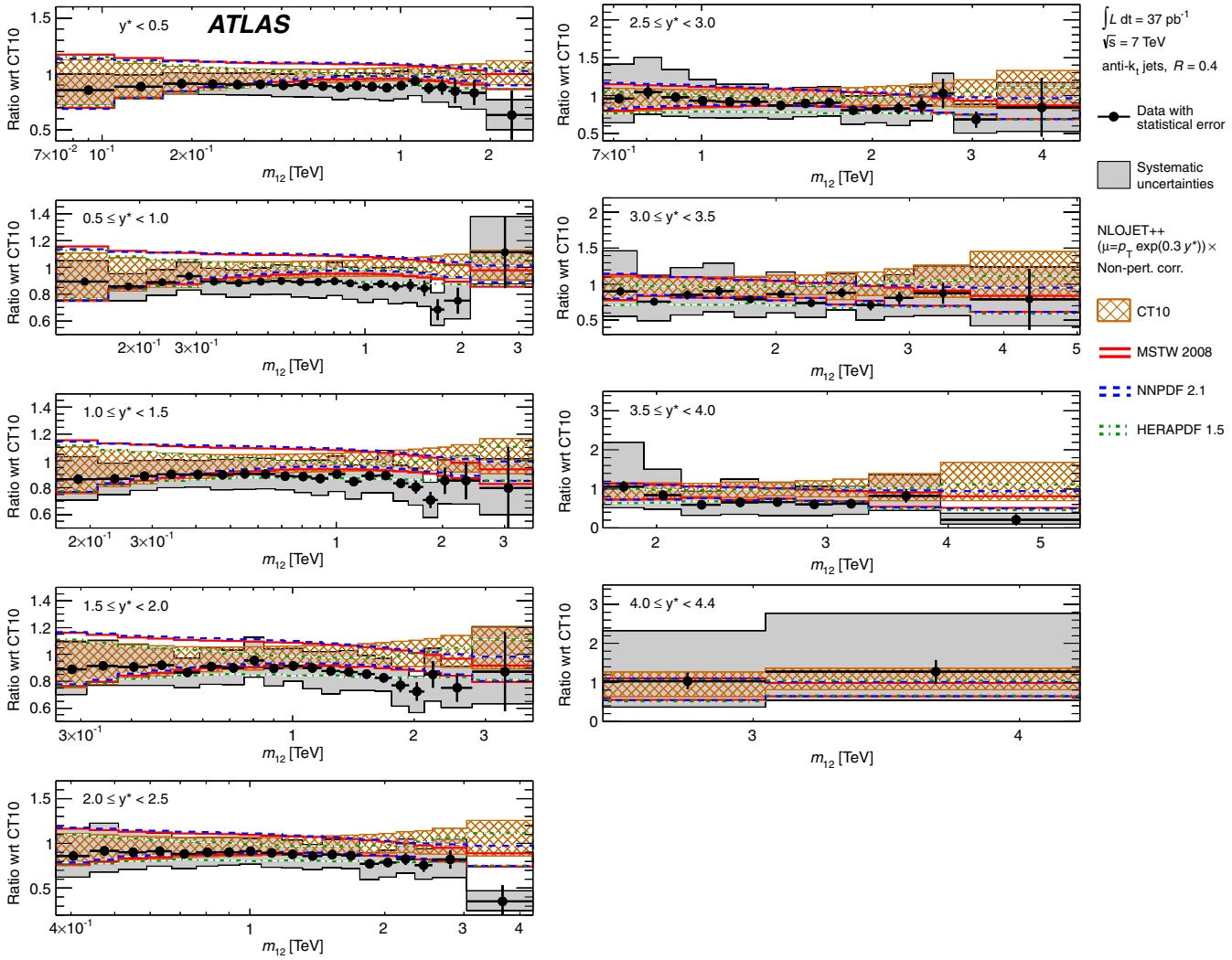

FIG. 16 (color online). Ratios of dijet double-differential cross section to the theoretical prediction obtained using NLOJET++ with the CT10 PDF set. The ratios are shown as a function of dijet mass, binned in half the rapidity separation between the two leading jets, $y^* = |y_1 - y_2|/2$. The results are shown for jets identified using the anti-k_t algorithm with $R = 0.4$. The theoretical error bands obtained by using NLOJET++ with different PDF sets (CT10, MSTW 2008, NNPDF 2.1, HERAPDF 1.5) are shown. The systematic and theoretical uncertainties are calculated as described in Fig. 14.

respectively in Figs. 18 and 19, where the data and all theory predictions have been normalized to the NLOJET++ prediction with CT10. The NLOJET++ prediction has been corrected for nonperturbative effects calculated using the PYTHIA MC with the AUET2B tune. The POWHEG predictions shown are interfaced to the PYTHIA parton shower with the AUET2B or Perugia2011 tune, and to the HERWIG parton shower using the AUET2 tune. The data are also compared to the POWHEG fixed-order NLO prediction (corrected for nonperturbative effects), where the POWHEG prediction has been calculated using a scale choice of $\mu_R = \mu_F = p_T^{\mathrm{Born}}$.

The data are in best agreement with the POWHEG prediction showered with PYTHIA using the AUET2B tune. The other POWHEG showered predictions exhibit discrepancies at low dijet mass in all y^* slices, where they predict larger cross sections than are observed in the data.

X. CONCLUSIONS

Cross section measurements have been presented for inclusive jets and dijets reconstructed with the anti-k_t algorithm using two values of the clustering parameter ($R = 0.4$ and $R = 0.6$). Inclusive jet production has been measured as a function of jet transverse momentum, in bins of jet rapidity. Dijet production has been measured as a function of the invariant mass of the two leading jets, in bins of half their rapidity difference. These results are based on the data sample collected with the ATLAS detector during 2010, which corresponds to (37.3 ± 1.2) pb^{-1} of integrated luminosity.

Two different sizes of the jet clustering parameter have been used in order to probe the relative effects of the parton shower, hadronization, and the underlying event. The measurements have been corrected for all detector effects

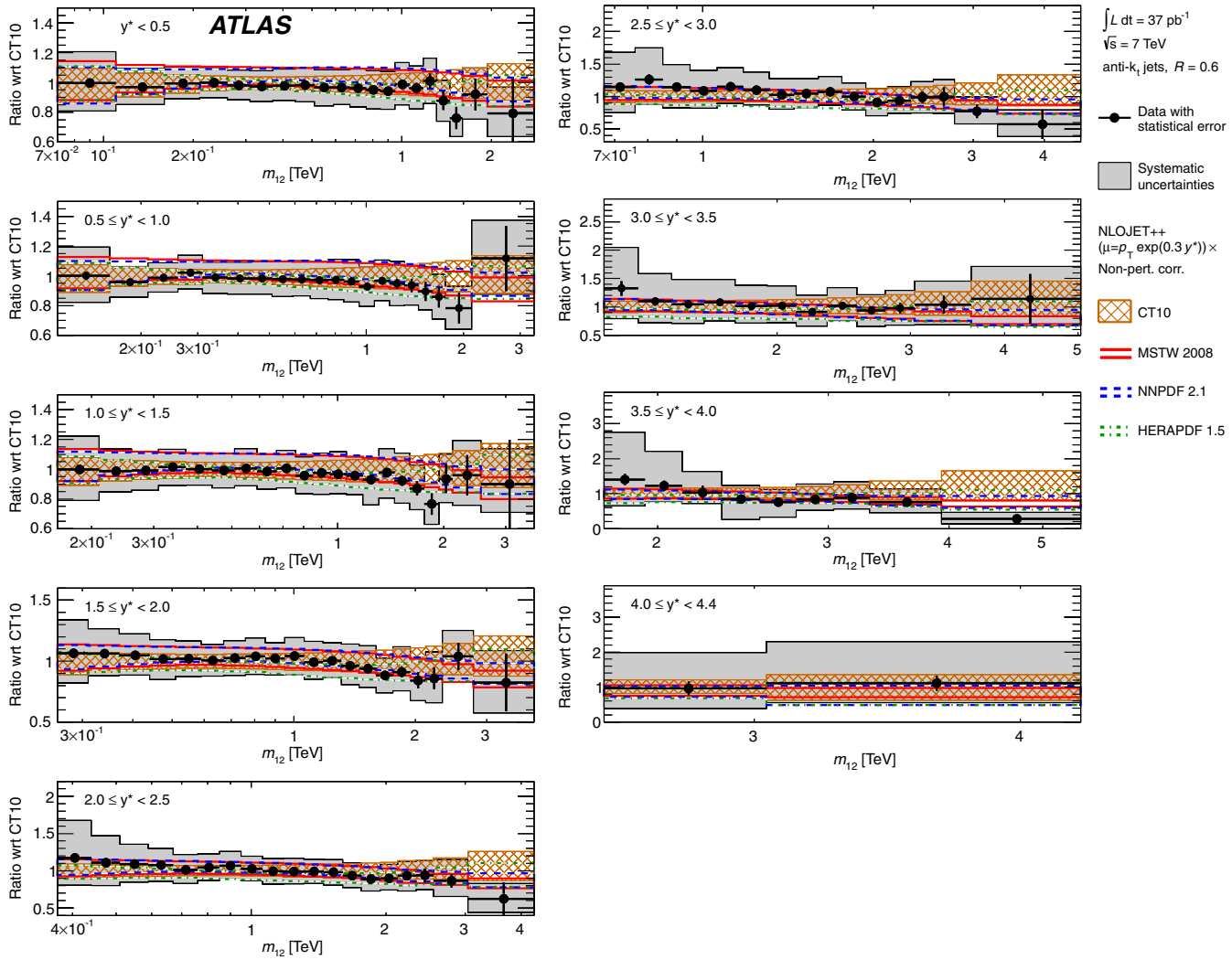

FIG. 17 (color online). Ratios of dijet double-differential cross section to the theoretical prediction obtained using NLOJET++ with the CT10 PDF set. The ratios are shown as a function of dijet mass, binned in half the rapidity separation between the two leading jets, $y^* = |y_1 - y_2|/2$. The results are shown for jets identified using the anti-k_t algorithm with $R = 0.6$. The theoretical error bands obtained by using NLOJET++ with different PDF sets (CT10, MSTW 2008, NNPDF 2.1, HERAPDF 1.5) are shown. The systematic and theoretical uncertainties are calculated as described in Fig. 14.

to the particle level so that they can be compared to any theoretical calculation. In this paper, they have been compared to fixed-order NLO pQCD calculations corrected for nonperturbative effects, as well as to parton shower Monte Carlo simulations with NLO matrix elements. The latter predictions have only recently become available for inclusive jet and dijet production.

The current results reflect a number of significant experimental accomplishments:

(i) The cross section measurements extend to 1.5 TeV in jet transverse momentum and 5 TeV in dijet invariant mass, the highest ever measured. These results probe NLO pQCD in a large, new kinematic regime.

(ii) Using data taken with minimum-bias and forward jet triggers, these measurements extend to both the low-p_T region (down to jet transverse momentum of 20 GeV and dijet invariant mass of 70 GeV) and to the forward region (out to rapidities of $|y| = 4.4$). The forward region, in particular, has never been explored before with such precision at a hadron-hadron collider.

(iii) High-precision measurements of the data collected during LHC beam position scans have determined the uncertainty on the collected luminosity to 3.4%.

(iv) Detailed understanding of the detector performance has precisely determined systematic uncertainties, in particular, those arising from the jet energy scale. In the central region ($|\eta| < 0.8$) the JES uncertainty is lower than 4.6% for all jets with $p_T > 20$ GeV, while for jet transverse momenta between 60 and 800 GeV the JES uncertainty is below 2.5%.

(v) The correlations of the cross section measurement across various p_T, m_{12}, and rapidity bins have been studied for 22 independent sources of systematic

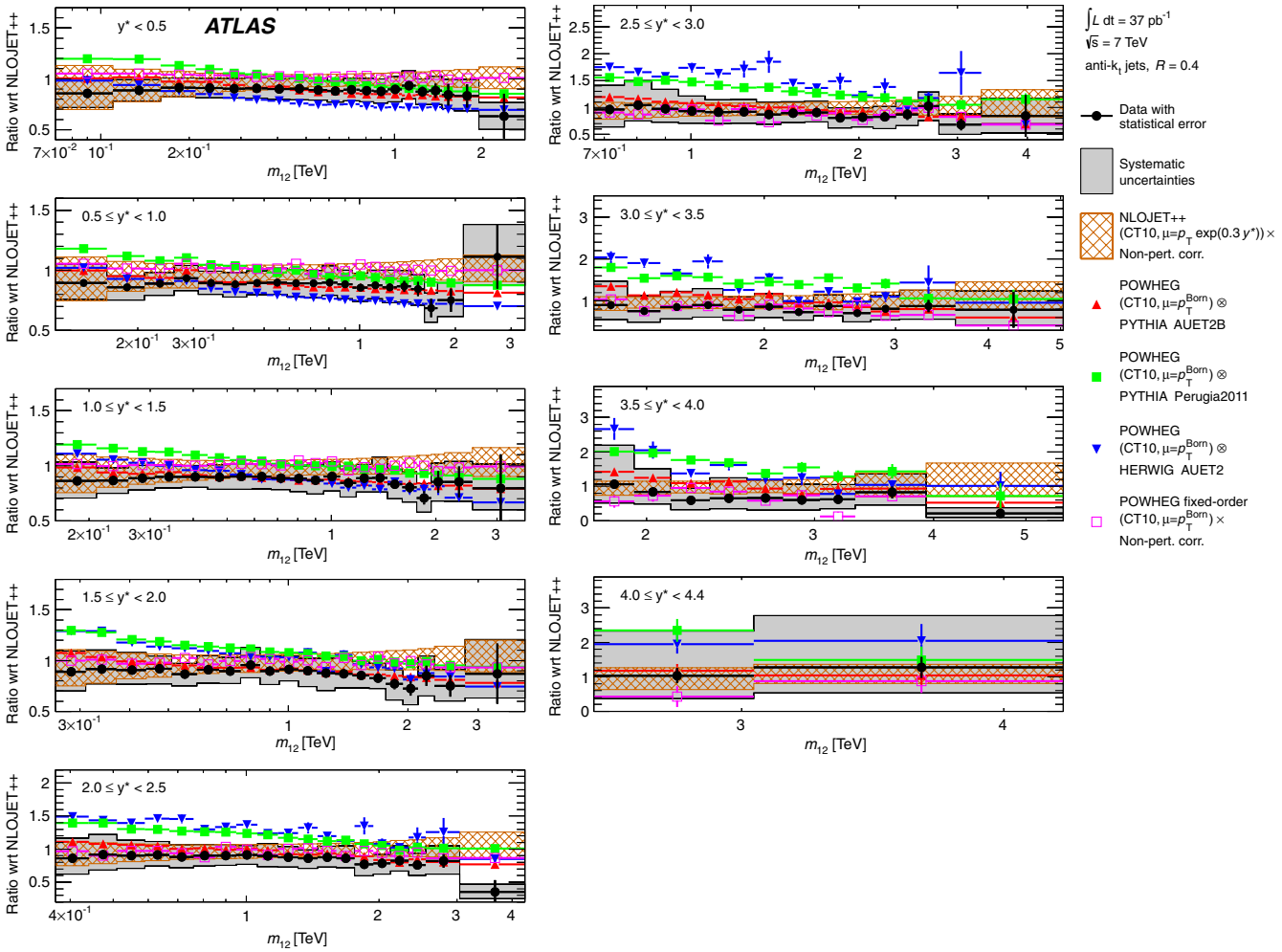

FIG. 18 (color online). Ratios of dijet double-differential cross section to the theoretical prediction obtained using NLOJET++ with the CT10 PDF set. The ratios are shown as a function of dijet mass, binned in half the rapidity separation between the two leading jets, $y^* = |y_1 - y_2|/2$. The results are shown for jets identified using the anti-k_t algorithm with $R = 0.4$. The ratios of POWHEG predictions showered using either PYTHIA or HERWIG to the NLOJET++ predictions corrected for nonperturbative effects are shown and can be compared to the corresponding ratios for data. Only the statistical uncertainty on the POWHEG predictions is shown. The total systematic uncertainties on the theory and the measurement are indicated. The NLOJET++ prediction and the POWHEG ME calculations use the CT10 PDF set.

uncertainty. These have been provided in the form of 87 nuisance parameters, each of which is fully correlated in p_T and y (dijet mass and y^*), for use in PDF fits.

The experimental uncertainties achieved are similar in size to the theoretical uncertainties in some regions of phase space, thereby providing some sensitivity to different theoretical predictions.

The measurements are compared to fixed-order NLO pQCD calculations, as well as to new calculations in which NLO pQCD matrix elements are matched to leading-logarithmic parton showers. Overall, both sets of calculations agree with the data over many orders of magnitude, although the cross sections predicted by the theory tend to be larger than the measured values at large jet transverse momentum and dijet invariant mass. The matched NLO parton shower calculations predict significant effects of the parton shower in some regions of phase space, in some cases improving and in others degrading the agreement with data with respect to the fixed-order calculations.

These measurements probe and may constrain the largely unexplored area of parton distribution functions at large x and high momentum transfer. The results reported here constitute a comprehensive test of QCD across a large kinematic regime.

ACKNOWLEDGMENTS

We thank S. Ellis, M. Mangano, D. Soper, and R. Thorne for useful discussions regarding the scales used for the dijet theory predictions; the POWHEG authors for assistance with the POWHEG predictions; and P. Skands for advice regarding the nonperturbative corrections. We thank CERN for

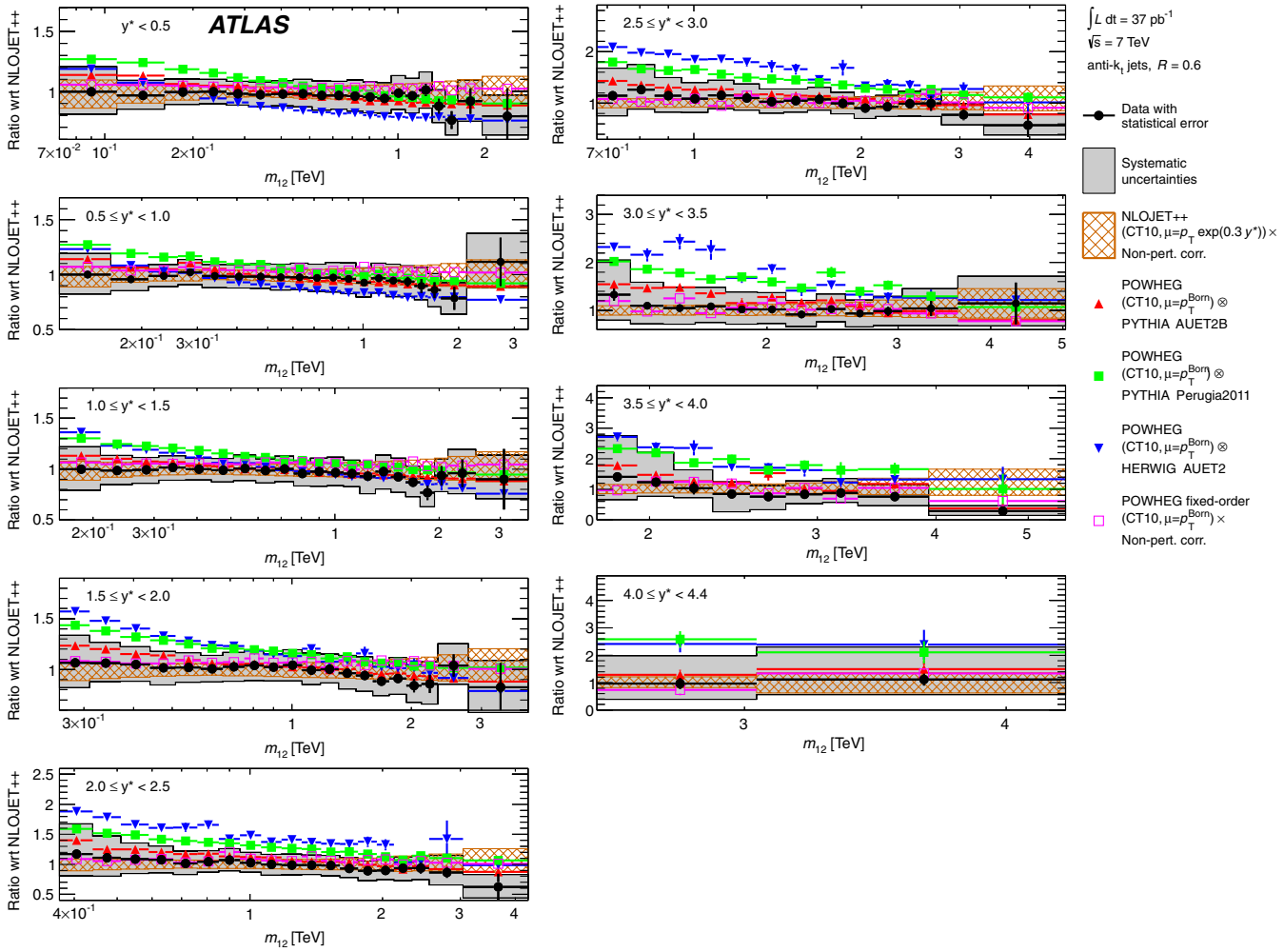

FIG. 19 (color online). Ratios of dijet double-differential cross section to the theoretical prediction obtained using NLOJET++ with the CT10 PDF set. The ratios are shown as a function of dijet mass, binned in half the rapidity separation between the two leading jets, $y^* = |y_1 - y_2|/2$. The results are shown for jets identified using the anti-k_t algorithm with $R = 0.6$. The ratios of POWHEG predictions showered using either PYTHIA or HERWIG to the NLOJET++ predictions corrected for nonperturbative effects are shown and can be compared to the corresponding ratios for data. Only the statistical uncertainty on the POWHEG predictions is shown. The total systematic uncertainties on the theory and the measurement are indicated. The NLOJET++ prediction and the POWHEG ME calculations use the CT10 PDF set.

the very successful operation of the LHC, as well as the support staff from our institutions without whom ATLAS could not be operated efficiently. We acknowledge the support of ANPCyT, Argentina; YerPhI, Armenia; ARC, Australia; BMWF, Austria; ANAS, Azerbaijan; SSTC, Belarus; CNPq and FAPESP, Brazil; NSERC, NRC and CFI, Canada; CERN; CONICYT, Chile; CAS, MOST and NSFC, China; COLCIENCIAS, Colombia; MSMT CR, MPO CR and VSC CR, Czech Republic; DNRF, DNSRC and Lundbeck Foundation, Denmark; ARTEMIS, European Union; IN2P3-CNRS and CEA-DSM/IRFU, France; GNAS, Georgia; BMBF, DFG, HGF, MPG and AvH Foundation, Germany; GSRT, Greece; ISF, MINERVA, GIF, DIP and Benoziyo Center, Israel; INFN, Italy; MEXT and JSPS, Japan; CNRST, Morocco; FOM and NWO, Netherlands; RCN, Norway; MNiSW, Poland; GRICES and FCT, Portugal; MERYS (MECTS), Romania; MES of Russia and ROSATOM, Russian Federation; JINR; MSTD, Serbia; MSSR, Slovakia; ARRS and MVZT, Slovenia; DST/NRF, South Africa; MICINN, Spain; SRC and Wallenberg Foundation, Sweden; SER, SNSF and Cantons of Bern and Geneva, Switzerland; NSC, Taiwan; TAEK, Turkey; STFC, the Royal Society and Leverhulme Trust, United Kingdom; DOE and NSF, United States of America. The crucial computing support from all WLCG partners is acknowledged gratefully, in particular, from CERN and the ATLAS Tier-1 facilities at TRIUMF (Canada), NDGF (Denmark, Norway, Sweden), CC-IN2P3 (France), KIT/GridKA (Germany), INFN-CNAF (Italy), NL-T1 (Netherlands), PIC (Spain), ASGC (Taiwan), RAL (UK) and BNL (USA) and in the Tier-2 facilities worldwide.

APPENDIX A: NON-PERTURBATIVE CORRECTIONS

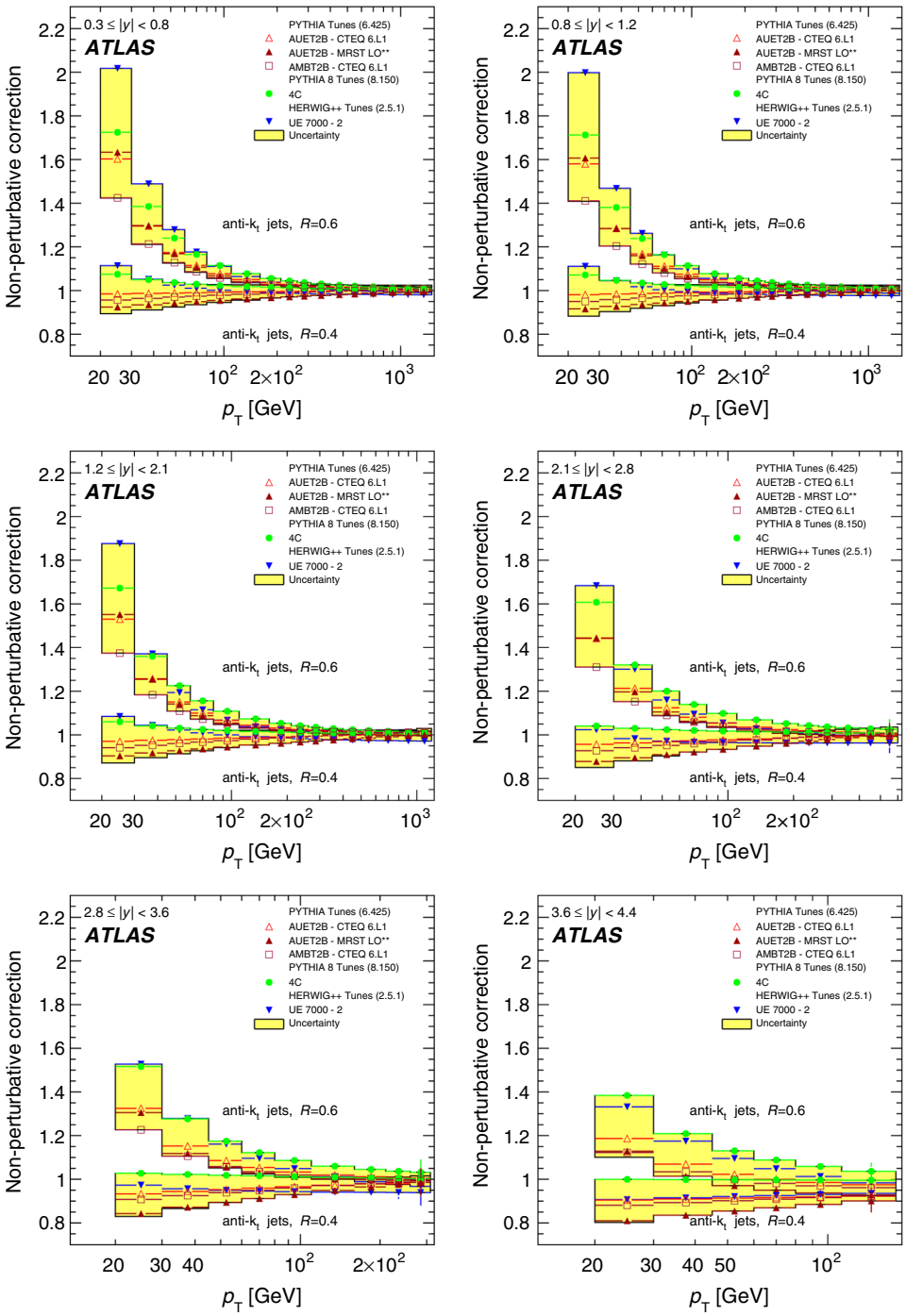

FIG. 20 (color online). Nonperturbative correction factors for inclusive jets identified using the anti-k_t algorithm with clustering parameters $R = 0.4$ and $R = 0.6$ in various rapidity regions, derived using various Monte Carlo generators. The correction derived using PYTHIA 6.425 with the AUET2B CTEQ6L1 tune is used for the fixed-order NLO calculations presented in this analysis.

APPENDIX B: INCLUSIVE JET TABLES

TABLE V. Measured jet cross section for $R = 0.4$, $|y| < 0.3$. NPC stands for multiplicative nonperturbative corrections with error × 100 in parentheses, i.e., 1.25(10) means 1.25 ± 0.10. σ is the measured cross section. δ_{stat} is the statistical uncertainty. γ_i and u_i are the correlated and uncorrelated systematic uncertainties, as described in Sec. VIII D and Table III. All uncertainties are given in %. An overall luminosity uncertainty of 3.4%, which is applicable to all ATLAS data samples based on 2010 data, is not shown. All tables are available on HEPDATA [71].

p_T-bin [GeV]	NPC	σ [pb/GeV]	δ_{stat} %	γ_1	γ_7	γ_{13}	γ_{19}	γ_{25}	γ_{31}	γ_{32}	γ_{38}	γ_{44}	γ_{50}	γ_{56}	γ_{62}	γ_{68}	γ_{74}	γ_{75}	γ_{76}	γ_{82}	γ_{83}	u_1	u_2	u_3
20–30	0.99(11)	4.70×10^6	0.86	$^{+10}_{-9.6}$	$^{+10}_{-9.9}$	$^{+7.0}_{-7.1}$	$^{+8.3}_{-8.6}$	$^{+3.7}_{-4.0}$	0.0	$^{+2.0}_{-2.2}$	$^{+4.9}_{-5.0}$	$^{+4.1}_{-4.7}$	0.0	0.0	$^{+1.8}_{-2.0}$	0.0	0.0	±1.5	±4.2	±0.2	±2.0	0.70	1.00	0.33
30–45	0.99(7)	7.17×10^5	1.33	$^{+4.7}_{-4.8}$	$^{+8.9}_{-8.3}$	$^{+5.9}_{-6.0}$	$^{+10}_{-9.0}$	$^{+1.4}_{-1.7}$	0.0	$^{+2.3}_{-2.4}$	$^{+4.0}_{-3.8}$	$^{+4.1}_{-4.4}$	0.0	0.0	$^{+3.3}_{-3.5}$	0.0	0.0	±1.1	±0.9	0.0	±1.0	0.41	1.00	0.22
45–60	0.99(5)	1.48×10^5	3.03	$^{+1.8}_{-1.7}$	$^{+7.8}_{-6.8}$	$^{+4.1}_{-3.5}$	$^{+5.3}_{-4.7}$	$^{+0.4}_{-0.1}$	0.0	$^{+2.9}_{-2.8}$	$^{+2.4}_{-2.3}$	$^{+4.0}_{-3.7}$	$^{+0.2}_{+0.2}$	$^{+0.3}_{+0.0}$	$^{+4.6}_{-4.4}$	0.0	0.0	±0.7	±0.7	0.0	±1.0	0.27	1.00	0.19
60–80	0.99(5)	3.81×10^4	1.10	∓0.6	$^{+6.2}_{-6.0}$	$^{+2.5}_{-2.4}$	$^{+3.3}_{-3.4}$	$^{+0.9}_{-1.0}$	0.0	±3.2	$^{+1.5}_{-1.6}$	$^{+4.1}_{-3.9}$	$^{+0.4}_{-0.3}$	0.0	$^{+4.6}_{-4.2}$	∓0.1	0.0	±0.4	0.0	0.0	±1.0	0.27	1.00	0.15
80–110	0.99(4)	8.52×10^3	0.68	∓0.4	$^{+6.4}_{-6.8}$	$^{+3.6}_{-4.1}$	$^{+3.2}_{-3.3}$	$^{+1.7}_{-2.2}$	0.0	$^{+2.7}_{-3.1}$	$^{+1.1}_{-1.6}$	$^{+4.2}_{-4.9}$	$^{+0.5}_{-1.0}$	0.0	±2.4	$^{-0.6}_{+0.2}$	0.0	±2.0	±2.3	0.0	±1.0	0.40	1.00	0.10
110–160	0.99(3)	1.48×10^3	0.62	0.0	$^{+5.4}_{-4.9}$	$^{+3.5}_{-3.3}$	$^{+3.3}_{-3.4}$	±0.7	0.0	$^{+3.2}_{-2.9}$	$^{+1.2}_{-1.0}$	$^{+5.3}_{-4.9}$	$^{+1.7}_{-1.6}$	0.0	0.0	$^{+1.3}_{-1.1}$	0.0	0.0	±0.8	0.0	±1.0	0.35	1.00	0.07
160–210	1.00(3)	2.54×10^2	0.69	0.0	$^{+3.8}_{-3.5}$	$^{+3.8}_{-3.9}$	$^{+3.0}_{-2.6}$	$^{+1.4}_{-0.9}$	0.0	$^{+2.5}_{-2.6}$	$^{+0.8}_{-0.4}$	$^{+6.1}_{-5.5}$	$^{+2.5}_{-1.9}$	$^{+0.3}_{+0.2}$	∓0.3	±4.5	±0.1	±0.1	±0.4	0.0	±1.0	0.34	1.00	0.06
210–260	1.00(3)	6.34×10^1	0.91	0.0	$^{+5.4}_{-5.6}$	$^{+5.7}_{-5.9}$	$^{+2.1}_{-2.7}$	$^{+1.1}_{-1.7}$	0.0	$^{+2.8}_{-2.9}$	$^{+0.5}_{-0.8}$	$^{+6.1}_{-6.5}$	$^{+3.2}_{-3.8}$	$^{+0.2}_{-0.5}$	0.0	$^{+6.2}_{-6.6}$	±0.2	0.0	±0.4	±0.1	±1.0	0.37	1.00	0.05
260–310	1.00(3)	2.07×10^1	0.86	0.0	$^{+5.4}_{-4.9}$	$^{+4.0}_{-3.7}$	$^{+2.1}_{-1.9}$	$^{+1.8}_{-1.5}$	0.0	$^{+2.4}_{-2.0}$	$^{+0.6}_{-0.3}$	$^{+6.1}_{-5.7}$	$^{+4.1}_{-3.8}$	$^{+0.6}_{-0.4}$	0.0	$^{+6.9}_{-6.4}$	±0.2	0.0	±0.7	0.0	±1.0	0.28	1.00	0.05
310–400	1.00(2)	5.96×10^0	1.03	0.0	$^{+3.7}_{-3.2}$	$^{+2.3}_{-1.9}$	$^{+1.1}_{-0.5}$	$^{+1.9}_{-1.8}$	0.0	$^{+2.0}_{-1.9}$	$^{+0.7}_{-0.1}$	$^{+6.3}_{-6.1}$	$^{+4.5}_{-3.8}$	$^{+0.7}_{-0.2}$	0.0	$^{+7.0}_{-6.5}$	±0.1	0.0	±0.8	0.0	±1.0	0.26	1.00	0.05
400–500	1.00(2)	1.33×10^0	2.02	0.0	$^{+0.4}_{-0.8}$	0.0	$^{+1.6}_{-2.0}$	$^{+1.8}_{-2.2}$	0.0	$^{+1.1}_{-1.5}$	$^{+0.3}_{-0.7}$	$^{+6.7}_{-6.6}$	$^{+5.0}_{-5.3}$	$^{+0.1}_{-0.6}$	0.0	$^{+7.7}_{-7.8}$	±0.2	0.0	±0.4	0.0	±1.0	0.21	1.00	0.05
500–600	1.00(2)	3.47×10^{-1}	3.22	0.0	±2.3	$^{+1.0}_{-0.8}$	$^{+1.9}_{-1.8}$	$^{+3.0}_{-2.7}$	0.0	$^{+1.6}_{-1.3}$	$^{+0.3}_{-0.4}$	$^{+7.2}_{-6.7}$	$^{+6.2}_{-5.5}$	$^{+0.5}_{-0.6}$	0.0	$^{+9.6}_{-8.8}$	±0.3	0.0	±0.7	0.0	±1.0	0.19	1.00	0.05
600–800	1.00(2)	6.44×10^{-2}	5.73	0.0	±4.2	$^{+3.3}_{-3.4}$	$^{+0.8}_{-0.6}$	$^{+1.8}_{-2.1}$	0.0	$^{+1.2}_{-1.5}$	$^{+0.5}_{-0.4}$	$^{+7.7}_{-6.8}$	$^{+6.0}_{-5.8}$	$^{+1.0}_{-0.9}$	0.0	$^{+10}_{-9.4}$	±0.3	0.0	±0.7	0.0	±1.0	0.17	1.00	0.21
800–1000	1.00(2)	1.01×10^{-2}	16.7	0.0	$^{+3.0}_{-2.6}$	$^{+5.4}_{-4.9}$	$^{+1.1}_{-0.9}$	$^{+1.7}_{-1.5}$	0.0	$^{+1.1}_{-1.0}$	$^{+0.3}_{+0.1}$	$^{+8.4}_{-7.8}$	$^{+7.9}_{-6.8}$	$^{+1.8}_{-2.1}$	0.0	$^{+12}_{-11}$	±0.5	0.0	±0.9	0.0	±1.0	0.11	1.00	0.21
1000–1200	1.00(2)	1.14×10^{-3}	37.3	0.0	$^{+2.4}_{-2.5}$	$^{+5.6}_{-5.3}$	$^{+0.9}_{-0.7}$	±3.1	0.0	$^{+1.0}_{-0.6}$	$^{+0.5}_{-0.3}$	$^{+8.8}_{-7.9}$	$^{+8.8}_{-8.4}$	±4.9	0.0	$^{+16}_{-14}$	±0.7	0.0	±0.4	0.0	±1.0	0.12	1.00	0.21
1200–1500	1.00(2)	4.00×10^{-4}	58.6	0.0	$^{+2.3}_{-2.5}$	$^{+6.3}_{-6.4}$	$^{+1.0}_{-0.8}$	$^{+2.4}_{-2.7}$	0.0	$^{+0.5}_{-0.8}$	$^{+0.6}_{-0.5}$	$^{+9.7}_{-8.9}$	$^{+10}_{-9.5}$	$^{+9.3}_{-8.6}$	0.0	$^{+20}_{-18}$	±0.5	0.0	±3.0	±0.1	±1.0	0.08	1.00	0.21

TABLE VI. Measured jet cross section for $R = 0.4$, $0.3 \leq |y| < 0.8$. See Table V for description of the columns. All tables are available on HEPDATA [71].

p_T-bin [GeV]	NPC	σ[pb/GeV]	δ_{stat} %	γ_1	γ_7	γ_{13}	γ_{19}	γ_{25}	γ_{31}	γ_{32}	γ_{38}	γ_{44}	γ_{50}	γ_{56}	γ_{62}	γ_{68}	γ_{74}	γ_{75}	γ_{76}	γ_{82}	γ_{83}	u_1	u_2	u_3
20–30	0.98(11)	4.61×10^6	0.61	$^{+10}_{-9.5}$	$^{+8.1}_{-8.3}$	$^{+10}_{-9.6}$	± 7.3	± 4.2	0.0	± 2.1	± 4.3	$^{+4.6}_{-4.5}$	0.0	0.0	± 2.9	0.0	0.0	± 1.3	± 3.9	± 0.2	± 2.0	0.70	1.00	0.30
30–45	0.99(7)	7.30×10^5	1.19	$^{+4.9}_{-4.7}$	$^{+11}_{-9.5}$	$^{+6.8}_{-6.3}$	$^{+8.8}_{-7.5}$	$^{+2.4}_{-2.1}$	0.0	± 2.4	± 3.2	$^{+4.6}_{-4.4}$	0.0	0.0	± 3.2	$^{-0.2}_{+0.1}$	0.0	± 1.0	± 1.7	0.0	± 1.0	0.43	1.00	0.20
45–60	0.99(6)	1.49×10^5	2.15	$^{+2.0}_{-1.5}$	$^{+7.5}_{-6.7}$	$^{+6.0}_{-5.3}$	$^{+4.9}_{-4.2}$	$^{+1.7}_{-1.1}$	0.0	$^{+3.2}_{-2.6}$	$^{+1.9}_{-1.3}$	$^{+4.4}_{-3.8}$	$^{+0.1}_{+0.2}$	$^{+0.3}_{+0.0}$	$^{+2.7}_{-2.3}$	$^{+0.3}_{+0.1}$	± 0.1	± 0.5	± 1.2	0.0	± 1.0	0.28	1.00	0.19
60–80	0.99(5)	3.71×10^4	0.83	∓ 0.6	$^{+6.2}_{-5.3}$	$^{+5.1}_{-4.4}$	$^{+3.9}_{-3.4}$	$^{+2.4}_{-2.1}$	0.0	$^{+3.2}_{-2.7}$	$^{+1.5}_{-1.2}$	$^{+4.6}_{-3.9}$	$^{+0.5}_{-0.2}$	0.0	$^{+0.9}_{-0.7}$	$^{+1.6}_{-1.3}$	0.0	0.0	± 0.6	0.0	± 1.0	0.30	1.00	0.16
80–110	0.99(4)	8.35×10^3	0.56	∓ 0.4	± 5.8	$^{+3.6}_{-3.8}$	$^{+2.7}_{-3.0}$	$^{+0.5}_{-0.9}$	0.0	$^{+2.5}_{-2.8}$	$^{+0.8}_{-1.3}$	$^{+4.6}_{-4.8}$	$^{+0.8}_{-1.2}$	0.0	∓ 0.3	$^{+3.6}_{-3.7}$	0.0	± 0.3	± 0.7	0.0	± 1.0	0.38	1.00	0.11
110–160	0.99(3)	1.44×10^3	0.44	0.0	$^{+5.6}_{-5.4}$	$^{+3.8}_{-3.5}$	$^{+3.4}_{-3.2}$	± 0.8	0.0	$^{+2.5}_{-2.4}$	$^{+0.8}_{-0.7}$	$^{+5.2}_{-4.7}$	$^{+1.6}_{-1.5}$	0.0	∓ 0.1	$^{+5.0}_{-4.9}$	0.0	0.0	± 1.3	0.0	± 1.0	0.35	1.00	0.08
160–210	0.99(3)	2.41×10^2	0.58	0.0	$^{+4.6}_{-4.0}$	$^{+3.8}_{-3.4}$	$^{+3.0}_{-2.6}$	$^{+1.7}_{-1.1}$	0.0	$^{+2.4}_{-1.9}$	$^{+1.1}_{-0.4}$	$^{+5.7}_{-5.4}$	$^{+2.5}_{-1.9}$	$^{+0.4}_{+0.1}$	0.0	$^{+6.7}_{-5.9}$	± 0.1	0.0	± 0.7	0.0	± 1.0	0.39	1.00	0.07
210–260	1.00(3)	6.06×10^1	0.72	0.0	$^{+4.0}_{-4.6}$	$^{+3.3}_{-3.9}$	$^{+2.2}_{-2.3}$	$^{+1.5}_{-2.1}$	0.0	$^{+1.8}_{-2.0}$	0.0	$^{+6.2}_{-6.4}$	$^{+3.0}_{-3.5}$	0.0	0.0	$^{+7.8}_{-7.6}$	± 0.1	0.0	± 0.4	0.0	± 1.0	0.30	1.00	0.07
260–310	1.00(3)	1.96×10^1	0.68	0.0	$^{+4.1}_{-3.2}$	$^{+3.1}_{-2.1}$	$^{+2.0}_{-1.2}$	$^{+3.0}_{-2.2}$	0.0	$^{+2.1}_{-1.4}$	$^{+0.7}_{-0.2}$	$^{+6.9}_{-6.2}$	$^{+3.9}_{-3.3}$	$^{+0.3}_{0.0}$	0.0	$^{+8.8}_{-7.6}$	± 0.2	0.0	± 0.7	0.0	± 1.0	0.25	1.00	0.07
310–400	1.00(2)	5.64×10^0	0.92	0.0	$^{+3.6}_{-3.0}$	$^{+2.6}_{-2.4}$	$^{+1.8}_{-1.6}$	$^{+3.3}_{-2.7}$	0.0	$^{+1.9}_{-1.3}$	$^{+0.4}_{-0.3}$	$^{+7.1}_{-6.3}$	$^{+4.3}_{-4.2}$	$^{+0.5}_{+0.1}$	0.0	$^{+9.4}_{-8.8}$	± 0.1	0.0	± 0.7	0.0	± 1.0	0.30	1.00	0.07
400–500	1.00(2)	1.19×10^0	1.76	0.0	$^{+3.5}_{-3.6}$	$^{+2.5}_{-2.9}$	$^{+1.0}_{-1.5}$	$^{+2.5}_{-2.9}$	0.0	$^{+0.9}_{-1.4}$	± 0.3	± 6.4	$^{+4.3}_{-4.5}$	0.0	0.0	$^{+9.4}_{-9.0}$	± 0.3	0.0	± 0.4	0.0	± 1.0	0.24	1.00	0.07
500–600	1.00(2)	3.16×10^{-1}	3.23	0.0	$^{+3.3}_{-2.9}$	$^{+2.4}_{-2.2}$	± 0.6	$^{+2.0}_{-1.9}$	0.0	$^{+1.1}_{-0.9}$	$^{+0.4}_{-0.3}$	$^{+6.7}_{-6.9}$	$^{+5.2}_{-4.9}$	$^{+0.5}_{-0.3}$	0.0	$^{+11}_{-10}$	± 0.2	0.0	± 0.4	0.0	± 1.0	0.21	1.00	0.25
600–800	1.00(2)	6.60×10^{-2}	4.20	0.0	$^{+3.1}_{-3.6}$	$^{+0.7}_{-1.2}$	$^{+0.7}_{-0.6}$	$^{+2.1}_{-2.0}$	0.0	$^{+0.7}_{-1.2}$	± 0.4	$^{+7.4}_{-7.3}$	$^{+6.3}_{-5.9}$	$^{+0.9}_{-1.3}$	0.0	$^{+13}_{-12}$	± 0.2	0.0	± 0.2	0.0	± 1.0	0.14	1.00	0.25
800–1000	1.00(2)	7.80×10^{-3}	11.9	0.0	$^{+5.5}_{-5.2}$	$^{+3.6}_{-2.7}$	$^{+1.4}_{-0.9}$	$^{+3.0}_{-2.9}$	0.0	$^{+0.9}_{-0.2}$	$^{+0.4}_{+0.1}$	$^{+9.0}_{-8.0}$	$^{+7.1}_{-6.7}$	$^{+3.2}_{-2.9}$	0.0	$^{+16}_{-14}$	± 0.5	0.0	± 1.0	0.0	± 1.0	0.13	1.00	0.25
1000–1200	1.00(2)	1.38×10^{-3}	30.6	0.0	$^{+5.7}_{-5.2}$	$^{+3.5}_{-3.7}$	$^{+0.5}_{-0.4}$	$^{+3.6}_{-3.4}$	0.0	$^{+0.5}_{-0.9}$	$^{+0.6}_{-0.5}$	$^{+10}_{-8.5}$	$^{+8.4}_{-7.7}$	$^{+6.5}_{-6.1}$	0.0	$^{+19}_{-16}$	± 0.6	0.0	± 2.2	0.0	± 1.0	0.14	1.00	0.25
1200–1500	1.00(2)	2.35×10^{-4}	66.6	0.0	$^{+6.8}_{-7.1}$	$^{+4.4}_{-5.6}$	$^{+0.4}_{-1.2}$	$^{+3.3}_{-3.5}$	0.0	$^{+0.4}_{-1.3}$	0.0	± 11	$^{+9.4}_{-9.7}$	$^{+11}_{-12}$	0.0	$^{+23}_{-21}$	± 0.5	0.0	± 2.4	± 0.1	± 1.0	0.15	1.00	0.25

TABLE VII. Measured jet cross section for $R = 0.4$, $0.8 \leq |y| < 1.2$. See Table V for description of the columns. All tables are available on HEPDATA [71].

p_T-bin [GeV]	NPC	σ [pb/GeV]	δ_{stat} %	γ_2	γ_8	γ_{14}	γ_{20}	γ_{26}	γ_{31}	γ_{33}	γ_{39}	γ_{45}	γ_{51}	γ_{57}	γ_{63}	γ_{69}	γ_{74}	γ_{75}	γ_{77}	γ_{82}	γ_{83}	u_1	u_2	u_3
20–30	0.98(11)	3.92×10^6	0.68	± 9.1	$^{+7.0}_{-8.0}$	$^{+8.9}_{-9.3}$	± 13	$^{+3.7}_{-3.9}$	$^{+7.0}_{-7.5}$	$^{+1.8}_{-1.9}$	$^{+3.9}_{-4.1}$	$^{+4.1}_{-4.4}$	0.0	0.0	$^{+2.5}_{-2.8}$	0.0	0.0	± 1.0	± 9.4	± 1.2	± 2.0	1.02	1.00	0.25
30–45	0.98(7)	6.66×10^5	1.51	$^{+5.0}_{-4.5}$	$^{+11}_{-9.4}$	$^{+7.2}_{-6.2}$	$^{+5.7}_{-4.8}$	$^{+2.5}_{-1.9}$	$^{+8.7}_{-7.4}$	$^{+2.6}_{-2.3}$	$^{+3.4}_{-3.0}$	$^{+4.9}_{-4.3}$	0.0	0.0	$^{+3.4}_{-3.0}$	$^{-0.2}_{+0.1}$	0.0	± 0.7	± 6.5	± 0.2	± 1.0	0.72	1.00	0.20
45–60	0.99(6)	1.39×10^5	2.59	$^{+1.9}_{-1.4}$	$^{+8.2}_{-6.7}$	$^{+6.3}_{-5.3}$	$^{+2.0}_{-1.2}$	$^{+1.8}_{-1.2}$	$^{+7.2}_{-6.0}$	$^{+3.2}_{-2.6}$	$^{+1.9}_{-1.4}$	$^{+4.7}_{-3.8}$	$^{+0.2}_{+0.2}$	$^{+0.3}_{+0.0}$	$^{+2.7}_{-2.2}$	$^{+0.2}_{+0.1}$	0.0	± 0.5	± 3.1	± 0.3	± 1.0	0.46	1.00	0.21
60–80	0.99(5)	3.39×10^4	0.99	∓ 0.7	$^{+6.0}_{-5.3}$	$^{+4.8}_{-4.5}$	± 2.4	$^{+2.3}_{-2.2}$	$^{+5.3}_{-5.0}$	± 2.8	$^{+1.5}_{-1.3}$	$^{+4.4}_{-4.1}$	$^{+0.3}_{-0.2}$	0.0	± 0.8	$^{+1.6}_{-1.5}$	0.0	± 0.1	± 1.5	± 0.2	± 1.0	0.47	1.00	0.18
80–110	0.99(4)	7.55×10^3	0.71	$^{-0.5}_{+0.4}$	$^{+5.7}_{-5.8}$	$^{+3.8}_{-3.9}$	$^{+2.6}_{-2.8}$	$^{+0.6}_{-1.0}$	$^{+4.3}_{-4.1}$	$^{+2.7}_{-2.9}$	$^{+1.0}_{-1.3}$	± 4.8	$^{+1.0}_{-1.3}$	0.0	∓ 0.3	$^{+3.9}_{-3.8}$	± 0.2	± 0.3	± 1.4	± 0.2	± 1.0	0.70	1.00	0.12
110–160	0.99(3)	1.28×10^3	0.50	0.0	$^{+5.6}_{-5.9}$	$^{+3.7}_{-3.8}$	± 2.5	$^{+0.8}_{-1.0}$	± 3.0	$^{+2.5}_{-2.6}$	$^{+0.7}_{-0.9}$	$^{+5.2}_{-5.1}$	$^{+1.6}_{-1.8}$	0.0	∓ 0.1	$^{+5.0}_{-5.3}$	± 0.2	0.0	± 1.7	± 0.1	± 1.0	0.63	1.00	0.08
160–210	0.99(3)	2.05×10^2	0.58	0.0	$^{+4.8}_{-4.0}$	$^{+3.9}_{-3.3}$	$^{+2.3}_{-1.9}$	$^{+1.8}_{-1.3}$	$^{+3.6}_{-3.1}$	$^{+2.3}_{-1.9}$	$^{+1.0}_{-0.4}$	$^{+5.9}_{-5.6}$	$^{+2.6}_{-2.0}$	$^{+0.4}_{+0.1}$	0.0	$^{+6.8}_{-6.1}$	± 0.2	0.0	± 1.2	± 0.1	± 1.0	0.63	1.00	0.06
210–260	1.00(3)	5.01×10^1	1.00	0.0	± 4.3	± 3.5	$^{+2.2}_{-1.9}$	$^{+1.8}_{-2.0}$	± 3.9	$^{+2.1}_{-1.8}$	$^{+0.2}_{-0.6}$	$^{+6.4}_{-6.0}$	$^{+3.3}_{-3.2}$	0.0	0.0	$^{+8.1}_{-7.3}$	± 0.1	0.0	± 1.6	0.0	± 1.0	0.53	1.00	0.06
260–310	1.00(3)	1.59×10^1	0.98	0.0	$^{+3.7}_{-3.5}$	$^{+2.7}_{-2.4}$	$^{+1.6}_{-1.2}$	$^{+2.6}_{-2.5}$	$^{+4.0}_{-3.7}$	$^{+1.8}_{-1.5}$	$^{+0.6}_{-0.3}$	$^{+6.6}_{-6.8}$	$^{+3.6}_{-3.7}$	$^{+0.2}_{0.0}$	0.0	$^{+8.5}_{-8.4}$	0.0	0.0	± 0.9	± 0.2	± 1.0	0.39	1.00	0.06
310–400	1.00(2)	4.38×10^0	1.06	0.0	$^{+3.3}_{-2.7}$	$^{+2.5}_{-2.2}$	$^{+1.4}_{-1.0}$	$^{+3.1}_{-2.5}$	$^{+4.2}_{-3.5}$	$^{+1.7}_{-1.2}$	$^{+0.4}_{-0.3}$	$^{+7.2}_{-6.1}$	$^{+4.1}_{-3.8}$	$^{+0.5}_{+0.2}$	0.0	$^{+9.6}_{-8.5}$	± 0.2	0.0	± 1.2	0.0	± 1.0	0.48	1.00	0.06
400–500	1.00(2)	9.18×10^{-1}	1.94	0.0	$^{+3.6}_{-4.0}$	$^{+2.8}_{-3.0}$	$^{+0.9}_{-0.7}$	$^{+2.8}_{-3.0}$	$^{+4.2}_{-4.6}$	$^{+1.2}_{-1.5}$	$^{+0.3}_{-0.4}$	$^{+6.7}_{-6.8}$	$^{+4.3}_{-4.8}$	0.0	0.0	± 9.9	± 0.2	0.0	± 1.2	0.0	± 1.0	0.43	1.00	0.06
500–600	1.00(2)	2.14×10^{-1}	3.67	0.0	$^{+3.4}_{-3.2}$	± 2.7	$^{+0.2}_{-0.3}$	$^{+2.3}_{-2.4}$	$^{+4.5}_{-4.3}$	$^{+1.4}_{-1.3}$	$^{+0.4}_{-0.5}$	$^{+7.3}_{-7.4}$	± 5.6	± 0.7	0.0	± 11	± 0.2	0.0	± 1.5	0.0	± 1.0	0.41	1.00	0.28
600–800	1.00(2)	4.07×10^{-2}	6.66	0.0	$^{+3.5}_{-3.9}$	$^{+0.9}_{-1.2}$	$^{+0.7}_{-0.8}$	± 2.3	$^{+5.0}_{-5.4}$	$^{+0.7}_{-1.1}$	$^{+0.3}_{-0.4}$	$^{+8.0}_{-8.1}$	$^{+7.0}_{-6.5}$	$^{+1.2}_{-1.3}$	0.0	$^{+14}_{-13}$	± 0.2	0.0	± 2.0	0.0	± 1.0	0.25	1.00	0.51
800–1000	1.00(2)	2.70×10^{-3}	22.3	0.0	$^{+5.9}_{-6.0}$	$^{+3.8}_{-3.3}$	$^{+1.1}_{-0.5}$	± 3.4	$^{+6.5}_{-5.8}$	$^{+1.0}_{-0.4}$	$^{+0.5}_{+0.1}$	$^{+11}_{-9.1}$	$^{+8.2}_{-7.7}$	$^{+3.6}_{-3.7}$	0.0	$^{+18}_{-16}$	± 0.5	0.0	± 0.8	0.0	± 1.0	0.26	1.00	0.87
1000–1200	1.00(2)	4.66×10^{-4}	61.7	0.0	$^{+7.8}_{-6.3}$	$^{+4.9}_{-4.4}$	$^{+0.6}_{-0.5}$	$^{+4.9}_{-4.0}$	$^{+8.0}_{-7.4}$	$^{+0.6}_{-1.1}$	$^{+0.7}_{-0.6}$	$^{+13}_{-10}$	$^{+11}_{-9.5}$	$^{+8.5}_{-7.8}$	0.0	$^{+24}_{-20}$	± 0.6	0.0	± 6.6	0.0	± 1.0	0.30	1.00	1.24
1200–1500	1.00(2)	1.02×10^{-4}	104	∓ 0.1	$^{+8.8}_{-11}$	$^{+6.9}_{-8.7}$	$^{+0.2}_{-1.8}$	$^{+5.1}_{-5.9}$	$^{+9.8}_{-11}$	$^{+0.4}_{-1.9}$	0.0	$^{+14}_{-16}$	$^{+13}_{-14}$	$^{+16}_{-17}$	0.0	$^{+33}_{-28}$	± 1.0	0.0	± 9.5	0.0	± 1.0	0.26	1.00	1.69

TABLE VIII. Measured jet cross section for $R = 0.4$, $1.2 \leq |y| < 2.1$. See Table V for description of the columns. All tables are available on HEPDATA [71].

p_T-bin [GeV]	NPC	σ [pb/GeV]	δ_{stat} %	γ_3	γ_9	γ_{15}	γ_{21}	γ_{27}	γ_{31}	γ_{34}	γ_{40}	γ_{46}	γ_{52}	γ_{58}	γ_{64}	γ_{70}	γ_{74}	γ_{75}	γ_{78}	γ_{82}	γ_{83}	u_1	u_2	u_3
20–30	0.97(11)	3.70×10^6	0.55	$^{+9.5}_{-9.0}$	$^{+7.0}_{-7.6}$	$^{+9.3}_{-9.1}$	$^{+9.5}_{-8.7}$	± 3.7	± 14	$^{+1.7}_{-1.8}$	± 3.8	$^{+4.0}_{-4.1}$	0.0	0.0	$^{+2.5}_{-2.6}$	0.0	∓ 0.1	± 0.9	± 10	± 0.6	± 2.0	1.10	1.00	0.30
30–45	0.97(7)	5.62×10^5	1.17	$^{+4.7}_{-4.6}$	$^{+11}_{-9.5}$	$^{+6.8}_{-6.3}$	$^{+2.4}_{-1.9}$	$^{+2.3}_{-1.9}$	$^{+16}_{-14}$	$^{+2.3}_{-2.2}$	$^{+3.1}_{-3.0}$	$^{+4.4}_{-4.3}$	0.0	0.0	$^{+3.1}_{-3.0}$	∓ 0.2	0.0	± 0.9	± 4.7	0.0	± 1.0	0.77	1.00	0.15
45–60	0.98(6)	1.09×10^5	2.01	$^{+2.0}_{-1.8}$	$^{+8.1}_{-6.7}$	$^{+6.3}_{-5.4}$	$^{+0.2}_{0.0}$	$^{+1.7}_{-1.4}$	$^{+12}_{-9.2}$	$^{+3.1}_{-2.8}$	$^{+2.0}_{-1.7}$	$^{+4.4}_{-3.8}$	$^{+0.2}_{+0.2}$	$^{+0.3}_{+0.0}$	$^{+2.8}_{-2.5}$	$^{+0.3}_{+0.0}$	0.0	± 0.6	± 1.8	0.0	± 1.0	0.51	1.00	0.13
60–80	0.98(5)	2.67×10^4	0.73	∓ 0.5	$^{+6.7}_{-6.6}$	± 5.4	± 0.4	$^{+2.5}_{-2.6}$	$^{+8.0}_{-7.6}$	± 3.1	$^{+1.5}_{-1.7}$	± 4.9	$^{+0.3}_{-0.2}$	0.0	± 0.9	$^{+1.7}_{-1.8}$	± 0.1	± 0.4	± 0.6	0.0	± 1.0	0.48	1.00	0.10
80–110	0.98(4)	5.84×10^3	1.11	∓ 0.4	$^{+6.5}_{-5.9}$	$^{+4.3}_{-4.1}$	$^{+0.9}_{-1.0}$	$^{+0.8}_{-1.0}$	$^{+5.8}_{-5.5}$	$^{+3.2}_{-3.1}$	$^{+1.2}_{-1.4}$	$^{+5.3}_{-5.0}$	$^{+1.2}_{-1.3}$	0.0	∓ 0.3	$^{+4.2}_{-4.0}$	± 0.1	± 0.2	± 2.3	0.0	± 1.0	0.42	1.00	0.07
110–160	0.99(3)	9.58×10^2	0.71	0.0	$^{+5.6}_{-5.7}$	± 3.7	$^{+0.7}_{-1.1}$	± 0.8	$^{+4.5}_{-4.4}$	± 2.4	± 0.7	$^{+5.1}_{-5.0}$	± 1.5	0.0	∓ 0.1	$^{+4.9}_{-5.2}$	± 0.2	0.0	± 1.1	0.0	± 1.0	0.49	1.00	0.05
160–210	0.99(3)	1.51×10^2	0.81	0.0	$^{+5.0}_{-4.3}$	$^{+4.2}_{-3.4}$	$^{+1.1}_{-0.7}$	$^{+1.7}_{-1.2}$	$^{+5.4}_{-5.1}$	$^{+2.4}_{-2.1}$	$^{+1.0}_{-0.5}$	$^{+6.3}_{-5.9}$	$^{+2.6}_{-2.2}$	$^{+0.4}_{+0.1}$	0.0	$^{+7.4}_{-6.3}$	± 0.4	0.0	± 1.2	0.0	± 1.0	0.44	1.00	0.05
210–260	0.99(3)	3.38×10^1	0.66	0.0	$^{+4.2}_{-4.5}$	$^{+3.3}_{-3.7}$	± 1.3	$^{+1.6}_{-2.2}$	$^{+5.8}_{-5.3}$	± 2.0	$^{+0.2}_{-0.8}$	$^{+6.4}_{-6.3}$	$^{+3.0}_{-3.4}$	0.0	0.0	$^{+8.2}_{-7.7}$	± 0.6	0.0	± 1.3	0.0	± 1.0	0.58	1.00	0.05
260–310	0.99(3)	9.58×10^0	1.28	0.0	$^{+4.1}_{-3.8}$	$^{+3.1}_{-2.6}$	$^{+1.7}_{-1.5}$	$^{+3.1}_{-2.8}$	$^{+6.3}_{-6.1}$	$^{+2.1}_{-1.7}$	$^{+0.6}_{-0.4}$	$^{+7.4}_{-7.1}$	$^{+3.9}_{-4.1}$	$^{+0.2}_{0.0}$	0.0	$^{+9.5}_{-8.7}$	± 0.2	0.0	± 0.9	± 0.1	± 1.0	0.47	1.00	0.06
310–400	1.00(2)	2.35×10^0	1.06	0.0	$^{+4.0}_{-3.2}$	$^{+2.8}_{-2.6}$	$^{+1.4}_{-1.0}$	$^{+3.6}_{-2.8}$	$^{+6.7}_{-6.3}$	$^{+1.9}_{-1.4}$	$^{+0.4}_{-0.3}$	$^{+8.0}_{-7.0}$	$^{+5.0}_{-4.5}$	$^{+0.5}_{+0.1}$	0.0	$^{+10}_{-9.7}$	0.0	0.0	± 1.5	0.0	± 1.0	0.38	1.00	0.06
400–500	1.00(2)	3.91×10^{-1}	1.98	0.0	$^{+3.9}_{-4.7}$	$^{+2.7}_{-3.6}$	$^{+1.5}_{-1.7}$	$^{+2.8}_{-3.6}$	$^{+7.4}_{-7.1}$	$^{+1.0}_{-1.8}$	$^{+0.3}_{-0.4}$	$^{+7.8}_{-7.9}$	$^{+5.0}_{-5.6}$	0.0	0.0	$^{+12}_{-11}$	± 0.4	0.0	± 1.0	± 0.1	± 1.0	0.46	1.00	0.07
500–600	1.00(2)	7.25×10^{-2}	4.72	0.0	$^{+4.1}_{-3.9}$	$^{+3.0}_{-2.9}$	$^{+2.2}_{-2.1}$	$^{+2.6}_{-2.7}$	$^{+8.4}_{-8.2}$	± 1.5	± 0.4	$^{+8.8}_{-9.0}$	$^{+6.8}_{-6.7}$	$^{+0.6}_{-0.7}$	0.0	± 14	± 0.5	0.0	± 1.2	0.0	± 1.0	0.44	1.00	0.58
600–800	1.00(2)	9.51×10^{-3}	8.77	0.0	$^{+4.9}_{-5.2}$	$^{+1.6}_{-2.0}$	$^{+1.1}_{-1.7}$	$^{+3.3}_{-3.2}$	$^{+11}_{-9.1}$	$^{+1.1}_{-1.6}$	$^{+0.5}_{-0.7}$	$^{+11}_{-9.9}$	$^{+9.8}_{-8.2}$	$^{+1.9}_{-2.2}$	0.0	$^{+20}_{-16}$	± 0.6	0.0	± 2.1	± 0.2	± 1.0	0.41	1.00	0.62
800–1000	1.00(3)	4.86×10^{-4}	39.2	0.0	$^{+8.2}_{-7.9}$	$^{+5.4}_{-4.5}$	$^{+0.8}_{-0.2}$	$^{+4.4}_{-4.6}$	± 12	$^{+1.2}_{-0.6}$	$^{+0.7}_{+0.1}$	$^{+14}_{-13}$	$^{+11}_{-10}$	$^{+5.5}_{-5.2}$	0.0	$^{+25}_{-21}$	± 1.1	0.0	± 3.9	± 0.3	± 1.0	0.38	1.00	0.68
1000–1200	1.01(3)	6.93×10^{-5}	103	∓ 0.1	$^{+8.4}_{-8.8}$	$^{+6.7}_{-6.8}$	$^{+7.6}_{-8.1}$	$^{+6.5}_{-5.3}$	$^{+15}_{-14}$	$^{+0.5}_{-0.9}$	$^{+0.6}_{-0.4}$	$^{+16}_{-15}$	± 14	$^{+11}_{-12}$	0.0	$^{+34}_{-27}$	± 2.3	0.0	± 9.2	± 0.5	± 1.0	0.15	1.00	0.77

TABLE IX. Measured jet cross section for $R = 0.4$, $2.1 \leq |y| < 2.8$. See Table V for description of the columns. All tables are available on HEPDATA [71].

p_T-bin [GeV]	NPC	σ [pb/GeV]	δ_{stat} %	γ_4	γ_{10}	γ_{16}	γ_{22}	γ_{28}	γ_{31}	γ_{35}	γ_{41}	γ_{47}	γ_{53}	γ_{59}	γ_{65}	γ_{71}	γ_{74}	γ_{75}	γ_{79}	γ_{82}	γ_{84}	u_1	u_2	u_3
20–30	0.96(10)	2.76×10^6	0.69	$^{+10}_{-9.1}$	± 7.4	$^{+10}_{-9.1}$	$^{+6.5}_{-6.1}$	± 4.0	$^{+26}_{-23}$	$^{+2.0}_{-1.9}$	$^{+4.2}_{-4.1}$	$^{+4.4}_{-4.3}$	0.0	0.0	± 2.7	0.0	0.0	± 1.2	± 15	± 0.1	± 2.0	1.27	1.00	0.02
30–45	0.96(7)	4.07×10^5	1.37	$^{+4.8}_{-4.3}$	$^{+11}_{-9.1}$	$^{+6.7}_{-5.8}$	$^{+4.7}_{-4.0}$	$^{+2.3}_{-1.8}$	$^{+28}_{-21}$	$^{+2.4}_{-2.2}$	$^{+3.3}_{-2.9}$	$^{+4.5}_{-4.1}$	0.0	0.0	$^{+3.2}_{-2.9}$	$^{-0.2}_{+0.1}$	0.0	± 0.7	± 5.1	0.0	± 1.0	0.85	1.00	0.02
45–60	0.97(6)	8.00×10^4	2.84	$^{+2.5}_{-2.1}$	$^{+8.1}_{-7.1}$	$^{+6.7}_{-5.8}$	$^{+2.5}_{-2.0}$	$^{+2.1}_{-1.4}$	$^{+16}_{-13}$	$^{+3.5}_{-2.6}$	$^{+2.2}_{-1.7}$	$^{+4.7}_{-3.9}$	$^{+0.1}_{+0.2}$	$^{+0.3}_{+0.0}$	$^{+3.1}_{-2.6}$	$^{+0.3}_{+0.2}$	± 0.2	± 0.1	± 1.6	0.0	± 1.0	0.55	1.00	0.02
60–80	0.97(5)	1.71×10^4	1.05	$^{-0.5}_{+0.4}$	± 7.0	$^{+5.5}_{-5.6}$	$^{+1.3}_{-1.5}$	$^{+2.5}_{-2.8}$	$^{+10}_{-9.4}$	$^{+3.1}_{-3.5}$	$^{+1.7}_{-1.9}$	$^{+5.0}_{-5.2}$	± 0.3	0.0	$^{+0.8}_{-1.0}$	$^{+1.7}_{-1.9}$	± 0.2	± 0.3	± 0.8	0.0	± 1.0	0.57	1.00	0.02
80–110	0.98(4)	3.44×10^3	0.60	∓ 0.3	$^{+6.2}_{-6.3}$	$^{+3.9}_{-4.5}$	$^{+0.5}_{-0.7}$	$^{+0.6}_{-1.2}$	$^{+6.8}_{-6.7}$	$^{+2.8}_{-3.4}$	$^{+1.0}_{-1.5}$	$^{+5.0}_{-5.4}$	$^{+1.0}_{-1.5}$	0.0	$^{-0.3}_{+0.2}$	$^{+3.8}_{-4.4}$	± 0.3	± 0.1	± 1.1	0.0	± 1.0	0.78	1.00	0.02
110–160	0.98(3)	4.98×10^2	0.61	0.0	± 6.4	$^{+4.2}_{-4.0}$	$^{+1.3}_{-1.1}$	$^{+1.1}_{-0.9}$	$^{+6.1}_{-6.2}$	$^{+2.9}_{-2.5}$	$^{+0.9}_{-0.8}$	$^{+6.1}_{-5.6}$	$^{+1.9}_{-1.7}$	0.0	∓ 0.1	$^{+5.9}_{-5.8}$	± 0.4	0.0	± 1.5	0.0	± 1.0	0.66	1.00	0.00
160–210	0.99(3)	5.93×10^1	0.89	0.0	$^{+6.0}_{-5.0}$	$^{+5.1}_{-4.2}$	$^{+1.5}_{-0.9}$	$^{+2.3}_{-1.5}$	$^{+8.2}_{-6.8}$	$^{+3.2}_{-2.5}$	$^{+1.2}_{-0.5}$	$^{+7.4}_{-6.7}$	$^{+3.4}_{-2.8}$	$^{+0.4}_{+0.1}$	0.0	$^{+9.0}_{-7.3}$	± 0.7	0.0	± 1.6	0.0	± 1.0	0.81	1.00	0.00
210–260	0.99(3)	1.00×10^1	1.31	0.0	± 5.9	$^{+4.7}_{-4.9}$	$^{+0.8}_{-1.2}$	$^{+2.2}_{-2.7}$	$^{+9.5}_{-9.2}$	± 2.4	$^{+0.3}_{-0.8}$	$^{+9.0}_{-8.8}$	$^{+4.6}_{-4.8}$	0.0	0.0	$^{+11}_{-10}$	± 0.6	0.0	± 1.9	0.0	± 1.0	0.71	1.00	0.00
260–310	0.99(3)	1.85×10^0	2.04	0.0	$^{+6.2}_{-3.8}$	$^{+4.7}_{-2.6}$	$^{+3.6}_{-2.0}$	$^{+4.8}_{-2.9}$	$^{+10}_{-8.3}$	$^{+3.4}_{-1.8}$	$^{+1.0}_{-0.1}$	$^{+10.0}_{-8.6}$	$^{+6.1}_{-4.4}$	$^{+0.5}_{0.0}$	0.0	$^{+13}_{-12}$	± 0.9	0.0	± 2.8	± 0.1	± 1.0	0.56	1.00	0.22
310–400	0.99(3)	2.76×10^{-1}	3.07	0.0	$^{+6.5}_{-5.3}$	$^{+5.1}_{-4.2}$	$^{+3.3}_{-2.7}$	$^{+6.1}_{-4.5}$	$^{+14}_{-12}$	$^{+3.0}_{-2.5}$	$^{+0.5}_{-0.8}$	$^{+13}_{-11}$	$^{+8.4}_{-6.9}$	$^{+0.6}_{+0.1}$	0.0	$^{+18}_{-15}$	± 0.7	0.0	± 0.8	0.0	± 1.0	0.92	1.00	0.13
400–500	1.00(3)	1.66×10^{-2}	11.5	0.0	$^{+9.3}_{-8.0}$	$^{+6.0}_{-6.1}$	$^{+1.0}_{-2.7}$	$^{+6.0}_{-6.1}$	$^{+17}_{-15}$	$^{+2.3}_{-3.1}$	$^{+1.2}_{-1.4}$	$^{+15}_{-14}$	$^{+11}_{-10}$	0.0	0.0	$^{+26}_{-19}$	± 1.2	0.0	± 5.6	± 0.2	± 1.0	1.07	1.00	0.14
500–600	1.00(4)	3.13×10^{-4}	91.4	0.0	± 2.4	$^{+1.1}_{-2.6}$	± 2.7	$^{+0.9}_{-2.6}$	$^{+9.5}_{-16}$	0.0	0.0	$^{+8.0}_{-16}$	$^{+5.4}_{-10}$	0.0	0.0	$^{+19}_{-25}$	± 1.1	0.0	± 8.0	± 1.5	± 1.0	-0.07	1.00	0.16

TABLE X. Measured jet cross section for $R = 0.4$, $2.8 \leq |y| < 3.6$. See Table V for description of the columns. All tables are available on HEPDATA [71].

p_T-bin [GeV]	NPC	σ [pb/GeV]	δ_{stat} %	γ_5	γ_{11}	γ_{17}	γ_{23}	γ_{29}	γ_{31}	γ_{36}	γ_{42}	γ_{48}	γ_{54}	γ_{60}	γ_{66}	γ_{72}	γ_{74}	γ_{75}	γ_{80}	γ_{82}	γ_{85}	u_1	u_2	u_3
20–30	0.93(10)	1.89×10^6	0.78	$^{+11}_{-9.0}$	$^{+7.8}_{-7.6}$	$^{+10}_{-9.2}$	$^{+17}_{-14}$	$^{+4.1}_{-3.9}$	$^{+37}_{-30}$	$^{+1.8}_{-1.9}$	$^{+4.3}_{-4.0}$	$^{+4.5}_{-4.2}$	0.0	0.0	$^{+2.7}_{-2.6}$	0.0	∓ 0.2	± 0.6	± 14	± 0.3	± 2.0	3.83	1.00	0.00
30–45	0.94(8)	2.67×10^5	1.67	$^{+4.9}_{-5.0}$	$^{+12}_{-11}$	$^{+6.8}_{-7.0}$	$^{+10}_{-9.3}$	$^{+2.5}_{-2.4}$	$^{+41}_{-28}$	$^{+2.6}_{-2.7}$	$^{+3.4}_{-3.6}$	$^{+4.8}_{-5.1}$	0.0	0.0	$^{+3.3}_{-3.6}$	∓ 0.1	0.0	± 0.9	± 6.5	0.0	± 1.0	2.67	1.00	0.00
45–60	0.95(6)	4.25×10^4	3.69	$^{+2.2}_{-2.0}$	$^{+9.1}_{-8.0}$	$^{+7.3}_{-6.5}$	$^{+7.5}_{-6.8}$	$^{+2.2}_{-1.7}$	$^{+28}_{-20}$	$^{+3.8}_{-3.3}$	$^{+2.4}_{-1.9}$	$^{+5.4}_{-4.7}$	$^{+0.3}_{+0.2}$	$^{+0.4}_{+0.0}$	$^{+3.1}_{-2.7}$	$^{+0.5}_{-0.1}$	± 0.3	± 0.2	± 2.1	0.0	± 1.0	1.78	1.00	0.00
60–80	0.96(5)	8.57×10^3	1.69	∓ 0.7	$^{+7.4}_{-6.4}$	$^{+5.6}_{-5.1}$	$^{+7.9}_{-6.7}$	± 2.5	$^{+18}_{-14}$	$^{+3.5}_{-3.2}$	$^{+1.7}_{-1.6}$	$^{+5.3}_{-4.6}$	± 0.4	0.0	$^{+1.0}_{-0.7}$	$^{+2.1}_{-2.0}$	± 0.3	± 0.3	± 1.7	0.0	± 1.0	3.35	1.00	0.00
80–110	0.97(4)	1.31×10^3	3.41	$^{-0.6}_{+0.5}$	$^{+7.5}_{-8.3}$	$^{+4.8}_{-5.4}$	$^{+8.1}_{-8.4}$	$^{+0.8}_{-1.0}$	± 13	$^{+3.2}_{-3.9}$	$^{+1.1}_{-1.5}$	$^{+6.4}_{-7.4}$	$^{+1.3}_{-1.7}$	0.0	$^{-0.5}_{+0.4}$	$^{+5.2}_{-5.8}$	± 0.2	± 0.7	± 2.2	± 0.1	± 1.0	4.17	1.00	0.00
110–160	0.97(3)	1.16×10^2	1.54	0.0	$^{+7.1}_{-8.6}$	$^{+4.6}_{-5.4}$	$^{+6.5}_{-7.6}$	± 1.3	$^{+14}_{-13}$	$^{+3.1}_{-3.5}$	± 1.0	$^{+7.0}_{-8.0}$	$^{+2.2}_{-2.5}$	0.0	∓ 0.2	$^{+7.0}_{-8.5}$	± 0.2	± 0.2	± 3.8	± 0.3	± 1.0	2.42	1.00	0.00
160–210	0.98(3)	5.57×10^0	3.92	0.0	$^{+10}_{-7.1}$	$^{+8.2}_{-5.8}$	$^{+12}_{-10}$	$^{+3.9}_{-2.4}$	$^{+22}_{-18}$	$^{+4.5}_{-3.0}$	$^{+1.7}_{-0.7}$	$^{+13}_{-11}$	$^{+5.1}_{-4.3}$	$^{+0.4}_{+0.1}$	0.0	$^{+16}_{-13}$	± 1.0	± 0.5	± 6.1	± 0.4	± 1.0	2.61	1.00	0.17
210–260	0.98(4)	2.89×10^{-1}	8.18	0.0	$^{+8.6}_{-8.3}$	$^{+6.6}_{-7.3}$	$^{+17}_{-16}$	$^{+4.0}_{-4.7}$	± 25	$^{+3.6}_{-3.3}$	$^{+0.3}_{-0.9}$	± 14	$^{+7.5}_{-8.1}$	0.0	0.0	$^{+18}_{-17}$	± 1.1	0.0	± 13	± 0.3	± 1.0	2.97	1.00	0.19
260–310	0.99(4)	9.17×10^{-3}	39.3	0.0	$^{+26}_{-14}$	$^{+20}_{-11}$	$^{+41}_{-28}$	$^{+22}_{-12}$	$^{+51}_{-38}$	± 12	$^{+3.1}_{+0.1}$	$^{+38}_{-28}$	$^{+28}_{-18}$	$^{+3.4}_{+0.1}$	0.0	$^{+41}_{-27}$	∓ 0.7	± 0.1	± 5.6	± 1.6	± 1.0	6.77	1.00	0.21

TABLE XI. Measured jet cross section for $R = 0.4$, $3.6 \leq |y| < 4.4$. See Table V for description of the columns. All tables are available on HEPDATA [71].

p_T-bin [GeV]	NPC	σ [pb/GeV]	δ_{stat}%	γ_6	γ_{12}	γ_{18}	γ_{24}	γ_{30}	γ_{31}	γ_{37}	γ_{43}	γ_{49}	γ_{55}	γ_{61}	γ_{67}	γ_{73}	γ_{74}	γ_{75}	γ_{81}	γ_{82}	γ_{86}	u_1	u_2	u_3
20–30	0.90(10)	8.19×10^5	1.04	$^{+12}_{-10}$	$^{+8.8}_{-8.7}$	$^{+11}_{-10}$	$^{+3.3}_{-3.4}$	$^{+4.7}_{-4.5}$	$^{+68}_{-48}$	$^{+2.3}_{-2.2}$	$^{+4.9}_{-4.5}$	$^{+5.2}_{-4.9}$	0.0	0.0	$^{+3.1}_{-3.2}$	0.0	0.0	± 0.3	± 15	± 1.0	± 2.0	4.69	1.00	0.00
30–45	0.91(8)	8.64×10^4	1.13	± 5.2	$^{+13}_{-11}$	$^{+7.9}_{-7.2}$	$^{+2.2}_{-2.0}$	$^{+2.6}_{-2.2}$	$^{+83}_{-44}$	$^{+2.8}_{-2.9}$	$^{+3.4}_{-3.5}$	$^{+5.4}_{-5.3}$	0.0	0.0	$^{+3.5}_{-3.6}$	0.0	0.0	± 0.7	± 4.4	± 0.5	± 1.0	7.98	1.00	0.00
45–60	0.91(7)	8.83×10^3	1.95	$^{+2.3}_{-2.6}$	$^{+10}_{-9.1}$	$^{+8.4}_{-7.8}$	$^{+1.7}_{-1.9}$	$^{+2.3}_{-2.6}$	$^{+60}_{-34}$	$^{+3.9}_{-4.2}$	$^{+2.4}_{-2.7}$	$^{+6.3}_{-5.5}$	$^{+0.3}_{+0.1}$	$^{+0.4}_{+0.0}$	$^{+3.3}_{-3.4}$	$^{+0.7}_{-0.5}$	± 0.2	± 0.7	± 1.0	± 0.4	± 1.0	5.37	1.00	0.00
60–80	0.92(6)	9.20×10^2	2.78	∓ 0.9	$^{+11}_{-10}$	$^{+8.9}_{-8.4}$	$^{+3.0}_{-1.5}$	$^{+5.0}_{-3.6}$	$^{+41}_{-29}$	$^{+6.5}_{-5.7}$	$^{+3.8}_{-2.4}$	$^{+8.7}_{-8.1}$	$^{+1.1}_{-0.7}$	0.0	$^{+1.2}_{-1.1}$	$^{+5.0}_{-3.5}$	0.0	± 1.8	± 2.1	± 0.4	± 1.0	5.40	1.00	0.02
80–110	0.92(6)	5.38×10^1	3.94	∓ 0.6	± 13	$^{+8.1}_{-9.9}$	$^{+1.1}_{-2.2}$	$^{+1.6}_{-3.0}$	$^{+31}_{-23}$	$^{+5.4}_{-7.7}$	$^{+2.2}_{-3.4}$	$^{+11}_{-12}$	$^{+2.6}_{-3.9}$	0.0	∓ 0.6	$^{+9.1}_{-11}$	± 1.0	± 0.2	± 6.7	± 0.7	± 1.0	6.66	1.00	0.02
110–160	0.92(5)	5.42×10^{-1}	15.7	0.0	$^{+15}_{-17}$	$^{+13}_{-11}$	$^{+19}_{-30}$	$^{+2.9}_{-6.9}$	$^{+23}_{-30}$	$^{+8.9}_{-9.1}$	$^{+3.0}_{-5.8}$	$^{+16}_{-15}$	$^{+4.9}_{-8.8}$	0.0	∓ 0.3	$^{+17}_{-16}$	± 1.3	0.0	± 6.1	± 0.5	± 1.0	8.54	1.00	0.02

TABLE XII. Measured jet cross section for $R = 0.6$, $|y| < 0.3$. NPC stands for multiplicative nonperturbative corrections with error × 100 in parentheses, i.e., 1.25(10) means 1.25 ± 0.10. σ is the measured cross section. δ_{stat} is the statistical uncertainty. γ_i and u_i are the correlated and uncorrelated systematic uncertainties, as described in Sec. VIII D and Table III. All uncertainties are given in %. An overall luminosity uncertainty of 3.4%, which is applicable to all ATLAS data samples based on 2010 data, is not shown. All tables are available on HEPDATA [71].

p_T-bin [GeV]	NPC	σ [pb/GeV]	δ_{stat}%	γ_1	γ_7	γ_{13}	γ_{19}	γ_{25}	γ_{31}	γ_{32}	γ_{38}	γ_{44}	γ_{50}	γ_{56}	γ_{62}	γ_{68}	γ_{74}	γ_{75}	γ_{76}	γ_{82}	γ_{83}	u_1	u_2	u_3
20–30	1.61(30)	1.00×10^7	0.57	$^{+13}_{-12}$	± 11	$^{+16}_{-15}$	$^{+9.7}_{-9.1}$	$^{+5.7}_{-5.6}$	0.0	$^{+2.2}_{-2.3}$	$^{+5.6}_{-5.4}$	$^{+4.7}_{-5.1}$	0.0	0.0	$^{+2.1}_{-2.2}$	0.0	0.0	± 1.3	± 3.3	0.0	± 2.0	0.69	1.00	0.33
30–45	1.30(10)	1.23×10^6	1.21	$^{+8.4}_{-7.3}$	$^{+10}_{-8.9}$	$^{+10}_{-8.7}$	$^{+8.0}_{-6.9}$	$^{+2.4}_{-2.1}$	0.0	± 2.5	$^{+4.1}_{-3.8}$	$^{+4.4}_{-4.3}$	0.0	0.0	$^{+3.5}_{-3.6}$	0.0	0.0	± 0.8	± 3.0	0.0	± 1.0	0.47	1.00	0.22
45–60	1.18(6)	2.19×10^5	2.63	$^{+2.1}_{-1.2}$	$^{+8.4}_{-6.4}$	$^{+5.1}_{-3.5}$	$^{+4.6}_{-3.1}$	$^{+1.2}_{-0.5}$	0.0	$^{+3.5}_{-2.4}$	$^{+2.8}_{-1.8}$	$^{+4.9}_{-3.4}$	$^{+0.2}_{+0.2}$	$^{+0.4}_{+0.0}$	$^{+5.6}_{-4.1}$	0.0	0.0	± 1.0	± 1.4	± 0.1	± 1.0	0.30	1.00	0.19
60–80	1.12(4)	5.45×10^4	0.96	∓ 1.1	$^{+6.9}_{-5.9}$	$^{+1.1}_{-0.8}$	$^{+3.7}_{-3.1}$	$^{+0.8}_{-0.6}$	0.0	$^{+3.2}_{-2.7}$	$^{+1.7}_{-1.3}$	$^{+4.3}_{-3.6}$	$^{+0.4}_{-0.3}$	$^{+0.0}_{+0.1}$	$^{+4.6}_{-3.7}$	$^{-0.1}_{+0.2}$	0.0	± 0.4	± 1.3	0.0	± 1.0	0.28	1.00	0.15
80–110	1.08(3)	1.14×10^4	0.84	$^{-0.5}_{+0.4}$	$^{+6.4}_{-6.1}$	$^{+1.1}_{-1.6}$	$^{+3.9}_{-4.3}$	$^{+1.0}_{-1.5}$	0.0	$^{+3.0}_{-3.4}$	$^{+1.2}_{-1.8}$	$^{+4.9}_{-5.0}$	$^{+0.8}_{-1.0}$	0.0	$^{+2.5}_{-2.7}$	0.0	0.0	± 0.3	± 0.5	0.0	± 1.0	0.48	1.00	0.10
110–160	1.05(2)	1.93×10^3	0.61	0.0	$^{+3.9}_{-4.7}$	$^{+2.3}_{-3.0}$	$^{+3.0}_{-3.3}$	$^{+1.0}_{-1.2}$	0.0	$^{+3.0}_{-3.2}$	$^{+1.0}_{-1.2}$	$^{+4.9}_{-5.4}$	$^{+1.5}_{-1.7}$	0.0	0.0	$^{+1.1}_{-1.3}$	± 0.2	0.0	0.0	0.0	± 1.0	0.37	1.00	0.07
160–210	1.04(2)	3.21×10^2	0.67	0.0	$^{+5.9}_{-5.6}$	$^{+4.6}_{-4.0}$	$^{+2.2}_{-1.8}$	$^{+1.5}_{-1.1}$	0.0	$^{+2.7}_{-2.6}$	$^{+0.9}_{-0.6}$	$^{+6.1}_{-5.6}$	$^{+2.7}_{-2.2}$	$^{+0.4}_{+0.1}$	∓ 0.3	$^{+4.8}_{-4.4}$	± 0.1	0.0	± 0.8	0.0	± 1.0	0.45	1.00	0.06
210–260	1.03(1)	7.78×10^1	0.90	0.0	$^{+7.0}_{-6.8}$	± 3.6	$^{+1.0}_{-1.5}$	$^{+1.1}_{-1.6}$	0.0	$^{+2.2}_{-2.6}$	$^{+0.4}_{-0.6}$	$^{+5.6}_{-6.1}$	$^{+2.4}_{-3.1}$	± 0.2	0.0	$^{+5.7}_{-6.2}$	± 0.1	± 0.1	0.0	0.0	± 1.0	0.26	1.00	0.05
260–310	1.02(1)	2.54×10^1	0.83	0.0	$^{+5.2}_{-3.6}$	$^{+2.5}_{-2.2}$	$^{+1.4}_{-0.9}$	$^{+2.2}_{-1.8}$	0.0	$^{+2.5}_{-1.6}$	$^{+0.6}_{-0.2}$	$^{+6.2}_{-5.6}$	$^{+4.2}_{-3.3}$	$^{+0.6}_{-0.3}$	0.0	$^{+7.1}_{-6.3}$	± 0.2	± 0.3	± 0.7	0.0	± 1.0	0.24	1.00	0.05
310–400	1.02(1)	7.16×10^0	0.93	0.0	$^{+2.4}_{-2.5}$	$^{+2.8}_{-2.5}$	$^{+0.6}_{-0.5}$	$^{+2.5}_{-2.7}$	0.0	± 1.9	$^{+0.7}_{-0.2}$	± 6.3	$^{+4.3}_{-4.0}$	$^{+0.7}_{-0.2}$	0.0	± 6.9	± 0.2	± 0.2	± 0.4	0.0	± 1.0	0.27	1.00	0.05
400–500	1.02(1)	1.60×10^0	1.60	0.0	$^{+2.5}_{-3.3}$	$^{+1.8}_{-2.3}$	0.0	$^{+2.3}_{-2.4}$	0.0	$^{+1.1}_{-2.0}$	$^{+0.2}_{-0.8}$	$^{+6.5}_{-6.8}$	$^{+4.9}_{-5.6}$	0.0	0.0	$^{+7.7}_{-7.9}$	± 0.3	0.0	± 0.8	0.0	± 1.0	0.21	1.00	0.05
500–600	1.01(1)	4.10×10^{-1}	2.98	0.0	$^{+3.0}_{-2.7}$	$^{+2.3}_{-2.1}$	$^{+0.9}_{-0.8}$	$^{+3.1}_{-2.8}$	0.0	$^{+1.7}_{-1.4}$	± 0.5	$^{+7.0}_{-7.1}$	$^{+6.2}_{-5.6}$	± 0.7	0.0	$^{+9.4}_{-9.0}$	± 0.3	0.0	± 0.4	± 0.1	± 1.0	0.32	1.00	0.05
600–800	1.01(1)	7.61×10^{-2}	5.26	0.0	$^{+3.1}_{-3.4}$	± 4.8	± 0.9	$^{+3.3}_{-3.2}$	0.0	$^{+1.1}_{-1.6}$	$^{+0.3}_{-0.4}$	$^{+8.5}_{-7.1}$	$^{+6.5}_{-6.1}$	± 1.0	0.0	$^{+11}_{-9.3}$	± 0.2	0.0	± 0.6	0.0	± 1.0	0.14	1.00	0.21
800–1000	1.01(1)	1.18×10^{-2}	14.3	0.0	$^{+3.2}_{-2.7}$	$^{+6.3}_{-5.5}$	$^{+0.5}_{+0.2}$	$^{+2.5}_{-1.8}$	0.0	$^{+1.4}_{-0.8}$	$^{+0.5}_{+0.1}$	$^{+8.4}_{-8.0}$	$^{+7.8}_{-7.1}$	± 2.2	0.0	$^{+13}_{-11}$	± 0.5	0.0	± 0.7	0.0	± 1.0	0.17	1.00	0.21
1000–1200	1.01(1)	1.54×10^{-3}	34.0	0.0	$^{+2.4}_{-2.3}$	± 6.5	$^{+0.4}_{0.0}$	$^{+3.0}_{-2.9}$	0.0	$^{+1.1}_{-0.7}$	$^{+0.5}_{-0.3}$	$^{+8.6}_{-7.9}$	$^{+8.7}_{-8.5}$	$^{+4.9}_{-5.1}$	0.0	$^{+17}_{-14}$	± 0.7	0.0	± 1.3	0.0	± 1.0	0.10	1.00	0.21
1200–1500	1.01(1)	3.99×10^{-4}	58.9	0.0	$^{+1.7}_{-2.3}$	$^{+7.2}_{-7.4}$	$^{+0.8}_{-2.1}$	$^{+4.4}_{-5.1}$	0.0	$^{+0.3}_{-1.4}$	$^{+0.4}_{-0.8}$	$^{+9.3}_{-9.7}$	$^{+9.8}_{-10}$	$^{+8.9}_{-9.1}$	0.0	$^{+20}_{-18}$	± 0.6	0.0	± 2.2	± 0.1	± 1.0	0.13	1.00	0.21

TABLE XIII. Measured jet cross section for $R = 0.6$, $0.3 \leq |y| < 0.8$. See Table XII for description of the columns. All tables are available on HEPDATA [71].

p_T-bin [GeV]	NPC	σ [pb/GeV]	δ_{stat}%	γ_1	γ_7	γ_{13}	γ_{19}	γ_{25}	γ_{31}	γ_{32}	γ_{38}	γ_{44}	γ_{50}	γ_{56}	γ_{62}	γ_{68}	γ_{74}	γ_{75}	γ_{76}	γ_{82}	γ_{83}	u_1	u_2	u_3
20–30	1.60(30)	9.95×10^6	0.48	$^{+12}_{-11}$	$^{+9.4}_{-9.5}$	$^{+14}_{-13}$	$^{+8.0}_{-8.3}$	$^{+4.7}_{-4.6}$	0.0	$^{+2.2}_{-2.1}$	$^{+4.4}_{-4.3}$	$^{+4.7}_{-4.6}$	0.0	0.0	$^{+3.0}_{-2.9}$	0.0	0.0	± 0.9	± 2.7	0.0	± 2.0	0.71	1.00	0.30
30–45	1.30(14)	1.25×10^6	1.03	$^{+8.6}_{-7.6}$	$^{+9.9}_{-9.2}$	$^{+10}_{-9.3}$	$^{+7.9}_{-7.1}$	$^{+3.0}_{-2.5}$	0.0	$^{+2.6}_{-2.5}$	$^{+3.5}_{-3.2}$	$^{+4.9}_{-4.6}$	0.0	0.0	$^{+3.5}_{-3.2}$	$^{-0.2}_{+0.1}$	0.0	± 0.7	± 2.8	± 0.1	± 1.0	0.47	1.00	0.20
45–60	1.17(8)	2.25×10^5	2.04	$^{+2.2}_{-1.6}$	$^{+8.9}_{-7.2}$	$^{+7.4}_{-5.8}$	$^{+4.2}_{-3.4}$	$^{+1.9}_{-1.3}$	0.0	$^{+3.4}_{-2.7}$	$^{+2.1}_{-1.6}$	$^{+4.7}_{-3.9}$	$^{+0.2}_{+0.2}$	$^{+0.4}_{+0.0}$	$^{+2.9}_{-2.4}$	$^{+0.4}_{+0.1}$	0.0	± 0.5	± 1.6	± 0.1	± 1.0	0.31	1.00	0.19
60–80	1.12(5)	5.32×10^4	0.81	$^{-1.1}_{+1.0}$	$^{+6.4}_{-5.5}$	$^{+4.0}_{-3.5}$	$^{+2.7}_{-2.6}$	$^{+3.5}_{-3.4}$	0.0	$^{+3.0}_{-2.9}$	$^{+1.5}_{-1.3}$	$^{+4.7}_{-4.2}$	$^{+0.4}_{-0.2}$	0.0	$^{+0.9}_{-0.8}$	$^{+1.7}_{-1.5}$	0.0	± 0.3	± 1.2	0.0	± 1.0	0.30	1.00	0.16
80–110	1.08(3)	1.13×10^4	0.47	∓ 0.5	$^{+5.3}_{-5.9}$	$^{+2.6}_{-3.2}$	$^{+2.4}_{-3.0}$	$^{+2.1}_{-2.6}$	0.0	$^{+2.5}_{-3.2}$	$^{+1.0}_{-1.4}$	$^{+4.6}_{-5.2}$	$^{+0.9}_{-1.4}$	0.0	∓ 0.3	$^{+3.5}_{-4.1}$	0.0	± 0.3	± 0.4	0.0	± 1.0	0.44	1.00	0.11
110–160	1.05(2)	1.88×10^3	0.46	0.0	$^{+5.4}_{-5.2}$	$^{+2.5}_{-2.6}$	$^{+2.1}_{-2.3}$	$^{+0.4}_{-0.3}$	0.0	$^{+2.5}_{-2.3}$	± 0.7	$^{+5.2}_{-4.9}$	$^{+1.6}_{-1.4}$	0.0	∓ 0.1	$^{+5.0}_{-5.1}$	± 0.1	0.0	± 0.8	0.0	± 1.0	0.37	1.00	0.08
160–210	1.04(2)	3.03×10^2	0.49	0.0	$^{+4.0}_{-3.2}$	$^{+2.7}_{-2.5}$	$^{+2.4}_{-1.8}$	$^{+1.6}_{-1.1}$	0.0	$^{+2.6}_{-2.1}$	$^{+1.0}_{-0.5}$	$^{+6.1}_{-5.4}$	$^{+2.8}_{-2.1}$	$^{+0.4}_{+0.1}$	0.0	$^{+7.1}_{-5.9}$	± 0.2	0.0	± 0.5	0.0	± 1.0	0.42	1.00	0.07
210–260	1.03(1)	7.47×10^1	0.62	0.0	$^{+2.8}_{-3.5}$	$^{+2.7}_{-3.3}$	$^{+1.1}_{-1.6}$	$^{+1.9}_{-2.5}$	0.0	$^{+1.7}_{-1.8}$	$^{+0.2}_{-0.7}$	$^{+6.2}_{-6.4}$	$^{+2.9}_{-3.4}$	0.0	0.0	$^{+8.0}_{-7.7}$	± 0.2	0.0	± 0.8	0.0	± 1.0	0.33	1.00	0.07
260–310	1.02(1)	2.39×10^1	0.59	0.0	$^{+4.7}_{-3.6}$	$^{+2.9}_{-2.5}$	$^{+1.4}_{-1.5}$	$^{+2.9}_{-2.7}$	0.0	$^{+2.1}_{-1.7}$	$^{+0.8}_{-0.4}$	$^{+6.9}_{-6.7}$	$^{+3.7}_{-3.6}$	$^{+0.3}_{0.0}$	0.0	$^{+8.6}_{-8.3}$	± 0.1	± 0.1	± 0.7	0.0	± 1.0	0.27	1.00	0.07
310–400	1.02(1)	6.79×10^0	0.70	0.0	$^{+4.2}_{-3.5}$	$^{+3.1}_{-2.8}$	$^{+1.1}_{-0.5}$	$^{+3.4}_{-2.6}$	0.0	$^{+1.8}_{-1.2}$	± 0.3	$^{+7.6}_{-6.1}$	$^{+4.5}_{-3.8}$	$^{+0.4}_{+0.1}$	0.0	$^{+9.8}_{-8.5}$	± 0.2	± 0.2	± 0.4	0.0	± 1.0	0.28	1.00	0.07
400–500	1.02(1)	1.44×10^0	1.47	0.0	$^{+4.3}_{-4.9}$	$^{+3.1}_{-3.2}$	0.0	$^{+1.8}_{-2.4}$	0.0	$^{+0.9}_{-1.4}$	$^{+0.2}_{-0.3}$	$^{+6.7}_{-6.5}$	$^{+4.2}_{-4.6}$	0.0	0.0	$^{+10}_{-9.2}$	± 0.1	± 0.2	± 0.8	0.0	± 1.0	0.23	1.00	0.07
500–600	1.01(1)	3.68×10^{-1}	2.72	0.0	$^{+3.5}_{-3.0}$	$^{+1.7}_{-1.4}$	$^{+0.9}_{-0.8}$	$^{+2.2}_{-2.3}$	0.0	$^{+1.3}_{-1.0}$	$^{+0.4}_{-0.3}$	$^{+6.7}_{-6.9}$	$^{+5.2}_{-5.1}$	$^{+0.6}_{-0.4}$	0.0	$^{+11}_{-10}$	± 0.3	0.0	± 0.5	0.0	± 1.0	0.21	1.00	0.25
600–800	1.01(1)	7.50×10^{-2}	4.46	0.0	$^{+2.3}_{-2.5}$	$^{+0.8}_{-0.9}$	± 0.4	$^{+3.3}_{-2.9}$	0.0	$^{+0.7}_{-1.2}$	$^{+0.4}_{-0.5}$	$^{+7.4}_{-7.2}$	$^{+6.4}_{-5.8}$	$^{+0.9}_{-1.3}$	0.0	$^{+13}_{-12}$	± 0.3	0.0	± 0.4	0.0	± 1.0	0.18	1.00	0.25
800–1000	1.01(1)	9.09×10^{-3}	11.9	0.0	$^{+5.3}_{-4.7}$	$^{+1.8}_{-1.1}$	$^{+0.9}_{-0.4}$	$^{+3.5}_{-3.0}$	0.0	$^{+0.9}_{-0.3}$	$^{+0.4}_{+0.1}$	$^{+9.2}_{-7.8}$	$^{+7.2}_{-6.7}$	$^{+3.0}_{-3.1}$	0.0	$^{+16}_{-14}$	± 0.4	0.0	± 0.9	0.0	± 1.0	0.14	1.00	0.25
1000–1200	1.01(1)	1.61×10^{-3}	28.8	0.0	$^{+6.1}_{-5.1}$	$^{+1.8}_{-1.9}$	$^{+0.8}_{-0.4}$	$^{+3.9}_{-3.3}$	0.0	$^{+0.7}_{-0.8}$	$^{+0.8}_{-0.4}$	$^{+11}_{-9.1}$	$^{+8.6}_{-7.9}$	$^{+6.6}_{-6.2}$	0.0	$^{+19}_{-17}$	± 0.6	0.0	± 1.4	0.0	± 1.0	0.12	1.00	0.25
1200–1500	1.01(1)	2.35×10^{-4}	58.7	0.0	$^{+6.0}_{-7.5}$	$^{+1.6}_{-2.7}$	0.0	$^{+3.1}_{-4.3}$	0.0	$^{+0.4}_{-1.6}$	0.0	$^{+9.9}_{-11}$	$^{+8.8}_{-9.9}$	$^{+11}_{-12}$	0.0	$^{+23}_{-21}$	± 0.3	0.0	± 1.8	0.0	± 1.0	0.13	1.00	0.25

TABLE XIV. Measured jet cross section for $R = 0.6$, $0.8 \leq |y| < 1.2$. See Table XII for description of the columns. All tables are available on HEPDATA [71].

p_T-bin [GeV]	NPC	σ [pb/GeV]	δ_{stat}%	γ_2	γ_8	γ_{14}	γ_{20}	γ_{26}	γ_{31}	γ_{33}	γ_{39}	γ_{45}	γ_{51}	γ_{57}	γ_{63}	γ_{69}	γ_{74}	γ_{75}	γ_{77}	γ_{82}	γ_{83}	u_1	u_2	u_3
20–30	1.58(29)	8.54×10^6	0.55	$^{+10}_{-11}$	$^{+7.9}_{-8.6}$	± 12	$^{+8.0}_{-8.4}$	$^{+3.9}_{-4.1}$	± 4.2	± 1.8	$^{+3.7}_{-3.8}$	$^{+3.9}_{-4.0}$	0.0	0.0	$^{+2.5}_{-2.6}$	0.0	0.0	± 1.6	± 8.1	± 1.4	± 2.0	0.97	1.00	0.25
30–45	1.28(13)	1.12×10^6	1.15	$^{+8.3}_{-7.6}$	$^{+9.6}_{-9.4}$	$^{+10}_{-9.5}$	$^{+5.3}_{-4.8}$	$^{+3.0}_{-2.6}$	$^{+5.3}_{-4.9}$	$^{+2.6}_{-2.5}$	$^{+3.5}_{-3.2}$	$^{+4.9}_{-4.6}$	0.0	0.0	$^{+3.5}_{-3.3}$	∓ 0.1	0.0	± 0.4	± 8.3	0.0	± 1.0	0.84	1.00	0.20
45–60	1.17(7)	1.99×10^5	2.37	$^{+2.2}_{-1.8}$	$^{+9.2}_{-8.1}$	$^{+7.7}_{-6.5}$	$^{+3.6}_{-2.7}$	$^{+1.8}_{-1.5}$	$^{+4.9}_{-4.5}$	$^{+3.3}_{-3.0}$	$^{+2.0}_{-1.7}$	$^{+4.9}_{-4.5}$	$^{+0.2}_{+0.2}$	$^{+0.4}_{+0.0}$	$^{+2.8}_{-2.6}$	$^{+0.3}_{-0.1}$	± 0.1	± 0.3	± 3.8	± 0.4	± 1.0	0.54	1.00	0.21
60–80	1.11(4)	4.84×10^4	0.91	∓ 1.1	$^{+6.8}_{-6.1}$	$^{+4.2}_{-3.7}$	$^{+2.0}_{-1.9}$	$^{+3.7}_{-3.5}$	$^{+4.0}_{-3.6}$	$^{+3.2}_{-3.1}$	± 1.5	$^{+5.0}_{-4.5}$	$^{+0.4}_{-0.3}$	0.0	± 0.9	± 1.8	0.0	± 0.2	± 1.5	± 0.2	± 1.0	0.51	1.00	0.18
80–110	1.07(3)	1.03×10^4	0.61	∓ 0.5	$^{+5.5}_{-5.6}$	$^{+2.6}_{-3.0}$	$^{+0.8}_{-1.3}$	$^{+2.1}_{-2.6}$	$^{+3.0}_{-3.4}$	$^{+2.6}_{-3.1}$	$^{+1.0}_{-1.4}$	$^{+4.8}_{-5.0}$	$^{+1.0}_{-1.4}$	0.0	∓ 0.3	$^{+3.7}_{-4.0}$	0.0	± 0.3	± 1.3	± 0.2	± 1.0	0.71	1.00	0.12
110–160	1.05(2)	1.66×10^3	0.55	0.0	$^{+5.6}_{-5.3}$	$^{+2.6}_{-3.0}$	$^{+1.5}_{-2.0}$	$^{+0.4}_{-0.5}$	$^{+2.9}_{-3.0}$	$^{+2.5}_{-2.6}$	± 0.8	$^{+5.5}_{-5.1}$	$^{+1.6}_{-1.8}$	0.0	∓ 0.1	$^{+5.3}_{-5.4}$	± 0.1	0.0	± 1.9	± 0.2	± 1.0	0.61	1.00	0.08
160–210	1.04(2)	2.60×10^2	0.64	0.0	$^{+3.7}_{-3.3}$	$^{+2.6}_{-2.4}$	$^{+2.4}_{-1.7}$	$^{+1.6}_{-1.1}$	± 3.2	$^{+2.5}_{-2.0}$	$^{+1.0}_{-0.6}$	$^{+6.0}_{-5.7}$	$^{+2.7}_{-2.1}$	$^{+0.4}_{+0.1}$	0.0	$^{+7.0}_{-6.2}$	± 0.2	0.0	± 1.6	± 0.1	± 1.0	0.68	1.00	0.06
210–260	1.03(1)	6.17×10^1	0.96	0.0	$^{+2.8}_{-3.5}$	$^{+2.9}_{-3.3}$	$^{+1.6}_{-2.1}$	$^{+2.1}_{-2.5}$	$^{+3.3}_{-3.4}$	± 1.9	$^{+0.2}_{-0.7}$	$^{+6.1}_{-6.6}$	$^{+3.0}_{-3.3}$	0.0	0.0	$^{+7.8}_{-7.9}$	± 0.2	0.0	± 1.5	± 0.1	± 1.0	0.52	1.00	0.06
260–310	1.02(1)	1.95×10^1	0.81	0.0	$^{+4.7}_{-3.8}$	$^{+2.6}_{-2.5}$	$^{+1.7}_{-1.6}$	$^{+2.7}_{-2.8}$	$^{+4.1}_{-3.5}$	± 1.8	$^{+0.7}_{-0.3}$	$^{+7.1}_{-6.5}$	± 3.8	$^{+0.3}_{0.0}$	0.0	$^{+9.1}_{-8.1}$	± 0.2	± 0.1	± 1.7	0.0	± 1.0	0.48	1.00	0.06
310–400	1.02(1)	5.24×10^0	1.12	0.0	$^{+4.3}_{-3.7}$	$^{+3.2}_{-3.0}$	± 1.0	$^{+3.4}_{-2.7}$	$^{+3.8}_{-3.6}$	$^{+1.8}_{-1.3}$	± 0.3	$^{+7.3}_{-6.3}$	$^{+4.6}_{-4.1}$	$^{+0.4}_{+0.1}$	0.0	$^{+9.7}_{-8.5}$	± 0.1	± 0.1	± 1.4	± 0.1	± 1.0	0.47	1.00	0.06
400–500	1.02(1)	1.10×10^0	1.96	0.0	$^{+4.5}_{-4.9}$	± 3.1	$^{+0.5}_{-1.0}$	$^{+1.7}_{-2.2}$	$^{+3.7}_{-3.6}$	$^{+0.9}_{-1.4}$	$^{+0.2}_{-0.3}$	$^{+6.5}_{-6.8}$	$^{+4.2}_{-4.7}$	0.0	0.0	$^{+9.5}_{-9.7}$	± 0.2	± 0.3	± 0.7	± 0.1	± 1.0	0.35	1.00	0.06
500–600	1.01(1)	2.52×10^{-1}	3.33	0.0	$^{+3.6}_{-3.0}$	± 1.5	$^{+1.0}_{-0.8}$	$^{+2.4}_{-2.5}$	$^{+4.0}_{-4.2}$	$^{+1.2}_{-1.0}$	± 0.4	± 7.2	± 5.5	$^{+0.6}_{-0.4}$	0.0	± 11	± 0.3	± 0.3	± 0.2	± 0.2	± 1.0	0.37	1.00	0.28
600–800	1.01(1)	4.72×10^{-2}	6.53	0.0	$^{+2.3}_{-2.8}$	$^{+0.8}_{-0.9}$	0.0	± 3.2	$^{+4.5}_{-4.3}$	$^{+0.6}_{-1.2}$	$^{+0.3}_{-0.4}$	$^{+8.3}_{-7.7}$	$^{+7.1}_{-6.1}$	$^{+0.9}_{-1.3}$	0.0	$^{+14}_{-13}$	± 0.3	0.0	± 2.3	0.0	± 1.0	0.26	1.00	0.51
800–1000	1.01(1)	2.97×10^{-3}	22.0	0.0	$^{+6.3}_{-5.5}$	$^{+2.0}_{-1.3}$	$^{+0.4}_{+0.2}$	$^{+4.3}_{-3.5}$	$^{+5.7}_{-5.4}$	$^{+0.9}_{-0.3}$	$^{+0.5}_{+0.1}$	$^{+10}_{-8.8}$	$^{+8.3}_{-7.6}$	$^{+4.0}_{-3.7}$	0.0	$^{+18}_{-15}$	± 0.5	0.0	± 2.1	0.0	± 1.0	0.25	1.00	0.87
1000–1200	1.01(1)	4.54×10^{-4}	62.5	0.0	$^{+7.3}_{-6.8}$	$^{+1.7}_{-2.7}$	$^{+0.6}_{-0.5}$	$^{+4.5}_{-4.4}$	$^{+7.1}_{-6.7}$	$^{+0.6}_{-1.3}$	$^{+0.7}_{-0.6}$	± 12	± 10	$^{+8.2}_{-8.6}$	0.0	$^{+23}_{-21}$	± 0.6	0.0	± 3.0	0.0	± 1.0	0.28	1.00	1.24
1200–1500	1.01(2)	1.01×10^{-4}	114	$^{-0.2}_{+0.1}$	$^{+8.3}_{-11}$	$^{+2.4}_{-3.3}$	$^{+2.0}_{-2.2}$	$^{+4.2}_{-5.8}$	$^{+8.4}_{-9.7}$	$^{+1.3}_{-1.1}$	0.0	$^{+14}_{-16}$	$^{+13}_{-15}$	$^{+16}_{-18}$	0.0	$^{+33}_{-28}$	± 1.3	0.0	± 7.8	0.0	± 1.0	0.17	1.00	1.69

TABLE XV. Measured jet cross section for $R = 0.6$, $1.2 \leq |y| < 2.1$. See Table XII for description of the columns. All tables are available on HEPDATA [71].

p_T-bin [GeV]	NPC	σ [pb/GeV]	δ_{stat}%	γ_3	γ_9	γ_{15}	γ_{21}	γ_{27}	γ_{31}	γ_{34}	γ_{40}	γ_{46}	γ_{52}	γ_{58}	γ_{64}	γ_{70}	γ_{74}	γ_{75}	γ_{78}	γ_{82}	γ_{83}	u_1	u_2	u_3
20–30	1.53(25)	7.65×10^6	0.40	± 11	$^{+9.0}_{-9.2}$	± 13	$^{+11}_{-10}$	± 4.5	± 14	± 2.0	$^{+4.1}_{-4.2}$	$^{+4.5}_{-4.4}$	0.0	0.0	$^{+2.7}_{-2.8}$	0.0	0.0	± 1.3	± 11	± 0.6	± 2.0	1.18	1.00	0.30
30–45	1.26(9)	9.38×10^5	0.72	$^{+8.6}_{-8.0}$	$^{+10}_{-9.6}$	$^{+11}_{-9.8}$	$^{+5.8}_{-5.3}$	$^{+3.1}_{-2.8}$	$^{+15}_{-13}$	$^{+2.6}_{-2.7}$	$^{+3.5}_{-3.4}$	$^{+4.9}_{-4.7}$	0.0	0.0	$^{+3.5}_{-3.4}$	$^{-0.2}_{+0.1}$	0.0	± 0.6	± 7.0	0.0	± 1.0	0.86	1.00	0.15
45–60	1.15(6)	1.59×10^5	1.73	$^{+2.3}_{-1.6}$	$^{+9.2}_{-7.8}$	$^{+7.7}_{-6.3}$	$^{+3.8}_{-3.1}$	$^{+1.9}_{-1.3}$	$^{+10}_{-8.4}$	$^{+3.4}_{-2.8}$	$^{+2.1}_{-1.6}$	$^{+5.0}_{-4.1}$	$^{+0.1}_{+0.2}$	$^{+0.3}_{+0.0}$	$^{+3.0}_{-2.4}$	$^{+0.3}_{+0.1}$	0.0	± 0.7	± 2.1	0.0	± 1.0	0.54	1.00	0.13
60–80	1.10(4)	3.78×10^4	0.66	∓ 1.0	$^{+6.9}_{-6.0}$	$^{+4.3}_{-3.8}$	$^{+1.9}_{-1.6}$	$^{+3.7}_{-3.4}$	$^{+7.1}_{-6.1}$	$^{+3.2}_{-2.9}$	$^{+1.6}_{-1.4}$	$^{+5.1}_{-4.7}$	$^{+0.4}_{-0.3}$	0.0	± 0.9	$^{+1.9}_{-1.7}$	± 0.1	± 0.2	± 1.6	0.0	± 1.0	0.50	1.00	0.10
80–110	1.07(3)	7.76×10^3	0.93	$^{-0.5}_{+0.4}$	$^{+5.6}_{-6.0}$	$^{+2.7}_{-3.4}$	$^{+0.7}_{-1.2}$	$^{+2.2}_{-2.8}$	± 5.2	$^{+2.6}_{-3.3}$	$^{+1.0}_{-1.6}$	$^{+4.8}_{-5.3}$	$^{+1.0}_{-1.6}$	0.0	∓ 0.3	$^{+3.7}_{-4.2}$	± 0.1	± 0.3	± 1.0	0.0	± 1.0	0.40	1.00	0.07
110–160	1.04(2)	1.25×10^3	0.81	0.0	$^{+5.7}_{-5.5}$	$^{+2.7}_{-3.0}$	± 1.1	$^{+0.4}_{-0.5}$	$^{+4.6}_{-4.9}$	± 2.6	± 0.8	$^{+5.5}_{-5.3}$	± 1.7	0.0	∓ 0.1	$^{+5.2}_{-5.5}$	± 0.2	0.0	± 1.0	0.0	± 1.0	0.53	1.00	0.05
160–210	1.03(2)	1.86×10^2	0.74	0.0	$^{+4.1}_{-3.3}$	$^{+2.8}_{-2.5}$	$^{+1.1}_{-1.0}$	$^{+1.7}_{-1.2}$	$^{+5.7}_{-4.9}$	$^{+2.8}_{-2.2}$	$^{+1.1}_{-0.5}$	$^{+6.4}_{-6.0}$	$^{+3.0}_{-2.2}$	$^{+0.4}_{+0.1}$	0.0	$^{+7.4}_{-6.5}$	± 0.3	0.0	± 1.0	± 0.1	± 1.0	0.49	1.00	0.05
210–260	1.03(2)	4.12×10^1	0.71	0.0	$^{+2.9}_{-3.6}$	$^{+3.0}_{-3.4}$	$^{+0.1}_{-0.7}$	$^{+2.1}_{-2.6}$	$^{+5.4}_{-5.8}$	± 1.9	$^{+0.2}_{-0.7}$	$^{+6.5}_{-6.6}$	$^{+3.2}_{-3.5}$	0.0	0.0	$^{+8.2}_{-7.9}$	± 0.3	± 0.2	± 1.1	± 0.1	± 1.0	0.57	1.00	0.05
260–310	1.02(1)	1.14×10^1	1.28	0.0	$^{+5.0}_{-4.0}$	$^{+2.8}_{-2.6}$	$^{+0.2}_{0.0}$	± 2.9	$^{+6.2}_{-5.7}$	$^{+2.1}_{-1.9}$	$^{+0.6}_{-0.3}$	$^{+7.5}_{-7.3}$	$^{+3.8}_{-4.0}$	$^{+0.2}_{0.0}$	0.0	$^{+9.5}_{-9.0}$	± 0.3	± 0.1	± 0.8	0.0	± 1.0	0.42	1.00	0.06
310–400	1.02(1)	2.85×10^0	0.91	0.0	$^{+4.7}_{-4.0}$	$^{+3.6}_{-3.1}$	$^{+1.2}_{-0.4}$	$^{+3.9}_{-2.8}$	$^{+6.9}_{-5.7}$	$^{+2.1}_{-1.3}$	$^{+0.4}_{-0.3}$	$^{+8.0}_{-6.8}$	$^{+5.0}_{-4.4}$	$^{+0.5}_{+0.1}$	0.0	$^{+11}_{-9.6}$	± 0.2	0.0	± 1.7	0.0	± 1.0	0.40	1.00	0.06
400–500	1.02(1)	4.60×10^{-1}	1.87	0.0	$^{+5.3}_{-5.7}$	$^{+3.7}_{-3.8}$	$^{+1.7}_{-2.5}$	$^{+2.2}_{-3.0}$	$^{+7.2}_{-7.1}$	$^{+1.1}_{-1.8}$	$^{+0.4}_{-0.3}$	$^{+8.1}_{-7.7}$	$^{+5.5}_{-5.6}$	0.0	0.0	$^{+12}_{-11}$	± 0.3	0.0	± 1.3	0.0	± 1.0	0.47	1.00	0.07
500–600	1.01(1)	8.54×10^{-2}	4.18	0.0	$^{+4.2}_{-3.6}$	$^{+1.9}_{-1.8}$	$^{+2.4}_{-1.6}$	$^{+2.9}_{-3.1}$	$^{+8.7}_{-8.1}$	$^{+1.5}_{-1.4}$	$^{+0.5}_{-0.4}$	$^{+8.8}_{-8.9}$	$^{+6.7}_{-6.4}$	$^{+0.9}_{-0.8}$	0.0	$^{+14}_{-13}$	± 0.6	0.0	± 1.9	± 0.2	± 1.0	0.44	1.00	0.58
600–800	1.01(1)	1.15×10^{-2}	8.21	0.0	$^{+3.7}_{-3.8}$	$^{+1.3}_{-1.2}$	$^{+0.3}_{-1.0}$	$^{+4.9}_{-4.2}$	$^{+11}_{-9.8}$	$^{+0.8}_{-1.5}$	$^{+0.4}_{-0.7}$	$^{+12}_{-11}$	$^{+10}_{-8.9}$	$^{+1.6}_{-2.0}$	0.0	$^{+20}_{-17}$	± 0.6	0.0	± 2.7	± 0.2	± 1.0	0.35	1.00	0.62
800–1000	1.01(1)	6.85×10^{-4}	35.1	0.0	$^{+8.9}_{-7.4}$	$^{+2.9}_{-1.9}$	$^{+0.5}_{+0.3}$	$^{+5.8}_{-4.6}$	$^{+13}_{-11}$	$^{+1.5}_{-0.5}$	$^{+0.8}_{+0.1}$	$^{+15}_{-12}$	$^{+12}_{-10}$	$^{+5.8}_{-5.3}$	0.0	$^{+27}_{-21}$	± 1.1	0.0	± 3.7	± 0.3	± 1.0	0.41	1.00	0.68
1000–1200	1.01(1)	6.75×10^{-5}	104	∓ 0.1	$^{+10.0}_{-9.5}$	$^{+2.2}_{-3.1}$	± 2.4	$^{+6.1}_{-6.3}$	± 15	$^{+0.6}_{-1.5}$	$^{+0.6}_{-0.3}$	$^{+17}_{-15}$	± 14	± 13	0.0	$^{+39}_{-26}$	± 1.9	0.0	± 7.5	± 0.5	± 1.0	0.21	1.00	0.77

TABLE XVI. Measured jet cross section for $R = 0.6$, $2.1 \leq |y| < 2.8$. See Table XII for description of the columns. All tables are available on HEPDATA [71].

p_T-bin [GeV]	NPC	σ [pb/GeV]	δ_{stat} %	γ_4	γ_{10}	γ_{16}	γ_{22}	γ_{28}	γ_{31}	γ_{35}	γ_{41}	γ_{47}	γ_{53}	γ_{59}	γ_{65}	γ_{71}	γ_{74}	γ_{75}	γ_{79}	γ_{82}	γ_{84}	u_1	u_2	u_3
20–30	1.44(19)	5.82×10^6	0.54	$^{+13}_{-11}$	$^{+9.9}_{-9.3}$	$^{+15}_{-13}$	$^{+5.7}_{-5.4}$	$^{+4.9}_{-4.8}$	$^{+22}_{-20}$	$^{+2.2}_{-2.1}$	$^{+4.5}_{-4.4}$	$^{+4.8}_{-4.6}$	0.0	0.0	$^{+3.0}_{-2.9}$	0.0	0.0	±0.4	±17	±0.5	±2.0	1.42	1.00	0.02
30–45	1.21(8)	6.89×10^5	1.02	$^{+8.9}_{-8.0}$	$^{+10}_{-9.8}$	$^{+11}_{-9.9}$	$^{+5.6}_{-5.4}$	$^{+3.1}_{-2.8}$	$^{+23}_{-18}$	$^{+2.6}_{-2.7}$	±3.5	$^{+5.0}_{-4.8}$	0.0	0.0	±3.5	$^{-0.2}_{+0.1}$	0.0	±0.5	±7.7	±0.2	±1.0	0.99	1.00	0.02
45–60	1.12(6)	1.19×10^5	2.32	$^{+2.7}_{-2.0}$	$^{+9.4}_{-8.0}$	$^{+7.9}_{-6.5}$	$^{+4.1}_{-3.5}$	$^{+2.1}_{-1.5}$	$^{+14}_{-11}$	$^{+3.6}_{-3.0}$	$^{+2.2}_{-1.7}$	$^{+5.0}_{-4.4}$	$^{+0.2}_{+0.2}$	$^{+0.4}_{+0.0}$	$^{+3.2}_{-2.5}$	$^{+0.3}_{-0.1}$	±0.2	±0.3	±2.4	±0.2	±1.0	0.59	1.00	0.02
60–80	1.08(4)	2.42×10^4	0.87	$^{-0.9}_{+0.8}$	$^{+7.0}_{-5.8}$	$^{+4.5}_{-3.7}$	$^{+2.4}_{-1.8}$	$^{+4.1}_{-3.3}$	$^{+8.5}_{-6.9}$	$^{+3.5}_{-2.7}$	$^{+2.1}_{-1.5}$	$^{+5.2}_{-4.5}$	$^{+0.6}_{-0.3}$	0.0	$^{+1.2}_{-0.8}$	$^{+2.1}_{-1.5}$	±0.2	±0.3	±1.5	0.0	±1.0	0.55	1.00	0.02
80–110	1.05(3)	4.72×10^3	0.58	$^{-0.4}_{+0.3}$	$^{+6.3}_{-5.9}$	$^{+3.5}_{-3.3}$	$^{+0.7}_{-0.6}$	±2.5	$^{+5.9}_{-5.6}$	$^{+3.2}_{-3.1}$	$^{+1.2}_{-1.4}$	$^{+5.5}_{-5.2}$	$^{+1.1}_{-1.3}$	0.0	$^{-0.3}_{+0.2}$	$^{+4.3}_{-4.1}$	±0.1	±0.2	±2.3	0.0	±1.0	0.80	1.00	0.02
110–160	1.03(3)	6.40×10^2	0.58	0.0	$^{+6.2}_{-6.0}$	$^{+2.9}_{-3.3}$	$^{+0.3}_{-0.5}$	$^{+0.4}_{-0.7}$	$^{+5.3}_{-5.2}$	$^{+2.8}_{-2.9}$	$^{+0.7}_{-1.0}$	$^{+6.0}_{-5.8}$	±1.9	0.0	0.0	$^{+5.7}_{-6.0}$	±0.2	0.0	±1.3	0.0	±1.0	0.69	1.00	0.00
160–210	1.02(2)	7.31×10^1	0.71	0.0	$^{+4.5}_{-4.1}$	$^{+2.9}_{-3.3}$	$^{+0.9}_{-0.6}$	±1.8	$^{+6.8}_{-6.5}$	±2.7	$^{+1.1}_{-0.7}$	$^{+7.4}_{-7.2}$	$^{+3.1}_{-3.0}$	$^{+0.4}_{+0.1}$	0.0	$^{+8.7}_{-7.9}$	±0.4	0.0	±2.2	0.0	±1.0	0.79	1.00	0.00
210–260	1.02(2)	1.21×10^1	1.25	0.0	$^{+3.9}_{-4.8}$	$^{+3.6}_{-4.4}$	$^{+1.3}_{-1.4}$	$^{+2.8}_{-3.6}$	$^{+7.7}_{-7.5}$	±2.4	0.0	±8.5	$^{+3.9}_{-4.6}$	0.0	0.0	±11	±0.5	±0.1	±1.6	0.0	±1.0	0.74	1.00	0.00
260–310	1.02(2)	2.26×10^0	1.80	0.0	$^{+7.5}_{-5.4}$	$^{+4.9}_{-3.3}$	$^{+2.1}_{-1.5}$	$^{+5.0}_{-3.6}$	$^{+9.7}_{-8.0}$	$^{+3.6}_{-2.3}$	$^{+1.4}_{-0.6}$	$^{+10}_{-9.6}$	$^{+6.0}_{-5.4}$	$^{+0.8}_{0.0}$	0.0	$^{+14}_{-12}$	±0.5	0.0	±1.7	0.0	±1.0	0.71	1.00	0.22
310–400	1.01(2)	3.24×10^{-1}	2.89	0.0	$^{+6.9}_{-6.6}$	$^{+5.1}_{-4.8}$	$^{+2.0}_{-1.5}$	$^{+5.3}_{-4.3}$	$^{+11}_{-9.7}$	$^{+2.8}_{-2.2}$	$^{+0.7}_{-0.5}$	$^{+13}_{-10}$	$^{+7.6}_{-7.1}$	$^{+0.8}_{+0.1}$	0.0	$^{+17}_{-14}$	±0.3	±0.2	±1.8	0.0	±1.0	0.84	1.00	0.13
400–500	1.01(2)	2.09×10^{-2}	11.7	0.0	$^{+11}_{-9.7}$	$^{+5.8}_{-6.3}$	$^{+2.7}_{-3.4}$	$^{+3.9}_{-5.6}$	$^{+15}_{-14}$	$^{+1.8}_{-2.7}$	$^{+0.7}_{-0.3}$	$^{+16}_{-14}$	$^{+12}_{-11}$	0.0	0.0	$^{+23}_{-20}$	±1.1	±0.3	±3.0	±0.5	±1.0	0.58	1.00	0.14
500–600	1.01(2)	5.83×10^{-4}	63.9	0.0	$^{+2.4}_{-1.1}$	$^{+1.1}_{+0.3}$	$^{+5.0}_{-4.0}$	$^{+0.8}_{-1.1}$	$^{+13}_{-5.1}$	$^{+1.1}_{+0.2}$	0.0	$^{+13}_{-7.8}$	$^{+9.2}_{-3.8}$	0.0	0.0	$^{+27}_{-16}$	±0.9	0.0	±12	±0.8	±1.0	0.08	1.00	0.16

TABLE XVII. Measured jet cross section for $R = 0.6$, $2.8 \leq |y| < 3.6$. See Table XII for description of the columns. All tables are available on HEPDATA [71].

p_T-bin [GeV]	NPC	σ [pb/GeV]	δ_{stat} %	γ_5	γ_{11}	γ_{17}	γ_{23}	γ_{29}	γ_{31}	γ_{36}	γ_{42}	γ_{48}	γ_{54}	γ_{60}	γ_{66}	γ_{72}	γ_{74}	γ_{75}	γ_{80}	γ_{82}	γ_{85}	u_1	u_2	u_3
20–30	1.32(15)	3.90×10^6	0.61	$^{+14}_{-12}$	$^{+11}_{-9.8}$	$^{+16}_{-14}$	$^{+8.6}_{-7.8}$	$^{+5.2}_{-4.9}$	$^{+35}_{-28}$	$^{+2.3}_{-2.2}$	$^{+4.9}_{-4.5}$	$^{+5.2}_{-4.8}$	0.0	0.0	$^{+3.3}_{-3.0}$	0.0	0.0	±0.4	±16	±0.1	±2.0	4.37	1.00	0.00
30–45	1.15(9)	4.26×10^5	1.42	$^{+9.0}_{-7.8}$	$^{+11}_{-10.0}$	$^{+11}_{-9.9}$	$^{+9.4}_{-8.0}$	$^{+3.1}_{-2.8}$	$^{+37}_{-26}$	±2.8	$^{+3.5}_{-3.6}$	$^{+5.3}_{-5.2}$	0.0	0.0	$^{+3.6}_{-3.7}$	$\mp$0.1	0.0	±0.8	±9.7	±0.1	±1.0	2.99	1.00	0.00
45–60	1.09(6)	6.42×10^4	3.20	$^{+2.1}_{-2.4}$	$^{+8.8}_{-9.4}$	$^{+7.2}_{-7.9}$	$^{+7.1}_{-7.8}$	$^{+2.1}_{-2.3}$	$^{+24}_{-19}$	$^{+3.5}_{-3.8}$	$^{+2.2}_{-2.3}$	$^{+4.8}_{-5.5}$	$^{+0.1}_{+0.2}$	$^{+0.3}_{+0.0}$	$^{+3.0}_{-3.3}$	$^{+0.5}_{-0.3}$	±0.2	±0.4	±1.3	0.0	±1.0	1.83	1.00	0.00
60–80	1.05(5)	1.24×10^4	1.36	$^{-1.2}_{+1.1}$	$^{+7.5}_{-6.6}$	$^{+4.4}_{-4.0}$	$^{+5.9}_{-5.3}$	$^{+4.1}_{-3.7}$	$^{+17}_{-13}$	$^{+3.7}_{-3.2}$	$^{+2.0}_{-1.4}$	$^{+5.6}_{-4.9}$	$^{+0.6}_{-0.4}$	0.0	$^{+1.0}_{-0.8}$	$^{+2.5}_{-2.0}$	±0.3	±0.5	±2.3	0.0	±1.0	3.47	1.00	0.00
80–110	1.03(4)	1.78×10^3	2.35	$\mp$0.5	$^{+6.8}_{-6.7}$	$^{+3.9}_{-3.7}$	±6.1	$^{+2.6}_{-3.0}$	±11	$^{+3.6}_{-3.8}$	$^{+1.3}_{-1.8}$	$^{+6.1}_{-6.2}$	$^{+1.5}_{-2.0}$	0.0	$\mp$0.4	$^{+5.2}_{-5.1}$	±0.3	±0.2	±3.4	0.0	±1.0	4.12	1.00	0.00
110–160	1.02(3)	1.51×10^2	1.36	0.0	$^{+8.0}_{-8.1}$	$^{+3.9}_{-4.3}$	$^{+9.7}_{-9.6}$	$^{+0.7}_{-0.9}$	$^{+13}_{-12}$	$^{+3.5}_{-3.7}$	$^{+1.0}_{-1.3}$	$^{+8.1}_{-8.2}$	$^{+2.4}_{-2.7}$	0.0	$\mp$0.2	$^{+8.1}_{-8.6}$	±0.2	0.0	±2.4	±0.1	±1.0	2.62	1.00	0.00
160–210	1.01(3)	7.23×10^0	3.16	0.0	$^{+7.6}_{-5.2}$	$^{+5.3}_{-4.2}$	$^{+9.4}_{-7.4}$	$^{+3.5}_{-2.4}$	$^{+21}_{-17}$	$^{+5.1}_{-3.5}$	$^{+2.0}_{-0.4}$	$^{+13}_{-10}$	$^{+5.9}_{-4.3}$	$^{+0.7}_{+0.1}$	0.0	$^{+16}_{-12}$	±0.6	0.0	±4.7	±0.1	±1.0	2.56	1.00	0.17
210–260	1.01(3)	3.75×10^{-1}	6.88	0.0	$^{+8.3}_{-7.7}$	$^{+7.5}_{-6.6}$	$^{+8.0}_{-6.0}$	$^{+5.2}_{-5.7}$	$^{+26}_{-20}$	$^{+3.5}_{-4.0}$	$^{+0.6}_{-1.2}$	$^{+17}_{-14}$	$^{+8.8}_{-7.3}$	0.0	0.0	$^{+21}_{-18}$	±1.0	0.0	±6.1	±0.4	±1.0	3.36	1.00	0.19
260–310	1.01(3)	1.09×10^{-2}	35.8	0.0	$^{+14}_{-8.1}$	$^{+8.4}_{-6.1}$	$^{+11}_{-5.5}$	$^{+9.4}_{-6.7}$	$^{+41}_{-31}$	$^{+3.8}_{-3.9}$	$^{+2.2}_{+0.4}$	$^{+25}_{-20}$	$^{+12}_{-8.8}$	$^{+2.6}_{+0.2}$	0.0	$^{+35}_{-22}$	$\mp$0.3	±0.7	±19	±1.3	±1.0	3.53	1.00	0.21

TABLE XVIII. Measured jet cross section for $R = 0.6$, $3.6 \leq |y| < 4.4$. See Table XII for description of the columns. All tables are available on HEPDATA [71].

p_T-bin [GeV]	NPC	σ [pb/GeV]	δ_{stat}%	γ_6	γ_{12}	γ_{18}	γ_{24}	γ_{30}	γ_{31}	γ_{37}	γ_{43}	γ_{49}	γ_{55}	γ_{61}	γ_{67}	γ_{73}	γ_{74}	γ_{75}	γ_{81}	γ_{82}	γ_{86}	u_1	u_2	u_3
20–30	1.19(14)	1.51×10^6	0.81	$^{+14}_{-13}$	± 11	$^{+17}_{-15}$	$^{+3.1}_{-3.2}$	$^{+5.3}_{-5.5}$	$^{+60}_{-42}$	$^{+2.4}_{-2.5}$	$^{+5.0}_{-5.1}$	$^{+5.3}_{-5.4}$	0.0	0.0	$^{+3.2}_{-3.4}$	0.0	0.0	± 0.3	± 13	± 1.2	± 2.0	5.01	1.00	0.00
30–45	1.07(10)	1.38×10^5	0.86	$^{+10}_{-8.9}$	$^{+13}_{-11}$	$^{+13}_{-11}$	$^{+3.0}_{-2.8}$	$^{+3.6}_{-2.9}$	$^{+65}_{-37}$	$^{+3.3}_{-3.0}$	$^{+4.1}_{-3.8}$	$^{+6.3}_{-5.7}$	0.0	0.0	$^{+4.1}_{-3.9}$	0.0	0.0	± 0.9	± 6.2	± 0.7	± 1.0	9.22	1.00	0.00
45–60	1.02(8)	1.29×10^4	2.08	$^{+2.5}_{-2.4}$	$^{+12}_{-11}$	$^{+9.8}_{-9.4}$	$^{+2.0}_{-1.8}$	$^{+2.9}_{-2.6}$	$^{+39}_{-26}$	$^{+5.0}_{-4.7}$	$^{+2.5}_{-2.6}$	± 6.8	$^{+0.6}_{+0.2}$	$^{+0.7}_{+0.0}$	$^{+3.7}_{-3.3}$	$^{+1.0}_{-0.2}$	± 0.4	± 0.5	± 1.5	± 0.3	± 1.0	5.64	1.00	0.00
60–80	1.00(7)	1.27×10^3	2.23	$^{-1.3}_{+1.2}$	$^{+8.9}_{-11}$	$^{+5.9}_{-7.4}$	$^{+0.8}_{-2.6}$	$^{+5.0}_{-7.0}$	$^{+24}_{-19}$	$^{+4.4}_{-6.4}$	$^{+2.0}_{-4.0}$	$^{+7.7}_{-8.8}$	$^{+0.3}_{-1.7}$	0.0	$^{+0.5}_{-2.2}$	$^{+3.5}_{-4.9}$	± 0.3	± 0.6	± 4.3	± 0.8	± 1.0	5.27	1.00	0.02
80–110	0.99(6)	7.70×10^1	3.19	∓ 0.5	$^{+13}_{-10}$	$^{+6.1}_{-5.1}$	$^{+4.7}_{-2.6}$	$^{+4.6}_{-3.2}$	$^{+17}_{-13}$	$^{+6.0}_{-4.7}$	± 1.9	$^{+11}_{-9.5}$	$^{+2.2}_{-2.3}$	0.0	∓ 0.5	$^{+8.3}_{-7.7}$	∓ 0.2	± 0.2	± 5.1	± 0.6	± 1.0	5.55	1.00	0.02
110–160	0.98(6)	8.28×10^{-1}	12.2	0.0	$^{+10}_{-15}$	$^{+7.1}_{-9.4}$	$^{+9.3}_{-11}$	$^{+0.3}_{-3.7}$	$^{+13}_{-14}$	$^{+2.7}_{-9.7}$	$^{+0.8}_{-4.2}$	$^{+10}_{-15}$	$^{+3.5}_{-6.9}$	0.0	$^{-0.2}_{+0.4}$	$^{+11}_{-16}$	± 2.3	± 0.1	± 11	± 3.1	± 1.0	8.01	1.00	0.02

APPENDIX C: DIJET TABLES

TABLE XIX. Measured dijet cross section for $R = 0.4$ and $y^* < 0.5$. NPC stands for multiplicative nonperturbative corrections with error × 100 in parentheses, i.e., 1.25(10) means 1.25 ± 0.10. σ is the measured cross section. δ_{stat} is the statistical uncertainty. γ_i and u_i are the correlated and uncorrelated systematic uncertainties, as described in Sec. VIII D and Table IV. All uncertainties are given in %. An overall luminosity uncertainty of 3.4%, which is applicable to all ATLAS data samples based on 2010 data, is not shown. All tables are available on HEPDATA [71].

m_{12}-bin [TeV]	NPC	σ [pb/TeV]	δ_{stat}%	γ_1	γ_7	γ_{13}	γ_{19}	γ_{25}	γ_{31}	γ_{32}	γ_{38}	γ_{44}	γ_{50}	γ_{56}	γ_{62}	γ_{68}	γ_{74}	γ_{75}	γ_{76}	γ_{82}	γ_{83}	u_1	u_2	u_3
0.07–0.11	1.04 (8)	2.4×10^8	1.3	$^{+4.0}_{-4.1}$	$^{+8.2}_{-7.7}$	$^{+5.9}_{-5.8}$	$^{+4.3}_{-4.2}$	$^{+1.5}_{-1.7}$	$^{+9.8}_{-8.5}$	$^{+2.0}_{-2.3}$	$^{+2.5}_{-2.7}$	$^{+3.7}_{-3.9}$	0.0	0.02	$^{+2.7}_{-2.8}$	$^{+0.15}_{-0.14}$	0.0	N/A	2.1	0.01	2.1	$^{+2.4}_{-2.7}$	1.0	1.0
0.11–0.16	1.03 (5)	3.4×10^7	0.67	$^{+0.95}_{-0.93}$	$^{+6.4}_{-6.2}$	$^{+4.9}_{-4.8}$	2.7	1.9	$^{+5.6}_{-4.9}$	2.6	$^{+1.7}_{-1.6}$	$^{+4.1}_{-4.0}$	$^{+0.18}_{-0.24}$	$^{+0.0}_{-0.03}$	$^{+1.9}_{-1.7}$	$^{+0.81}_{-0.87}$	0.04	N/A	0.76	0.12	2.0	$^{+1.6}_{-1.7}$	1.0	1.0
0.16–0.21	1.02 (4)	7.1×10^6	0.52	$^{+0.35}_{-0.33}$	$^{+6.0}_{-5.5}$	$^{+3.9}_{-3.7}$	$^{+2.2}_{-2.0}$	$^{+1.3}_{-1.2}$	$^{+3.3}_{-3.0}$	$^{+2.8}_{-2.5}$	$^{+1.3}_{-1.1}$	$^{+4.5}_{-4.1}$	$^{+0.85}_{-0.77}$	$^{+0.06}_{-0.04}$	$^{+0.49}_{-0.47}$	$^{+2.5}_{-2.4}$	0.04	N/A	0.61	0.1	2.0	$^{+1.2}_{-1.1}$	1.0	1.0
0.21–0.26	1.02 (4)	2.0×10^6	0.88	0.12	$^{+5.7}_{-5.6}$	$^{+3.7}_{-4.0}$	2.2	$^{+0.79}_{-0.84}$	$^{+2.2}_{-2.3}$	2.6	$^{+0.99}_{-0.98}$	$^{+4.7}_{-4.8}$	$^{+1.3}_{-1.4}$	$^{+0.04}_{-0.07}$	$^{+0.03}_{-0.02}$	$^{+3.4}_{-3.7}$	0.2	N/A	0.34	0.04	2.0	$^{+1.0}_{-0.98}$	1.0	1.0
0.26–0.31	1.02 (3)	7.2×10^5	0.67	0.03	$^{+5.5}_{-4.9}$	$^{+3.9}_{-3.2}$	$^{+2.5}_{-2.4}$	$^{+1.2}_{-1.0}$	$^{+2.6}_{-2.1}$	$^{+2.7}_{-2.4}$	$^{+0.88}_{-0.9}$	$^{+5.5}_{-4.8}$	$^{+1.7}_{-1.6}$	$^{+0.06}_{-0.04}$	$^{+0.03}_{-0.04}$	$^{+4.8}_{-4.3}$	0.1	N/A	0.62	0.11	2.0	$^{+0.77}_{-0.83}$	1.0	1.0
0.31–0.37	1.02 (3)	2.8×10^5	0.55	0.0	$^{+4.9}_{-4.6}$	$^{+3.4}_{-3.3}$	$^{+2.5}_{-2.2}$	$^{+1.4}_{-1.3}$	$^{+2.4}_{-2.3}$	$^{+2.5}_{-2.3}$	0.67	$^{+5.7}_{-5.3}$	$^{+2.1}_{-2.0}$	$^{+0.08}_{-0.07}$	$^{+0.01}_{-0.02}$	$^{+5.5}_{-5.1}$	0.0	N/A	0.57	0.03	2.0	$^{+0.64}_{-0.67}$	1.0	1.0
0.37–0.44	1.02 (2)	1.1×10^5	0.61	0.0	$^{+4.3}_{-4.2}$	$^{+3.7}_{-3.8}$	$^{+1.9}_{-2.0}$	1.4	$^{+2.3}_{-2.0}$	$^{+2.0}_{-2.1}$	$^{+0.55}_{-0.59}$	5.5	$^{+2.2}_{-2.3}$	$^{+0.1}_{-0.12}$	0.0	$^{+6.0}_{-5.9}$	0.06	N/A	0.29	0.01	2.0	$^{+0.56}_{-0.65}$	1.0	1.0
0.44–0.51	1.02 (2)	4.3×10^4	0.64	0.0	$^{+4.5}_{-4.3}$	$^{+4.1}_{-3.9}$	$^{+1.9}_{-2.0}$	$^{+1.7}_{-1.8}$	2.1	$^{+2.1}_{-2.0}$	$^{+0.61}_{-0.63}$	$^{+6.0}_{-5.7}$	$^{+3.0}_{-2.9}$	$^{+0.13}_{-0.16}$	0.0	$^{+6.8}_{-6.6}$	0.0	N/A	0.24	0.0	2.0	$^{+0.63}_{-0.75}$	1.0	1.0
0.51–0.59	1.01 (2)	1.8×10^4	0.82	0.0	$^{+4.5}_{-3.8}$	$^{+3.3}_{-2.6}$	$^{+2.0}_{-1.6}$	$^{+2.2}_{-1.7}$	$^{+2.5}_{-1.8}$	$^{+2.1}_{-1.7}$	$^{+0.64}_{-0.42}$	$^{+6.4}_{-5.8}$	$^{+3.6}_{-2.9}$	$^{+0.27}_{-0.15}$	0.0	$^{+7.7}_{-6.8}$	0.0	N/A	0.66	0.16	2.0	$^{+0.7}_{-0.52}$	1.0	1.0
0.59–0.67	1.01 (2)	7.9×10^3	1.1	0.0	$^{+3.5}_{-3.8}$	$^{+2.6}_{-2.9}$	$^{+1.3}_{-1.4}$	$^{+2.0}_{-2.4}$	$^{+1.7}_{-2.2}$	$^{+1.6}_{-1.7}$	$^{+0.31}_{-0.4}$	$^{+6.2}_{-6.4}$	$^{+3.2}_{-3.7}$	$^{+0.13}_{-0.2}$	0.0	$^{+7.4}_{-7.6}$	0.1	N/A	0.12	0.0	2.0	$^{+0.36}_{-0.51}$	1.0	1.0
0.67–0.76	1.01 (2)	3.7×10^3	1.3	0.0	$^{+3.2}_{-3.3}$	$^{+2.3}_{-2.4}$	$^{+1.2}_{-1.3}$	$^{+2.3}_{-2.4}$	$^{+1.6}_{-1.9}$	$^{+1.4}_{-1.6}$	$^{+0.33}_{-0.39}$	$^{+6.5}_{-6.2}$	$^{+3.8}_{-3.9}$	$^{+0.12}_{-0.18}$	0.0	$^{+8.3}_{-7.9}$	0.07	N/A	0.3	0.0	2.0	$^{+0.34}_{-0.39}$	1.0	1.0
0.76–0.85	1.01 (2)	1.8×10^3	1.8	0.0	$^{+3.2}_{-3.1}$	$^{+2.0}_{-1.9}$	$^{+1.5}_{-1.4}$	$^{+2.6}_{-2.5}$	$^{+2.2}_{-1.8}$	$^{+1.7}_{-1.6}$	$^{+0.48}_{-0.38}$	$^{+6.8}_{-6.3}$	$^{+4.5}_{-4.3}$	$^{+0.26}_{-0.17}$	0.0	$^{+9.0}_{-8.1}$	0.04	N/A	0.41	0.06	2.0	$^{+0.46}_{-0.39}$	1.0	1.0
0.85–0.95	1.01 (1)	8.6×10^2	2.2	0.0	$^{+3.2}_{-3.0}$	$^{+2.3}_{-2.2}$	$^{+1.5}_{-1.4}$	$^{+2.6}_{-2.5}$	$^{+1.9}_{-1.8}$	$^{+1.5}_{-1.4}$	$^{+0.28}_{-0.44}$	$^{+6.9}_{-6.8}$	$^{+4.8}_{-4.7}$	$^{+0.12}_{-0.23}$	0.0	$^{+9.2}_{-8.6}$	0.08	N/A	0.34	0.0	2.0	$^{+0.27}_{-0.42}$	1.0	1.0
0.95–1.06	1.01 (1)	4.2×10^2	3.2	0.0	2.7	$^{+2.5}_{-2.6}$	1.4	$^{+2.4}_{-2.3}$	1.7	1.3	$^{+0.35}_{-0.36}$	$^{+7.1}_{-6.5}$	$^{+5.1}_{-4.8}$	$^{+0.23}_{-0.1}$	0.0	$^{+9.5}_{-9.2}$	0.06	N/A	0.37	0.0	2.0	$^{+0.3}_{-0.31}$	1.0	1.0
1.06–1.18	1.01 (1)	2.1×10^2	4.4	0.0	$^{+3.2}_{-3.1}$	2.4	$^{+1.1}_{-1.3}$	$^{+2.3}_{-2.5}$	1.8	$^{+1.4}_{-1.5}$	$^{+0.45}_{-0.43}$	$^{+7.4}_{-6.6}$	$^{+5.5}_{-5.3}$	$^{+0.49}_{-0.55}$	0.0	$^{+11}_{-9.1}$	0.0	N/A	0.55	0.0	2.0	$^{+0.47}_{-0.36}$	1.0	1.0
1.18–1.31	1.01 (1)	9.6×10^1	5.8	0.0	$^{+3.3}_{-3.4}$	$^{+1.1}_{-1.4}$	$^{+0.48}_{-0.7}$	$^{+1.9}_{-2.0}$	$^{+1.5}_{-1.3}$	$^{+0.99}_{-1.3}$	$^{+0.33}_{-0.32}$	6.7	5.4	$^{+0.43}_{-0.73}$	0.0	10	0.1	N/A	0.1	0.0	2.0	$^{+0.26}_{-0.3}$	1.0	1.0
1.31–1.45	1.01 (1)	4.7×10^1	7.7	0.0	$^{+3.7}_{-3.6}$	1.6	$^{+0.84}_{-0.58}$	$^{+2.2}_{-2.0}$	$^{+1.3}_{-1.2}$	$^{+1.2}_{-0.92}$	$^{+0.34}_{-0.26}$	$^{+7.5}_{-7.2}$	$^{+6.1}_{-5.9}$	$^{+0.97}_{-0.77}$	0.0	$^{+12}_{-11}$	0.06	N/A	0.23	0.06	2.0	0.2	1.0	1.0
1.45–1.6	1.01 (1)	2.1×10^1	13	0.0	3.9	$^{+2.8}_{-2.9}$	$^{+1.1}_{-1.2}$	2.6	$^{+1.3}_{-1.4}$	$^{+1.1}_{-1.2}$	$^{+0.34}_{-0.31}$	$^{+8.3}_{-7.5}$	$^{+6.6}_{-6.2}$	$^{+1.4}_{-1.5}$	0.0	$^{+12}_{-11}$	0.09	N/A	0.35	0.0	2.0	$^{+0.22}_{-0.18}$	1.0	1.0
1.6–1.94	1.01 (1)	7.2×10^0	14	0.0	$^{+4.3}_{-4.2}$	$^{+3.7}_{-3.8}$	$^{+1.3}_{-1.2}$	2.6	1.1	$^{+1.0}_{-0.99}$	$^{+0.37}_{-0.34}$	$^{+8.6}_{-8.0}$	$^{+7.2}_{-6.7}$	$^{+2.2}_{-2.3}$	0.0	$^{+14}_{-12}$	0.07	N/A	0.52	0.03	2.0	$^{+0.25}_{-0.21}$	1.0	1.0
1.94–2.78	1.01 (1)	6.4×10^{-1}	35	$^{+0.0}_{-0.01}$	$^{+4.3}_{-4.2}$	$^{+4.2}_{-4.1}$	$^{+0.61}_{-0.83}$	$^{+2.9}_{-3.0}$	$^{+0.76}_{-0.74}$	$^{+0.72}_{-0.92}$	$^{+0.35}_{-0.46}$	$^{+8.5}_{-8.4}$	7.7	$^{+4.4}_{-4.6}$	0.0	$^{+16}_{-15}$	0.3	N/A	0.45	0.01	2.0	$^{+0.12}_{-0.2}$	1.0	1.0

TABLE XX. Measured dijet cross section for $R = 0.4$ and $0.5 \leq y^* < 1.0$. See Table XIX for a description of the columns. All tables are available on HEPDATA [71].

m_{12}-bin [TeV]	NPC	σ [pb/TeV]	δ_{stat} %	γ_1	γ_7	γ_{13}	γ_{19}	γ_{25}	γ_{31}	γ_{32}	γ_{38}	γ_{44}	γ_{50}	γ_{56}	γ_{62}	γ_{68}	γ_{74}	γ_{75}	γ_{76}	γ_{82}	γ_{83}	u_1	u_2	u_3
0.11–0.16	1.04 (6)	7.9×10^7	1.2	$^{+3.9}_{-3.5}$	$^{+7.8}_{-7.2}$	$^{+6.2}_{-5.6}$	$^{+4.2}_{-3.8}$	$^{+1.9}_{-1.7}$	$^{+10}_{-8.3}$	$^{+2.5}_{-2.3}$	$^{+2.6}_{-2.3}$	$^{+4.1}_{-3.8}$	$^{+0.02}_{-0.0}$	$^{+0.02}_{-0.0}$	$^{+2.7}_{-2.5}$	$^{+0.04}_{-0.0}$	0.05	N/A	2.1	0.25	2.1	$^{+2.7}_{-2.3}$	1.0	1.0
0.16–0.21	1.03 (5)	1.6×10^7	0.77	$^{+0.48}_{-0.63}$	6.2	$^{+4.4}_{-4.6}$	$^{+2.0}_{-2.7}$	$^{+1.8}_{-2.5}$	$^{+4.4}_{-4.9}$	$^{+2.9}_{-3.5}$	$^{+1.2}_{-1.9}$	$^{+4.3}_{-4.7}$	$^{+0.4}_{-0.93}$	$^{+0.0}_{-0.04}$	$^{+1.3}_{-1.9}$	$^{+1.4}_{-2.2}$	0.1	N/A	0.0	0.0	1.9	$^{+1.0}_{-2.3}$	1.0	1.0
0.21–0.26	1.03 (4)	4.7×10^6	0.62	$^{+0.39}_{-0.45}$	$^{+6.0}_{-5.9}$	$^{+4.0}_{-4.1}$	$^{+2.2}_{-2.3}$	$^{+1.2}_{-1.3}$	$^{+3.4}_{-3.6}$	2.8	1.1	$^{+4.5}_{-4.6}$	$^{+0.8}_{-0.87}$	$^{+0.04}_{-0.03}$	$^{+0.43}_{-0.39}$	$^{+2.5}_{-2.7}$	0.06	N/A	0.26	0.0	2.0	$^{+1.1}_{-1.4}$	1.0	1.0
0.26–0.31	1.02 (3)	1.7×10^6	0.66	0.11	$^{+6.2}_{-6.1}$	$^{+4.2}_{-4.1}$	$^{+2.4}_{-2.2}$	$^{+0.96}_{-0.67}$	$^{+2.9}_{-3.1}$	$^{+2.7}_{-2.6}$	$^{+1.1}_{-0.88}$	5.0	$^{+1.3}_{-1.1}$	$^{+0.08}_{-0.05}$	$^{+0.11}_{-0.0}$	$^{+3.6}_{-3.7}$	0.04	N/A	0.6	0.0	2.0	$^{+1.2}_{-0.96}$	1.0	1.0
0.31–0.37	1.02 (3)	6.5×10^5	0.63	0.02	$^{+5.5}_{-5.2}$	3.7	2.4	$^{+0.95}_{-1.0}$	$^{+3.0}_{-2.6}$	$^{+2.7}_{-2.5}$	$^{+0.88}_{-0.84}$	$^{+5.1}_{-4.8}$	$^{+1.7}_{-1.6}$	$^{+0.06}_{-0.07}$	$^{+0.0}_{-0.04}$	$^{+4.3}_{-4.2}$	0.07	N/A	0.54	0.1	2.0	$^{+0.89}_{-0.9}$	1.0	1.0
0.37–0.44	1.02 (3)	2.5×10^5	0.77	0.0	$^{+4.9}_{-5.2}$	$^{+3.4}_{-3.7}$	$^{+2.2}_{-2.8}$	$^{+1.4}_{-1.6}$	$^{+2.8}_{-3.1}$	$^{+2.4}_{-2.8}$	$^{+0.88}_{-1.1}$	$^{+5.3}_{-5.6}$	$^{+1.8}_{-2.3}$	$^{+0.06}_{-0.13}$	0.0	$^{+4.9}_{-5.4}$	0.08	N/A	0.14	0.02	2.0	$^{+0.79}_{-1.2}$	1.0	1.0
0.44–0.51	1.02 (2)	1.0×10^5	0.68	0.0	$^{+4.7}_{-4.4}$	3.4	$^{+1.9}_{-2.0}$	$^{+1.2}_{-1.4}$	$^{+2.5}_{-2.6}$	$^{+2.0}_{-2.1}$	$^{+0.61}_{-0.68}$	$^{+5.7}_{-5.2}$	$^{+1.9}_{-2.1}$	0.09	0.0	$^{+5.8}_{-5.4}$	0.0	N/A	0.55	0.03	2.0	$^{+0.66}_{-0.68}$	1.0	1.0
0.51–0.59	1.02 (2)	4.4×10^4	0.82	0.0	$^{+4.9}_{-4.1}$	$^{+4.2}_{-3.7}$	$^{+2.0}_{-1.7}$	$^{+1.7}_{-1.5}$	$^{+2.9}_{-2.5}$	$^{+2.2}_{-1.8}$	$^{+0.6}_{-0.56}$	$^{+6.6}_{-5.2}$	$^{+2.8}_{-2.4}$	$^{+0.1}_{-0.14}$	0.0	$^{+7.3}_{-5.8}$	0.08	N/A	0.82	0.14	2.0	$^{+0.75}_{-0.65}$	1.0	1.0
0.59–0.67	1.02 (2)	1.9×10^4	0.94	0.0	$^{+4.3}_{-4.6}$	$^{+3.8}_{-3.6}$	$^{+1.8}_{-1.7}$	$^{+1.8}_{-1.7}$	$^{+2.8}_{-2.7}$	$^{+2.1}_{-2.0}$	$^{+0.62}_{-0.52}$	$^{+6.1}_{-6.3}$	3.1	$^{+0.19}_{-0.16}$	0.0	$^{+7.1}_{-7.3}$	0.0	N/A	0.42	0.06	2.0	$^{+0.69}_{-0.66}$	1.0	1.0
0.67–0.76	1.02 (2)	9.0×10^3	1.0	0.0	$^{+3.9}_{-4.4}$	$^{+3.0}_{-3.3}$	$^{+1.6}_{-2.0}$	$^{+2.0}_{-2.4}$	$^{+2.6}_{-2.9}$	$^{+1.8}_{-2.3}$	$^{+0.3}_{-0.56}$	$^{+5.9}_{-6.5}$	$^{+3.2}_{-3.7}$	$^{+0.05}_{-0.15}$	0.0	$^{+7.1}_{-7.9}$	0.0	N/A	0.0	0.0	2.0	$^{+0.37}_{-0.77}$	1.0	1.0
0.76–0.85	1.02 (2)	4.3×10^3	1.3	0.0	$^{+4.7}_{-3.2}$	$^{+3.4}_{-2.4}$	$^{+2.0}_{-1.4}$	$^{+2.9}_{-2.2}$	$^{+3.4}_{-2.3}$	$^{+2.2}_{-1.6}$	$^{+0.62}_{-0.48}$	$^{+7.9}_{-6.0}$	$^{+4.5}_{-3.2}$	$^{+0.31}_{-0.15}$	0.0	$^{+9.6}_{-7.5}$	0.09	N/A	0.99	0.12	2.0	$^{+0.75}_{-0.53}$	1.0	1.0
0.85–0.95	1.01 (2)	2.1×10^3	1.6	0.0	$^{+3.3}_{-3.6}$	$^{+2.4}_{-2.5}$	$^{+1.3}_{-1.4}$	$^{+2.4}_{-2.6}$	$^{+2.5}_{-2.8}$	$^{+1.6}_{-1.7}$	$^{+0.49}_{-0.33}$	$^{+6.8}_{-7.0}$	$^{+3.9}_{-4.1}$	$^{+0.24}_{-0.09}$	0.0	$^{+9.0}_{-8.5}$	0.04	N/A	0.33	0.0	2.0	$^{+0.55}_{-0.33}$	1.0	1.0
0.95–1.06	1.01 (1)	9.8×10^2	2.1	0.0	$^{+3.4}_{-3.3}$	$^{+2.4}_{-2.2}$	1.3	$^{+2.7}_{-2.6}$	$^{+2.8}_{-2.7}$	1.6	$^{+0.37}_{-0.44}$	$^{+7.1}_{-6.7}$	$^{+4.6}_{-4.3}$	$^{+0.16}_{-0.21}$	0.0	$^{+9.1}_{-8.7}$	0.06	N/A	0.36	0.0	2.0	$^{+0.36}_{-0.45}$	1.0	1.0
1.06–1.18	1.01 (1)	4.9×10^2	2.7	0.0	$^{+3.3}_{-3.0}$	$^{+2.3}_{-2.2}$	$^{+1.5}_{-1.4}$	$^{+2.6}_{-2.4}$	$^{+2.7}_{-2.6}$	$^{+1.6}_{-1.5}$	$^{+0.37}_{-0.43}$	$^{+7.1}_{-6.3}$	$^{+4.7}_{-4.4}$	$^{+0.21}_{-0.23}$	0.0	$^{+9.2}_{-8.6}$	0.0	N/A	0.37	0.03	2.0	$^{+0.34}_{-0.42}$	1.0	1.0
1.18–1.31	1.01 (1)	2.3×10^2	3.9	0.0	$^{+3.8}_{-3.2}$	$^{+3.1}_{-2.7}$	$^{+1.4}_{-1.5}$	$^{+3.0}_{-2.7}$	$^{+3.3}_{-2.9}$	$^{+1.6}_{-1.5}$	$^{+0.5}_{-0.3}$	$^{+7.9}_{-7.0}$	$^{+5.7}_{-5.1}$	$^{+0.31}_{-0.19}$	0.0	$^{+11}_{-10}$	0.01	N/A	0.66	0.0	2.0	$^{+0.52}_{-0.3}$	1.0	1.0
1.31–1.45	1.01 (1)	1.1×10^2	5.2	0.0	$^{+3.3}_{-3.4}$	$^{+2.4}_{-2.6}$	1.2	2.4	$^{+2.8}_{-2.7}$	$^{+1.4}_{-1.3}$	$^{+0.38}_{-0.34}$	$^{+7.3}_{-7.4}$	$^{+5.4}_{-5.5}$	$^{+0.42}_{-0.21}$	0.0	10	0.02	N/A	0.28	0.02	2.0	$^{+0.36}_{-0.32}$	1.0	1.0
1.45–1.6	1.01 (1)	5.2×10^1	6.8	0.0	$^{+2.9}_{-3.7}$	$^{+1.8}_{-2.4}$	$^{+0.91}_{-0.94}$	$^{+1.8}_{-2.3}$	$^{+2.4}_{-3.2}$	$^{+1.0}_{-1.3}$	$^{+0.34}_{-0.41}$	$^{+6.5}_{-7.8}$	$^{+4.9}_{-6.5}$	$^{+0.41}_{-0.63}$	0.0	$^{+11}_{-10}$	0.06	N/A	0.0	0.08	2.0	$^{+0.26}_{-0.34}$	1.0	1.0
1.6–1.76	1.01 (1)	2.0×10^1	11	0.0	$^{+3.7}_{-4.0}$	2.0	$^{+0.83}_{-0.82}$	$^{+2.1}_{-2.3}$	$^{+3.2}_{-3.3}$	1.1	$^{+0.2}_{-0.29}$	$^{+8.4}_{-7.7}$	$^{+6.4}_{-6.3}$	$^{+0.79}_{-0.76}$	0.0	$^{+13}_{-12}$	0.1	N/A	0.4	0.0	2.0	$^{+0.08}_{-0.23}$	1.0	1.0
1.76–2.12	1.01 (1)	7.6×10^0	13	0.0	$^{+4.3}_{-4.0}$	$^{+2.3}_{-2.4}$	$^{+0.98}_{-1.1}$	$^{+2.7}_{-2.5}$	$^{+3.2}_{-3.1}$	$^{+1.0}_{-1.1}$	$^{+0.41}_{-0.42}$	$^{+8.5}_{-7.9}$	$^{+7.0}_{-6.6}$	$^{+1.3}_{-1.5}$	0.0	$^{+14}_{-13}$	0.1	N/A	0.44	0.11	2.0	$^{+0.32}_{-0.21}$	1.0	1.0
2.12–3.31	1.01 (1)	9.8×10^{-1}	24	0.0	$^{+5.6}_{-5.1}$	$^{+4.1}_{-3.7}$	$^{+0.94}_{-0.86}$	$^{+3.6}_{-3.3}$	$^{+3.6}_{-3.4}$	$^{+1.0}_{-0.86}$	$^{+0.42}_{-0.45}$	$^{+10}_{-8.9}$	$^{+8.6}_{-7.6}$	$^{+3.9}_{-3.6}$	0.0	$^{+17}_{-15}$	0.3	N/A	0.99	0.05	2.0	0.31	1.0	1.0

TABLE XXI. Measured dijet cross section for $R = 0.4$ and $1.0 \leq y^* < 1.5$. See Table XIX for a description of the columns. All tables are available on HEPDATA [71].

m_{12}-bin [TeV]	NPC	σ [pb/TeV]	δ_{stat} %	γ_2	γ_8	γ_{14}	γ_{20}	γ_{26}	γ_{31}	γ_{33}	γ_{39}	γ_{45}	γ_{51}	γ_{57}	γ_{63}	γ_{69}	γ_{74}	γ_{75}	γ_{77}	γ_{82}	γ_{83}	u_1	u_2	u_3
0.16–0.21	1.04 (6)	4.3×10^7	1.5	$^{+4.2}_{-3.9}$	$^{+8.3}_{-7.8}$	$^{+6.5}_{-6.1}$	$^{+4.4}_{-4.1}$	$^{+2.0}_{-1.9}$	$^{+13}_{-11}$	2.5	$^{+2.7}_{-2.6}$	$^{+4.2}_{-4.0}$	$^{+0.08}_{-0.07}$	0.01	2.8	$^{+0.1}_{-0.04}$	0.04	N/A	2.3	0.2	2.1	$^{+3.1}_{-2.8}$	2.0	1.0
0.21–0.26	1.04 (5)	1.3×10^7	1.1	$^{+0.37}_{-0.61}$	6.5	$^{+5.0}_{-5.3}$	$^{+2.1}_{-2.3}$	$^{+1.4}_{-1.7}$	$^{+7.9}_{-7.4}$	$^{+2.8}_{-2.9}$	$^{+1.4}_{-1.5}$	$^{+4.2}_{-4.6}$	$^{+0.26}_{-0.36}$	$^{+0.03}_{-0.04}$	1.8	$^{+0.71}_{-0.85}$	0.0	N/A	0.22	0.12	1.9	$^{+1.5}_{-2.1}$	2.0	1.0
0.26–0.31	1.03 (4)	4.8×10^6	1.0	$^{+0.04}_{-0.09}$	$^{+7.0}_{-6.4}$	$^{+4.8}_{-4.5}$	$^{+2.5}_{-2.2}$	$^{+1.8}_{-1.5}$	$^{+6.7}_{-5.7}$	$^{+3.0}_{-2.6}$	$^{+1.3}_{-1.1}$	$^{+4.7}_{-4.4}$	$^{+0.49}_{-0.32}$	$^{+0.06}_{-0.02}$	$^{+1.1}_{-0.93}$	$^{+1.8}_{-1.6}$	0.1	N/A	0.76	0.12	2.0	$^{+1.4}_{-1.5}$	2.0	1.0
0.31–0.37	1.03 (4)	1.9×10^6	0.95	0.14	$^{+6.1}_{-5.8}$	$^{+4.5}_{-4.0}$	$^{+2.5}_{-2.2}$	$^{+1.6}_{-1.4}$	$^{+5.1}_{-4.6}$	$^{+3.1}_{-2.5}$	$^{+1.5}_{-1.2}$	$^{+4.7}_{-4.4}$	$^{+0.88}_{-0.8}$	$^{+0.05}_{-0.03}$	$^{+0.57}_{-0.36}$	$^{+2.8}_{-2.6}$	0.3	N/A	0.8	0.0	2.0	$^{+1.7}_{-1.4}$	2.0	1.0
0.37–0.44	1.03 (3)	7.3×10^5	0.89	0.07	$^{+5.9}_{-5.3}$	$^{+4.0}_{-3.7}$	2.1	$^{+1.0}_{-0.98}$	$^{+4.2}_{-3.8}$	$^{+2.5}_{-2.6}$	1.1	$^{+4.8}_{-4.4}$	$^{+1.1}_{-1.2}$	$^{+0.1}_{-0.07}$	$^{+0.06}_{-0.07}$	$^{+3.3}_{-3.5}$	0.5	N/A	0.51	0.0	2.0	$^{+1.2}_{-1.3}$	2.0	1.0
0.44–0.51	1.02 (3)	3.0×10^5	1.1	0.02	$^{+6.3}_{-6.1}$	$^{+4.3}_{-4.2}$	$^{+2.3}_{-2.5}$	1.1	$^{+4.0}_{-4.1}$	3.0	1.0	$^{+5.6}_{-5.5}$	$^{+1.8}_{-1.6}$	$^{+0.05}_{-0.04}$	$^{+0.01}_{-0.04}$	$^{+4.7}_{-4.6}$	0.2	N/A	1.0	0.0	2.0	$^{+1.1}_{-1.3}$	2.0	1.0
0.51–0.59	1.02 (3)	1.3×10^5	1.3	0.0	$^{+5.8}_{-5.9}$	$^{+3.9}_{-4.3}$	$^{+2.3}_{-2.2}$	$^{+1.4}_{-1.2}$	$^{+4.0}_{-4.6}$	$^{+2.7}_{-2.9}$	$^{+1.0}_{-0.66}$	$^{+6.0}_{-5.8}$	$^{+2.1}_{-1.9}$	$^{+0.05}_{-0.13}$	$^{+0.0}_{-0.02}$	5.7	0.07	N/A	0.7	0.02	2.0	$^{+1.2}_{-0.85}$	2.0	1.0
0.59–0.67	1.02 (2)	5.7×10^4	1.4	0.0	$^{+5.5}_{-5.3}$	$^{+3.9}_{-3.6}$	$^{+2.1}_{-2.0}$	$^{+1.3}_{-1.4}$	$^{+4.0}_{-3.9}$	$^{+2.3}_{-2.5}$	$^{+0.77}_{-0.8}$	$^{+6.3}_{-5.7}$	$^{+2.0}_{-2.3}$	$^{+0.12}_{-0.06}$	$^{+0.0}_{-0.01}$	$^{+6.4}_{-5.9}$	0.1	N/A	0.69	0.0	2.0	$^{+0.82}_{-0.92}$	2.0	1.0
0.67–0.76	1.02 (2)	2.6×10^4	1.1	0.0	$^{+5.1}_{-4.3}$	$^{+4.0}_{-3.4}$	$^{+2.0}_{-1.8}$	$^{+1.6}_{-1.4}$	$^{+4.1}_{-3.2}$	$^{+2.3}_{-2.0}$	$^{+0.8}_{-0.72}$	$^{+6.1}_{-5.7}$	$^{+2.4}_{-2.2}$	0.07	0.0	$^{+6.5}_{-6.1}$	0.1	N/A	0.34	0.31	2.0	$^{+0.78}_{-0.91}$	2.0	1.0
0.76–0.85	1.02 (2)	1.3×10^4	1.4	0.0	$^{+4.9}_{-5.1}$	4.0	$^{+1.9}_{-1.7}$	$^{+1.9}_{-2.0}$	$^{+3.9}_{-4.4}$	$^{+2.4}_{-2.2}$	$^{+0.63}_{-0.67}$	$^{+6.2}_{-6.3}$	$^{+2.7}_{-3.0}$	$^{+0.15}_{-0.13}$	0.0	$^{+7.2}_{-7.0}$	0.09	N/A	0.4	0.0	2.0	$^{+0.96}_{-0.85}$	2.0	1.0
0.85–0.95	1.02 (2)	6.1×10^3	1.5	0.0	$^{+5.2}_{-5.0}$	$^{+4.5}_{-4.0}$	1.8	$^{+2.3}_{-2.4}$	$^{+5.1}_{-4.5}$	$^{+2.4}_{-2.3}$	$^{+0.47}_{-0.39}$	$^{+7.7}_{-6.7}$	$^{+3.8}_{-3.4}$	$^{+0.14}_{-0.08}$	0.0	$^{+8.6}_{-8.2}$	0.1	N/A	0.72	0.0	2.0	$^{+0.75}_{-0.77}$	2.0	1.0
0.95–1.06	1.02 (2)	3.1×10^3	1.6	0.0	$^{+4.8}_{-4.6}$	$^{+3.4}_{-3.3}$	1.7	$^{+2.0}_{-2.2}$	$^{+4.6}_{-4.2}$	1.9	$^{+0.67}_{-0.52}$	$^{+7.1}_{-7.2}$	$^{+3.6}_{-3.5}$	$^{+0.08}_{-0.16}$	0.0	$^{+8.8}_{-8.7}$	0.02	N/A	0.73	0.12	2.0	$^{+0.9}_{-0.79}$	2.0	1.0
1.06–1.18	1.02 (2)	1.4×10^3	2.1	0.0	$^{+4.1}_{-4.2}$	$^{+2.8}_{-2.6}$	$^{+1.4}_{-1.8}$	$^{+2.5}_{-2.2}$	$^{+3.8}_{-4.5}$	$^{+1.8}_{-2.1}$	$^{+0.48}_{-0.95}$	$^{+7.2}_{-8.0}$	$^{+4.0}_{-4.2}$	$^{+0.16}_{-0.22}$	0.0	9.3	0.1	N/A	0.26	0.0	2.0	$^{+0.66}_{-1.0}$	2.0	1.0
1.18–1.31	1.02 (2)	7.2×10^2	2.7	0.0	$^{+2.9}_{-4.0}$	$^{+2.4}_{-2.9}$	$^{+1.1}_{-1.8}$	$^{+2.6}_{-3.0}$	$^{+3.5}_{-4.5}$	$^{+1.3}_{-1.9}$	$^{+0.25}_{-0.54}$	$^{+6.7}_{-6.9}$	$^{+3.4}_{-4.4}$	$^{+0.23}_{-0.07}$	0.0	$^{+9.4}_{-8.1}$	0.08	N/A	0.49	0.03	2.0	$^{+0.35}_{-0.89}$	2.0	1.0
1.31–1.45	1.02 (2)	3.5×10^2	2.9	0.0	$^{+5.6}_{-3.4}$	$^{+4.1}_{-2.7}$	$^{+2.5}_{-1.6}$	$^{+4.1}_{-3.0}$	$^{+6.7}_{-4.6}$	$^{+2.8}_{-1.5}$	$^{+0.9}_{-0.36}$	$^{+9.7}_{-7.0}$	$^{+6.3}_{-4.0}$	$^{+0.18}_{-0.16}$	0.0	$^{+13}_{-8.9}$	0.2	N/A	1.7	0.12	2.0	$^{+1.2}_{-0.48}$	2.0	1.0
1.45–1.6	1.01 (1)	1.5×10^2	4.5	0.0	$^{+4.2}_{-4.0}$	$^{+3.0}_{-3.1}$	1.5	$^{+3.2}_{-3.3}$	$^{+5.1}_{-4.8}$	$^{+1.8}_{-1.7}$	$^{+0.43}_{-0.38}$	$^{+7.6}_{-7.2}$	$^{+5.1}_{-4.8}$	$^{+0.04}_{-0.12}$	0.0	$^{+10}_{-9.9}$	0.1	N/A	0.58	0.1	2.0	0.46	2.0	1.0
1.6–1.76	1.01 (1)	7.3×10^1	6.0	0.0	$^{+4.2}_{-4.1}$	$^{+3.2}_{-2.7}$	$^{+1.6}_{-1.1}$	$^{+3.1}_{-2.7}$	$^{+5.8}_{-5.1}$	$^{+2.0}_{-1.4}$	$^{+0.48}_{-0.37}$	$^{+8.1}_{-7.9}$	$^{+5.9}_{-5.2}$	$^{+0.34}_{-0.22}$	0.0	11	0.1	N/A	0.51	0.02	2.0	$^{+0.54}_{-0.42}$	2.0	1.0
1.76–1.94	1.01 (1)	2.9×10^1	8.5	0.0	4.0	$^{+2.8}_{-3.1}$	$^{+1.4}_{-1.3}$	$^{+2.3}_{-2.9}$	$^{+5.3}_{-6.4}$	$^{+1.5}_{-1.6}$	$^{+0.56}_{-0.43}$	8.5	$^{+5.9}_{-6.3}$	$^{+0.34}_{-0.18}$	0.0	$^{+13}_{-12}$	0.2	N/A	0.47	0.04	2.0	$^{+0.62}_{-0.43}$	2.0	1.0
1.94–2.12	1.01 (1)	1.7×10^1	11	0.0	$^{+4.3}_{-4.8}$	$^{+3.1}_{-3.9}$	$^{+1.2}_{-2.2}$	$^{+2.8}_{-3.6}$	$^{+7.0}_{-6.9}$	$^{+1.4}_{-2.4}$	$^{+0.61}_{-0.72}$	$^{+9.2}_{-8.6}$	$^{+6.8}_{-7.1}$	$^{+0.36}_{-0.63}$	0.0	13	0.05	N/A	0.17	0.02	2.0	$^{+0.6}_{-0.72}$	2.0	1.0
2.12–2.55	1.01 (1)	5.2×10^0	16	0.0	$^{+5.0}_{-4.7}$	$^{+2.9}_{-2.6}$	$^{+1.0}_{-1.3}$	$^{+3.0}_{-2.5}$	$^{+6.2}_{-6.6}$	$^{+1.2}_{-1.4}$	$^{+0.24}_{-0.45}$	9.2	6.8	$^{+0.53}_{-1.1}$	0.0	$^{+16}_{-14}$	0.2	N/A	0.71	0.0	2.0	$^{+0.23}_{-0.43}$	2.0	1.0
2.55–3.61	1.01 (1)	4.3×10^{-1}	39	0.01	$^{+5.9}_{-5.4}$	$^{+3.0}_{-2.2}$	$^{+1.5}_{-0.82}$	$^{+4.2}_{-3.3}$	$^{+8.9}_{-8.4}$	$^{+2.2}_{-0.95}$	$^{+0.37}_{-0.42}$	$^{+11}_{-10}$	$^{+9.6}_{-8.9}$	$^{+3.4}_{-2.0}$	0.0	$^{+19}_{-17}$	0.4	N/A	1.3	0.0	2.0	$^{+0.26}_{-0.29}$	2.0	1.0

TABLE XXII. Measured dijet cross section for $R = 0.4$ and $1.5 \leq y^* < 2.0$. See Table XIX for a description of the columns. All tables are available on HEPDATA [71].

m_{12}-bin [TeV]	NPC	σ [pb/TeV]	δ_{stat} %	γ_3	γ_9	γ_{15}	γ_{21}	γ_{27}	γ_{31}	γ_{34}	γ_{40}	γ_{46}	γ_{52}	γ_{58}	γ_{64}	γ_{70}	γ_{74}	γ_{75}	γ_{78}	γ_{82}	γ_{83}	u_1	u_2	u_3
0.26–0.31	1.04 (6)	1.3×10^7	2.6	$^{+4.2}_{-3.6}$	$^{+8.8}_{-8.6}$	$^{+6.7}_{-6.8}$	$^{+4.1}_{-3.8}$	$^{+1.9}_{-2.1}$	$^{+18}_{-15}$	$^{+2.8}_{-2.7}$	$^{+2.8}_{-2.5}$	$^{+4.5}_{-4.4}$	$^{+0.1}_{-0.01}$	$^{+0.02}_{-0.0}$	$^{+3.2}_{-2.9}$	$^{+0.14}_{-0.07}$	0.07	N/A	2.6	0.22	$^{+2.1}_{-2.0}$	$^{+3.7}_{-3.2}$	2.0	1.0
0.31–0.37	1.03 (5)	5.4×10^6	1.9	$^{+2.0}_{-1.7}$	$^{+8.4}_{-6.6}$	$^{+7.3}_{-5.6}$	$^{+3.6}_{-2.6}$	$^{+2.2}_{-1.7}$	$^{+15}_{-11}$	$^{+3.4}_{-2.6}$	$^{+2.2}_{-1.9}$	$^{+5.4}_{-4.3}$	$^{+0.17}_{-0.13}$	$^{+0.01}_{-0.03}$	$^{+2.4}_{-2.1}$	$^{+0.62}_{-0.52}$	0.01	N/A	1.6	0.04	2.0	$^{+3.2}_{-2.5}$	2.0	1.0
0.37–0.44	1.03 (5)	2.2×10^6	1.7	$^{+0.92}_{-0.67}$	$^{+8.3}_{-6.9}$	$^{+6.4}_{-5.3}$	$^{+2.7}_{-2.1}$	2.2	$^{+13}_{-9.6}$	$^{+3.4}_{-2.7}$	$^{+1.9}_{-1.7}$	$^{+5.6}_{-4.8}$	$^{+0.65}_{-0.47}$	0.0	$^{+1.6}_{-1.4}$	$^{+1.7}_{-1.2}$	0.06	N/A	1.5	0.38	2.0	$^{+2.5}_{-2.2}$	2.0	1.0
0.44–0.51	1.03 (4)	8.9×10^5	1.7	$^{+0.0}_{-0.36}$	$^{+6.8}_{-7.6}$	$^{+4.3}_{-5.6}$	$^{+1.7}_{-2.5}$	$^{+1.4}_{-2.2}$	$^{+9.3}_{-9.4}$	$^{+2.4}_{-3.5}$	$^{+0.9}_{-1.7}$	$^{+4.1}_{-5.7}$	$^{+0.17}_{-0.85}$	$^{+0.03}_{-0.05}$	$^{+0.39}_{-1.0}$	$^{+1.6}_{-3.1}$	0.2	N/A	0.45	0.0	2.0	$^{+1.5}_{-2.4}$	2.0	1.0
0.51–0.59	1.03 (4)	3.7×10^5	1.6	$^{+0.0}_{-0.08}$	$^{+5.8}_{-6.1}$	$^{+4.2}_{-4.3}$	$^{+2.2}_{-2.8}$	$^{+1.2}_{-1.9}$	6.4	$^{+2.7}_{-3.3}$	$^{+0.99}_{-1.8}$	$^{+4.6}_{-4.7}$	$^{+0.67}_{-1.6}$	$^{+0.02}_{-0.13}$	$^{+0.08}_{-0.64}$	$^{+3.4}_{-3.6}$	0.2	N/A	0.96	0.0	2.0	$^{+1.4}_{-2.6}$	2.0	1.0
0.59–0.67	1.03 (3)	1.7×10^5	1.9	$^{+0.08}_{-0.02}$	7.0	$^{+5.2}_{-5.0}$	$^{+2.7}_{-2.8}$	$^{+1.7}_{-1.4}$	$^{+6.7}_{-6.6}$	$^{+3.8}_{-3.6}$	$^{+2.1}_{-1.5}$	$^{+6.0}_{-5.7}$	$^{+2.3}_{-1.9}$	$^{+0.06}_{-0.14}$	$^{+0.05}_{-0.02}$	$^{+5.1}_{-4.9}$	0.08	N/A	0.74	0.39	2.0	2.4	2.0	1.0
0.67–0.76	1.02 (3)	8.1×10^4	1.9	$^{+0.04}_{-0.02}$	$^{+7.4}_{-6.5}$	$^{+4.7}_{-4.3}$	2.2	$^{+1.1}_{-0.97}$	$^{+6.7}_{-6.4}$	$^{+3.2}_{-2.7}$	$^{+1.2}_{-0.89}$	$^{+6.1}_{-5.7}$	$^{+1.6}_{-1.5}$	$^{+0.04}_{-0.07}$	$^{+0.09}_{-0.03}$	$^{+5.4}_{-5.1}$	0.02	N/A	0.9	0.19	2.0	$^{+1.4}_{-1.5}$	2.0	1.0
0.76–0.85	1.02 (3)	4.0×10^4	2.1	0.0	$^{+8.2}_{-5.8}$	$^{+5.2}_{-4.3}$	$^{+3.8}_{-1.6}$	$^{+1.4}_{-1.2}$	$^{+7.7}_{-5.6}$	$^{+3.7}_{-2.8}$	$^{+1.2}_{-0.95}$	$^{+7.6}_{-5.6}$	$^{+2.8}_{-1.8}$	$^{+0.05}_{-0.14}$	$^{+0.0}_{-0.03}$	$^{+7.2}_{-5.4}$	0.2	N/A	1.7	0.0	2.0	$^{+2.7}_{-1.2}$	2.0	1.0
0.85–0.95	1.02 (3)	1.9×10^4	2.5	0.0	$^{+7.0}_{-6.3}$	$^{+5.1}_{-4.4}$	$^{+2.8}_{-2.6}$	$^{+1.9}_{-1.7}$	$^{+6.5}_{-5.8}$	3.2	$^{+0.87}_{-0.73}$	$^{+7.1}_{-6.5}$	$^{+2.9}_{-2.6}$	$^{+0.02}_{-0.04}$	$^{+0.0}_{-0.02}$	$^{+7.1}_{-6.6}$	0.3	N/A	1.3	0.0	2.0	$^{+1.7}_{-1.6}$	2.0	1.0
0.95–1.06	1.02 (3)	9.5×10^3	2.2	0.0	$^{+6.0}_{-5.2}$	$^{+3.9}_{-2.9}$	$^{+1.6}_{-1.2}$	$^{+0.97}_{-1.2}$	$^{+6.2}_{-5.6}$	$^{+2.1}_{-1.6}$	$^{+0.57}_{-0.58}$	$^{+6.4}_{-5.9}$	$^{+2.1}_{-1.5}$	$^{+0.04}_{-0.03}$	$^{+0.01}_{-0.0}$	$^{+6.8}_{-6.3}$	0.03	N/A	0.89	0.0	2.0	$^{+0.42}_{-0.95}$	2.0	1.0
1.06–1.18	1.02 (2)	4.6×10^3	2.8	0.0	$^{+5.0}_{-6.0}$	$^{+3.5}_{-5.0}$	$^{+1.6}_{-1.8}$	$^{+1.8}_{-2.1}$	$^{+5.7}_{-6.9}$	$^{+2.2}_{-2.9}$	$^{+0.33}_{-1.5}$	$^{+6.3}_{-7.8}$	$^{+2.4}_{-3.4}$	$^{+0.05}_{-0.14}$	0.0	$^{+6.8}_{-9.4}$	0.2	N/A	0.0	0.03	2.0	$^{+1.1}_{-1.7}$	2.0	1.0
1.18–1.31	1.02 (2)	2.2×10^3	2.9	0.0	$^{+5.5}_{-7.2}$	$^{+4.6}_{-5.7}$	$^{+1.9}_{-2.8}$	$^{+2.5}_{-3.6}$	$^{+6.9}_{-8.2}$	$^{+3.0}_{-4.2}$	$^{+0.87}_{-1.1}$	$^{+7.5}_{-8.5}$	$^{+3.7}_{-4.5}$	$^{+0.21}_{-0.08}$	0.0	$^{+8.8}_{-9.4}$	0.1	N/A	0.14	0.0	2.0	$^{+1.3}_{-1.5}$	2.0	1.0
1.31–1.45	1.02 (2)	1.0×10^3	3.3	0.0	$^{+6.2}_{-5.7}$	$^{+4.8}_{-3.3}$	$^{+2.0}_{-1.1}$	$^{+2.4}_{-1.4}$	$^{+7.6}_{-7.4}$	$^{+2.6}_{-1.5}$	$^{+0.61}_{-0.45}$	$^{+8.3}_{-7.4}$	$^{+4.4}_{-3.2}$	$^{+0.14}_{-0.12}$	0.0	$^{+9.9}_{-8.8}$	0.02	N/A	1.0	0.23	2.0	$^{+0.98}_{-0.57}$	2.0	1.0
1.45–1.6	1.02 (2)	4.9×10^2	4.0	0.0	$^{+4.8}_{-3.6}$	$^{+4.0}_{-3.4}$	$^{+1.5}_{-1.3}$	$^{+2.7}_{-1.6}$	5.9	$^{+1.9}_{-1.5}$	$^{+0.12}_{-0.37}$	$^{+7.3}_{-6.8}$	$^{+3.8}_{-3.4}$	$^{+0.0}_{-0.4}$	0.0	$^{+10}_{-8.1}$	0.4	N/A	1.9	0.0	2.0	$^{+0.56}_{-0.21}$	2.0	1.0
1.6–1.76	1.02 (2)	2.3×10^2	4.5	0.0	$^{+4.2}_{-2.7}$	$^{+2.7}_{-2.9}$	$^{+1.4}_{-1.3}$	$^{+2.8}_{-2.1}$	$^{+7.7}_{-4.0}$	$^{+2.0}_{-1.5}$	$^{+0.8}_{-0.42}$	$^{+8.3}_{-5.0}$	$^{+3.6}_{-3.0}$	$^{+0.22}_{-0.08}$	0.0	$^{+11}_{-7.9}$	0.0	N/A	1.6	0.2	2.0	$^{+1.2}_{-1.1}$	2.0	1.0
1.76–1.94	1.02 (2)	9.8×10^1	6.5	0.0	$^{+4.1}_{-6.1}$	$^{+2.0}_{-3.6}$	$^{+1.2}_{-0.34}$	$^{+2.2}_{-3.5}$	$^{+7.5}_{-9.1}$	$^{+1.9}_{-1.2}$	$^{+0.34}_{-0.0}$	$^{+9.0}_{-9.7}$	$^{+4.2}_{-5.9}$	$^{+0.15}_{-0.0}$	0.0	11	0.1	N/A	0.32	0.0	2.0	$^{+0.92}_{-0.1}$	2.0	1.0
1.94–2.12	1.02 (2)	4.3×10^1	9.5	0.0	$^{+4.3}_{-5.7}$	$^{+2.6}_{-3.5}$	$^{+1.7}_{-4.1}$	$^{+2.5}_{-4.3}$	$^{+5.9}_{-8.3}$	$^{+0.62}_{-3.3}$	$^{+0.0}_{-1.4}$	$^{+6.9}_{-10}$	$^{+4.6}_{-6.1}$	$^{+0.04}_{-0.0}$	0.0	$^{+9.9}_{-13}$	0.1	N/A	0.0	0.0	2.0	$^{+0.2}_{-2.5}$	2.0	1.0
2.12–2.33	1.02 (2)	2.3×10^1	12	0.0	$^{+6.0}_{-5.7}$	$^{+5.0}_{-4.9}$	$^{+1.0}_{-2.0}$	$^{+2.8}_{-3.4}$	$^{+9.4}_{-11}$	$^{+0.78}_{-2.1}$	$^{+0.0}_{-0.44}$	$^{+10}_{-11}$	$^{+7.3}_{-6.3}$	$^{+0.0}_{-0.21}$	0.0	$^{+14}_{-13}$	0.7	N/A	1.2	0.05	2.0	$^{+0.23}_{-0.7}$	2.0	1.0
2.33–2.78	1.01 (2)	5.9×10^0	14	0.0	$^{+5.7}_{-4.4}$	$^{+3.9}_{-3.3}$	$^{+2.4}_{-1.7}$	$^{+4.2}_{-3.1}$	$^{+9.0}_{-7.9}$	$^{+2.8}_{-1.9}$	$^{+1.1}_{-0.63}$	$^{+9.1}_{-8.7}$	$^{+6.9}_{-6.2}$	$^{+0.73}_{-0.66}$	0.0	12	0.4	N/A	0.9	0.0	2.0	$^{+1.1}_{-0.51}$	2.0	1.0
2.78–3.93	1.01 (1)	5.4×10^{-1}	34	0.01	$^{+10}_{-7.1}$	$^{+7.2}_{-4.5}$	$^{+2.3}_{-2.4}$	$^{+6.3}_{-4.3}$	$^{+15}_{-11}$	$^{+2.7}_{-2.0}$	1.2	$^{+17}_{-11}$	$^{+13}_{-9.3}$	$^{+0.84}_{-0.93}$	0.0	$^{+24}_{-17}$	0.2	N/A	3.1	0.0	2.0	1.2	2.0	1.0

TABLE XXIII. Measured dijet cross section for $R = 0.4$ and $2.0 \leq y^* < 2.5$. See Table XIX for a description of the columns. All tables are available on HEPDATA [71].

m_{12}-bin [TeV]	NPC	σ [pb/TeV]	δ_{stat} %	$\gamma 4$	γ_{10}	γ_{16}	γ_{22}	γ_{28}	γ_{31}	γ_{35}	γ_{41}	γ_{47}	γ_{53}	γ_{59}	γ_{65}	γ_{71}	γ_{74}	γ_{75}	γ_{79}	γ_{82}	γ_{84}	u_1	u_2	u_3
0.37–0.44	1.03 (7)	5.8×10^6	3.9	$^{+5.1}_{-5.2}$	$^{+11}_{-9.3}$	$^{+7.9}_{-7.5}$	$^{+4.1}_{-4.5}$	$^{+2.1}_{-2.7}$	$^{+30}_{-22}$	$^{+2.8}_{-3.2}$	$^{+3.0}_{-3.5}$	5.3	$^{+0.0}_{-0.08}$	$^{+0.02}_{-0.08}$	$^{+3.0}_{-3.7}$	$^{+0.12}_{-0.07}$	0.06	N/A	4.8	0.0	2.1	$^{+5.7}_{-4.3}$	1.0	$^{+1.6}_{-0.44}$
0.44–0.51	1.03 (6)	2.6×10^6	3.7	$^{+4.7}_{-3.9}$	$^{+11}_{-9.3}$	$^{+8.6}_{-7.6}$	$^{+4.3}_{-3.8}$	$^{+2.4}_{-2.5}$	$^{+28}_{-20}$	$^{+4.0}_{-3.4}$	$^{+3.5}_{-3.0}$	$^{+6.0}_{-5.3}$	$^{+0.28}_{-0.24}$	$^{+0.03}_{-0.02}$	$^{+3.8}_{-3.2}$	$^{+0.44}_{-0.4}$	0.1	N/A	3.7	0.07	2.0	$^{+5.2}_{-4.3}$	1.0	$^{+1.1}_{-0.92}$
0.51–0.59	1.03 (6)	1.1×10^6	2.7	$^{+2.4}_{-2.0}$	$^{+9.4}_{-7.9}$	$^{+7.6}_{-6.6}$	$^{+3.7}_{-2.6}$	$^{+2.4}_{-2.2}$	$^{+21}_{-16}$	$^{+3.5}_{-3.3}$	$^{+2.7}_{-2.1}$	$^{+5.9}_{-4.9}$	$^{+0.39}_{-0.17}$	$^{+0.02}_{-0.0}$	$^{+2.7}_{-2.2}$	$^{+0.96}_{-0.92}$	0.05	N/A	2.1	0.0	2.0	$^{+3.6}_{-3.7}$	1.0	$^{+0.9}_{-1.1}$
0.59–0.67	1.03 (5)	5.2×10^5	2.2	$^{+0.99}_{-0.86}$	$^{+8.3}_{-7.3}$	$^{+6.8}_{-5.9}$	$^{+2.9}_{-2.5}$	$^{+2.6}_{-2.2}$	$^{+17}_{-13}$	$^{+3.4}_{-3.0}$	$^{+2.1}_{-1.8}$	$^{+5.4}_{-4.8}$	$^{+0.55}_{-0.41}$	$^{+0.03}_{-0.0}$	$^{+1.6}_{-1.4}$	$^{+1.8}_{-1.6}$	0.03	N/A	1.9	0.14	2.0	$^{+3.1}_{-3.0}$	1.0	$^{+0.96}_{-1.0}$
0.67–0.76	1.03 (5)	2.4×10^5	2.1	$^{+0.36}_{-0.33}$	$^{+8.1}_{-7.5}$	$^{+6.0}_{-5.9}$	2.8	$^{+2.2}_{-2.1}$	$^{+15}_{-13}$	3.4	$^{+1.6}_{-1.7}$	$^{+5.4}_{-5.6}$	$^{+0.63}_{-0.82}$	$^{+0.02}_{-0.03}$	$^{+0.86}_{-0.98}$	$^{+2.5}_{-2.8}$	0.04	N/A	2.7	1.9	2.0	$^{+2.9}_{-3.1}$	1.0	$^{+0.99}_{-1.0}$
0.76–0.85	1.03 (5)	1.2×10^5	1.9	$^{+0.04}_{-0.0}$	$^{+7.8}_{-7.4}$	$^{+5.7}_{-5.4}$	$^{+2.5}_{-2.8}$	1.9	$^{+13}_{-11}$	$^{+3.3}_{-3.4}$	$^{+1.5}_{-1.7}$	5.8	$^{+0.91}_{-0.97}$	$^{+0.03}_{-0.06}$	$^{+0.34}_{-0.5}$	$^{+3.4}_{-3.6}$	0.03	N/A	2.6	1.6	2.0	$^{+2.4}_{-2.9}$	1.0	1.0
0.85–0.95	1.03 (4)	5.8×10^4	1.9	$^{+0.09}_{-0.06}$	$^{+8.1}_{-7.4}$	$^{+5.6}_{-4.9}$	$^{+2.4}_{-2.1}$	$^{+1.7}_{-1.3}$	$^{+12}_{-10}$	$^{+3.4}_{-2.9}$	$^{+1.6}_{-1.3}$	$^{+6.4}_{-5.6}$	$^{+1.4}_{-1.1}$	$^{+0.05}_{-0.07}$	$^{+0.19}_{-0.08}$	$^{+4.4}_{-3.8}$	0.05	N/A	3.1	1.8	2.0	$^{+2.5}_{-2.1}$	1.0	1.0
0.95–1.06	1.02 (4)	2.8×10^4	2.2	$^{+0.04}_{-0.05}$	$^{+6.9}_{-7.1}$	$^{+4.7}_{-4.9}$	$^{+2.3}_{-2.2}$	$^{+1.1}_{-1.0}$	$^{+9.5}_{-9.2}$	$^{+2.7}_{-3.0}$	$^{+1.2}_{-1.1}$	$^{+5.6}_{-5.7}$	1.3	$^{+0.04}_{-0.01}$	$^{+0.06}_{-0.0}$	4.8	0.05	N/A	2.3	0.43	2.0	$^{+1.9}_{-1.8}$	1.0	1.0
1.06–1.18	1.02 (4)	1.4×10^4	2.1	0.02	$^{+8.6}_{-7.5}$	$^{+6.1}_{-5.4}$	$^{+3.2}_{-2.7}$	$^{+1.8}_{-1.3}$	$^{+11}_{-9.5}$	$^{+4.3}_{-3.6}$	$^{+1.5}_{-1.1}$	$^{+7.5}_{-6.7}$	$^{+2.4}_{-1.9}$	$^{+0.08}_{-0.0}$	$^{+0.02}_{-0.03}$	$^{+7.0}_{-6.1}$	0.04	N/A	4.3	2.8	2.0	$^{+2.9}_{-2.4}$	1.0	1.0
1.18–1.31	1.02 (4)	6.7×10^3	2.6	0.0	$^{+8.1}_{-7.3}$	$^{+5.5}_{-5.1}$	$^{+2.6}_{-2.7}$	1.5	$^{+9.7}_{-8.7}$	$^{+3.8}_{-3.4}$	$^{+1.2}_{-1.1}$	$^{+7.3}_{-6.9}$	$^{+2.3}_{-2.2}$	$^{+0.06}_{-0.15}$	$^{+0.01}_{-0.03}$	$^{+6.9}_{-6.7}$	0.05	N/A	1.7	0.86	2.0	2.2	1.0	1.0
1.31–1.45	1.02 (3)	3.2×10^3	3.1	0.0	$^{+6.4}_{-7.5}$	$^{+4.3}_{-4.9}$	$^{+1.7}_{-2.6}$	$^{+1.1}_{-2.0}$	$^{+8.2}_{-8.8}$	$^{+2.3}_{-3.4}$	$^{+0.71}_{-1.2}$	$^{+6.3}_{-7.5}$	$^{+1.8}_{-2.7}$	$^{+0.01}_{-0.18}$	$^{+0.0}_{-0.01}$	$^{+6.2}_{-7.8}$	0.05	N/A	0.23	0.0	2.0	$^{+1.2}_{-1.8}$	1.0	1.0
1.45–1.6	1.02 (3)	1.5×10^3	3.9	0.0	$^{+7.7}_{-6.4}$	$^{+5.2}_{-4.3}$	$^{+2.7}_{-2.0}$	$^{+2.2}_{-1.6}$	$^{+10}_{-8.7}$	$^{+3.1}_{-2.6}$	$^{+1.2}_{-0.8}$	$^{+8.3}_{-7.1}$	$^{+3.1}_{-2.3}$	$^{+0.08}_{-0.0}$	$^{+0.0}_{-0.01}$	$^{+9.0}_{-7.6}$	0.07	N/A	1.3	0.36	2.0	$^{+2.0}_{-1.5}$	1.0	1.0
1.6–1.76	1.02 (3)	7.3×10^2	3.9	0.0	$^{+7.9}_{-6.2}$	$^{+5.8}_{-4.5}$	$^{+3.1}_{-2.4}$	$^{+2.8}_{-2.0}$	$^{+11}_{-8.5}$	$^{+4.1}_{-2.6}$	$^{+1.2}_{-1.1}$	$^{+9.4}_{-7.4}$	$^{+3.9}_{-2.7}$	$^{+0.26}_{-0.29}$	0.0	$^{+10}_{-8.0}$	0.08	N/A	0.3	0.0	2.0	$^{+2.3}_{-1.9}$	1.0	1.0
1.76–1.94	1.02 (3)	3.1×10^2	4.5	0.0	$^{+5.2}_{-8.1}$	$^{+3.8}_{-6.5}$	$^{+1.6}_{-3.5}$	$^{+1.4}_{-3.2}$	$^{+8.6}_{-11}$	$^{+2.4}_{-4.3}$	$^{+0.8}_{-1.3}$	$^{+7.4}_{-9.7}$	$^{+2.8}_{-5.6}$	$^{+0.13}_{-0.19}$	0.0	$^{+8.5}_{-11}$	0.08	N/A	0.0	0.0	2.0	$^{+0.81}_{-2.3}$	1.0	1.0
1.94–2.12	1.02 (3)	1.5×10^2	5.9	0.0	$^{+5.1}_{-6.6}$	$^{+4.3}_{-5.5}$	$^{+2.3}_{-2.4}$	$^{+1.7}_{-2.9}$	$^{+9.0}_{-10}$	$^{+1.8}_{-3.1}$	$^{+0.83}_{-1.1}$	$^{+7.9}_{-9.3}$	$^{+3.3}_{-4.3}$	$^{+0.05}_{-0.0}$	0.0	$^{+9.5}_{-11}$	0.1	N/A	0.66	0.0	2.0	$^{+1.2}_{-2.0}$	1.0	1.0
2.12–2.33	1.02 (3)	7.3×10^1	7.7	0.0	$^{+8.5}_{-5.6}$	$^{+7.1}_{-3.9}$	$^{+4.7}_{-2.1}$	$^{+4.6}_{-2.3}$	$^{+13}_{-9.5}$	$^{+4.3}_{-2.1}$	$^{+0.89}_{-0.95}$	$^{+12}_{-8.8}$	$^{+6.4}_{-3.5}$	$^{+0.21}_{-0.46}$	0.0	$^{+14}_{-9.9}$	0.02	N/A	2.4	0.42	2.0	$^{+3.4}_{-1.3}$	1.0	1.0
2.33–2.55	1.02 (3)	2.6×10^1	9.7	0.0	$^{+6.6}_{-5.9}$	$^{+4.5}_{-4.6}$	$^{+2.4}_{-3.3}$	$^{+3.0}_{-3.5}$	$^{+12}_{-9.9}$	$^{+2.6}_{-2.7}$	$^{+0.85}_{-1.2}$	$^{+11}_{-8.7}$	$^{+4.9}_{-5.2}$	$^{+0.28}_{-0.37}$	0.0	$^{+14}_{-11}$	0.1	N/A	1.3	0.21	2.0	$^{+1.7}_{-2.0}$	1.0	1.0
2.55–3.04	1.02 (2)	8.0	12	0.0	$^{+7.6}_{-6.7}$	$^{+5.6}_{-5.2}$	$^{+3.6}_{-3.2}$	$^{+4.8}_{-4.2}$	$^{+14}_{-11}$	$^{+3.7}_{-3.0}$	0.69	$^{+13}_{-11}$	$^{+7.2}_{-6.5}$	$^{+0.14}_{-0.23}$	0.0	$^{+15}_{-14}$	0.1	N/A	2.8	0.08	2.0	$^{+1.7}_{-1.6}$	1.0	1.0
3.04–4.27	1.02 (2)	2.3×10^{-1}	51	0.0	$^{+7.4}_{-6.7}$	$^{+5.4}_{-4.8}$	3.4	$^{+5.6}_{-5.1}$	$^{+16}_{-13}$	$^{+2.6}_{-3.3}$	$^{+0.7}_{-0.78}$	$^{+15}_{-13}$	$^{+8.6}_{-8.0}$	$^{+0.3}_{-0.29}$	0.0	$^{+20}_{-18}$	0.4	N/A	2.5	0.18	2.0	$^{+1.3}_{-1.4}$	1.0	1.0

TABLE XXIV. Measured dijet cross section for $R = 0.4$ and $2.5 \leq y^* < 3.0$. See Table XIX for a description of the columns. All tables are available on HEPDATA [71].

m_{12}-bin [TeV]	NPC	σ [pb/TeV]	δ_{stat} %	$\gamma 4$	γ_{10}	γ_{16}	γ_{22}	γ_{28}	γ_{31}	γ_{35}	γ_{41}	γ_{47}	γ_{53}	γ_{59}	γ_{65}	γ_{71}	γ_{74}	γ_{75}	γ_{79}	γ_{82}	γ_{84}	u_1	u_2	u_3
0.67–0.76	1.03 (7)	7.3×10^5	7.1	$^{+4.9}_{-4.8}$	10	8.0	4.2	$^{+2.8}_{-2.6}$	$^{+43}_{-28}$	$^{+3.5}_{-3.3}$	$^{+3.5}_{-3.3}$	$^{+5.3}_{-5.6}$	$^{+0.19}_{-0.09}$	$^{+0.04}_{-0.01}$	$^{+3.6}_{-3.4}$	$^{+0.35}_{-0.22}$	0.1	N/A	4.8	0.17	2.1	$^{+5.5}_{-5.9}$	1.0	$^{+0.75}_{-1.2}$
0.76–0.85	1.03 (6)	3.9×10^5	8.5	$^{+4.2}_{-3.0}$	$^{+11}_{-8.9}$	$^{+9.0}_{-7.4}$	$^{+4.2}_{-3.5}$	$^{+2.7}_{-2.4}$	$^{+39}_{-23}$	$^{+4.1}_{-3.3}$	$^{+3.5}_{-2.6}$	$^{+6.7}_{-5.6}$	$^{+0.16}_{-0.14}$	$^{+0.05}_{-0.0}$	$^{+3.6}_{-2.7}$	$^{+0.68}_{-0.5}$	0.2	N/A	4.7	0.4	2.0	$^{+6.1}_{-4.4}$	1.0	$^{+0.94}_{-1.1}$
0.85–0.95	1.03 (6)	1.9×10^5	4.9	$^{+2.5}_{-2.0}$	$^{+10}_{-8.5}$	$^{+9.0}_{-6.9}$	$^{+4.4}_{-3.1}$	2.6	$^{+32}_{-21}$	$^{+3.9}_{-3.6}$	$^{+2.6}_{-2.4}$	$^{+7.2}_{-5.4}$	$^{+0.31}_{-0.25}$	$^{+0.02}_{-0.0}$	$^{+2.5}_{-2.2}$	$^{+1.2}_{-1.1}$	0.05	N/A	3.1	0.11	2.0	$^{+5.6}_{-4.0}$	1.0	$^{+1.1}_{-0.95}$
0.95–1.06	1.02 (5)	9.1×10^4	3.3	1.3	$^{+9.4}_{-8.1}$	$^{+7.7}_{-6.6}$	$^{+3.4}_{-3.5}$	$^{+2.6}_{-2.7}$	$^{+25}_{-19}$	$^{+3.6}_{-4.0}$	$^{+2.0}_{-2.4}$	$^{+6.0}_{-5.6}$	$^{+0.56}_{-0.53}$	0.0	$^{+1.7}_{-1.9}$	$^{+2.0}_{-2.1}$	0.03	N/A	2.0	0.08	2.0	$^{+4.2}_{-4.5}$	1.0	$^{+1.0}_{-0.97}$
1.06–1.18	1.02 (5)	4.3×10^4	3.4	$^{+0.63}_{-0.61}$	$^{+8.8}_{-8.5}$	$^{+6.5}_{-6.7}$	$^{+3.2}_{-3.6}$	$^{+2.7}_{-2.6}$	$^{+20}_{-17}$	$^{+3.8}_{-4.0}$	$^{+2.2}_{-2.1}$	$^{+5.8}_{-6.3}$	$^{+0.8}_{-0.81}$	$^{+0.09}_{-0.12}$	$^{+1.3}_{-1.2}$	$^{+2.7}_{-3.0}$	0.04	N/A	2.2	0.87	2.0	$^{+3.9}_{-4.5}$	1.0	$^{+1.0}_{-0.99}$
1.18–1.31	1.02 (5)	2.1×10^4	3.5	$^{+0.18}_{-0.16}$	$^{+8.6}_{-9.4}$	$^{+6.1}_{-6.9}$	3.5	2.1	$^{+20}_{-17}$	$^{+3.4}_{-3.7}$	1.7	$^{+6.1}_{-6.8}$	$^{+0.84}_{-0.96}$	$^{+0.07}_{-0.08}$	$^{+0.75}_{-0.58}$	$^{+3.2}_{-3.8}$	0.05	N/A	1.2	0.0	2.0	$^{+3.3}_{-4.1}$	1.0	1.0
1.31–1.45	1.02 (5)	9.9×10^3	3.0	$^{+0.03}_{-0.06}$	$^{+9.5}_{-8.6}$	$^{+6.7}_{-6.1}$	$^{+3.4}_{-3.2}$	$^{+1.6}_{-1.7}$	$^{+20}_{-15}$	$^{+4.2}_{-3.5}$	1.5	$^{+7.2}_{-6.6}$	$^{+1.1}_{-1.2}$	$^{+0.05}_{-0.08}$	$^{+0.24}_{-0.3}$	$^{+4.9}_{-4.5}$	0.06	N/A	0.0	0.0	2.0	$^{+4.1}_{-3.4}$	1.0	1.0
1.45–1.6	1.02 (4)	4.9×10^3	3.4	0.07	$^{+9.4}_{-8.1}$	$^{+6.8}_{-5.8}$	$^{+3.8}_{-3.4}$	$^{+1.8}_{-1.7}$	$^{+16}_{-13}$	$^{+4.4}_{-3.8}$	$^{+1.8}_{-1.6}$	$^{+7.8}_{-6.6}$	$^{+1.8}_{-1.7}$	$^{+0.01}_{-0.12}$	$^{+0.09}_{-0.18}$	$^{+5.9}_{-5.3}$	0.07	N/A	0.93	0.0	2.0	$^{+3.9}_{-3.5}$	1.0	1.0
1.6–1.76	1.02 (4)	2.4×10^3	4.2	0.04	$^{+9.2}_{-7.4}$	$^{+6.6}_{-5.2}$	$^{+4.0}_{-3.4}$	$^{+1.6}_{-1.1}$	$^{+15}_{-12}$	$^{+3.9}_{-3.5}$	$^{+1.4}_{-1.1}$	$^{+7.9}_{-6.4}$	$^{+2.0}_{-1.7}$	$^{+0.0}_{-0.09}$	$^{+0.03}_{-0.0}$	$^{+6.7}_{-5.6}$	0.07	N/A	3.4	2.4	2.0	$^{+3.2}_{-2.9}$	1.0	1.0
1.76–1.94	1.02 (4)	1.0×10^3	5.5	0.02	$^{+9.5}_{-9.3}$	$^{+6.4}_{-6.7}$	$^{+4.3}_{-4.8}$	$^{+1.8}_{-2.0}$	$^{+15}_{-13}$	$^{+4.2}_{-4.3}$	$^{+1.5}_{-2.2}$	8.5	$^{+2.5}_{-2.8}$	$^{+0.07}_{-0.1}$	$^{+0.08}_{-0.02}$	$^{+7.9}_{-8.0}$	0.06	N/A	3.0	0.92	2.0	$^{+3.1}_{-3.4}$	1.0	1.0
1.94–2.12	1.02 (4)	4.7×10^2	6.0	0.0	8.7	$^{+5.9}_{-6.1}$	$^{+4.5}_{-4.3}$	$^{+1.9}_{-1.5}$	13	$^{+4.0}_{-3.6}$	1.5	$^{+8.2}_{-8.4}$	$^{+2.8}_{-2.4}$	$^{+0.17}_{-0.04}$	0.03	$^{+7.9}_{-8.2}$	0.07	N/A	0.89	0.0	2.0	$^{+2.9}_{-2.6}$	1.0	1.0
2.12–2.33	1.02 (4)	2.2×10^2	9.0	0.0	$^{+8.9}_{-10}$	$^{+5.9}_{-7.6}$	$^{+4.7}_{-6.1}$	$^{+2.1}_{-4.0}$	$^{+14}_{-15}$	$^{+3.6}_{-5.4}$	$^{+1.3}_{-1.0}$	$^{+9.0}_{-10}$	$^{+2.9}_{-4.7}$	$^{+0.12}_{-0.13}$	$^{+0.0}_{-0.02}$	$^{+9.0}_{-11}$	0.07	N/A	0.76	0.0	2.0	$^{+3.0}_{-4.5}$	1.0	1.0
2.33–2.55	1.02 (4)	9.6×10^1	11	0.0	$^{+10}_{-8.3}$	$^{+6.9}_{-5.9}$	$^{+5.5}_{-4.7}$	$^{+2.5}_{-3.1}$	$^{+16}_{-13}$	4.3	$^{+1.3}_{-1.0}$	$^{+11}_{-8.9}$	$^{+3.9}_{-4.1}$	$^{+0.09}_{-0.14}$	0.0	$^{+11}_{-9.7}$	0.1	N/A	4.4	2.6	2.0	$^{+3.6}_{-3.2}$	1.0	1.0
2.55–2.78	1.02 (4)	4.6×10^1	19	0.0	$^{+8.0}_{-8.5}$	$^{+5.8}_{-6.5}$	$^{+4.9}_{-5.3}$	$^{+2.4}_{-2.9}$	$^{+16}_{-15}$	$^{+3.8}_{-4.1}$	$^{+0.97}_{-1.6}$	$^{+9.9}_{-10}$	$^{+3.8}_{-4.4}$	$^{+0.07}_{-0.14}$	0.0	$^{+11}_{-12}$	0.1	N/A	3.4	0.67	2.0	$^{+3.0}_{-2.5}$	1.0	1.0
2.78–3.31	1.02 (4)	8.0	16	0.0	$^{+8.8}_{-7.7}$	$^{+5.7}_{-6.1}$	$^{+4.9}_{-5.1}$	$^{+3.3}_{-2.9}$	$^{+18}_{-16}$	$^{+3.8}_{-3.5}$	$^{+0.83}_{-1.1}$	$^{+12}_{-10}$	4.5	$^{+0.2}_{-0.13}$	0.0	$^{+14}_{-12}$	0.07	N/A	3.5	0.24	2.0	$^{+2.2}_{-3.0}$	1.0	1.0
3.31–4.64	1.02 (3)	5.5×10^{-1}	46	0.0	11	$^{+8.5}_{-9.2}$	$^{+8.3}_{-9.1}$	$^{+5.3}_{-5.5}$	$^{+22}_{-21}$	$^{+4.6}_{-4.9}$	$^{+1.7}_{-0.78}$	$^{+16}_{-15}$	$^{+8.5}_{-8.4}$	$^{+0.55}_{-0.13}$	0.0	$^{+19}_{-18}$	0.2	N/A	2.5	0.0	2.0	$^{+4.0}_{-4.7}$	1.0	1.0

TABLE XXV. Measured dijet cross section for $R = 0.4$ and $3.0 \leq y^* < 3.5$. See Table XIX for a description of the columns. All tables are available on HEPDATA [71].

m_{12}-bin [TeV]	NPC	σ [pb/TeV]	δ_{stat} %	$\gamma 5$	γ_{11}	γ_{17}	γ_{23}	γ_{29}	γ_{31}	γ_{36}	γ_{42}	γ_{48}	γ_{54}	γ_{60}	γ_{66}	γ_{72}	γ_{74}	γ_{75}	γ_{80}	γ_{82}	γ_{85}	u_1	u_2	u_3
1.18–1.31	1.02 (7)	5.6×10^4	6.6	$^{+3.8}_{-4.4}$	$^{+12}_{-11}$	$^{+8.9}_{-8.7}$	$^{+4.7}_{-4.8}$	$^{+2.3}_{-3.0}$	$^{+59}_{-33}$	$^{+3.7}_{-4.2}$	$^{+2.7}_{-3.4}$	$^{+6.0}_{-6.6}$	$^{+0.17}_{-0.16}$	0.02	$^{+2.9}_{-3.5}$	$^{+0.53}_{-0.59}$	0.4	N/A	5.8	0.69	2.0	$^{+6.6}_{-7.1}$	2.0	$^{+0.95}_{-1.1}$
1.31–1.45	1.02 (7)	2.6×10^4	6.2	$^{+2.9}_{-3.1}$	$^{+12}_{-10}$	$^{+8.6}_{-8.5}$	$^{+5.3}_{-4.5}$	$^{+2.4}_{-2.9}$	$^{+44}_{-30}$	$^{+4.1}_{-4.5}$	$^{+2.6}_{-2.9}$	$^{+6.3}_{-6.7}$	$^{+0.26}_{-0.27}$	$^{+0.04}_{-0.0}$	$^{+2.8}_{-3.0}$	$^{+1.1}_{-1.2}$	0.3	N/A	3.0	0.7	2.0	$^{+5.6}_{-6.8}$	2.0	$^{+0.78}_{-1.2}$
1.45–1.6	1.01 (7)	1.4×10^4	7.2	$^{+2.4}_{-2.1}$	$^{+11}_{-10}$	$^{+8.2}_{-8.3}$	$^{+5.0}_{-4.9}$	$^{+3.2}_{-3.0}$	$^{+40}_{-27}$	$^{+4.6}_{-4.3}$	$^{+3.0}_{-2.8}$	6.7	$^{+0.48}_{-0.44}$	$^{+0.05}_{-0.0}$	$^{+2.9}_{-2.7}$	1.8	0.0	N/A	3.3	1.4	2.0	$^{+5.6}_{-6.3}$	2.0	$^{+0.88}_{-1.1}$
1.6–1.76	1.01 (7)	7.2×10^3	7.3	$^{+1.6}_{-1.3}$	11	8.4	5.1	$^{+3.6}_{-3.3}$	$^{+39}_{-25}$	$^{+4.9}_{-4.6}$	$^{+3.1}_{-2.6}$	$^{+7.3}_{-7.2}$	$^{+0.73}_{-0.77}$	0.03	$^{+2.2}_{-1.9}$	2.8	0.06	N/A	3.1	0.94	2.0	$^{+6.1}_{-6.6}$	2.0	$^{+0.96}_{-1.0}$
1.76–1.94	1.01 (7)	3.1×10^3	5.0	$^{+0.54}_{-0.43}$	11	$^{+8.5}_{-8.8}$	$^{+5.3}_{-5.5}$	3.2	$^{+34}_{-25}$	$^{+4.7}_{-5.2}$	$^{+2.6}_{-2.4}$	8.0	$^{+0.9}_{-1.1}$	$^{+0.04}_{-0.05}$	$^{+1.0}_{-1.1}$	$^{+3.7}_{-4.3}$	0.0	N/A	3.6	1.8	2.0	$^{+6.3}_{-6.4}$	2.0	$^{+0.99}_{-1.0}$
1.94–2.12	1.01 (6)	1.5×10^3	4.4	$^{+0.06}_{-0.02}$	$^{+11}_{-10}$	$^{+7.7}_{-7.8}$	5.5	$^{+2.7}_{-2.5}$	$^{+30}_{-22}$	$^{+4.6}_{-4.7}$	2.1	7.9	$^{+1.2}_{-1.4}$	$^{+0.09}_{-0.06}$	$^{+0.59}_{-0.63}$	$^{+4.6}_{-4.8}$	0.04	N/A	5.7	3.5	2.0	5.4	2.0	1.0
2.12–2.33	1.01 (6)	6.4×10^2	5.3	$^{+0.1}_{-0.11}$	$^{+11}_{-9.6}$	$^{+7.5}_{-6.8}$	$^{+5.8}_{-5.4}$	$^{+2.3}_{-1.9}$	$^{+26}_{-20}$	$^{+4.6}_{-4.2}$	$^{+2.1}_{-1.7}$	$^{+8.2}_{-7.5}$	$^{+1.7}_{-1.5}$	$^{+0.1}_{-0.07}$	$^{+0.37}_{-0.42}$	$^{+5.8}_{-5.3}$	0.2	N/A	0.09	0.0	2.0	$^{+5.1}_{-4.8}$	2.0	1.0
2.33–2.55	1.01 (6)	2.7×10^2	7.2	$^{+0.0}_{-0.1}$	$^{+10}_{-9.3}$	$^{+7.1}_{-6.8}$	5.7	1.8	$^{+23}_{-20}$	$^{+4.2}_{-4.5}$	$^{+1.7}_{-1.8}$	$^{+8.2}_{-7.9}$	$^{+1.8}_{-2.0}$	$^{+0.05}_{-0.07}$	$^{+0.11}_{-0.28}$	$^{+6.3}_{-6.6}$	0.1	N/A	0.0	0.0	2.0	$^{+4.4}_{-4.7}$	2.0	1.0
2.55–2.78	1.01 (6)	1.1×10^2	9.9	$^{+0.0}_{-0.07}$	11	$^{+7.3}_{-7.9}$	$^{+7.0}_{-7.4}$	$^{+1.8}_{-2.6}$	$^{+32}_{-20}$	$^{+4.5}_{-5.5}$	$^{+1.7}_{-2.5}$	$^{+9.4}_{-9.6}$	$^{+2.3}_{-3.1}$	$^{+0.1}_{-0.12}$	$^{+0.02}_{-0.05}$	$^{+8.1}_{-8.6}$	0.09	N/A	0.0	0.0	2.0	$^{+4.4}_{-5.5}$	2.0	1.0
2.78–3.04	1.01 (6)	4.3×10^1	11	$^{+0.05}_{-0.04}$	$^{+13}_{-12}$	$^{+9.1}_{-8.0}$	$^{+9.1}_{-8.3}$	$^{+2.2}_{-2.7}$	$^{+30}_{-21}$	$^{+5.9}_{-5.4}$	$^{+1.8}_{-2.3}$	$^{+12}_{-11}$	$^{+3.2}_{-3.5}$	$^{+0.15}_{-0.13}$	$^{+0.07}_{-0.03}$	$^{+11}_{-9.8}$	0.09	N/A	5.1	3.1	2.0	$^{+5.5}_{-5.1}$	2.0	1.0
3.04–3.61	1.01 (6)	1.2×10^1	17	$^{+0.03}_{-0.02}$	$^{+14}_{-12}$	$^{+10}_{-8.3}$	$^{+12}_{-9.7}$	$^{+3.1}_{-2.9}$	$^{+28}_{-22}$	$^{+6.7}_{-5.4}$	2.1	$^{+14}_{-12}$	$^{+4.6}_{-4.1}$	$^{+0.09}_{-0.11}$	$^{+0.07}_{-0.05}$	$^{+14}_{-12}$	0.09	N/A	9.6	5.6	2.0	$^{+5.9}_{-4.5}$	2.0	1.0
3.61–5.04	1.01 (5)	4.4×10^{-1}	54	$^{+0.01}_{-0.0}$	$^{+18}_{-15}$	$^{+13}_{-11}$	$^{+17}_{-15}$	$^{+5.0}_{-4.4}$	$^{+35}_{-28}$	$^{+7.7}_{-6.3}$	$^{+2.0}_{-2.5}$	$^{+21}_{-17}$	$^{+7.6}_{-6.1}$	$^{+0.14}_{-0.16}$	0.03	$^{+22}_{-19}$	0.7	N/A	9.9	2.6	2.0	$^{+5.9}_{-4.6}$	2.0	1.0

TABLE XXVI. Measured dijet cross section for $R = 0.4$ and $3.5 \leq y^* < 4.0$. See Table XIX for a description of the columns. All tables are available on HEPDATA [71].

m_{12}-bin [TeV]	NPC	σ [pb/TeV]	δ_{stat} %	$\gamma 6$	γ_{12}	γ_{18}	γ_{24}	γ_{30}	γ_{31}	γ_{37}	γ_{43}	γ_{49}	γ_{55}	γ_{61}	γ_{67}	γ_{73}	γ_{74}	γ_{75}	γ_{81}	γ_{82}	γ_{86}	u_1	u_2	u_3
1.76–1.94	0.989 (10)	8.9×10^3	13	$^{+6.2}_{-5.2}$	$^{+14}_{-12}$	$^{+10}_{-9.1}$	4.9	$^{+3.2}_{-3.0}$	$^{+100}_{-46}$	$^{+4.4}_{-4.1}$	$^{+4.1}_{-3.8}$	$^{+7.4}_{-6.7}$	$^{+0.07}_{-0.2}$	0.01	$^{+4.3}_{-4.0}$	$^{+0.22}_{-0.48}$	0.0	N/A	6.8	0.0	2.1	$^{+11}_{-8.1}$	2.0	$^{+2.3}_{-0.0}$
1.94–2.12	0.989 (10)	3.6×10^3	14	$^{+4.3}_{-4.4}$	$^{+13}_{-11}$	$^{+9.5}_{-9.1}$	$^{+4.1}_{-5.1}$	$^{+3.1}_{-2.8}$	$^{+76}_{-37}$	4.1	$^{+3.6}_{-3.3}$	$^{+7.0}_{-6.9}$	$^{+0.06}_{-0.18}$	$^{+0.0}_{-0.02}$	$^{+3.5}_{-3.6}$	$^{+0.58}_{-0.79}$	0.5	N/A	2.8	0.0	2.0	$^{+7.3}_{-6.9}$	2.0	$^{+0.72}_{-1.3}$
2.12–2.33	0.989 (10)	1.3×10^3	8.9	$^{+1.7}_{-3.0}$	$^{+12}_{-9.6}$	$^{+9.9}_{-8.4}$	$^{+2.8}_{-3.6}$	$^{+2.3}_{-2.0}$	$^{+58}_{-42}$	$^{+3.6}_{-3.5}$	$^{+2.2}_{-2.3}$	6.2	$^{+0.43}_{-0.32}$	0.02	$^{+2.1}_{-2.3}$	$^{+0.81}_{-0.59}$	0.4	N/A	0.0	0.0	2.0	$^{+4.9}_{-6.3}$	2.0	$^{+0.33}_{-1.7}$
2.33–2.55	0.989 (10)	6.1×10^2	8.8	$^{+1.9}_{-2.4}$	$^{+18}_{-12}$	$^{+13}_{-9.9}$	$^{+2.8}_{-4.1}$	$^{+3.6}_{-3.2}$	$^{+86}_{-42}$	$^{+4.3}_{-4.8}$	$^{+3.1}_{-3.0}$	$^{+7.6}_{-7.9}$	$^{+0.27}_{-0.42}$	$^{+0.05}_{-0.02}$	$^{+2.8}_{-2.5}$	$^{+1.8}_{-2.3}$	0.2	N/A	1.3	0.0	2.0	$^{+6.5}_{-7.9}$	2.0	$^{+0.68}_{-1.3}$
2.55–2.78	0.989 (9)	3.0×10^2	8.4	$^{+4.0}_{-1.5}$	$^{+18}_{-16}$	13	$^{+4.5}_{-8.3}$	$^{+6.6}_{-7.4}$	$^{+71}_{-41}$	$^{+7.9}_{-8.8}$	$^{+5.8}_{-6.7}$	$^{+11}_{-12}$	$^{+3.5}_{-4.5}$	$^{+0.09}_{-0.03}$	$^{+4.9}_{-5.8}$	$^{+5.8}_{-6.9}$	0.08	N/A	4.9	4.5	2.0	$^{+9.1}_{-11}$	2.0	$^{+0.91}_{-1.1}$
2.78–3.04	0.989 (9)	1.0×10^2	11	$^{+1.7}_{-0.78}$	$^{+20}_{-15}$	$^{+16}_{-12}$	$^{+9.6}_{-7.3}$	$^{+5.2}_{-5.9}$	$^{+64}_{-37}$	$^{+11}_{-8.2}$	$^{+3.9}_{-5.3}$	$^{+15}_{-12}$	$^{+2.3}_{-2.9}$	$^{+0.06}_{-0.03}$	$^{+2.4}_{-3.7}$	$^{+9.8}_{-7.1}$	0.08	N/A	13	0.32	2.0	$^{+13}_{-9.2}$	2.0	$^{+0.98}_{-1.0}$
3.04–3.31	0.989 (9)	4.0×10^1	15	$^{+0.0}_{-0.2}$	$^{+20}_{-14}$	$^{+16}_{-11}$	$^{+7.8}_{-5.7}$	$^{+4.3}_{-3.9}$	$^{+60}_{-34}$	$^{+9.0}_{-6.9}$	$^{+3.3}_{-3.6}$	$^{+14}_{-12}$	$^{+2.0}_{-1.5}$	$^{+0.06}_{-0.02}$	$^{+0.99}_{-0.91}$	$^{+8.9}_{-7.5}$	0.1	N/A	8.7	0.0	2.0	$^{+9.9}_{-6.9}$	2.0	1.0
3.31–3.93	0.989 (9)	9.3×10^0	21	$^{+0.1}_{-0.33}$	$^{+19}_{-16}$	$^{+13}_{-11}$	$^{+5.6}_{-4.9}$	$^{+3.6}_{-3.2}$	$^{+57}_{-35}$	$^{+7.4}_{-7.2}$	$^{+3.3}_{-3.0}$	$^{+14}_{-13}$	$^{+2.6}_{-2.4}$	$^{+0.15}_{-0.07}$	$^{+0.53}_{-0.12}$	$^{+9.5}_{-9.2}$	0.2	N/A	5.0	0.39	2.0	$^{+6.6}_{-6.5}$	2.0	1.0
3.93–5.47	0.989 (8)	8.6×10^{-2}	68	$^{+0.18}_{-0.24}$	$^{+22}_{-18}$	$^{+15}_{-11}$	$^{+9.2}_{-7.9}$	$^{+3.3}_{-3.5}$	$^{+65}_{-36}$	$^{+11}_{-9.2}$	$^{+3.0}_{-3.5}$	$^{+19}_{-15}$	$^{+4.6}_{-4.7}$	$^{+0.12}_{-0.15}$	$^{+0.22}_{-0.0}$	$^{+17}_{-13}$	0.4	N/A	17	13	2.0	$^{+7.4}_{-6.0}$	2.0	1.0

TABLE XXVII. Measured dijet cross section for $R = 0.4$ and $4.0 \leq y^* < 4.4$. See Table XIX for a description of the columns. All tables are available on HEPDATA [71].

m_{12}-bin [TeV]	NPC	σ [pb/TeV]	δ_{stat} %	$\gamma 6$	γ_{12}	γ_{18}	γ_{24}	γ_{30}	γ_{31}	γ_{37}	γ_{43}	γ_{49}	γ_{55}	γ_{61}	γ_{67}	γ_{73}	γ_{74}	γ_{75}	γ_{81}	γ_{82}	γ_{86}	u_1	u_2	u_3
2.55–3.04	0.937 (15)	2.6×10^2	21	$^{+5.8}_{-6.2}$	$^{+16}_{-14}$	12	$^{+2.0}_{-2.4}$	$^{+2.8}_{-3.1}$	$^{+120}_{-59}$	$^{+4.5}_{-4.7}$	$^{+3.9}_{-4.0}$	$^{+7.7}_{-8.4}$	$^{+0.08}_{-0.29}$	0.0	$^{+4.1}_{-4.5}$	$^{+0.42}_{-0.87}$	0.3	N/A	7.2	3.2	$^{+2.1}_{-2.0}$	$^{+8.9}_{-9.0}$	2.0	1.0
3.04–4.27	0.937 (15)	1.8×10^1	24	$^{+3.9}_{-2.8}$	$^{+18}_{-15}$	$^{+14}_{-13}$	$^{+4.2}_{-2.6}$	$^{+5.8}_{-4.3}$	$^{+110}_{-50}$	7.7	$^{+5.4}_{-3.1}$	11	$^{+2.1}_{-1.1}$	$^{+0.0}_{-0.28}$	$^{+5.1}_{-3.0}$	$^{+4.1}_{-2.5}$	3.0	N/A	2.9	4.1	2.0	$^{+7.9}_{-9.3}$	2.0	1.0

TABLE XXVIII. Measured dijet cross section for $R = 0.6$ and $y^* < 0.5$. See Table XIX for a description of the columns. All tables are available on HEPDATA [71].

m_{12}-bin [TeV]	NPC	σ [pb/TeV]	δ_{stat} %	γ_1	γ_7	γ_{13}	γ_{19}	γ_{25}	γ_{31}	γ_{32}	γ_{38}	γ_{44}	γ_{50}	γ_{56}	γ_{62}	γ_{68}	γ_{74}	γ_{75}	γ_{76}	γ_{82}	γ_{83}	u_1	u_2	u_3
0.07–0.11	1.35 (9)	4.6×10^8	0.97	$^{+6.9}_{-6.2}$	$^{+9.3}_{-8.5}$	$^{+9.6}_{-8.6}$	$^{+5.6}_{-5.1}$	$^{+2.4}_{-2.3}$	$^{+9.6}_{-7.5}$	$^{+2.7}_{-2.6}$	$^{+3.1}_{-2.9}$	$^{+4.5}_{-4.3}$	$^{+0.03}_{-0.02}$	0.0	$^{+3.3}_{-3.1}$	$^{+0.11}_{-0.12}$	0.0	N/A	2.8	0.45	2.1	$^{+5.5}_{-4.9}$	1.0	1.0
0.11–0.16	1.22 (5)	5.6×10^7	0.59	$^{+0.91}_{-0.87}$	$^{+6.9}_{-6.5}$	$^{+5.2}_{-4.8}$	$^{+3.2}_{-2.9}$	$^{+2.5}_{-2.4}$	$^{+4.9}_{-4.2}$	$^{+2.8}_{-2.6}$	1.7	$^{+4.3}_{-4.1}$	$^{+0.22}_{-0.25}$	$^{+0.04}_{-0.03}$	$^{+2.0}_{-1.9}$	$^{+0.74}_{-0.76}$	0.03	N/A	0.89	0.17	2.0	$^{+2.8}_{-2.9}$	1.0	1.0
0.16–0.21	1.15 (3)	1.1×10^7	0.44	$^{+0.57}_{-0.6}$	$^{+6.0}_{-5.6}$	$^{+2.9}_{-2.7}$	2.1	$^{+2.5}_{-2.3}$	$^{+3.1}_{-2.9}$	$^{+3.0}_{-2.9}$	1.3	$^{+4.8}_{-4.5}$	$^{+0.92}_{-0.86}$	$^{+0.05}_{-0.03}$	$^{+0.47}_{-0.49}$	$^{+2.9}_{-2.7}$	0.02	N/A	0.58	0.15	2.0	$^{+1.9}_{-2.2}$	1.0	1.0
0.21–0.26	1.12 (3)	2.9×10^6	0.6	$^{+0.14}_{-0.15}$	$^{+5.7}_{-5.3}$	$^{+2.8}_{-2.9}$	$^{+1.9}_{-2.0}$	1.1	2.3	$^{+2.6}_{-2.7}$	$^{+0.99}_{-1.1}$	$^{+5.0}_{-4.7}$	$^{+1.3}_{-1.4}$	$^{+0.03}_{-0.07}$	$^{+0.04}_{-0.03}$	$^{+3.7}_{-3.6}$	0.0	N/A	0.51	0.05	2.0	$^{+1.6}_{-1.7}$	1.0	1.0
0.26–0.31	1.1 (2)	1.0×10^6	0.65	0.03	$^{+5.2}_{-4.7}$	$^{+2.7}_{-2.4}$	$^{+2.0}_{-1.7}$	$^{+0.76}_{-0.69}$	$^{+2.3}_{-2.1}$	$^{+2.6}_{-2.3}$	$^{+0.89}_{-0.69}$	$^{+5.3}_{-5.0}$	$^{+1.7}_{-1.6}$	$^{+0.04}_{-0.03}$	$^{+0.03}_{-0.0}$	$^{+4.6}_{-4.4}$	0.03	N/A	0.65	0.06	2.0	$^{+1.3}_{-1.1}$	1.0	1.0
0.31–0.37	1.08 (2)	3.8×10^5	0.54	0.0	$^{+4.7}_{-4.5}$	$^{+2.5}_{-2.4}$	$^{+2.0}_{-1.9}$	$^{+1.1}_{-1.0}$	$^{+2.2}_{-2.1}$	$^{+2.5}_{-2.3}$	$^{+0.78}_{-0.71}$	5.4	$^{+2.1}_{-2.0}$	0.11	0.02	5.3	0.08	N/A	0.45	0.07	2.0	$^{+1.2}_{-1.3}$	1.0	1.0
0.37–0.44	1.07 (2)	1.4×10^5	0.5	0.0	$^{+3.7}_{-3.4}$	$^{+3.0}_{-2.8}$	$^{+1.6}_{-1.3}$	$^{+1.6}_{-1.3}$	$^{+2.4}_{-2.0}$	$^{+2.2}_{-2.0}$	$^{+0.69}_{-0.63}$	$^{+6.0}_{-5.3}$	$^{+2.5}_{-2.2}$	$^{+0.1}_{-0.12}$	0.0	$^{+6.3}_{-5.6}$	0.05	N/A	0.55	0.09	2.0	$^{+1.2}_{-0.99}$	1.0	1.0
0.44–0.51	1.06 (1)	5.8×10^4	0.59	0.0	$^{+3.9}_{-3.6}$	$^{+3.4}_{-3.1}$	$^{+1.4}_{-1.3}$	$^{+2.2}_{-2.0}$	$^{+2.2}_{-2.1}$	$^{+2.3}_{-2.1}$	$^{+0.61}_{-0.57}$	$^{+6.3}_{-5.7}$	$^{+3.1}_{-2.9}$	$^{+0.21}_{-0.15}$	0.0	$^{+7.1}_{-6.4}$	0.03	N/A	0.45	0.0	2.0	$^{+0.99}_{-1.1}$	1.0	1.0
0.51–0.59	1.05 (1)	2.4×10^4	0.67	0.0	$^{+4.5}_{-4.6}$	$^{+2.6}_{-2.8}$	1.3	$^{+2.2}_{-2.5}$	$^{+1.9}_{-2.1}$	$^{+1.8}_{-1.9}$	$^{+0.51}_{-0.5}$	6.4	$^{+3.2}_{-3.4}$	$^{+0.19}_{-0.14}$	0.0	$^{+7.5}_{-7.6}$	0.1	N/A	0.19	0.0	2.0	1.0	1.0	1.0
0.59–0.67	1.05 (1)	1.1×10^4	1.0	0.0	$^{+3.6}_{-3.5}$	2.2	$^{+0.91}_{-0.98}$	$^{+2.4}_{-2.5}$	$^{+1.7}_{-1.9}$	$^{+1.5}_{-1.7}$	$^{+0.39}_{-0.35}$	6.2	3.3	$^{+0.13}_{-0.16}$	0.0	$^{+7.8}_{-7.4}$	0.1	N/A	0.41	0.0	2.0	$^{+0.6}_{-0.7}$	1.0	1.0
0.67–0.76	1.04 (1)	4.8×10^3	1.3	0.0	$^{+3.6}_{-3.5}$	$^{+3.0}_{-2.9}$	$^{+0.96}_{-0.85}$	$^{+2.9}_{-2.7}$	$^{+1.9}_{-1.8}$	$^{+1.7}_{-1.6}$	$^{+0.45}_{-0.37}$	$^{+6.9}_{-6.6}$	4.1	$^{+0.21}_{-0.16}$	0.0	$^{+8.8}_{-8.3}$	0.04	N/A	0.36	0.08	2.0	$^{+0.73}_{-0.6}$	1.0	1.0
0.76–0.85	1.04 (1)	2.3×10^3	1.7	0.0	$^{+3.8}_{-4.1}$	$^{+3.5}_{-3.7}$	$^{+0.54}_{-0.64}$	$^{+2.4}_{-2.5}$	$^{+1.8}_{-1.9}$	1.6	$^{+0.31}_{-0.44}$	$^{+6.4}_{-6.6}$	$^{+4.2}_{-4.4}$	$^{+0.14}_{-0.18}$	0.0	8.5	0.05	N/A	0.08	0.0	2.0	$^{+0.56}_{-0.65}$	1.0	1.0
0.85–0.95	1.03 (1)	1.1×10^3	2.1	0.0	$^{+4.2}_{-4.1}$	3.1	$^{+0.61}_{-0.75}$	$^{+2.2}_{-2.3}$	1.7	1.5	$^{+0.32}_{-0.37}$	$^{+6.7}_{-6.2}$	$^{+4.6}_{-4.5}$	$^{+0.11}_{-0.23}$	0.0	$^{+9.1}_{-8.3}$	0.05	N/A	0.35	0.0	2.0	$^{+0.48}_{-0.57}$	1.0	1.0
0.95–1.06	1.03 (1)	5.5×10^2	2.7	0.0	$^{+4.2}_{-4.0}$	$^{+2.3}_{-2.1}$	$^{+0.95}_{-0.9}$	2.3	$^{+1.9}_{-1.6}$	1.5	$^{+0.38}_{-0.42}$	$^{+7.1}_{-6.8}$	$^{+5.2}_{-4.8}$	$^{+0.24}_{-0.23}$	0.0	$^{+10}_{-9.1}$	0.04	N/A	0.43	0.07	2.0	$^{+0.57}_{-0.59}$	1.0	1.0
1.06–1.18	1.03 (1)	2.6×10^2	3.6	0.0	$^{+3.7}_{-3.3}$	$^{+1.8}_{-1.6}$	$^{+0.95}_{-0.78}$	$^{+2.9}_{-2.6}$	$^{+1.8}_{-1.6}$	$^{+1.5}_{-1.3}$	$^{+0.41}_{-0.32}$	$^{+7.4}_{-7.2}$	5.6	$^{+0.55}_{-0.42}$	0.0	10	0.1	N/A	0.25	0.0	2.0	$^{+0.58}_{-0.44}$	1.0	1.0
1.18–1.31	1.03 (1)	1.3×10^2	5.0	0.0	$^{+2.2}_{-2.5}$	$^{+1.7}_{-2.0}$	$^{+0.81}_{-0.73}$	$^{+2.6}_{-3.0}$	$^{+1.2}_{-1.5}$	$^{+1.0}_{-1.1}$	$^{+0.39}_{-0.45}$	$^{+7.2}_{-6.9}$	$^{+5.8}_{-5.6}$	$^{+0.52}_{-0.59}$	0.0	11	0.0	N/A	0.1	0.0	2.0	$^{+0.49}_{-0.46}$	1.0	1.0
1.31–1.45	1.02 (1)	5.4×10^1	7.0	0.0	$^{+2.4}_{-2.7}$	$^{+2.0}_{-2.3}$	$^{+0.51}_{-0.55}$	$^{+3.0}_{-3.1}$	$^{+1.2}_{-1.3}$	$^{+1.1}_{-1.2}$	$^{+0.29}_{-0.37}$	$^{+7.2}_{-7.3}$	$^{+6.0}_{-6.1}$	$^{+0.94}_{-0.96}$	0.0	11	0.02	N/A	0.09	0.0	2.0	$^{+0.28}_{-0.4}$	1.0	1.0
1.45–1.6	1.02 (1)	2.2×10^1	9.8	0.0	$^{+3.5}_{-3.4}$	$^{+2.6}_{-2.3}$	$^{+0.33}_{-0.31}$	$^{+2.9}_{-2.8}$	$^{+1.1}_{-1.2}$	$^{+1.1}_{-0.98}$	$^{+0.33}_{-0.29}$	$^{+8.1}_{-7.6}$	$^{+6.5}_{-6.2}$	$^{+1.3}_{-1.2}$	0.0	$^{+12}_{-11}$	0.1	N/A	0.32	0.0	2.0	$^{+0.32}_{-0.3}$	1.0	1.0
1.6–1.94	1.02 (1)	9.2×10^0	11	0.0	$^{+4.2}_{-4.3}$	$^{+2.9}_{-3.0}$	$^{+0.3}_{-0.49}$	$^{+2.9}_{-3.0}$	1.0	$^{+0.95}_{-1.2}$	$^{+0.33}_{-0.49}$	$^{+8.7}_{-8.1}$	$^{+7.2}_{-6.9}$	$^{+2.1}_{-2.5}$	0.0	$^{+14}_{-13}$	0.04	N/A	0.31	0.0	2.0	$^{+0.33}_{-0.46}$	1.0	1.0
1.94–2.78	1.02 (0)	9.2×10^{-1}	29	0.0	$^{+4.2}_{-3.8}$	$^{+3.6}_{-3.4}$	$^{+0.61}_{-0.53}$	$^{+3.0}_{-2.7}$	$^{+0.74}_{-0.68}$	$^{+0.95}_{-0.86}$	$^{+0.47}_{-0.43}$	$^{+9.0}_{-8.2}$	$^{+8.2}_{-7.5}$	$^{+4.7}_{-4.5}$	0.0	$^{+17}_{-14}$	0.2	N/A	0.85	0.09	2.0	$^{+0.29}_{-0.28}$	1.0	1.0

TABLE XXIX. Measured dijet cross section for $R = 0.6$ and $0.5 \leq y^* < 1.0$. See Table XIX for a description of the columns. All tables are available on HEPDATA [71].

m_{12}-bin [TeV]	NPC	σ [pb/TeV]	δ_{stat}%	γ_1	γ_7	γ_{13}	γ_{19}	γ_{25}	γ_{31}	γ_{32}	γ_{38}	γ_{44}	γ_{50}	γ_{56}	γ_{62}	γ_{68}	γ_{74}	γ_{75}	γ_{76}	γ_{82}	γ_{83}	u_1	u_2	u_3
0.11–0.16	1.28 (6)	1.4×10^8	0.91	$^{+5.3}_{-4.9}$	$^{+8.8}_{-8.1}$	$^{+8.8}_{-8.0}$	$^{+4.9}_{-4.6}$	$^{+2.2}_{-2.3}$	$^{+9.1}_{-7.8}$	$^{+2.5}_{-2.6}$	2.7	$^{+4.4}_{-4.2}$	$^{+0.07}_{-0.03}$	$^{+0.0}_{-0.01}$	2.8	$^{+0.07}_{-0.06}$	0.07	N/A	2.3	0.28	2.1	$^{+5.3}_{-4.6}$	1.0	1.0
0.16–0.21	1.2 (4)	2.5×10^7	0.69	1.2	$^{+6.4}_{-6.0}$	$^{+3.3}_{-3.1}$	2.0	2.4	$^{+4.0}_{-3.6}$	$^{+3.0}_{-2.9}$	$^{+1.2}_{-1.1}$	$^{+4.4}_{-4.3}$	$^{+0.43}_{-0.38}$	0.03	1.2	1.4	0.1	N/A	0.07	0.0	1.9	$^{+1.8}_{-2.6}$	1.0	1.0
0.21–0.26	1.15 (3)	7.1×10^6	0.59	$^{+0.58}_{-0.59}$	$^{+5.8}_{-5.4}$	$^{+2.8}_{-2.5}$	$^{+2.0}_{-1.9}$	$^{+2.4}_{-2.1}$	$^{+3.1}_{-2.9}$	$^{+2.8}_{-2.6}$	$^{+1.2}_{-1.1}$	$^{+4.4}_{-4.3}$	$^{+0.82}_{-0.83}$	$^{+0.06}_{-0.04}$	0.43	$^{+2.7}_{-2.5}$	0.0	N/A	0.63	0.0	2.0	$^{+2.0}_{-2.1}$	1.0	1.0
0.26–0.31	1.12 (3)	2.5×10^6	0.49	$^{+0.12}_{-0.13}$	$^{+6.0}_{-5.9}$	$^{+3.1}_{-3.0}$	2.1	$^{+1.5}_{-1.3}$	$^{+3.1}_{-3.0}$	$^{+2.8}_{-2.7}$	$^{+1.2}_{-1.1}$	$^{+5.3}_{-5.1}$	1.3	0.04	$^{+0.22}_{-0.04}$	$^{+3.9}_{-3.8}$	0.02	N/A	0.61	0.0	2.0	2.1	1.0	1.0
0.31–0.37	1.1 (2)	9.4×10^5	0.61	0.02	$^{+5.5}_{-5.4}$	$^{+2.7}_{-2.8}$	2.0	$^{+0.87}_{-0.91}$	$^{+2.6}_{-2.8}$	2.6	$^{+0.92}_{-0.94}$	$^{+5.1}_{-5.2}$	1.6	$^{+0.06}_{-0.1}$	$^{+0.01}_{-0.02}$	$^{+4.2}_{-4.4}$	0.03	N/A	0.48	0.15	2.0	$^{+1.6}_{-1.7}$	1.0	1.0
0.37–0.44	1.09 (2)	3.5×10^5	0.73	0.0	$^{+5.1}_{-4.8}$	$^{+2.6}_{-2.7}$	$^{+1.9}_{-1.7}$	$^{+1.0}_{-0.94}$	$^{+2.7}_{-2.6}$	2.5	$^{+0.83}_{-0.68}$	$^{+5.6}_{-5.4}$	$^{+1.9}_{-1.8}$	$^{+0.07}_{-0.06}$	$^{+0.0}_{-0.03}$	$^{+5.3}_{-5.2}$	0.02	N/A	0.54	0.08	2.0	$^{+1.3}_{-1.4}$	1.0	1.0
0.44–0.51	1.08 (2)	1.4×10^5	0.71	0.0	$^{+4.5}_{-4.0}$	$^{+3.0}_{-2.7}$	1.6	1.3	$^{+2.8}_{-2.4}$	$^{+2.4}_{-2.3}$	$^{+0.75}_{-0.72}$	$^{+6.1}_{-5.5}$	$^{+2.4}_{-2.2}$	$^{+0.1}_{-0.13}$	0.0	$^{+6.3}_{-5.8}$	0.01	N/A	0.63	0.17	2.0	$^{+1.2}_{-1.4}$	1.0	1.0
0.51–0.59	1.07 (1)	5.9×10^4	0.74	0.0	3.9	$^{+3.2}_{-3.1}$	$^{+1.4}_{-1.5}$	$^{+1.7}_{-1.8}$	$^{+2.8}_{-2.6}$	2.2	0.68	$^{+6.3}_{-6.1}$	2.8	$^{+0.17}_{-0.12}$	0.0	$^{+6.9}_{-6.7}$	0.09	N/A	0.54	0.06	2.0	$^{+1.3}_{-1.2}$	1.0	1.0
0.59–0.67	1.06 (1)	2.6×10^4	0.82	0.0	$^{+4.2}_{-3.6}$	$^{+3.3}_{-2.8}$	1.3	$^{+2.3}_{-2.0}$	$^{+2.8}_{-2.6}$	2.1	0.56	$^{+6.9}_{-5.6}$	$^{+3.2}_{-2.8}$	$^{+0.13}_{-0.14}$	0.0	$^{+7.9}_{-6.6}$	0.08	N/A	0.7	0.1	2.0	$^{+1.0}_{-1.2}$	1.0	1.0
0.67–0.76	1.05 (1)	1.2×10^4	1.0	0.0	$^{+4.1}_{-4.0}$	2.8	$^{+1.1}_{-1.0}$	$^{+2.4}_{-2.5}$	$^{+2.3}_{-2.4}$	$^{+2.0}_{-1.8}$	$^{+0.4}_{-0.43}$	$^{+6.3}_{-6.5}$	$^{+3.4}_{-3.5}$	$^{+0.1}_{-0.15}$	0.0	$^{+7.7}_{-7.9}$	0.01	N/A	0.21	0.12	2.0	$^{+0.98}_{-0.93}$	1.0	1.0
0.76–0.85	1.05 (1)	5.6×10^3	1.2	0.0	$^{+4.3}_{-4.1}$	$^{+2.8}_{-2.9}$	$^{+1.0}_{-1.2}$	$^{+2.9}_{-3.0}$	2.8	$^{+1.9}_{-2.0}$	$^{+0.34}_{-0.57}$	$^{+7.1}_{-6.8}$	$^{+4.1}_{-3.8}$	$^{+0.17}_{-0.22}$	0.0	$^{+8.5}_{-8.3}$	0.07	N/A	0.37	0.0	2.0	$^{+0.87}_{-1.1}$	1.0	1.0
0.85–0.95	1.04 (1)	2.7×10^3	1.4	0.0	$^{+4.3}_{-4.2}$	$^{+3.4}_{-3.0}$	$^{+0.93}_{-0.81}$	$^{+3.1}_{-2.8}$	$^{+3.0}_{-2.7}$	$^{+1.8}_{-1.7}$	$^{+0.56}_{-0.34}$	$^{+7.4}_{-7.0}$	$^{+4.6}_{-4.3}$	$^{+0.23}_{-0.07}$	0.0	$^{+9.6}_{-9.0}$	0.06	N/A	0.43	0.17	2.0	$^{+0.82}_{-0.61}$	1.0	1.0
0.95–1.06	1.04 (1)	1.3×10^3	1.8	0.0	$^{+4.0}_{-4.1}$	3.5	$^{+0.74}_{-0.64}$	2.8	$^{+2.6}_{-2.7}$	$^{+1.6}_{-1.7}$	$^{+0.38}_{-0.39}$	$^{+7.3}_{-7.1}$	$^{+4.4}_{-4.6}$	$^{+0.13}_{-0.2}$	0.0	$^{+9.3}_{-9.0}$	0.04	N/A	0.19	0.0	2.0	$^{+0.62}_{-0.63}$	1.0	1.0
1.06–1.18	1.04 (1)	6.4×10^2	2.6	0.0	$^{+4.1}_{-4.0}$	$^{+3.2}_{-3.0}$	$^{+0.7}_{-0.71}$	$^{+2.3}_{-2.2}$	$^{+2.6}_{-2.5}$	$^{+1.5}_{-1.4}$	$^{+0.33}_{-0.39}$	$^{+6.8}_{-6.6}$	4.7	$^{+0.18}_{-0.16}$	0.0	$^{+9.4}_{-8.8}$	0.0	N/A	0.49	0.0	2.0	$^{+0.58}_{-0.65}$	1.0	1.0
1.18–1.31	1.03 (1)	3.0×10^2	3.5	0.0	$^{+4.5}_{-4.6}$	2.9	$^{+1.2}_{-1.3}$	$^{+2.5}_{-2.7}$	$^{+2.8}_{-3.2}$	$^{+1.6}_{-1.8}$	$^{+0.49}_{-0.52}$	$^{+7.5}_{-7.4}$	$^{+5.2}_{-5.3}$	$^{+0.36}_{-0.42}$	0.0	$^{+11}_{-9.9}$	0.08	N/A	0.25	0.0	2.0	$^{+0.76}_{-0.71}$	1.0	1.0
1.31–1.45	1.03 (1)	1.4×10^2	4.8	0.0	$^{+3.9}_{-3.3}$	$^{+2.0}_{-1.9}$	$^{+1.0}_{-0.88}$	$^{+2.4}_{-2.1}$	$^{+2.7}_{-2.4}$	$^{+1.3}_{-1.1}$	$^{+0.45}_{-0.26}$	$^{+7.6}_{-6.6}$	$^{+5.3}_{-5.0}$	$^{+0.24}_{-0.18}$	0.0	$^{+11}_{-10}$	0.04	N/A	0.49	0.02	2.0	$^{+0.59}_{-0.34}$	1.0	1.0
1.45–1.6	1.03 (1)	6.5×10^1	7.1	0.0	$^{+3.9}_{-2.5}$	$^{+2.4}_{-1.5}$	$^{+0.97}_{-0.87}$	$^{+3.6}_{-2.3}$	$^{+3.5}_{-2.1}$	$^{+1.3}_{-1.0}$	$^{+0.37}_{-0.4}$	$^{+8.8}_{-6.3}$	$^{+7.0}_{-4.9}$	$^{+0.62}_{-0.46}$	0.0	$^{+13}_{-10}$	0.08	N/A	1.1	0.14	2.0	$^{+0.45}_{-0.51}$	1.0	1.0
1.6–1.76	1.03 (1)	3.0×10^1	8.4	0.0	$^{+2.7}_{-3.2}$	$^{+1.9}_{-2.2}$	$^{+0.81}_{-1.0}$	$^{+3.1}_{-3.4}$	$^{+2.8}_{-3.1}$	$^{+1.4}_{-1.3}$	$^{+0.35}_{-0.44}$	$^{+7.7}_{-7.9}$	6.5	$^{+1.0}_{-0.88}$	0.0	$^{+13}_{-12}$	0.1	N/A	0.18	0.13	2.0	$^{+0.55}_{-0.64}$	1.0	1.0
1.76–2.12	1.02 (1)	9.2×10^0	13	0.0	$^{+3.3}_{-3.6}$	$^{+1.9}_{-2.2}$	$^{+0.49}_{-0.37}$	$^{+3.1}_{-3.2}$	$^{+3.0}_{-3.2}$	$^{+1.1}_{-1.3}$	$^{+0.36}_{-0.32}$	$^{+8.3}_{-8.4}$	$^{+6.5}_{-6.8}$	$^{+1.4}_{-1.6}$	0.0	$^{+14}_{-13}$	0.09	N/A	0.24	0.12	2.0	$^{+0.41}_{-0.36}$	1.0	1.0
2.12–3.31	1.02 (1)	1.1×10^0	20	0.0	$^{+5.1}_{-5.0}$	$^{+2.2}_{-2.1}$	$^{+0.41}_{-0.33}$	$^{+3.5}_{-3.4}$	$^{+3.2}_{-3.1}$	$^{+0.97}_{-0.93}$	$^{+0.42}_{-0.37}$	$^{+10}_{-9.2}$	$^{+8.2}_{-7.9}$	3.7	0.0	$^{+17}_{-16}$	0.2	N/A	0.61	0.0	2.0	$^{+0.38}_{-0.34}$	1.0	1.0

TABLE XXX. Measured dijet cross section for $R = 0.6$ and $1.0 \leq y^* < 1.5$. See Table XIX for a description of the columns. All tables are available on HEPDATA [71].

m_{12}-bin [TeV]	NPC	σ [pb/TeV]	δ_{stat} %	γ_2	γ_8	γ_{14}	γ_{20}	γ_{26}	γ_{31}	γ_{33}	γ_{39}	γ_{45}	γ_{51}	γ_{57}	γ_{63}	γ_{69}	γ_{74}	γ_{75}	γ_{77}	γ_{82}	γ_{83}	u_1	u_2	u_3
0.16–0.21	1.3 (7)	7.9×10^7	1.5	$^{+6.2}_{-5.8}$	$^{+9.3}_{-8.9}$	$^{+9.7}_{-8.9}$	$^{+5.2}_{-5.0}$	$^{+2.6}_{-2.5}$	$^{+12}_{-11}$	2.8	$^{+3.1}_{-3.0}$	4.7	$^{+0.01}_{-0.06}$	$^{+0.01}_{-0.0}$	3.2	$^{+0.0}_{-0.02}$	0.03	N/A	2.8	0.4	2.1	$^{+6.5}_{-5.7}$	2.0	1.0
0.21–0.26	1.23 (5)	2.2×10^7	0.99	$^{+0.48}_{-0.62}$	$^{+8.0}_{-7.0}$	$^{+5.5}_{-5.2}$	$^{+3.2}_{-3.3}$	$^{+2.4}_{-2.5}$	$^{+7.3}_{-6.4}$	$^{+3.2}_{-3.3}$	$^{+2.0}_{-1.7}$	$^{+4.8}_{-4.7}$	$^{+0.37}_{-0.2}$	$^{+0.01}_{-0.0}$	$^{+2.3}_{-2.1}$	$^{+1.0}_{-0.82}$	0.0	N/A	0.72	0.27	1.9	$^{+3.3}_{-4.1}$	2.0	1.0
0.26–0.31	1.18 (4)	7.5×10^6	0.97	$^{+0.39}_{-0.41}$	6.8	$^{+3.8}_{-4.1}$	$^{+2.4}_{-2.6}$	$^{+2.8}_{-2.9}$	$^{+5.5}_{-5.7}$	$^{+2.9}_{-3.2}$	$^{+1.3}_{-1.6}$	$^{+4.5}_{-5.0}$	$^{+0.4}_{-0.42}$	$^{+0.06}_{-0.07}$	$^{+1.0}_{-1.2}$	1.9	0.07	N/A	0.2	0.09	2.0	$^{+2.8}_{-3.7}$	2.0	1.0
0.31–0.37	1.15 (3)	2.9×10^6	0.92	$^{+0.21}_{-0.28}$	$^{+6.2}_{-6.6}$	$^{+3.1}_{-3.4}$	2.1	$^{+2.2}_{-2.4}$	$^{+4.5}_{-4.7}$	$^{+2.6}_{-2.8}$	$^{+1.3}_{-1.5}$	$^{+4.9}_{-5.1}$	$^{+0.78}_{-1.0}$	$^{+0.03}_{-0.09}$	$^{+0.45}_{-0.75}$	$^{+2.5}_{-3.0}$	0.06	N/A	0.34	0.0	2.0	$^{+2.6}_{-2.9}$	2.0	1.0
0.37–0.44	1.13 (3)	1.1×10^6	0.8	$^{+0.07}_{-0.08}$	$^{+5.6}_{-5.5}$	$^{+3.1}_{-2.9}$	$^{+1.7}_{-1.9}$	$^{+1.4}_{-1.5}$	3.7	2.7	1.0	4.7	$^{+1.1}_{-1.3}$	$^{+0.08}_{-0.05}$	$^{+0.11}_{-0.1}$	$^{+3.4}_{-3.5}$	0.2	N/A	0.85	0.0	2.0	$^{+2.2}_{-2.3}$	2.0	1.0
0.44–0.51	1.11 (2)	4.3×10^5	1.0	0.02	$^{+5.6}_{-5.8}$	$^{+3.1}_{-3.0}$	$^{+1.9}_{-1.7}$	$^{+1.1}_{-0.87}$	3.7	$^{+2.8}_{-2.7}$	$^{+0.9}_{-0.81}$	$^{+5.1}_{-5.5}$	$^{+1.5}_{-1.4}$	$^{+0.01}_{-0.0}$	$^{+0.04}_{-0.02}$	$^{+4.5}_{-4.8}$	0.2	N/A	0.71	0.0	2.0	$^{+2.1}_{-1.9}$	2.0	1.0
0.51–0.59	1.1 (2)	1.8×10^5	1.1	0.0	$^{+6.1}_{-5.3}$	$^{+3.1}_{-3.0}$	$^{+2.1}_{-1.8}$	$^{+1.1}_{-1.0}$	$^{+4.3}_{-3.5}$	$^{+2.8}_{-2.7}$	$^{+0.85}_{-0.89}$	$^{+6.4}_{-5.5}$	$^{+2.1}_{-1.9}$	$^{+0.1}_{-0.07}$	$^{+0.04}_{-0.01}$	$^{+5.9}_{-5.2}$	0.06	N/A	0.82	0.06	2.0	$^{+2.0}_{-1.7}$	2.0	1.0
0.59–0.67	1.08 (2)	7.9×10^4	1.1	0.0	$^{+5.1}_{-4.9}$	$^{+2.8}_{-2.6}$	1.7	$^{+1.2}_{-1.1}$	$^{+3.6}_{-3.8}$	$^{+2.5}_{-2.4}$	$^{+0.82}_{-0.8}$	$^{+5.7}_{-6.0}$	$^{+2.2}_{-2.0}$	$^{+0.14}_{-0.19}$	$^{+0.01}_{-0.0}$	$^{+5.8}_{-6.3}$	0.1	N/A	0.27	0.0	2.0	$^{+1.6}_{-1.9}$	2.0	1.0
0.67–0.76	1.07 (2)	3.7×10^4	1.1	0.0	$^{+4.0}_{-4.5}$	$^{+2.8}_{-3.3}$	$^{+1.5}_{-1.8}$	$^{+1.4}_{-1.8}$	$^{+3.4}_{-3.9}$	$^{+2.4}_{-2.6}$	$^{+0.64}_{-1.2}$	6.2	$^{+2.4}_{-2.9}$	$^{+0.0}_{-0.09}$	0.0	$^{+6.9}_{-6.5}$	0.08	N/A	0.5	0.0	2.0	$^{+1.6}_{-1.8}$	2.0	1.0
0.76–0.85	1.07 (1)	1.7×10^4	1.4	0.0	$^{+4.0}_{-3.8}$	$^{+3.3}_{-3.2}$	$^{+1.5}_{-1.2}$	$^{+2.1}_{-1.8}$	$^{+4.0}_{-3.9}$	$^{+2.7}_{-2.5}$	$^{+0.83}_{-0.7}$	6.4	$^{+3.1}_{-2.9}$	$^{+0.17}_{-0.1}$	0.0	$^{+7.4}_{-7.0}$	0.07	N/A	0.69	0.0	2.0	$^{+1.6}_{-1.5}$	2.0	1.0
0.85–0.95	1.06 (1)	8.4×10^3	1.3	0.0	$^{+4.1}_{-4.4}$	$^{+2.9}_{-3.3}$	1.1	$^{+2.1}_{-2.5}$	4.4	$^{+2.0}_{-2.4}$	$^{+0.37}_{-0.39}$	$^{+7.2}_{-7.3}$	$^{+3.0}_{-3.7}$	$^{+0.1}_{-0.02}$	0.0	$^{+8.0}_{-8.8}$	0.03	N/A	0.18	0.0	2.0	$^{+1.1}_{-1.7}$	2.0	1.0
0.95–1.06	1.05 (1)	4.1×10^3	1.5	0.0	$^{+4.6}_{-4.1}$	$^{+3.4}_{-2.9}$	1.3	$^{+3.0}_{-2.6}$	$^{+4.2}_{-3.8}$	$^{+2.3}_{-2.1}$	$^{+0.81}_{-0.77}$	$^{+7.7}_{-6.5}$	$^{+3.9}_{-3.4}$	$^{+0.39}_{-0.17}$	0.0	$^{+9.3}_{-8.0}$	0.07	N/A	0.73	0.24	2.0	$^{+1.5}_{-1.6}$	2.0	1.0
1.06–1.18	1.05 (1)	2.0×10^3	1.9	0.0	$^{+3.7}_{-3.9}$	$^{+2.9}_{-3.3}$	$^{+1.1}_{-1.3}$	$^{+2.8}_{-3.1}$	$^{+3.7}_{-3.9}$	$^{+2.0}_{-2.1}$	$^{+0.84}_{-0.7}$	$^{+6.7}_{-6.5}$	$^{+3.8}_{-3.7}$	$^{+0.22}_{-0.35}$	0.0	$^{+8.3}_{-7.7}$	0.02	N/A	0.65	0.08	2.0	$^{+1.1}_{-1.4}$	2.0	1.0
1.18–1.31	1.05 (1)	9.0×10^2	2.6	0.0	$^{+3.6}_{-5.5}$	$^{+2.7}_{-4.1}$	$^{+1.2}_{-0.76}$	$^{+2.7}_{-3.6}$	$^{+4.3}_{-5.2}$	$^{+1.5}_{-2.1}$	$^{+0.21}_{-0.52}$	$^{+7.5}_{-8.8}$	$^{+3.5}_{-5.5}$	$^{+0.11}_{-0.14}$	0.0	$^{+9.9}_{-11}$	0.2	N/A	0.0	0.0	2.0	1.1	2.0	1.0
1.31–1.45	1.04 (1)	4.6×10^2	3.3	0.0	$^{+4.6}_{-5.0}$	3.8	$^{+0.95}_{-1.0}$	$^{+3.3}_{-3.5}$	$^{+4.7}_{-4.8}$	2.1	$^{+0.53}_{-0.36}$	$^{+7.3}_{-7.9}$	$^{+4.7}_{-5.2}$	$^{+0.18}_{-0.26}$	0.0	$^{+10}_{-11}$	0.03	N/A	0.39	0.0	2.0	$^{+1.1}_{-0.98}$	2.0	1.0
1.45–1.6	1.04 (1)	2.1×10^2	3.7	0.0	$^{+5.8}_{-4.4}$	$^{+4.1}_{-3.5}$	$^{+1.6}_{-1.0}$	$^{+3.2}_{-2.9}$	$^{+6.0}_{-4.6}$	$^{+2.0}_{-1.7}$	$^{+0.86}_{-0.39}$	$^{+9.5}_{-7.8}$	$^{+6.2}_{-4.7}$	$^{+0.53}_{-0.19}$	0.0	$^{+13}_{-10}$	0.2	N/A	0.98	0.26	2.0	$^{+1.3}_{-0.77}$	2.0	1.0
1.6–1.76	1.04 (1)	9.3×10^1	5.3	0.0	$^{+4.9}_{-4.7}$	$^{+3.6}_{-3.4}$	1.2	$^{+2.6}_{-2.5}$	$^{+5.1}_{-4.8}$	1.6	$^{+0.34}_{-0.52}$	$^{+8.2}_{-7.6}$	5.3	$^{+0.18}_{-0.14}$	0.0	$^{+12}_{-10}$	0.05	N/A	0.63	0.04	2.0	$^{+0.65}_{-0.74}$	2.0	1.0
1.76–1.94	1.03 (1)	3.8×10^1	9.3	0.0	$^{+5.6}_{-5.0}$	$^{+3.2}_{-3.0}$	$^{+1.4}_{-1.3}$	$^{+2.9}_{-2.4}$	$^{+5.8}_{-5.6}$	$^{+1.7}_{-1.5}$	$^{+0.44}_{-0.28}$	$^{+9.1}_{-7.8}$	$^{+6.5}_{-6.0}$	$^{+0.38}_{-0.0}$	0.0	12	0.2	N/A	0.42	0.0	2.0	$^{+0.6}_{-0.58}$	2.0	1.0
1.94–2.12	1.03 (1)	2.1×10^1	10	0.0	$^{+4.2}_{-3.8}$	$^{+2.1}_{-2.4}$	1.3	$^{+2.7}_{-2.8}$	$^{+4.8}_{-5.7}$	$^{+1.0}_{-1.4}$	$^{+0.07}_{-0.59}$	$^{+8.2}_{-7.2}$	$^{+6.0}_{-5.7}$	$^{+0.19}_{-0.74}$	0.0	$^{+12}_{-11}$	0.09	N/A	0.31	0.06	2.0	$^{+0.74}_{-0.79}$	2.0	1.0
2.12–2.55	1.03 (1)	6.9×10^0	14	0.0	$^{+4.7}_{-4.3}$	$^{+2.9}_{-1.9}$	$^{+2.1}_{-1.6}$	$^{+4.5}_{-3.9}$	$^{+7.5}_{-6.4}$	$^{+2.2}_{-1.3}$	$^{+0.63}_{-0.19}$	$^{+9.9}_{-9.6}$	$^{+8.1}_{-7.4}$	$^{+1.1}_{-0.74}$	0.0	$^{+17}_{-14}$	0.2	N/A	0.9	0.0	2.0	$^{+1.0}_{-0.5}$	2.0	1.0
2.55–3.61	1.02 (0)	5.8×10^{-1}	33	0.0	$^{+4.9}_{-3.9}$	$^{+1.8}_{-1.2}$	$^{+0.39}_{-0.34}$	$^{+4.5}_{-3.3}$	$^{+8.0}_{-6.2}$	$^{+1.5}_{-0.91}$	$^{+0.43}_{-0.35}$	$^{+11}_{-8.5}$	$^{+9.4}_{-7.1}$	2.2	0.0	$^{+19}_{-16}$	0.4	N/A	1.8	0.11	2.0	$^{+0.44}_{-0.39}$	2.0	1.0

TABLE XXXI. Measured dijet cross section for $R = 0.6$ and $1.5 \leq y^* < 2.0$. See Table XIX for a description of the columns. All tables are available on HEPDATA [71].

m_{12}-bin [TeV]	NPC	σ [pb/TeV]	δ_{stat} %	γ_3	γ_9	γ_{15}	γ_{21}	γ_{27}	γ_{31}	γ_{34}	γ_{40}	γ_{46}	γ_{52}	γ_{58}	γ_{64}	γ_{70}	γ_{74}	γ_{75}	γ_{78}	γ_{82}	γ_{83}	u_1	u_2	u_3
0.26–0.31	1.29 (7)	2.5×10^7	2.3	$^{+5.9}_{-5.5}$	$^{+10}_{-9.1}$	$^{+9.8}_{-8.9}$	$^{+5.2}_{-4.9}$	$^{+2.6}_{-2.5}$	$^{+16}_{-14}$	$^{+3.2}_{-3.1}$	$^{+3.2}_{-2.9}$	$^{+5.0}_{-4.9}$	$^{+0.03}_{-0.0}$	$^{+0.01}_{-0.0}$	$^{+3.5}_{-3.3}$	$^{+0.05}_{-0.0}$	0.1	N/A	3.2	0.35	$^{+2.1}_{-2.0}$	$^{+7.4}_{-6.8}$	2.0	1.0
0.31–0.37	1.24 (6)	9.6×10^6	2.3	$^{+1.8}_{-1.9}$	$^{+8.9}_{-7.6}$	$^{+7.3}_{-6.3}$	$^{+3.3}_{-3.2}$	2.3	$^{+12}_{-9.6}$	$^{+3.0}_{-2.9}$	$^{+2.0}_{-2.1}$	$^{+4.6}_{-4.8}$	$^{+0.07}_{-0.17}$	$^{+0.02}_{-0.1}$	$^{+2.4}_{-2.5}$	$^{+0.53}_{-0.71}$	0.04	N/A	1.7	0.13	2.0	$^{+4.9}_{-5.0}$	2.0	1.0
0.37–0.44	1.2 (5)	3.6×10^6	1.4	$^{+0.38}_{-0.35}$	$^{+7.9}_{-7.1}$	$^{+5.5}_{-5.2}$	$^{+3.4}_{-3.0}$	$^{+2.9}_{-3.0}$	$^{+9.4}_{-8.5}$	$^{+3.2}_{-3.0}$	$^{+1.7}_{-1.8}$	$^{+5.3}_{-4.8}$	$^{+0.54}_{-0.43}$	0.07	$^{+1.6}_{-1.8}$	1.4	0.04	N/A	1.4	0.06	2.0	$^{+4.9}_{-4.7}$	2.0	1.0
0.44–0.51	1.17 (4)	1.4×10^6	1.5	$^{+0.0}_{-0.14}$	$^{+7.1}_{-8.0}$	$^{+4.6}_{-4.7}$	$^{+2.8}_{-2.9}$	3.4	$^{+8.0}_{-8.3}$	$^{+3.7}_{-3.8}$	$^{+1.8}_{-2.0}$	$^{+5.6}_{-5.8}$	$^{+0.85}_{-1.1}$	0.0	$^{+0.73}_{-1.0}$	$^{+3.1}_{-3.0}$	0.0	N/A	0.63	0.0	2.0	$^{+4.5}_{-5.1}$	2.0	1.0
0.51–0.59	1.15 (4)	5.9×10^5	1.5	$^{+0.1}_{-0.12}$	$^{+7.2}_{-7.0}$	$^{+3.8}_{-3.9}$	$^{+1.7}_{-2.4}$	$^{+2.4}_{-2.7}$	$^{+7.4}_{-6.6}$	$^{+3.1}_{-3.3}$	$^{+1.1}_{-1.5}$	$^{+5.4}_{-5.5}$	$^{+0.63}_{-1.0}$	$^{+0.0}_{-0.06}$	$^{+0.17}_{-0.15}$	$^{+3.5}_{-3.7}$	0.2	N/A	0.54	0.0	2.0	$^{+3.3}_{-4.0}$	2.0	1.0
0.59–0.67	1.13 (3)	2.6×10^5	1.6	$^{+0.09}_{-0.07}$	$^{+6.5}_{-6.0}$	$^{+3.6}_{-3.4}$	$^{+2.1}_{-2.2}$	2.0	5.7	$^{+2.8}_{-3.0}$	$^{+1.4}_{-1.3}$	$^{+5.4}_{-5.2}$	$^{+1.5}_{-1.4}$	$^{+0.24}_{-0.07}$	$^{+0.07}_{-0.0}$	$^{+4.0}_{-4.1}$	0.09	N/A	1.0	0.0	2.0	3.0	2.0	1.0
0.67–0.76	1.12 (3)	1.2×10^5	1.7	0.02	6.4	3.6	$^{+2.0}_{-2.3}$	$^{+1.5}_{-1.3}$	$^{+5.8}_{-5.5}$	$^{+3.1}_{-3.3}$	$^{+1.2}_{-0.99}$	$^{+6.0}_{-6.1}$	$^{+2.2}_{-1.7}$	$^{+0.09}_{-0.04}$	0.03	$^{+5.2}_{-5.3}$	0.2	N/A	0.87	0.26	2.0	$^{+3.1}_{-3.2}$	2.0	1.0
0.76–0.85	1.1 (3)	5.7×10^4	2.1	0.0	$^{+7.0}_{-6.8}$	$^{+3.3}_{-3.2}$	$^{+1.7}_{-1.6}$	$^{+0.94}_{-0.54}$	6.0	$^{+3.0}_{-2.7}$	$^{+0.57}_{-0.58}$	6.6	$^{+1.9}_{-1.4}$	$^{+0.12}_{-0.0}$	$^{+0.02}_{-0.07}$	6.3	0.01	N/A	0.85	0.33	2.0	$^{+2.6}_{-2.3}$	2.0	1.0
0.85–0.95	1.09 (2)	2.8×10^4	2.1	0.0	$^{+5.6}_{-5.4}$	$^{+2.4}_{-2.6}$	$^{+1.4}_{-1.5}$	$^{+0.89}_{-0.83}$	$^{+5.1}_{-4.9}$	$^{+2.1}_{-2.3}$	$^{+0.6}_{-1.0}$	$^{+5.8}_{-6.2}$	$^{+1.5}_{-1.9}$	$^{+0.0}_{-0.13}$	$^{+0.0}_{-0.02}$	$^{+6.1}_{-6.8}$	0.2	N/A	0.08	0.17	2.0	$^{+1.8}_{-2.2}$	2.0	1.0
0.95–1.06	1.08 (2)	1.4×10^4	2.3	0.0	$^{+5.2}_{-5.6}$	$^{+3.7}_{-3.4}$	$^{+1.5}_{-1.6}$	$^{+1.7}_{-2.1}$	$^{+6.0}_{-6.1}$	$^{+3.7}_{-3.1}$	$^{+1.4}_{-0.94}$	$^{+6.6}_{-6.4}$	$^{+3.2}_{-3.0}$	$^{+0.17}_{-0.1}$	0.0	$^{+6.9}_{-7.1}$	0.1	N/A	0.58	0.25	2.0	$^{+2.6}_{-3.1}$	2.0	1.0
1.06–1.18	1.08 (2)	6.3×10^3	2.5	0.0	$^{+5.6}_{-4.0}$	$^{+4.1}_{-2.7}$	$^{+2.3}_{-1.2}$	$^{+2.6}_{-1.7}$	$^{+6.9}_{-5.8}$	$^{+3.5}_{-2.4}$	$^{+1.2}_{-0.58}$	$^{+8.0}_{-7.2}$	$^{+3.6}_{-2.6}$	$^{+0.17}_{-0.04}$	0.0	$^{+8.6}_{-7.7}$	0.1	N/A	1.4	1.0	2.0	$^{+2.9}_{-2.1}$	2.0	1.0
1.18–1.31	1.07 (2)	3.1×10^3	2.6	0.0	$^{+3.5}_{-3.3}$	$^{+1.5}_{-2.9}$	$^{+1.2}_{-1.6}$	$^{+1.2}_{-2.0}$	$^{+6.2}_{-5.3}$	$^{+1.3}_{-2.3}$	$^{+0.53}_{-1.1}$	$^{+8.1}_{-6.6}$	$^{+1.2}_{-3.1}$	$^{+0.0}_{-0.07}$	0.0	$^{+9.1}_{-7.5}$	0.4	N/A	1.6	0.38	2.0	$^{+1.1}_{-2.1}$	2.0	1.0
1.31–1.45	1.06 (2)	1.4×10^3	3.2	0.0	$^{+5.3}_{-4.1}$	$^{+4.3}_{-3.8}$	1.2	$^{+2.3}_{-3.2}$	$^{+7.3}_{-6.1}$	$^{+2.2}_{-2.9}$	$^{+0.58}_{-0.66}$	$^{+9.1}_{-7.3}$	$^{+4.7}_{-3.7}$	$^{+0.24}_{-0.26}$	0.0	$^{+10}_{-9.6}$	0.2	N/A	0.15	0.0	2.0	$^{+2.6}_{-2.0}$	2.0	1.0
1.45–1.6	1.06 (2)	6.7×10^2	3.7	0.0	$^{+5.5}_{-4.7}$	$^{+5.3}_{-4.0}$	$^{+1.6}_{-1.3}$	$^{+4.7}_{-3.3}$	$^{+7.7}_{-6.0}$	$^{+3.9}_{-2.3}$	$^{+0.52}_{-1.0}$	$^{+8.2}_{-7.7}$	$^{+5.6}_{-4.4}$	0.26	0.0	$^{+11}_{-9.0}$	0.05	N/A	1.8	0.0	2.0	$^{+3.1}_{-1.7}$	2.0	1.0
1.6–1.76	1.06 (2)	3.0×10^2	4.5	0.0	$^{+3.3}_{-4.0}$	$^{+2.2}_{-2.1}$	$^{+0.93}_{-0.76}$	$^{+1.6}_{-2.3}$	$^{+5.9}_{-6.6}$	$^{+1.2}_{-0.88}$	$^{+0.72}_{-0.0}$	$^{+7.9}_{-8.2}$	$^{+3.1}_{-3.5}$	$^{+0.0}_{-0.03}$	0.0	$^{+11}_{-9.8}$	0.4	N/A	1.9	0.42	2.0	$^{+1.3}_{-0.51}$	2.0	1.0
1.76–1.94	1.05 (1)	1.4×10^2	5.0	0.0	$^{+6.1}_{-4.3}$	$^{+4.1}_{-3.9}$	$^{+1.5}_{-1.9}$	$^{+3.6}_{-3.2}$	$^{+8.6}_{-6.3}$	$^{+2.7}_{-3.0}$	$^{+0.64}_{-1.2}$	$^{+11}_{-7.3}$	$^{+6.1}_{-4.6}$	$^{+0.11}_{-0.02}$	0.0	$^{+13}_{-9.8}$	0.06	N/A	1.5	0.02	2.0	$^{+1.4}_{-3.1}$	2.0	1.0
1.94–2.12	1.05 (1)	6.0×10^1	7.9	0.0	$^{+6.1}_{-6.4}$	$^{+5.5}_{-5.7}$	2.2	$^{+5.3}_{-5.1}$	$^{+9.0}_{-7.9}$	2.7	$^{+1.1}_{-0.33}$	$^{+11}_{-8.5}$	$^{+6.1}_{-5.7}$	$^{+0.87}_{-0.02}$	0.0	$^{+12}_{-9.9}$	0.5	N/A	0.76	0.0	2.0	$^{+2.3}_{-1.8}$	2.0	1.0
2.12–2.33	1.04 (1)	2.8×10^1	10	0.0	$^{+8.4}_{-7.0}$	$^{+6.2}_{-4.4}$	$^{+1.6}_{-1.8}$	$^{+5.3}_{-4.1}$	$^{+9.7}_{-9.0}$	$^{+2.2}_{-2.3}$	$^{+0.43}_{-0.15}$	$^{+11}_{-9.5}$	$^{+8.6}_{-7.1}$	$^{+0.4}_{-0.28}$	0.0	15	0.1	N/A	0.73	0.0	2.0	$^{+1.4}_{-1.1}$	2.0	1.0
2.33–2.78	1.04 (1)	9.8×10^0	11	0.0	$^{+5.8}_{-4.4}$	$^{+3.5}_{-3.2}$	$^{+1.2}_{-1.5}$	$^{+2.6}_{-2.4}$	$^{+7.3}_{-6.3}$	1.5	$^{+0.46}_{-0.73}$	$^{+9.4}_{-7.9}$	$^{+5.7}_{-4.6}$	$^{+0.14}_{-0.27}$	0.0	$^{+13}_{-12}$	0.09	N/A	1.6	0.0	2.0	$^{+0.81}_{-0.86}$	2.0	1.0
2.78–3.93	1.03 (1)	6.2×10^{-1}	29	0.02	$^{+7.4}_{-6.8}$	$^{+4.0}_{-3.5}$	$^{+2.8}_{-1.8}$	$^{+5.2}_{-3.9}$	$^{+12}_{-13}$	$^{+3.0}_{-2.1}$	$^{+0.29}_{-0.32}$	14	$^{+11}_{-10}$	$^{+0.36}_{-0.35}$	0.0	$^{+21}_{-19}$	0.6	N/A	1.1	0.0	2.0	$^{+1.5}_{-0.86}$	2.0	1.0

TABLE XXXII. Measured dijet cross section for $R = 0.6$ and $2.0 \leq y^* < 2.5$. See Table XIX for a description of the columns. All tables are available on HEPDATA [71].

m_{12}-bin [TeV]	NPC	σ [pb/TeV]	δ_{stat} %	$\gamma 4$	γ_{10}	γ_{16}	γ_{22}	γ_{28}	γ_{31}	γ_{35}	γ_{41}	γ_{47}	γ_{53}	γ_{59}	γ_{65}	γ_{71}	γ_{74}	γ_{75}	γ_{79}	γ_{82}	γ_{84}	u_1	u_2	u_3
0.37–0.44	1.3 (8)	1.3×10^7	3.2	$^{+10}_{-7.3}$	$^{+14}_{-11}$	$^{+15}_{-11}$	$^{+7.8}_{-5.8}$	$^{+3.7}_{-2.6}$	$^{+29}_{-21}$	$^{+3.8}_{-3.1}$	$^{+4.2}_{-3.3}$	$^{+6.8}_{-4.6}$	$^{+0.09}_{-0.0}$	$^{+0.01}_{-0.0}$	$^{+4.3}_{-3.5}$	$^{+0.06}_{-0.0}$	0.05	N/A	7.0	1.1	2.1	$^{+16}_{-8.4}$	1.0	$^{+2.7}_{-0.0}$
0.44–0.51	1.26 (7)	4.8×10^6	3.2	$^{+5.6}_{-5.5}$	$^{+11}_{-10}$	$^{+10}_{-9.4}$	$^{+5.0}_{-5.2}$	$^{+3.2}_{-2.9}$	$^{+25}_{-18}$	$^{+3.6}_{-3.5}$	$^{+3.3}_{-3.2}$	$^{+5.3}_{-5.7}$	$^{+0.1}_{-0.17}$	$^{+0.02}_{-0.04}$	$^{+3.5}_{-3.4}$	$^{+0.28}_{-0.25}$	0.1	N/A	4.2	0.74	2.0	$^{+9.2}_{-8.6}$	1.0	$^{+1.2}_{-0.83}$
0.51–0.59	1.23 (6)	2.0×10^6	3.0	$^{+1.9}_{-2.6}$	$^{+8.6}_{-8.3}$	$^{+7.7}_{-7.5}$	$^{+3.5}_{-3.9}$	$^{+2.7}_{-3.2}$	$^{+18}_{-15}$	$^{+3.4}_{-3.6}$	$^{+2.2}_{-2.5}$	5.5	$^{+0.32}_{-0.29}$	$^{+0.0}_{-0.02}$	$^{+2.3}_{-2.7}$	$^{+0.82}_{-0.91}$	0.02	N/A	2.3	0.31	2.0	$^{+6.3}_{-7.4}$	1.0	$^{+0.67}_{-1.3}$
0.59–0.67	1.2 (5)	8.9×10^5	1.9	$^{+0.67}_{-0.97}$	$^{+8.6}_{-8.2}$	6.4	$^{+2.7}_{-3.3}$	$^{+2.7}_{-3.5}$	$^{+15}_{-13}$	$^{+3.0}_{-3.7}$	$^{+1.7}_{-2.2}$	$^{+5.3}_{-5.8}$	$^{+0.4}_{-0.45}$	$^{+0.04}_{-0.0}$	$^{+1.4}_{-1.7}$	$^{+1.3}_{-1.9}$	0.03	N/A	2.1	0.64	2.0	$^{+6.0}_{-6.7}$	1.0	$^{+0.91}_{-1.1}$
0.67–0.76	1.18 (5)	3.9×10^5	1.9	$^{+0.24}_{-0.21}$	$^{+8.6}_{-7.7}$	$^{+5.6}_{-5.0}$	$^{+2.7}_{-2.6}$	$^{+3.5}_{-3.4}$	$^{+13}_{-11}$	$^{+3.6}_{-3.4}$	$^{+1.7}_{-1.8}$	$^{+5.9}_{-5.7}$	$^{+0.47}_{-0.59}$	0.03	$^{+0.84}_{-0.88}$	$^{+2.7}_{-2.6}$	0.05	N/A	2.9	1.3	2.0	$^{+6.3}_{-5.9}$	1.0	$^{+0.99}_{-1.0}$
0.76–0.85	1.16 (4)	1.9×10^5	1.5	$^{+0.0}_{-0.02}$	$^{+7.5}_{-7.3}$	$^{+4.6}_{-4.2}$	$^{+2.6}_{-2.4}$	$^{+3.4}_{-3.0}$	$^{+11}_{-9.9}$	$^{+3.6}_{-3.3}$	$^{+1.8}_{-1.7}$	$^{+5.7}_{-5.5}$	$^{+0.91}_{-1.0}$	$^{+0.03}_{-0.07}$	$^{+0.44}_{-0.55}$	$^{+3.3}_{-3.4}$	0.04	N/A	2.4	0.85	2.0	$^{+5.4}_{-5.1}$	1.0	1.0
0.85–0.95	1.15 (4)	9.4×10^4	1.4	$^{+0.06}_{-0.07}$	$^{+8.0}_{-7.3}$	$^{+4.6}_{-4.5}$	2.5	3.0	$^{+10}_{-9.1}$	3.7	$^{+1.6}_{-1.5}$	$^{+6.6}_{-6.0}$	1.3	$^{+0.01}_{-0.1}$	$^{+0.14}_{-0.26}$	$^{+4.7}_{-4.5}$	0.04	N/A	1.5	0.06	2.0	$^{+5.3}_{-5.1}$	1.0	1.0
0.95–1.06	1.13 (4)	4.3×10^4	1.6	$^{+0.05}_{-0.04}$	$^{+7.5}_{-6.9}$	$^{+4.2}_{-4.1}$	$^{+2.4}_{-2.3}$	2.2	$^{+9.0}_{-7.9}$	$^{+3.6}_{-3.4}$	1.3	$^{+6.4}_{-5.9}$	1.6	0.05	$^{+0.04}_{-0.0}$	$^{+5.0}_{-5.1}$	0.05	N/A	1.1	0.0	2.0	4.7	1.0	1.0
1.06–1.18	1.12 (3)	2.0×10^4	1.9	0.02	$^{+7.6}_{-7.8}$	$^{+4.0}_{-4.3}$	$^{+2.2}_{-2.4}$	$^{+1.5}_{-1.6}$	$^{+8.8}_{-8.6}$	$^{+3.4}_{-3.6}$	1.2	$^{+6.7}_{-7.2}$	1.8	$^{+0.05}_{-0.06}$	$^{+0.06}_{-0.01}$	$^{+6.1}_{-6.5}$	0.05	N/A	2.3	1.3	2.0	$^{+4.2}_{-4.6}$	1.0	1.0
1.18–1.31	1.11 (3)	9.9×10^3	2.5	0.0	$^{+7.8}_{-7.1}$	3.8	$^{+2.1}_{-2.4}$	$^{+1.3}_{-1.2}$	$^{+9.2}_{-7.9}$	3.3	$^{+1.3}_{-1.2}$	$^{+7.7}_{-6.8}$	2.1	$^{+0.11}_{-0.04}$	$^{+0.02}_{-0.03}$	$^{+7.5}_{-6.5}$	0.05	N/A	3.6	2.0	2.0	$^{+3.8}_{-3.7}$	1.0	1.0
1.31–1.45	1.1 (3)	4.7×10^3	2.7	0.0	$^{+7.0}_{-6.7}$	$^{+3.8}_{-3.6}$	$^{+2.1}_{-2.0}$	$^{+1.4}_{-1.1}$	8.1	$^{+3.4}_{-3.1}$	$^{+0.9}_{-1.0}$	$^{+7.2}_{-7.0}$	$^{+2.4}_{-2.2}$	$^{+0.06}_{-0.03}$	$^{+0.02}_{-0.01}$	$^{+7.2}_{-7.1}$	0.07	N/A	2.3	0.81	2.0	3.6	1.0	1.0
1.45–1.6	1.09 (3)	2.2×10^3	3.5	0.0	$^{+6.0}_{-6.5}$	$^{+3.0}_{-3.6}$	$^{+2.0}_{-2.1}$	$^{+1.4}_{-1.9}$	$^{+8.7}_{-8.3}$	$^{+2.9}_{-3.3}$	$^{+0.92}_{-1.1}$	$^{+8.2}_{-8.1}$	$^{+2.3}_{-3.0}$	$^{+0.05}_{-0.1}$	0.0	$^{+8.5}_{-8.6}$	0.07	N/A	0.0	0.0	2.0	$^{+3.2}_{-3.7}$	1.0	1.0
1.6–1.76	1.09 (3)	1.0×10^3	3.9	0.0	$^{+6.3}_{-5.6}$	$^{+4.2}_{-3.4}$	$^{+2.1}_{-1.8}$	$^{+2.6}_{-2.2}$	$^{+8.7}_{-8.0}$	$^{+3.8}_{-3.0}$	$^{+1.2}_{-0.78}$	$^{+8.6}_{-7.5}$	$^{+4.0}_{-3.3}$	$^{+0.09}_{-0.13}$	0.0	$^{+9.0}_{-8.3}$	0.06	N/A	0.0	0.0	2.0	3.7	1.0	1.0
1.76–1.94	1.08 (2)	4.6×10^2	4.1	0.0	$^{+5.0}_{-4.6}$	$^{+3.2}_{-3.6}$	$^{+1.5}_{-1.4}$	$^{+2.0}_{-1.7}$	$^{+9.0}_{-9.2}$	$^{+2.4}_{-2.7}$	$^{+0.84}_{-0.55}$	$^{+8.8}_{-8.4}$	$^{+2.9}_{-3.2}$	$^{+0.14}_{-0.1}$	0.0	$^{+9.8}_{-9.7}$	0.07	N/A	1.1	0.0	2.0	3.0	1.0	1.0
1.94–2.12	1.08 (2)	2.1×10^2	4.7	0.0	$^{+5.9}_{-3.8}$	$^{+4.9}_{-3.4}$	$^{+2.1}_{-1.7}$	$^{+3.5}_{-2.4}$	$^{+9.7}_{-8.6}$	$^{+3.3}_{-2.7}$	$^{+1.3}_{-0.9}$	$^{+9.4}_{-7.5}$	$^{+4.8}_{-3.0}$	$^{+0.32}_{-0.02}$	0.0	$^{+11}_{-9.3}$	0.1	N/A	2.2	0.18	2.0	$^{+3.9}_{-2.9}$	1.0	1.0
2.12–2.33	1.07 (2)	1.0×10^2	7.0	0.0	$^{+4.8}_{-6.2}$	$^{+3.9}_{-4.4}$	$^{+1.7}_{-1.8}$	$^{+2.8}_{-3.4}$	10	$^{+3.0}_{-2.9}$	$^{+0.65}_{-0.93}$	$^{+9.5}_{-10}$	$^{+4.2}_{-6.1}$	$^{+0.05}_{-0.44}$	0.0	$^{+11}_{-12}$	0.07	N/A	0.44	0.0	2.0	$^{+3.0}_{-3.3}$	1.0	1.0
2.33–2.55	1.07 (2)	4.1×10^1	9.9	0.0	$^{+5.0}_{-5.7}$	$^{+2.8}_{-4.4}$	$^{+1.6}_{-2.0}$	$^{+2.3}_{-4.0}$	$^{+10}_{-8.6}$	$^{+2.8}_{-3.2}$	$^{+0.51}_{-1.1}$	$^{+10}_{-9.0}$	$^{+4.4}_{-5.3}$	$^{+0.34}_{-0.5}$	0.0	$^{+13}_{-11}$	0.1	N/A	1.6	0.33	2.0	$^{+2.4}_{-3.4}$	1.0	1.0
2.55–3.04	1.06 (2)	1.1×10^1	10	0.0	$^{+9.5}_{-6.9}$	$^{+8.1}_{-5.0}$	$^{+2.4}_{-2.3}$	$^{+7.9}_{-4.7}$	$^{+14}_{-10}$	$^{+3.1}_{-3.2}$	$^{+0.8}_{-0.86}$	$^{+15}_{-11}$	$^{+9.1}_{-6.3}$	$^{+0.25}_{-0.18}$	0.0	$^{+18}_{-14}$	0.08	N/A	2.6	0.46	2.0	$^{+3.4}_{-3.2}$	1.0	1.0
3.04–4.27	1.05 (2)	5.1×10^{-1}	35	0.01	$^{+8.7}_{-8.1}$	$^{+6.4}_{-6.2}$	$^{+2.8}_{-3.0}$	$^{+5.6}_{-5.2}$	$^{+13}_{-12}$	$^{+3.1}_{-3.2}$	$^{+0.69}_{-0.88}$	$^{+15}_{-13}$	$^{+8.9}_{-8.8}$	$^{+0.23}_{-0.4}$	0.0	$^{+20}_{-18}$	0.4	N/A	2.1	0.11	2.0	$^{+2.8}_{-3.0}$	1.0	1.0

TABLE XXXIII. Measured dijet cross section for $R = 0.6$ and $2.5 \leq y^* < 3.0$. See Table XIX for a description of the columns. All tables are available on HEPDATA [71].

m_{12}-bin [TeV]	NPC	σ [pb/TeV]	δ_{stat} %	$\gamma 4$	γ_{10}	γ_{16}	γ_{22}	γ_{28}	γ_{31}	γ_{35}	γ_{41}	γ_{47}	γ_{53}	γ_{59}	γ_{65}	γ_{71}	γ_{74}	γ_{75}	γ_{79}	γ_{82}	γ_{84}	u_1	u_2	u_3
0.67–0.76	1.25 (7)	1.4×10^6	5.4	$^{+7.6}_{-5.9}$	$^{+13}_{-10}$	$^{+13}_{-10}$	$^{+5.2}_{-4.6}$	$^{+3.2}_{-2.6}$	$^{+37}_{-26}$	$^{+3.5}_{-3.1}$	$^{+3.6}_{-3.2}$	$^{+6.1}_{-5.3}$	$^{+0.05}_{-0.08}$	$^{+0.04}_{-0.05}$	$^{+3.7}_{-3.4}$	$^{+0.18}_{-0.06}$	0.2	N/A	6.4	0.28	2.1	$^{+15}_{-11}$	1.0	$^{+1.6}_{-0.4}$
0.76–0.85	1.23 (6)	7.3×10^5	6.5	$^{+5.0}_{-4.3}$	$^{+12}_{-11}$	$^{+11}_{-9.7}$	$^{+5.2}_{-4.8}$	$^{+3.5}_{-3.2}$	$^{+30}_{-21}$	$^{+4.5}_{-4.0}$	$^{+3.8}_{-3.2}$	$^{+6.6}_{-6.0}$	$^{+0.54}_{-0.24}$	0.0	$^{+4.0}_{-3.3}$	$^{+1.1}_{-0.55}$	0.2	N/A	3.7	0.69	2.0	$^{+11}_{-10}$	1.0	$^{+0.95}_{-1.1}$
0.85–0.95	1.21 (6)	3.2×10^5	3.8	$^{+2.6}_{-2.7}$	10	$^{+8.4}_{-9.1}$	$^{+4.0}_{-4.2}$	$^{+3.2}_{-3.5}$	$^{+23}_{-19}$	4.2	$^{+2.8}_{-2.5}$	$^{+6.4}_{-6.8}$	$^{+0.45}_{-0.27}$	$^{+0.02}_{-0.0}$	$^{+2.9}_{-2.6}$	$^{+1.4}_{-1.1}$	0.02	N/A	2.4	0.83	2.0	$^{+9.5}_{-9.7}$	1.0	$^{+0.86}_{-1.1}$
0.95–1.06	1.19 (5)	1.5×10^5	2.9	$^{+1.3}_{-1.4}$	$^{+9.9}_{-9.2}$	$^{+7.9}_{-7.2}$	3.5	$^{+3.5}_{-3.7}$	$^{+22}_{-17}$	$^{+4.0}_{-3.9}$	$^{+2.2}_{-2.3}$	$^{+6.6}_{-6.4}$	$^{+0.54}_{-0.57}$	$^{+0.01}_{-0.03}$	1.9	1.7	0.06	N/A	2.7	0.8	2.0	$^{+9.1}_{-8.8}$	1.0	$^{+0.95}_{-1.0}$
1.06–1.18	1.17 (5)	7.7×10^4	3.3	$^{+0.54}_{-0.6}$	$^{+9.2}_{-8.4}$	$^{+6.2}_{-5.8}$	$^{+3.3}_{-2.8}$	$^{+3.7}_{-3.6}$	$^{+19}_{-15}$	3.7	$^{+2.0}_{-2.1}$	$^{+6.0}_{-6.1}$	0.66	$^{+0.0}_{-0.04}$	$^{+1.4}_{-1.3}$	$^{+2.5}_{-2.6}$	0.08	N/A	1.9	0.59	2.0	$^{+8.8}_{-8.5}$	1.0	$^{+0.99}_{-1.0}$
1.18–1.31	1.16 (5)	3.6×10^4	2.8	$^{+0.11}_{-0.16}$	$^{+9.7}_{-8.0}$	$^{+5.5}_{-5.1}$	$^{+3.5}_{-3.2}$	$^{+3.7}_{-4.0}$	$^{+18}_{-14}$	4.0	$^{+1.7}_{-2.0}$	$^{+6.7}_{-6.1}$	$^{+0.89}_{-0.98}$	$^{+0.1}_{-0.04}$	$^{+0.91}_{-0.85}$	$^{+3.6}_{-3.8}$	0.1	N/A	2.2	0.7	2.0	$^{+8.4}_{-8.2}$	1.0	1.0
1.31–1.45	1.15 (4)	1.6×10^4	2.4	$^{+0.06}_{-0.05}$	$^{+9.5}_{-8.8}$	$^{+5.8}_{-5.2}$	$^{+3.4}_{-3.3}$	3.6	$^{+15}_{-13}$	$^{+4.6}_{-4.2}$	$^{+2.4}_{-1.8}$	$^{+7.5}_{-7.2}$	$^{+1.3}_{-1.5}$	$^{+0.08}_{-0.04}$	$^{+0.27}_{-0.4}$	$^{+5.1}_{-5.0}$	0.08	N/A	1.8	0.0	2.0	$^{+8.7}_{-7.4}$	1.0	1.0
1.45–1.6	1.14 (4)	7.8×10^3	2.8	$^{+0.06}_{-0.05}$	$^{+9.0}_{-8.5}$	$^{+5.2}_{-5.1}$	$^{+3.0}_{-3.2}$	$^{+2.8}_{-2.9}$	$^{+14}_{-12}$	4.1	1.7	$^{+7.3}_{-7.2}$	$^{+1.4}_{-1.8}$	$^{+0.05}_{-0.07}$	$^{+0.06}_{-0.1}$	5.7	0.1	N/A	1.2	0.0	2.0	$^{+7.3}_{-6.8}$	1.0	1.0
1.6–1.76	1.13 (4)	3.8×10^3	3.2	0.03	$^{+8.8}_{-8.0}$	$^{+4.6}_{-4.5}$	$^{+3.1}_{-3.2}$	$^{+2.3}_{-2.5}$	$^{+13}_{-10}$	3.9	$^{+1.6}_{-1.8}$	$^{+7.4}_{-7.0}$	2.1	$^{+0.08}_{-0.1}$	$^{+0.02}_{-0.15}$	$^{+6.3}_{-6.2}$	0.1	N/A	2.6	1.4	2.0	$^{+7.1}_{-6.2}$	1.0	1.0
1.76–1.94	1.12 (4)	1.6×10^3	4.6	$^{+0.01}_{-0.02}$	$^{+8.8}_{-8.1}$	$^{+4.6}_{-4.7}$	$^{+3.4}_{-3.5}$	1.9	$^{+12}_{-11}$	3.9	$^{+1.4}_{-1.6}$	$^{+8.2}_{-7.7}$	$^{+2.4}_{-2.3}$	$^{+0.06}_{-0.09}$	$^{+0.0}_{-0.03}$	$^{+7.4}_{-7.2}$	0.08	N/A	2.1	0.08	2.0	$^{+6.3}_{-6.2}$	1.0	1.0
1.94–2.12	1.11 (3)	7.0×10^2	4.8	0.0	$^{+9.7}_{-8.7}$	$^{+5.3}_{-5.4}$	4.4	$^{+1.9}_{-1.5}$	$^{+13}_{-12}$	$^{+4.6}_{-4.7}$	$^{+1.6}_{-1.3}$	$^{+9.8}_{-8.6}$	$^{+3.0}_{-3.5}$	$^{+0.16}_{-0.07}$	$^{+0.04}_{-0.02}$	$^{+9.3}_{-8.5}$	0.1	N/A	1.3	0.0	2.0	$^{+6.5}_{-6.6}$	1.0	1.0
2.12–2.33	1.1 (3)	3.2×10^2	7.9	0.0	$^{+8.8}_{-7.5}$	$^{+4.8}_{-3.9}$	$^{+4.1}_{-3.4}$	$^{+1.8}_{-1.5}$	$^{+13}_{-11}$	$^{+4.3}_{-3.6}$	$^{+1.4}_{-1.0}$	$^{+9.6}_{-8.4}$	$^{+3.3}_{-2.8}$	$^{+0.14}_{-0.08}$	$^{+0.02}_{-0.01}$	$^{+9.7}_{-8.6}$	0.1	N/A	2.2	0.63	2.0	$^{+6.3}_{-5.4}$	1.0	1.0
2.33–2.55	1.1 (3)	1.4×10^2	9.2	0.0	$^{+7.9}_{-8.2}$	$^{+4.5}_{-4.6}$	$^{+3.9}_{-4.0}$	$^{+2.1}_{-2.4}$	13	$^{+4.2}_{-4.3}$	$^{+1.2}_{-1.7}$	9.9	$^{+3.7}_{-3.8}$	$^{+0.08}_{-0.04}$	$^{+0.01}_{-0.0}$	10	0.1	N/A	5.1	4.0	2.0	5.9	1.0	1.0
2.55–2.78	1.09 (3)	5.8×10^1	15	0.0	$^{+7.8}_{-7.6}$	$^{+4.8}_{-5.1}$	$^{+3.8}_{-4.0}$	$^{+2.8}_{-2.9}$	$^{+15}_{-13}$	$^{+4.2}_{-4.3}$	$^{+1.2}_{-1.9}$	11	$^{+4.3}_{-4.6}$	$^{+0.09}_{-0.23}$	0.0	$^{+13}_{-12}$	0.2	N/A	4.8	2.5	2.0	$^{+6.0}_{-5.7}$	1.0	1.0
2.78–3.31	1.08 (3)	1.2×10^1	13	0.0	$^{+7.3}_{-6.5}$	$^{+5.1}_{-4.9}$	$^{+4.1}_{-4.3}$	$^{+3.1}_{-3.5}$	$^{+16}_{-13}$	$^{+3.8}_{-4.0}$	$^{+1.3}_{-0.96}$	$^{+13}_{-10}$	$^{+4.8}_{-5.1}$	$^{+0.18}_{-0.33}$	0.0	$^{+14}_{-12}$	0.1	N/A	3.1	0.0	2.0	$^{+6.0}_{-6.8}$	1.0	1.0
3.31–4.64	1.07 (2)	4.9×10^{-1}	39	0.0	$^{+8.5}_{-8.0}$	$^{+7.2}_{-6.9}$	$^{+6.4}_{-5.7}$	$^{+5.9}_{-5.3}$	$^{+22}_{-18}$	4.9	$^{+0.84}_{-1.5}$	$^{+16}_{-13}$	$^{+7.9}_{-7.7}$	$^{+0.14}_{-0.31}$	0.0	$^{+21}_{-16}$	0.5	N/A	3.8	0.0	2.0	$^{+8.1}_{-7.4}$	1.0	1.0

TABLE XXXIV. Measured dijet cross section for $R = 0.6$ and $3.0 \leq y^* < 3.5$. See Table XIX for a description of the columns. All tables are available on HEPDATA [71].

m_{12}-bin [TeV]	NPC	σ [pb/TeV]	δ_{stat} %	$\gamma 5$	γ_{11}	γ_{17}	γ_{23}	γ_{29}	γ_{31}	γ_{36}	γ_{42}	γ_{48}	γ_{54}	γ_{60}	γ_{66}	γ_{72}	γ_{74}	γ_{75}	γ_{80}	γ_{82}	γ_{85}	u_1	u_2	u_3
1.18–1.31	1.21 (7)	1.3×10^5	9.7	$^{+5.5}_{-6.4}$	13	12	$^{+4.4}_{-4.9}$	2.9	$^{+48}_{-29}$	3.9	$^{+3.1}_{-3.4}$	$^{+6.3}_{-7.3}$	$^{+0.27}_{-0.23}$	$^{+0.15}_{-0.04}$	$^{+3.2}_{-3.5}$	$^{+0.48}_{-0.54}$	0.2	N/A	5.0	0.23	2.0	$^{+15}_{-16}$	2.0	$^{+0.0}_{-2.4}$
1.31–1.45	1.19 (7)	5.4×10^4	6.8	$^{+3.3}_{-3.8}$	$^{+13}_{-11}$	$^{+11}_{-9.7}$	$^{+4.9}_{-4.4}$	$^{+3.5}_{-3.4}$	$^{+37}_{-25}$	$^{+4.3}_{-4.2}$	2.9	$^{+6.7}_{-7.3}$	$^{+0.22}_{-0.24}$	$^{+0.07}_{-0.05}$	$^{+3.0}_{-3.2}$	$^{+0.85}_{-1.0}$	0.0	N/A	3.1	0.49	2.0	$^{+15}_{-13}$	2.0	$^{+0.66}_{-1.3}$
1.45–1.6	1.18 (6)	2.4×10^4	6.5	2.4	$^{+13}_{-10}$	$^{+10}_{-8.3}$	$^{+4.8}_{-4.3}$	$^{+4.2}_{-4.0}$	$^{+33}_{-23}$	$^{+4.9}_{-4.5}$	$^{+2.8}_{-3.0}$	$^{+8.0}_{-7.0}$	$^{+0.58}_{-0.47}$	$^{+0.0}_{-0.04}$	$^{+2.6}_{-2.8}$	$^{+1.9}_{-1.7}$	0.02	N/A	3.9	1.9	2.0	$^{+14}_{-13}$	2.0	$^{+1.2}_{-0.84}$
1.6–1.76	1.16 (6)	1.2×10^4	5.5	$^{+1.2}_{-1.1}$	$^{+11}_{-10}$	$^{+8.5}_{-7.4}$	$^{+4.3}_{-3.9}$	$^{+4.4}_{-4.2}$	$^{+29}_{-22}$	$^{+4.8}_{-4.3}$	$^{+2.6}_{-2.5}$	$^{+7.7}_{-6.8}$	$^{+0.78}_{-0.72}$	$^{+0.0}_{-0.05}$	$^{+1.9}_{-1.8}$	$^{+2.7}_{-2.6}$	0.07	N/A	3.4	0.15	2.0	14	2.0	$^{+1.1}_{-0.9}$
1.76–1.94	1.15 (5)	5.6×10^3	4.4	$^{+0.55}_{-0.33}$	$^{+11}_{-10}$	$^{+8.0}_{-7.0}$	$^{+4.7}_{-3.9}$	$^{+5.1}_{-4.5}$	$^{+27}_{-21}$	$^{+5.3}_{-4.6}$	$^{+2.8}_{-2.4}$	$^{+8.2}_{-7.3}$	$^{+0.99}_{-0.93}$	$^{+0.14}_{-0.03}$	$^{+1.6}_{-1.2}$	$^{+4.0}_{-3.8}$	0.02	N/A	3.2	0.53	2.0	$^{+14}_{-12}$	2.0	$^{+1.0}_{-0.97}$
1.94–2.12	1.14 (5)	2.4×10^3	4.2	$^{+0.18}_{-0.09}$	$^{+11}_{-10}$	$^{+6.9}_{-6.5}$	$^{+4.9}_{-4.2}$	$^{+4.5}_{-4.2}$	$^{+25}_{-20}$	$^{+5.0}_{-4.6}$	$^{+2.4}_{-2.3}$	$^{+8.2}_{-8.0}$	$^{+1.2}_{-1.1}$	$^{+0.08}_{-0.03}$	$^{+0.86}_{-0.7}$	$^{+4.6}_{-4.5}$	0.05	N/A	4.0	2.3	2.0	12	2.0	$^{+1.0}_{-0.99}$
2.12–2.33	1.13 (5)	1.1×10^3	3.0	$^{+0.0}_{-0.06}$	11	$^{+6.3}_{-6.1}$	4.9	$^{+3.8}_{-3.9}$	$^{+22}_{-17}$	4.7	2.0	$^{+8.8}_{-8.2}$	$^{+1.4}_{-1.5}$	$^{+0.0}_{-0.07}$	$^{+0.28}_{-0.37}$	$^{+5.8}_{-5.6}$	0.08	N/A	3.8	1.6	2.0	$^{+13}_{-11}$	2.0	$^{+1.0}_{-0.99}$
2.33–2.55	1.12 (5)	4.5×10^2	5.0	$^{+0.05}_{-0.09}$	$^{+11}_{-10}$	$^{+6.2}_{-5.7}$	$^{+5.7}_{-5.4}$	$^{+3.6}_{-3.4}$	$^{+20}_{-16}$	$^{+5.0}_{-4.6}$	$^{+2.2}_{-2.0}$	$^{+9.3}_{-8.4}$	$^{+2.2}_{-2.0}$	$^{+0.13}_{-0.09}$	$^{+0.23}_{-0.15}$	$^{+7.2}_{-6.6}$	0.07	N/A	0.61	0.0	2.0	$^{+12}_{-10}$	2.0	1.0
2.55–2.78	1.12 (4)	1.9×10^2	7.7	0.05	$^{+11}_{-9.4}$	$^{+5.8}_{-5.2}$	$^{+6.3}_{-5.6}$	$^{+2.9}_{-2.6}$	$^{+19}_{-22}$	$^{+4.9}_{-4.4}$	$^{+2.1}_{-2.0}$	$^{+9.6}_{-8.7}$	$^{+2.6}_{-2.4}$	$^{+0.15}_{-0.05}$	$^{+0.14}_{-0.04}$	$^{+8.1}_{-7.5}$	0.08	N/A	0.0	0.0	2.0	$^{+10}_{-8.8}$	2.0	1.0
2.78–3.04	1.11 (4)	7.3×10^1	9.7	0.03	$^{+12}_{-11}$	6.2	$^{+7.7}_{-7.3}$	2.6	20	5.3	2.0	$^{+11}_{-10}$	$^{+3.2}_{-3.0}$	$^{+0.15}_{-0.11}$	$^{+0.03}_{-0.0}$	$^{+9.9}_{-9.6}$	0.1	N/A	1.2	0.0	2.0	$^{+10}_{-9.3}$	2.0	1.0
3.04–3.61	1.1 (4)	1.9×10^1	15	0.01	$^{+14}_{-12}$	$^{+7.6}_{-6.6}$	$^{+10}_{-8.9}$	$^{+2.9}_{-2.5}$	$^{+23}_{-18}$	$^{+6.4}_{-5.8}$	$^{+2.2}_{-1.8}$	$^{+14}_{-12}$	$^{+4.4}_{-4.0}$	$^{+0.2}_{-0.22}$	$^{+0.03}_{-0.05}$	$^{+14}_{-12}$	0.0	N/A	9.9	4.4	2.0	$^{+11}_{-10}$	2.0	1.0
3.61–5.04	1.09 (3)	8.9×10^{-1}	38	0.0	$^{+15}_{-12}$	$^{+8.2}_{-7.3}$	$^{+14}_{-12}$	$^{+4.0}_{-3.6}$	$^{+29}_{-22}$	$^{+7.1}_{-6.4}$	$^{+2.5}_{-2.1}$	$^{+19}_{-16}$	$^{+6.7}_{-6.2}$	$^{+0.41}_{-0.37}$	$^{+0.02}_{-0.03}$	$^{+20}_{-17}$	0.02	N/A	9.2	1.6	2.0	$^{+12}_{-10}$	2.0	1.0

TABLE XXXV. Measured dijet cross section for $R = 0.6$ and $3.5 \leq y^* < 4.0$. See Table XIX for a description of the columns. All tables are available on HEPDATA [71].

m_{12}-bin [TeV]	NPC	σ [pb/TeV]	δ_{stat} %	$\gamma 6$	γ_{12}	γ_{18}	γ_{24}	γ_{30}	γ_{31}	γ_{37}	γ_{43}	γ_{49}	γ_{55}	γ_{61}	γ_{67}	γ_{73}	γ_{74}	γ_{75}	γ_{81}	γ_{82}	γ_{86}	u_1	u_2	u_3
1.76–1.94	1.18 (10)	1.8×10^4	11	$^{+9.7}_{-8.4}$	$^{+18}_{-15}$	$^{+17}_{-15}$	$^{+6.0}_{-5.3}$	4.6	$^{+85}_{-42}$	$^{+5.4}_{-5.3}$	5.1	$^{+8.9}_{-9.0}$	$^{+0.26}_{-0.08}$	$^{+0.0}_{-0.02}$	$^{+5.4}_{-5.3}$	$^{+0.48}_{-0.24}$	0.6	N/A	8.3	0.71	2.1	$^{+32}_{-19}$	2.0	$^{+0.89}_{-1.1}$
1.94–2.12	1.17 (10)	8.0×10^3	12	$^{+6.3}_{-5.0}$	$^{+15}_{-8.9}$	$^{+14}_{-7.8}$	4.3	$^{+3.5}_{-2.9}$	$^{+72}_{-32}$	$^{+5.0}_{-3.9}$	$^{+3.6}_{-3.0}$	$^{+8.2}_{-3.2}$	$^{+0.48}_{-0.18}$	$^{+0.1}_{-0.0}$	$^{+4.2}_{-3.1}$	$^{+0.99}_{-0.66}$	0.08	N/A	6.7	0.42	2.0	$^{+25}_{-10}$	2.0	$^{+2.5}_{-0.0}$
2.12–2.33	1.16 (9)	3.4×10^3	19	$^{+4.3}_{-3.5}$	$^{+14}_{-7.0}$	$^{+11}_{-5.3}$	$^{+4.5}_{-3.8}$	$^{+4.3}_{-3.5}$	$^{+50}_{-25}$	$^{+5.4}_{-4.2}$	$^{+3.9}_{-3.0}$	$^{+8.0}_{-2.3}$	$^{+0.59}_{-0.26}$	$^{+0.12}_{-0.03}$	$^{+4.0}_{-3.0}$	$^{+1.8}_{-1.1}$	0.07	N/A	4.6	0.0	2.0	$^{+17}_{-9.5}$	2.0	$^{+1.5}_{-0.48}$
2.33–2.55	1.15 (9)	1.2×10^3	9.7	$^{+2.6}_{-2.0}$	$^{+12}_{-28}$	$^{+9.5}_{-26}$	$^{+4.2}_{-2.9}$	$^{+4.0}_{-3.4}$	$^{+39}_{-41}$	$^{+4.8}_{-4.0}$	$^{+2.9}_{-2.5}$	$^{+7.6}_{-25}$	$^{+0.62}_{-0.43}$	$^{+0.06}_{-0.03}$	$^{+2.7}_{-2.3}$	$^{+2.2}_{-1.7}$	0.1	N/A	0.0	0.0	2.0	$^{+15}_{-31}$	2.0	$^{+1.1}_{-0.94}$
2.55–2.78	1.14 (8)	4.8×10^2	8.0	$^{+1.5}_{-1.4}$	$^{+13}_{-22}$	$^{+10}_{-19}$	$^{+4.0}_{-3.9}$	$^{+4.4}_{-5.1}$	$^{+39}_{-36}$	$^{+4.9}_{-5.6}$	$^{+2.8}_{-3.1}$	$^{+8.8}_{-18}$	$^{+0.6}_{-0.84}$	$^{+0.02}_{-0.03}$	$^{+2.1}_{-2.3}$	$^{+2.8}_{-3.3}$	0.2	N/A	0.0	0.0	2.0	$^{+17}_{-25}$	2.0	$^{+1.0}_{-0.99}$
2.78–3.04	1.13 (8)	2.0×10^2	8.4	$^{+0.65}_{-0.77}$	$^{+16}_{-12}$	$^{+11}_{-8.1}$	$^{+4.8}_{-4.9}$	$^{+6.6}_{-6.7}$	$^{+42}_{-28}$	$^{+6.8}_{-7.0}$	$^{+3.2}_{-3.7}$	$^{+12}_{-8.7}$	$^{+1.2}_{-1.6}$	$^{+0.01}_{-0.09}$	$^{+1.7}_{-2.3}$	$^{+4.7}_{-5.2}$	0.1	N/A	2.8	0.0	2.0	$^{+19}_{-13}$	2.0	$^{+1.0}_{-0.99}$
3.04–3.31	1.12 (7)	8.0×10^1	13	0.21	$^{+16}_{-12}$	$^{+10}_{-7.4}$	$^{+5.5}_{-5.4}$	$^{+6.9}_{-6.2}$	$^{+42}_{-25}$	$^{+7.4}_{-6.7}$	$^{+3.6}_{-3.5}$	$^{+12}_{-9.3}$	$^{+2.0}_{-2.2}$	$^{+0.15}_{-0.09}$	$^{+1.5}_{-1.4}$	$^{+7.2}_{-6.6}$	0.4	N/A	4.6	0.0	2.0	$^{+16}_{-13}$	2.0	$^{+1.0}_{-0.99}$
3.31–3.93	1.11 (7)	1.3×10^1	17	$^{+0.02}_{-0.0}$	$^{+17}_{-15}$	$^{+9.6}_{-8.8}$	6.4	6.2	$^{+37}_{-25}$	7.4	$^{+3.4}_{-3.3}$	$^{+13}_{-12}$	$^{+2.8}_{-2.7}$	0.12	$^{+0.84}_{-0.55}$	$^{+9.0}_{-9.3}$	0.2	N/A	5.4	0.0	2.0	$^{+17}_{-15}$	2.0	1.0
3.93–5.47	1.1 (6)	1.7×10^{-1}	43	$^{+0.12}_{-0.14}$	$^{+24}_{-20}$	$^{+13}_{-11}$	$^{+11}_{-9.4}$	$^{+6.3}_{-5.6}$	$^{+37}_{-26}$	$^{+10}_{-9.5}$	$^{+3.7}_{-3.0}$	$^{+21}_{-18}$	$^{+5.3}_{-4.1}$	$^{+0.23}_{-0.32}$	$^{+0.0}_{-0.24}$	$^{+18}_{-16}$	0.4	N/A	16	8.7	2.0	$^{+22}_{-17}$	2.0	1.0

TABLE XXXVI. Measured dijet cross section for $R = 0.6$ and $4.0 \leq y^* < 4.4$. See Table XIX for a description of the columns. All tables are available on HEPDATA [71].

m_{12}-bin [TeV]	NPC	σ [pb/TeV]	δ_{stat} %	γ_6	γ_{12}	γ_{18}	γ_{24}	γ_{30}	γ_{31}	γ_{37}	γ_{43}	γ_{49}	γ_{55}	γ_{61}	γ_{67}	γ_{73}	γ_{74}	γ_{75}	γ_{81}	γ_{82}	γ_{86}	u_1	u_2	u_3
2.55–3.04	1.12 (14)	4.3×10^2	20	$^{+9.5}_{-9.3}$	17	16	$^{+4.2}_{-4.6}$	$^{+4.2}_{-4.7}$	$^{+98}_{-47}$	$^{+5.5}_{-5.8}$	$^{+5.1}_{-5.7}$	$^{+8.3}_{-8.7}$	$^{+0.14}_{-0.49}$	$^{+0.01}_{-0.07}$	$^{+5.6}_{-5.7}$	$^{+0.5}_{-0.98}$	1.0	N/A	7.8	2.8	$^{+2.1}_{-2.0}$	$^{+27}_{-21}$	2.0	1.0
3.04–4.27	1.11 (13)	2.8×10^1	19	$^{+5.9}_{-2.4}$	$^{+25}_{-16}$	$^{+22}_{-14}$	$^{+3.8}_{-2.0}$	$^{+6.7}_{-7.1}$	$^{+94}_{-36}$	$^{+8.9}_{-8.0}$	$^{+5.1}_{-4.1}$	$^{+14}_{-12}$	$^{+0.66}_{-0.86}$	$^{+0.04}_{-0.15}$	$^{+5.6}_{-5.0}$	$^{+3.5}_{-2.3}$	1.0	N/A	9.7	0.0	2.0	$^{+29}_{-18}$	2.0	1.0

[1] UA1 Collaboration, Phys. Lett. B **136**, 294 (1984).
[2] L3 Collaboration, Phys. Lett. B **248**, 464 (1990).
[3] UA2 Collaboration, Phys. Lett. B **257**, 232 (1991).
[4] ZEUS Collaboration, Eur. Phys. J. C **23**, 615 (2002).
[5] ZEUS Collaboration, Phys. Lett. B **547**, 164 (2002).
[6] ALEPH Collaboration, Eur. Phys. J. C **27**, 1 (2003).
[7] DELPHI Collaboration, Eur. Phys. J. C **38**, 413 (2005).
[8] ZEUS Collaboration, Eur. Phys. J. C **42**, 1 (2005).
[9] OPAL Collaboration, Eur. Phys. J. C **47**, 295 (2006).
[10] CDF Collaboration, Phys. Rev. D **75**, 092006 (2007).
[11] D0 Collaboration, Phys. Rev. Lett. **101**, 062001 (2008).
[12] CDF Collaboration, Phys. Rev. D **78**, 052006 (2008).
[13] D0 Collaboration, Phys. Rev. D **80**, 111107 (2009).
[14] D0 Collaboration, Phys. Rev. Lett. **103**, 191803 (2009).
[15] H1 Collaboration, Eur. Phys. J. C **67**, 1 (2010).
[16] H1 Collaboration, Eur. Phys. J. C **65**, 363 (2010).
[17] ZEUS Collaboration, Phys. Lett. B **691**, 127 (2010).
[18] D0 Collaboration, Phys. Lett. B **693**, 531 (2010).
[19] CMS Collaboration, Phys. Rev. Lett. **107**, 132001 (2011).
[20] CMS Collaboration, Phys. Lett. B **700**, 187 (2011).
[21] ATLAS Collaboration, Eur. Phys. J. C **71**, 1512 (2011).
[22] ATLAS Collaboration, JINST **3**, S08003 (2008).
[23] M. Cacciari, G. Salam, and G. Soyez, J. High Energy Phys. 04 (2008) 063.
[24] M. Cacciari and G. P. Salam, Phys. Lett. B **641**, 57 (2006).
[25] C. Buttar, J. D'Hondt, M. Kramer, G. Salam, M. Wobisch *et al.*, in Proceedings of the Workshop on Physics at TeV Colliders, Les Houches, France, 11-29 June 2007, arXiv:0803.0678.
[26] S. Frixione and G. Ridolfi, Nucl. Phys. **B507**, 315 (1997).
[27] T. Sjostrand, S. Mrenna, and P. Z. Skands, J. High Energy Phys. 05 (2006) 026.
[28] A. Sherstnev and R. Thorne, in 16th International Workshop on Deep Inelastic Scattering and Related Subjects (DIS 2008), London (UK), 7-11 Apr 2008, arXiv:0807.2132.
[29] ATLAS Collaboration, Report No. ATLAS-CONF-2010-031.
[30] ATLAS Collaboration, Eur. Phys. J. C **70**, 823 (2010).
[31] S. Agostinelli *et al.*, Nucl. Instrum. Methods Phys. Res., Sect. A **506**, 250 (2003).
[32] Z. Nagy, Phys. Rev. D **68**, 094002 (2003).
[33] S. Alioli, P. Nason, C. Oleari, and E. Re, J. High Energy Phys. 01 (2011) 095.
[34] P. Nason, arXiv:0709.2085.
[35] H.-L. Lai *et al.*, Phys. Rev. D **82**, 074024 (2010).
[36] S. D. Ellis, Z. Kunszt, and D. E. Soper, Phys. Rev. Lett. **69**, 1496 (1992).
[37] A. Martin, W. Stirling, R. Thorne, and G. Watt, Eur. Phys. J. C **63**, 189 (2009).
[38] R. D. Ball *et al.*, Nucl. Phys. **B838**, 136 (2010).
[39] S. Forte, E. Laenen, P. Nason, and J. Rojo, Nucl. Phys. **B834**, 116 (2010).
[40] H1 and ZEUS Collaborations, Reports Nos. H1prelim-10-142 and ZEUS-prel-10-018.
[41] T. Carli *et al.*, Eur. Phys. J. C **66**, 503 (2010).
[42] H.-L. Lai, J. Huston, Z. Li, P. Nadolsky, J. Pumplin *et al.*, Phys. Rev. D **82**, 054021 (2010).

[43] S. Moretti, M. Nolten, and D. Ross, Nucl. Phys. **B759**, 50 (2006).
[44] ATLAS Collaboration, Report No. ATL-PHYS-PUB-2011-009, 2011.
[45] ATLAS Collaboration, Report No. ATL-PHYS-PUB-2011-008, 2011.
[46] P. Z. Skands, in Proceedings of the First International Workshop on Multiple Partonic Interactions at the LHC MPI'08 October 27-31, 2008 Perugia, Italy, p. 284, http://www-library.desy.de/preparch/desy/proc/proc09-06.pdf.
[47] P. Z. Skands, Phys. Rev. D **82**, 074018 (2010).
[48] M. Bahr *et al.*, Eur. Phys. J. C **58**, 639 (2008).
[49] S. Alioli, K. Hamilton, P. Nason, C. Oleari, and E. Re, J. High Energy Phys. 04 (2011) 081.
[50] P. Nason, J. High Energy Phys. 11 (2004) 040.
[51] S. Frixione, P. Nason, and C. Oleari, J. High Energy Phys. 11 (2007) 070.
[52] S. Alioli, P. Nason, C. Oleari, and E. Re, J. High Energy Phys. 06 (2010) 043.
[53] G. Corcella *et al.*, J. High Energy Phys. 01 (2001) 010.
[54] J. M. Butterworth, J. R. Forshaw, and M. H. Seymour, Z. Phys. C **72**, 637 (1996).
[55] ATLAS Collaboration, Report No. ATL-PHYS-PUB-2010-014, 2010.
[56] ATLAS Collaboration, Phys. Lett. B **688**, 21 (2010).
[57] V. Lendermann *et al.*, Nucl. Instrum. Methods Phys. Res., Sect. A **604**, 707 (2009).
[58] W. Lampl *et al.*, Report No. ATLAS-LARG-PUB-2008-002, 2008.
[59] ATLAS Collaboration, arXiv:1112.6426 [Eur. Phys. J. C (to be published)].
[60] ATLAS Collaboration, Eur. Phys. J. C **72**, 1909 (2012).
[61] ATLAS Collaboration, Report No. ATL-TILECAL-2009-009, 2009.
[62] ATLAS Collaboration, Eur. Phys. J. C **71**, 1630 (2011).
[63] ATLAS Collaboration, Report No. ATLAS-CONF-2011-011, 2011.
[64] B. Malaescu, arXiv:0907.3791.
[65] G. D'Agostini, Nucl. Instrum. Methods Phys. Res., Sect. A **362**, 487 (1995).
[66] A. Hoecker and V. Kartvelishvili, Nucl. Instrum. Methods Phys. Res., Sect. A **372**, 469 (1996).
[67] K. Tackmann, A. Hoecker, and H. Lacker, http://root.cern.ch/root/html/TSVDUnfold.html
[68] ATLAS Collaboration, Phys. Rev. D **83**, 052003 (2011).
[69] ATLAS Collaboration, Report No. ATLAS-CONF-2010-054, 2010.
[70] ATLAS Collaboration, Report No. ATLAS-CONF-2011-028, 2011.
[71] ATLAS Collaboration, http://hepdata.cedar.ac.uk/view/irn9320911.

G. Aad,[47] B. Abbott,[110] J. Abdallah,[11] A. A. Abdelalim,[48] A. Abdesselam,[117] O. Abdinov,[10] B. Abi,[111] M. Abolins,[87] H. Abramowicz,[152] H. Abreu,[114] E. Acerbi,[88a,88b] B. S. Acharya,[163a,163b] D. L. Adams,[24] T. N. Addy,[55] J. Adelman,[174] M. Aderholz,[98] S. Adomeit,[97] P. Adragna,[74] T. Adye,[128] S. Aefsky,[22] J. A. Aguilar-Saavedra,[123b,a] M. Aharrouche,[80] S. P. Ahlen,[21] F. Ahles,[47] A. Ahmad,[147] M. Ahsan,[40] G. Aielli,[132a,132b] T. Akdogan,[18a] T. P. A. Åkesson,[78] G. Akimoto,[154] A. V. Akimov,[93] A. Akiyama,[66] A. Aktas,[47] M. S. Alam,[1] M. A. Alam,[75] J. Albert,[168] S. Albrand,[54] M. Aleksa,[29] I. N. Aleksandrov,[64] F. Alessandria,[88a] C. Alexa,[25a] G. Alexander,[152] G. Alexandre,[48] T. Alexopoulos,[9] M. Alhroob,[20] M. Aliev,[15] G. Alimonti,[88a] J. Alison,[119] M. Aliyev,[10] P. P. Allport,[72] S. E. Allwood-Spiers,[52] J. Almond,[81] A. Aloisio,[101a,101b] R. Alon,[170] A. Alonso,[78] B. Alvarez Gonzalez,[87] M. G. Alviggi,[101a,101b] K. Amako,[65] P. Amaral,[29] C. Amelung,[22] V. V. Ammosov,[127] A. Amorim,[123a,b] G. Amorós,[166] N. Amram,[152] C. Anastopoulos,[29] L. S. Ancu,[16] N. Andari,[114] T. Andeen,[34] C. F. Anders,[20] G. Anders,[57a] K. J. Anderson,[30] A. Andreazza,[88a,88b] V. Andrei,[57a] M-L. Andrieux,[54] X. S. Anduaga,[69] A. Angerami,[34] F. Anghinolfi,[29] N. Anjos,[123a] A. Annovi,[46] A. Antonaki,[8] M. Antonelli,[46] A. Antonov,[95] J. Antos,[143b] F. Anulli,[131a] S. Aoun,[82] L. Aperio Bella,[4] R. Apolle,[117,c] G. Arabidze,[87] I. Aracena,[142] Y. Arai,[65] A. T. H. Arce,[44] J. P. Archambault,[28] S. Arfaoui,[82] J-F. Arguin,[14] E. Arik,[18a,ii] M. Arik,[18a] A. J. Armbruster,[86] O. Arnaez,[80] C. Arnault,[114] A. Artamonov,[94] G. Artoni,[131a,131b] D. Arutinov,[20] S. Asai,[154] R. Asfandiyarov,[171] S. Ask,[27] B. Åsman,[145a,145b] L. Asquith,[5] K. Assamagan,[24] A. Astbury,[168] A. Astvatsatourov,[51] G. Atoian,[174] B. Aubert,[4] E. Auge,[114] K. Augsten,[126] M. Aurousseau,[144a] G. Avolio,[162] R. Avramidou,[9] D. Axen,[167] C. Ay,[53] G. Azuelos,[92,d] Y. Azuma,[154] M. A. Baak,[29] G. Baccaglioni,[88a] C. Bacci,[133a,133b] A. M. Bach,[14] H. Bachacou,[135] K. Bachas,[29] G. Bachy,[29] M. Backes,[48] M. Backhaus,[20] E. Badescu,[25a] P. Bagnaia,[131a,131b] S. Bahinipati,[2] Y. Bai,[32a] D. C. Bailey,[157] T. Bain,[157] J. T. Baines,[128] O. K. Baker,[174] M. D. Baker,[24] S. Baker,[76] E. Banas,[38] P. Banerjee,[92] Sw. Banerjee,[171] D. Banfi,[29] A. Bangert,[149] V. Bansal,[168] H. S. Bansil,[17] L. Barak,[170] S. P. Baranov,[93] A. Barashkou,[64] A. Barbaro Galtieri,[14] T. Barber,[47] E. L. Barberio,[85] D. Barberis,[49a,49b] M. Barbero,[20] D. Y. Bardin,[64] T. Barillari,[98] M. Barisonzi,[173] T. Barklow,[142] N. Barlow,[27] B. M. Barnett,[128] R. M. Barnett,[14] A. Baroncelli,[133a] G. Barone,[48] A. J. Barr,[117] F. Barreiro,[79] J. Barreiro Guimarães da Costa,[56] P. Barrillon,[114] R. Bartoldus,[142] A. E. Barton,[70] V. Bartsch,[148] R. L. Bates,[52] L. Batkova,[143a] J. R. Batley,[27] A. Battaglia,[16] M. Battistin,[29] G. Battistoni,[88a] F. Bauer,[135] H. S. Bawa,[142,e] B. Beare,[157] T. Beau,[77] P. H. Beauchemin,[160] R. Beccherle,[49a] P. Bechtle,[20] G. A. Beck,[74] H. P. Beck,[16] S. Becker,[97] M. Beckingham,[137] K. H. Becks,[173] A. J. Beddall,[18c] A. Beddall,[18c]

S. Bedikian,[174] V. A. Bednyakov,[64] C. P. Bee,[82] M. Begel,[24] S. Behar Harpaz,[151] P. K. Behera,[62] M. Beimforde,[98] C. Belanger-Champagne,[84] P. J. Bell,[48] W. H. Bell,[48] G. Bella,[152] L. Bellagamba,[19a] F. Bellina,[29] M. Bellomo,[29] A. Belloni,[56] O. Beloborodova,[106,f] K. Belotskiy,[95] O. Beltramello,[29] S. Ben Ami,[151] O. Benary,[152] D. Benchekroun,[134a] C. Benchouk,[82] M. Bendel,[80] N. Benekos,[164] Y. Benhammou,[152] J. A. Benitez Garcia,[158b] D. P. Benjamin,[44] M. Benoit,[114] J. R. Bensinger,[22] K. Benslama,[129] S. Bentvelsen,[104] M. Beretta,[46] D. Berge,[29] E. Bergeaas Kuutmann,[41] N. Berger,[4] F. Berghaus,[168] E. Berglund,[48] J. Beringer,[14] P. Bernat,[76] R. Bernhard,[47] C. Bernius,[24] T. Berry,[75] A. Bertin,[19a,19b] F. Bertinelli,[29] F. Bertolucci,[121a,121b] M. I. Besana,[88a,88b] N. Besson,[135] S. Bethke,[98] W. Bhimji,[45] R. M. Bianchi,[29] M. Bianco,[71a,71b] O. Biebel,[97] S. P. Bieniek,[76] K. Bierwagen,[53] J. Biesiada,[14] M. Biglietti,[133a] H. Bilokon,[46] M. Bindi,[19a,19b] S. Binet,[114] A. Bingul,[18c] C. Bini,[131a,131b] C. Biscarat,[176] U. Bitenc,[47] K. M. Black,[21] R. E. Blair,[5] J.-B. Blanchard,[114] G. Blanchot,[29] T. Blazek,[143a] C. Blocker,[22] J. Blocki,[38] A. Blondel,[48] W. Blum,[80] U. Blumenschein,[53] G. J. Bobbink,[104] V. B. Bobrovnikov,[106] S. S. Bocchetta,[78] A. Bocci,[44] C. R. Boddy,[117] M. Boehler,[41] J. Boek,[173] N. Boelaert,[35] S. Böser,[76] J. A. Bogaerts,[29] A. Bogdanchikov,[106] A. Bogouch,[89,ii] C. Bohm,[145a] V. Boisvert,[75] T. Bold,[37] V. Boldea,[25a] N. M. Bolnet,[135] M. Bona,[74] V. G. Bondarenko,[95] M. Bondioli,[162] M. Boonekamp,[135] G. Boorman,[75] C. N. Booth,[138] S. Bordoni,[77] C. Borer,[16] A. Borisov,[127] G. Borissov,[70] I. Borjanovic,[12a] S. Borroni,[86] K. Bos,[104] D. Boscherini,[19a] M. Bosman,[11] H. Boterenbrood,[104] D. Botterill,[128] J. Bouchami,[92] J. Boudreau,[122] E. V. Bouhova-Thacker,[70] C. Bourdarios,[114] N. Bousson,[82] A. Boveia,[30] J. Boyd,[29] I. R. Boyko,[64] N. I. Bozhko,[127] I. Bozovic-Jelisavcic,[12b] J. Bracinik,[17] A. Braem,[29] P. Branchini,[133a] G. W. Brandenburg,[56] A. Brandt,[7] G. Brandt,[15] O. Brandt,[53] U. Bratzler,[155] B. Brau,[83] J. E. Brau,[113] H. M. Braun,[173] B. Brelier,[157] J. Bremer,[29] R. Brenner,[165] S. Bressler,[170] D. Breton,[114] D. Britton,[52] F. M. Brochu,[27] I. Brock,[20] R. Brock,[87] T. J. Brodbeck,[70] E. Brodet,[152] F. Broggi,[88a] C. Bromberg,[87] G. Brooijmans,[34] W. K. Brooks,[31b] G. Brown,[81] H. Brown,[7] P. A. Bruckman de Renstrom,[38] D. Bruncko,[143b] R. Bruneliere,[47] S. Brunet,[60] A. Bruni,[19a] G. Bruni,[19a] M. Bruschi,[19a] T. Buanes,[13] F. Bucci,[48] J. Buchanan,[117] N. J. Buchanan,[2] P. Buchholz,[140] R. M. Buckingham,[117] A. G. Buckley,[45] S. I. Buda,[25a] I. A. Budagov,[64] B. Budick,[107] V. Büscher,[80] L. Bugge,[116] D. Buira-Clark,[117] O. Bulekov,[95] M. Bunse,[42] T. Buran,[116] H. Burckhart,[29] S. Burdin,[72] T. Burgess,[13] S. Burke,[128] E. Busato,[33] P. Bussey,[52] C. P. Buszello,[165] F. Butin,[29] B. Butler,[142] J. M. Butler,[21] C. M. Buttar,[52] J. M. Butterworth,[76] W. Buttinger,[27] J. Caballero,[24] S. Cabrera Urbán,[166] D. Caforio,[19a,19b] O. Cakir,[3a] P. Calafiura,[14] G. Calderini,[77] P. Calfayan,[97] R. Calkins,[105] L. P. Caloba,[23a] R. Caloi,[131a,131b] D. Calvet,[33] S. Calvet,[33] R. Camacho Toro,[33] P. Camarri,[132a,132b] M. Cambiaghi,[118a,118b] D. Cameron,[116] L. M. Caminada,[14] S. Campana,[29] M. Campanelli,[76] V. Canale,[101a,101b] F. Canelli,[30,g] A. Canepa,[158a] J. Cantero,[79] L. Capasso,[101a,101b] M. D. M. Capeans Garrido,[29] I. Caprini,[25a] M. Caprini,[25a] D. Capriotti,[98] M. Capua,[36a,36b] R. Caputo,[147] C. Caramarcu,[24] R. Cardarelli,[132a] T. Carli,[29] G. Carlino,[101a] L. Carminati,[88a,88b] B. Caron,[158a] S. Caron,[47] G. D. Carrillo Montoya,[171] A. A. Carter,[74] J. R. Carter,[27] J. Carvalho,[123a,h] D. Casadei,[107] M. P. Casado,[11] M. Cascella,[121a,121b] C. Caso,[49a,49b,ii] A. M. Castaneda Hernandez,[171] E. Castaneda-Miranda,[171] V. Castillo Gimenez,[166] N. F. Castro,[123a] G. Cataldi,[71a] F. Cataneo,[29] A. Catinaccio,[29] J. R. Catmore,[29] A. Cattai,[29] G. Cattani,[132a,132b] S. Caughron,[87] D. Cauz,[163a,163c] P. Cavalleri,[77] D. Cavalli,[88a] M. Cavalli-Sforza,[11] V. Cavasinni,[121a,121b] F. Ceradini,[133a,133b] A. S. Cerqueira,[23b] A. Cerri,[29] L. Cerrito,[74] F. Cerutti,[46] S. A. Cetin,[18b] F. Cevenini,[101a,101b] A. Chafaq,[134a] D. Chakraborty,[105] K. Chan,[2] B. Chapleau,[84] J. D. Chapman,[27] J. W. Chapman,[86] E. Chareyre,[77] D. G. Charlton,[17] V. Chavda,[81] C. A. Chavez Barajas,[29] S. Cheatham,[84] S. Chekanov,[5] S. V. Chekulaev,[158a] G. A. Chelkov,[64] M. A. Chelstowska,[103] C. Chen,[63] H. Chen,[24] S. Chen,[32c] T. Chen,[32c] X. Chen,[171] S. Cheng,[32a] A. Cheplakov,[64] V. F. Chepurnov,[64] R. Cherkaoui El Moursli,[134e] V. Chernyatin,[24] E. Cheu,[6] S. L. Cheung,[157] L. Chevalier,[135] G. Chiefari,[101a,101b] L. Chikovani,[50a] J. T. Childers,[57a] A. Chilingarov,[70] G. Chiodini,[71a] M. V. Chizhov,[64] G. Choudalakis,[30] S. Chouridou,[136] I. A. Christidi,[76] A. Christov,[47] D. Chromek-Burckhart,[29] M. L. Chu,[150] J. Chudoba,[124] G. Ciapetti,[131a,131b] K. Ciba,[37] A. K. Ciftci,[3a] R. Ciftci,[3a] D. Cinca,[33] V. Cindro,[73] M. D. Ciobotaru,[162] C. Ciocca,[19a] A. Ciocio,[14] M. Cirilli,[86] M. Citterio,[88a] M. Ciubancan,[25a] A. Clark,[48] P. J. Clark,[45] W. Cleland,[122] J. C. Clemens,[82] B. Clement,[54] C. Clement,[145a,145b] R. W. Clifft,[128] Y. Coadou,[82] M. Cobal,[163a,163c] A. Coccaro,[49a,49b] J. Cochran,[63] P. Coe,[117] J. G. Cogan,[142] J. Coggeshall,[164] E. Cogneras,[176] C. D. Cojocaru,[28] J. Colas,[4] A. P. Colijn,[104] N. J. Collins,[17] C. Collins-Tooth,[52] J. Collot,[54] G. Colon,[83] P. Conde Muiño,[123a] E. Coniavitis,[117] M. C. Conidi,[11] M. Consonni,[103] V. Consorti,[47] S. Constantinescu,[25a] C. Conta,[118a,118b] F. Conventi,[101a,i] J. Cook,[29] M. Cooke,[14] B. D. Cooper,[76] A. M. Cooper-Sarkar,[117] K. Copic,[14] T. Cornelissen,[173] M. Corradi,[19a] F. Corriveau,[84,j] A. Corso-Radu,[162] A. Cortes-Gonzalez,[164] G. Cortiana,[98] G. Costa,[88a] M. J. Costa,[166] D. Costanzo,[138] T. Costin,[30] D. Côté,[29]

R. Coura Torres,[23a] L. Courneyea,[168] G. Cowan,[75] C. Cowden,[27] B. E. Cox,[81] K. Cranmer,[107] J. Cranshaw,[5] F. Crescioli,[121a,121b] M. Cristinziani,[20] G. Crosetti,[36a,36b] R. Crupi,[71a,71b] S. Crépé-Renaudin,[54] C.-M. Cuciuc,[25a] C. Cuenca Almenar,[174] T. Cuhadar Donszelmann,[138] M. Curatolo,[46] C. J. Curtis,[17] P. Cwetanski,[60] H. Czirr,[140] Z. Czyczula,[174] S. D'Auria,[52] M. D'Onofrio,[72] A. D'Orazio,[131a,131b] P. V. M. Da Silva,[23a] C. Da Via,[81] W. Dabrowski,[37] T. Dai,[86] C. Dallapiccola,[83] M. Dam,[35] M. Dameri,[49a,49b] D. S. Damiani,[136] H. O. Danielsson,[29] D. Dannheim,[98] V. Dao,[48] G. Darbo,[49a] G. L. Darlea,[25b] C. Daum,[104] W. Davey,[20] T. Davidek,[125] N. Davidson,[85] R. Davidson,[70] E. Davies,[117,c] M. Davies,[92] A. R. Davison,[76] Y. Davygora,[57a] E. Dawe,[141] I. Dawson,[138] J. W. Dawson,[5,ii] R. K. Daya-Ishmukhametova,[39] K. De,[7] R. de Asmundis,[101a] S. De Castro,[19a,19b] P. E. De Castro Faria Salgado,[24] S. De Cecco,[77] J. de Graat,[97] N. De Groot,[103] P. de Jong,[104] C. De La Taille,[114] H. De la Torre,[79] B. De Lotto,[163a,163c] L. de Mora,[70] L. De Nooij,[104] D. De Pedis,[131a] A. De Salvo,[131a] U. De Sanctis,[163a,163c] A. De Santo,[148] J. B. De Vivie De Regie,[114] S. Dean,[76] R. Debbe,[24] C. Debenedetti,[45] D. V. Dedovich,[64] J. Degenhardt,[119] M. Dehchar,[117] C. Del Papa,[163a,163c] J. Del Peso,[79] T. Del Prete,[121a,121b] T. Delemontex,[54] M. Deliyergiyev,[73] A. Dell'Acqua,[29] L. Dell'Asta,[21] M. Della Pietra,[101a,i] D. della Volpe,[101a,101b] M. Delmastro,[29] N. Delruelle,[29] P. A. Delsart,[54] C. Deluca,[147] S. Demers,[174] M. Demichev,[64] B. Demirkoz,[11,k] J. Deng,[162] W. Deng,[24] S. P. Denisov,[127] D. Derendarz,[38] J. E. Derkaoui,[134d] F. Derue,[77] P. Dervan,[72] K. Desch,[20] E. Devetak,[147] P. O. Deviveiros,[157] A. Dewhurst,[128] B. DeWilde,[147] S. Dhaliwal,[157] R. Dhullipudi,[24,l] A. Di Ciaccio,[132a,132b] L. Di Ciaccio,[4] A. Di Girolamo,[29] B. Di Girolamo,[29] S. Di Luise,[133a,133b] A. Di Mattia,[171] B. Di Micco,[29] R. Di Nardo,[46] A. Di Simone,[132a,132b] R. Di Sipio,[19a,19b] M. A. Diaz,[31a] F. Diblen,[18c] E. B. Diehl,[86] J. Dietrich,[41] T. A. Dietzsch,[57a] S. Diglio,[85] K. Dindar Yagci,[39] J. Dingfelder,[20] C. Dionisi,[131a,131b] P. Dita,[25a] S. Dita,[25a] F. Dittus,[29] F. Djama,[82] T. Djobava,[50b] M. A. B. do Vale,[23c] A. Do Valle Wemans,[123a] T. K. O. Doan,[4] M. Dobbs,[84] R. Dobinson,[29,ii] D. Dobos,[29] E. Dobson,[29,m] J. Dodd,[34] C. Doglioni,[117] T. Doherty,[52] Y. Doi,[65,ii] J. Dolejsi,[125] I. Dolenc,[73] Z. Dolezal,[125] B. A. Dolgoshein,[95,ii] T. Dohmae,[154] M. Donadelli,[23d] M. Donega,[119] J. Donini,[54] J. Dopke,[29] A. Doria,[101a] A. Dos Anjos,[171] M. Dosil,[11] A. Dotti,[121a,121b] M. T. Dova,[69] J. D. Dowell,[17] A. D. Doxiadis,[104] A. T. Doyle,[52] Z. Drasal,[125] J. Drees,[173] N. Dressnandt,[119] H. Drevermann,[29] C. Driouichi,[35] M. Dris,[9] J. Dubbert,[98] S. Dube,[14] E. Duchovni,[170] G. Duckeck,[97] A. Dudarev,[29] F. Dudziak,[63] M. Dührssen,[29] I. P. Duerdoth,[81] L. Duflot,[114] M-A. Dufour,[84] M. Dunford,[29] H. Duran Yildiz,[3a] R. Duxfield,[138] M. Dwuznik,[37] F. Dydak,[29] M. Düren,[51] W. L. Ebenstein,[44] J. Ebke,[97] S. Eckweiler,[80] K. Edmonds,[80] C. A. Edwards,[75] N. C. Edwards,[52] W. Ehrenfeld,[41] T. Ehrich,[98] T. Eifert,[29] G. Eigen,[13] K. Einsweiler,[14] E. Eisenhandler,[74] T. Ekelof,[165] M. El Kacimi,[134c] M. Ellert,[165] S. Elles,[4] F. Ellinghaus,[80] K. Ellis,[74] N. Ellis,[29] J. Elmsheuser,[97] M. Elsing,[29] D. Emeliyanov,[128] R. Engelmann,[147] A. Engl,[97] B. Epp,[61] A. Eppig,[86] J. Erdmann,[53] A. Ereditato,[16] D. Eriksson,[145a] J. Ernst,[1] M. Ernst,[24] J. Ernwein,[135] D. Errede,[164] S. Errede,[164] E. Ertel,[80] M. Escalier,[114] C. Escobar,[122] X. Espinal Curull,[11] B. Esposito,[46] F. Etienne,[82] A. I. Etienvre,[135] E. Etzion,[152] D. Evangelakou,[53] H. Evans,[60] L. Fabbri,[19a,19b] C. Fabre,[29] R. M. Fakhrutdinov,[127] S. Falciano,[131a] Y. Fang,[171] M. Fanti,[88a,88b] A. Farbin,[7] A. Farilla,[133a] J. Farley,[147] T. Farooque,[157] S. M. Farrington,[117] P. Farthouat,[29] P. Fassnacht,[29] D. Fassouliotis,[8] B. Fatholahzadeh,[157] A. Favareto,[88a,88b] L. Fayard,[114] S. Fazio,[36a,36b] R. Febbraro,[33] P. Federic,[143a] O. L. Fedin,[120] W. Fedorko,[87] M. Fehling-Kaschek,[47] L. Feligioni,[82] D. Fellmann,[5] C. Feng,[32d] E. J. Feng,[30] A. B. Fenyuk,[127] J. Ferencei,[143b] J. Ferland,[92] W. Fernando,[108] S. Ferrag,[52] J. Ferrando,[52] V. Ferrara,[41] A. Ferrari,[165] P. Ferrari,[104] R. Ferrari,[118a] A. Ferrer,[166] M. L. Ferrer,[46] D. Ferrere,[48] C. Ferretti,[86] A. Ferretto Parodi,[49a,49b] M. Fiascaris,[30] F. Fiedler,[80] A. Filipčič,[73] A. Filippas,[9] F. Filthaut,[103] M. Fincke-Keeler,[168] M. C. N. Fiolhais,[123a,h] L. Fiorini,[166] A. Firan,[39] G. Fischer,[41] P. Fischer,[20] M. J. Fisher,[108] M. Flechl,[47] I. Fleck,[140] J. Fleckner,[80] P. Fleischmann,[172] S. Fleischmann,[173] T. Flick,[173] L. R. Flores Castillo,[171] M. J. Flowerdew,[98] M. Fokitis,[9] T. Fonseca Martin,[16] J. Fopma,[117] D. A. Forbush,[137] A. Formica,[135] A. Forti,[81] D. Fortin,[158a] J. M. Foster,[81] D. Fournier,[114] A. Foussat,[29] A. J. Fowler,[44] K. Fowler,[136] H. Fox,[70] P. Francavilla,[121a,121b] S. Franchino,[118a,118b] D. Francis,[29] T. Frank,[170] M. Franklin,[56] S. Franz,[29] M. Fraternali,[118a,118b] S. Fratina,[119] S. T. French,[27] F. Friedrich,[43] R. Froeschl,[29] D. Froidevaux,[29] J. A. Frost,[27] C. Fukunaga,[155] E. Fullana Torregrosa,[29] J. Fuster,[166] C. Gabaldon,[29] O. Gabizon,[170] T. Gadfort,[24] S. Gadomski,[48] G. Gagliardi,[49a,49b] P. Gagnon,[60] C. Galea,[97] E. J. Gallas,[117] V. Gallo,[16] B. J. Gallop,[128] P. Gallus,[124] K. K. Gan,[108] Y. S. Gao,[142,e] V. A. Gapienko,[127] A. Gaponenko,[14] F. Garberson,[174] M. Garcia-Sciveres,[14] C. García,[166] J. E. García Navarro,[48] R. W. Gardner,[30] N. Garelli,[29] H. Garitaonandia,[104] V. Garonne,[29] J. Garvey,[17] C. Gatti,[46] G. Gaudio,[118a] O. Gaumer,[48] B. Gaur,[140] L. Gauthier,[135] I. L. Gavrilenko,[93] C. Gay,[167] G. Gaycken,[20] J-C. Gayde,[29] E. N. Gazis,[9] P. Ge,[32d] C. N. P. Gee,[128] D. A. A. Geerts,[104] Ch. Geich-Gimbel,[20] K. Gellerstedt,[145a,145b] C. Gemme,[49a] A. Gemmell,[52] M. H. Genest,[97]

S. Gentile,[131a,131b] M. George,[53] S. George,[75] P. Gerlach,[173] A. Gershon,[152] C. Geweniger,[57a] H. Ghazlane,[134b] N. Ghodbane,[33] B. Giacobbe,[19a] S. Giagu,[131a,131b] V. Giakoumopoulou,[8] V. Giangiobbe,[121a,121b] F. Gianotti,[29] B. Gibbard,[24] A. Gibson,[157] S. M. Gibson,[29] L. M. Gilbert,[117] V. Gilewsky,[90] D. Gillberg,[28] A. R. Gillman,[128] D. M. Gingrich,[2,d] J. Ginzburg,[152] N. Giokaris,[8] M. P. Giordani,[163c] R. Giordano,[101a,101b] F. M. Giorgi,[15] P. Giovannini,[98] P. F. Giraud,[135] D. Giugni,[88a] M. Giunta,[92] P. Giusti,[19a] B. K. Gjelsten,[116] L. K. Gladilin,[96] C. Glasman,[79] J. Glatzer,[47] A. Glazov,[41] K. W. Glitza,[173] G. L. Glonti,[64] J. Godfrey,[141] J. Godlewski,[29] M. Goebel,[41] T. Göpfert,[43] C. Goeringer,[80] C. Gössling,[42] T. Göttfert,[98] S. Goldfarb,[86] T. Golling,[174] S. N. Golovnia,[127] A. Gomes,[123a,b] L. S. Gomez Fajardo,[41] R. Gonçalo,[75] J. Goncalves Pinto Firmino Da Costa,[41] L. Gonella,[20] A. Gonidec,[29] S. Gonzalez,[171] S. González de la Hoz,[166] G. Gonzalez Parra,[11] M. L. Gonzalez Silva,[26] S. Gonzalez-Sevilla,[48] J. J. Goodson,[147] L. Goossens,[29] P. A. Gorbounov,[94] H. A. Gordon,[24] I. Gorelov,[102] G. Gorfine,[173] B. Gorini,[29] E. Gorini,[71a,71b] A. Gorišek,[73] E. Gornicki,[38] S. A. Gorokhov,[127] V. N. Goryachev,[127] B. Gosdzik,[41] M. Gosselink,[104] M. I. Gostkin,[64] I. Gough Eschrich,[162] M. Gouighri,[134a] D. Goujdami,[134c] M. P. Goulette,[48] A. G. Goussiou,[137] C. Goy,[4] S. Gozpinar,[22] I. Grabowska-Bold,[37] P. Grafström,[29] K-J. Grahn,[41] F. Grancagnolo,[71a] S. Grancagnolo,[15] V. Grassi,[147] V. Gratchev,[120] N. Grau,[34] H. M. Gray,[29] J. A. Gray,[147] E. Graziani,[133a] O. G. Grebenyuk,[120] B. Green,[75] T. Greenshaw,[72] Z. D. Greenwood,[24,l] K. Gregersen,[35] I. M. Gregor,[41] P. Grenier,[142] J. Griffiths,[137] N. Grigalashvili,[64] A. A. Grillo,[136] S. Grinstein,[11] Y. V. Grishkevich,[96] J.-F. Grivaz,[114] M. Groh,[98] E. Gross,[170] J. Grosse-Knetter,[53] J. Groth-Jensen,[170] K. Grybel,[140] V. J. Guarino,[5] D. Guest,[174] C. Guicheney,[33] A. Guida,[71a,71b] S. Guindon,[53] H. Guler,[84,n] J. Gunther,[124] B. Guo,[157] J. Guo,[34] A. Gupta,[30] Y. Gusakov,[64] V. N. Gushchin,[127] A. Gutierrez,[92] P. Gutierrez,[110] N. Guttman,[152] O. Gutzwiller,[171] C. Guyot,[135] C. Gwenlan,[117] C. B. Gwilliam,[72] A. Haas,[142] S. Haas,[29] C. Haber,[14] H. K. Hadavand,[39] D. R. Hadley,[17] P. Haefner,[98] F. Hahn,[29] S. Haider,[29] Z. Hajduk,[38] H. Hakobyan,[175] J. Haller,[53] K. Hamacher,[173] P. Hamal,[112] M. Hamer,[53] A. Hamilton,[48] S. Hamilton,[160] H. Han,[32a] L. Han,[32b] K. Hanagaki,[115] K. Hanawa,[159] M. Hance,[14] C. Handel,[80] P. Hanke,[57a] J. R. Hansen,[35] J. B. Hansen,[35] J. D. Hansen,[35] P. H. Hansen,[35] P. Hansson,[142] K. Hara,[159] G. A. Hare,[136] T. Harenberg,[173] S. Harkusha,[89] D. Harper,[86] R. D. Harrington,[45] O. M. Harris,[137] K. Harrison,[17] J. Hartert,[47] F. Hartjes,[104] T. Haruyama,[65] A. Harvey,[55] S. Hasegawa,[100] Y. Hasegawa,[139] S. Hassani,[135] M. Hatch,[29] D. Hauff,[98] S. Haug,[16] M. Hauschild,[29] R. Hauser,[87] M. Havranek,[20] B. M. Hawes,[117] C. M. Hawkes,[17] R. J. Hawkings,[29] D. Hawkins,[162] T. Hayakawa,[66] T. Hayashi,[159] D. Hayden,[75] H. S. Hayward,[72] S. J. Haywood,[128] E. Hazen,[21] M. He,[32d] S. J. Head,[17] V. Hedberg,[78] L. Heelan,[7] S. Heim,[87] B. Heinemann,[14] S. Heisterkamp,[35] L. Helary,[4] M. Heller,[29] S. Hellman,[145a,145b] D. Hellmich,[20] C. Helsens,[11] T. Hemperek,[20] R. C. W. Henderson,[70] M. Henke,[57a] A. Henrichs,[53] A. M. Henriques Correia,[29] S. Henrot-Versille,[114] F. Henry-Couannier,[82] C. Hensel,[53] T. Henß,[173] C. M. Hernandez,[7] Y. Hernández Jiménez,[166] R. Herrberg,[15] A. D. Hershenhorn,[151] G. Herten,[47] R. Hertenberger,[97] L. Hervas,[29] N. P. Hessey,[104] E. Higón-Rodriguez,[166] D. Hill,[5,ii] J. C. Hill,[27] N. Hill,[5] K. H. Hiller,[41] S. Hillert,[20] S. J. Hillier,[17] I. Hinchliffe,[14] E. Hines,[119] M. Hirose,[115] F. Hirsch,[42] D. Hirschbuehl,[173] J. Hobbs,[147] N. Hod,[152] M. C. Hodgkinson,[138] P. Hodgson,[138] A. Hoecker,[29] M. R. Hoeferkamp,[102] J. Hoffman,[39] D. Hoffmann,[82] M. Hohlfeld,[80] M. Holder,[140] S. O. Holmgren,[145a] T. Holy,[126] J. L. Holzbauer,[87] Y. Homma,[66] T. M. Hong,[119] L. Hooft van Huysduynen,[107] T. Horazdovsky,[126] C. Horn,[142] S. Horner,[47] K. Horton,[117] J-Y. Hostachy,[54] S. Hou,[150] M. A. Houlden,[72] A. Hoummada,[134a] J. Howarth,[81] D. F. Howell,[117] I. Hristova,[15] J. Hrivnac,[114] I. Hruska,[124] T. Hryn'ova,[4] P. J. Hsu,[80] S.-C. Hsu,[14] G. S. Huang,[110] Z. Hubacek,[126] F. Hubaut,[82] F. Huegging,[20] T. B. Huffman,[117] E. W. Hughes,[34] G. Hughes,[70] R. E. Hughes-Jones,[81] M. Huhtinen,[29] P. Hurst,[56] M. Hurwitz,[14] U. Husemann,[41] N. Huseynov,[64,o] J. Huston,[87] J. Huth,[56] G. Iacobucci,[48] G. Iakovidis,[9] M. Ibbotson,[81] I. Ibragimov,[140] R. Ichimiya,[66] L. Iconomidou-Fayard,[114] J. Idarraga,[114] P. Iengo,[101a] O. Igonkina,[104] Y. Ikegami,[65] M. Ikeno,[65] Y. Ilchenko,[39] D. Iliadis,[153] D. Imbault,[77] M. Imori,[154] T. Ince,[20] J. Inigo-Golfin,[29] P. Ioannou,[8] M. Iodice,[133a] A. Irles Quiles,[166] C. Isaksson,[165] A. Ishikawa,[66] M. Ishino,[67] R. Ishmukhametov,[39] C. Issever,[117] S. Istin,[18a] A. V. Ivashin,[127] W. Iwanski,[38] H. Iwasaki,[65] J. M. Izen,[40] V. Izzo,[101a] B. Jackson,[119] J. N. Jackson,[72] P. Jackson,[142] M. R. Jaekel,[29] V. Jain,[60] K. Jakobs,[47] S. Jakobsen,[35] J. Jakubek,[126] D. K. Jana,[110] E. Jankowski,[157] E. Jansen,[76] A. Jantsch,[98] M. Janus,[20] G. Jarlskog,[78] L. Jeanty,[56] K. Jelen,[37] I. Jen-La Plante,[30] P. Jenni,[29] A. Jeremie,[4] P. Jež,[35] S. Jézéquel,[4] M. K. Jha,[19a] H. Ji,[171] W. Ji,[80] J. Jia,[147] Y. Jiang,[32b] M. Jimenez Belenguer,[41] G. Jin,[32b] S. Jin,[32a] O. Jinnouchi,[156] M. D. Joergensen,[35] D. Joffe,[39] L. G. Johansen,[13] M. Johansen,[145a,145b] K. E. Johansson,[145a] P. Johansson,[138] S. Johnert,[41] K. A. Johns,[6] K. Jon-And,[145a,145b] G. Jones,[81] R. W. L. Jones,[70] T. W. Jones,[76] T. J. Jones,[72] O. Jonsson,[29] C. Joram,[29] P. M. Jorge,[123a] J. Joseph,[14] T. Jovin,[12b] X. Ju,[129] C. A. Jung,[42] V. Juranek,[124] P. Jussel,[61] A. Juste Rozas,[11] V. V. Kabachenko,[127] S. Kabana,[16] M. Kaci,[166] A. Kaczmarska,[38]

P. Kadlecik,[35] M. Kado,[114] H. Kagan,[108] M. Kagan,[56] S. Kaiser,[98] E. Kajomovitz,[151] S. Kalinin,[173] L. V. Kalinovskaya,[64] S. Kama,[39] N. Kanaya,[154] M. Kaneda,[29] T. Kanno,[156] V. A. Kantserov,[95] J. Kanzaki,[65] B. Kaplan,[174] A. Kapliy,[30] J. Kaplon,[29] D. Kar,[43] M. Karagounis,[20] M. Karagoz,[117] M. Karnevskiy,[41] K. Karr,[5] V. Kartvelishvili,[70] A. N. Karyukhin,[127] L. Kashif,[171] G. Kasieczka,[57b] R. D. Kass,[108] A. Kastanas,[13] M. Kataoka,[4] Y. Kataoka,[154] E. Katsoufis,[9] J. Katzy,[41] V. Kaushik,[6] K. Kawagoe,[66] T. Kawamoto,[154] G. Kawamura,[80] M. S. Kayl,[104] V. A. Kazanin,[106] M. Y. Kazarinov,[64] J. R. Keates,[81] R. Keeler,[168] R. Kehoe,[39] M. Keil,[53] G. D. Kekelidze,[64] J. Kennedy,[97] C. J. Kenney,[142] M. Kenyon,[52] O. Kepka,[124] N. Kerschen,[29] B. P. Kerševan,[73] S. Kersten,[173] K. Kessoku,[154] J. Keung,[157] F. Khalil-zada,[10] H. Khandanyan,[164] A. Khanov,[111] D. Kharchenko,[64] A. Khodinov,[95] A. G. Kholodenko,[127] A. Khomich,[57a] T. J. Khoo,[27] G. Khoriauli,[20] A. Khoroshilov,[173] N. Khovanskiy,[64] V. Khovanskiy,[94] E. Khramov,[64] J. Khubua,[50b] H. Kim,[145a,145b] M. S. Kim,[2] P. C. Kim,[142] S. H. Kim,[159] N. Kimura,[169] O. Kind,[15] B. T. King,[72] M. King,[66] R. S. B. King,[117] J. Kirk,[128] L. E. Kirsch,[22] A. E. Kiryunin,[98] T. Kishimoto,[66] D. Kisielewska,[37] T. Kittelmann,[122] A. M. Kiver,[127] E. Kladiva,[143b] J. Klaiber-Lodewigs,[42] M. Klein,[72] U. Klein,[72] K. Kleinknecht,[80] M. Klemetti,[84] A. Klier,[170] A. Klimentov,[24] R. Klingenberg,[42] E. B. Klinkby,[35] T. Klioutchnikova,[29] P. F. Klok,[103] S. Klous,[104] E.-E. Kluge,[57a] T. Kluge,[72] P. Kluit,[104] S. Kluth,[98] N. S. Knecht,[157] E. Kneringer,[61] J. Knobloch,[29] E. B. F. G. Knoops,[82] A. Knue,[53] B. R. Ko,[44] T. Kobayashi,[154] M. Kobel,[43] M. Kocian,[142] P. Kodys,[125] K. Köneke,[29] A. C. König,[103] S. Koenig,[80] L. Köpke,[80] F. Koetsveld,[103] P. Koevesarki,[20] T. Koffas,[28] E. Koffeman,[104] F. Kohn,[53] Z. Kohout,[126] T. Kohriki,[65] T. Koi,[142] T. Kokott,[20] G. M. Kolachev,[106] H. Kolanoski,[15] V. Kolesnikov,[64] I. Koletsou,[88a] J. Koll,[87] D. Kollar,[29] M. Kollefrath,[47] S. D. Kolya,[81] A. A. Komar,[93] Y. Komori,[154] T. Kondo,[65] T. Kono,[41,p] A. I. Kononov,[47] R. Konoplich,[107,q] N. Konstantinidis,[76] A. Kootz,[173] S. Koperny,[37] S. V. Kopikov,[127] K. Korcyl,[38] K. Kordas,[153] V. Koreshev,[127] A. Korn,[117] A. Korol,[106] I. Korolkov,[11] E. V. Korolkova,[138] V. A. Korotkov,[127] O. Kortner,[98] S. Kortner,[98] V. V. Kostyukhin,[20] M. J. Kotamäki,[29] S. Kotov,[98] V. M. Kotov,[64] A. Kotwal,[44] C. Kourkoumelis,[8] V. Kouskoura,[153] A. Koutsman,[158a] R. Kowalewski,[168] T. Z. Kowalski,[37] W. Kozanecki,[135] A. S. Kozhin,[127] V. Kral,[126] V. A. Kramarenko,[96] G. Kramberger,[73] M. W. Krasny,[77] A. Krasznahorkay,[107] J. Kraus,[87] J. K. Kraus,[20] A. Kreisel,[152] F. Krejci,[126] J. Kretzschmar,[72] N. Krieger,[53] P. Krieger,[157] K. Kroeninger,[53] H. Kroha,[98] J. Kroll,[119] J. Kroseberg,[20] J. Krstic,[12a] U. Kruchonak,[64] H. Krüger,[20] T. Kruker,[16] N. Krumnack,[63] Z. V. Krumshteyn,[64] A. Kruth,[20] T. Kubota,[85] S. Kuehn,[47] A. Kugel,[57c] T. Kuhl,[41] D. Kuhn,[61] V. Kukhtin,[64] Y. Kulchitsky,[89] S. Kuleshov,[31b] C. Kummer,[97] M. Kuna,[77] N. Kundu,[117] J. Kunkle,[119] A. Kupco,[124] H. Kurashige,[66] M. Kurata,[159] Y. A. Kurochkin,[89] V. Kus,[124] M. Kuze,[156] J. Kvita,[29] R. Kwee,[15] A. La Rosa,[48] L. La Rotonda,[36a,36b] L. Labarga,[79] J. Labbe,[4] S. Lablak,[134a] C. Lacasta,[166] F. Lacava,[131a,131b] H. Lacker,[15] D. Lacour,[77] V. R. Lacuesta,[166] E. Ladygin,[64] R. Lafaye,[4] B. Laforge,[77] T. Lagouri,[79] S. Lai,[47] E. Laisne,[54] M. Lamanna,[29] C. L. Lampen,[6] W. Lampl,[6] E. Lancon,[135] U. Landgraf,[47] M. P. J. Landon,[74] H. Landsman,[151] J. L. Lane,[81] C. Lange,[41] A. J. Lankford,[162] F. Lanni,[24] K. Lantzsch,[173] A. Lanza,[118a] S. Laplace,[77] C. Lapoire,[20] J. F. Laporte,[135] T. Lari,[88a] A. V. Larionov,[127] A. Larner,[117] C. Lasseur,[29] M. Lassnig,[29] P. Laurelli,[46] W. Lavrijsen,[14] P. Laycock,[72] A. B. Lazarev,[64] O. Le Dortz,[77] E. Le Guirriec,[82] C. Le Maner,[157] E. Le Menedeu,[135] C. Lebel,[92] T. LeCompte,[5] F. Ledroit-Guillon,[54] H. Lee,[104] J. S. H. Lee,[115] S. C. Lee,[150] L. Lee,[174] M. Lefebvre,[168] M. Legendre,[135] A. Leger,[48] B. C. LeGeyt,[119] F. Legger,[97] C. Leggett,[14] M. Lehmacher,[20] G. Lehmann Miotto,[29] X. Lei,[6] M. A. L. Leite,[23d] R. Leitner,[125] D. Lellouch,[170] M. Leltchouk,[34] B. Lemmer,[53] V. Lendermann,[57a] K. J. C. Leney,[144b] T. Lenz,[104] G. Lenzen,[173] B. Lenzi,[29] K. Leonhardt,[43] S. Leontsinis,[9] C. Leroy,[92] J-R. Lessard,[168] J. Lesser,[145a] C. G. Lester,[27] A. Leung Fook Cheong,[171] J. Levêque,[4] D. Levin,[86] L. J. Levinson,[170] M. S. Levitski,[127] A. Lewis,[117] G. H. Lewis,[107] A. M. Leyko,[20] M. Leyton,[15] B. Li,[82] H. Li,[171,r] S. Li,[32b,s] X. Li,[86] Z. Liang,[39] Z. Liang,[117,t] H. Liao,[33] B. Liberti,[132a] P. Lichard,[29] M. Lichtnecker,[97] K. Lie,[164] W. Liebig,[13] R. Lifshitz,[151] C. Limbach,[20] A. Limosani,[85] M. Limper,[62] S. C. Lin,[150,u] F. Linde,[104] J. T. Linnemann,[87] E. Lipeles,[119] L. Lipinsky,[124] A. Lipniacka,[13] T. M. Liss,[164] D. Lissauer,[24] A. Lister,[48] A. M. Litke,[136] C. Liu,[28] D. Liu,[150] H. Liu,[86] J. B. Liu,[86] M. Liu,[32b] S. Liu,[2] Y. Liu,[32b] M. Livan,[118a,118b] S. S. A. Livermore,[117] A. Lleres,[54] J. Llorente Merino,[79] S. L. Lloyd,[74] E. Lobodzinska,[41] P. Loch,[6] W. S. Lockman,[136] T. Loddenkoetter,[20] F. K. Loebinger,[81] A. Loginov,[174] C. W. Loh,[167] T. Lohse,[15] K. Lohwasser,[47] M. Lokajicek,[124] J. Loken,[117] V. P. Lombardo,[4] R. E. Long,[70] L. Lopes,[123a,b] D. Lopez Mateos,[56] M. Losada,[161] P. Loscutoff,[14] F. Lo Sterzo,[131a,131b] M. J. Losty,[158a] X. Lou,[40] A. Lounis,[114] K. F. Loureiro,[161] J. Love,[21] P. A. Love,[70] A. J. Lowe,[142,e] F. Lu,[32a] H. J. Lubatti,[137] C. Luci,[131a,131b] A. Lucotte,[54] A. Ludwig,[43] D. Ludwig,[41] I. Ludwig,[47] J. Ludwig,[47] F. Luehring,[60] G. Luijckx,[104] D. Lumb,[47] L. Luminari,[131a] E. Lund,[116] B. Lund-Jensen,[146] B. Lundberg,[78] J. Lundberg,[145a,145b] J. Lundquist,[35] M. Lungwitz,[80] G. Lutz,[98] D. Lynn,[24] J. Lys,[14] E. Lytken,[78]

H. Ma,[24] L. L. Ma,[171] J. A. Macana Goia,[92] G. Maccarrone,[46] A. Macchiolo,[98] B. Maček,[73] J. Machado Miguens,[123a] R. Mackeprang,[35] R. J. Madaras,[14] W. F. Mader,[43] R. Maenner,[57c] T. Maeno,[24] P. Mättig,[173] S. Mättig,[41] L. Magnoni,[29] E. Magradze,[53] Y. Mahalalel,[152] K. Mahboubi,[47] G. Mahout,[17] C. Maiani,[131a,131b] C. Maidantchik,[23a] A. Maio,[123a,b] S. Majewski,[24] Y. Makida,[65] N. Makovec,[114] P. Mal,[135] B. Malaescu,[29] Pa. Malecki,[38] P. Malecki,[38] V. P. Maleev,[120] F. Malek,[54] U. Mallik,[62] D. Malon,[5] C. Malone,[142] S. Maltezos,[9] V. Malyshev,[106] S. Malyukov,[29] R. Mameghani,[97] J. Mamuzic,[12b] A. Manabe,[65] L. Mandelli,[88a] I. Mandić,[73] R. Mandrysch,[15] J. Maneira,[123a] P. S. Mangeard,[87] I. D. Manjavidze,[64] A. Mann,[53] P. M. Manning,[136] A. Manousakis-Katsikakis,[8] B. Mansoulie,[135] A. Manz,[98] A. Mapelli,[29] L. Mapelli,[29] L. March,[79] J. F. Marchand,[29] F. Marchese,[132a,132b] G. Marchiori,[77] M. Marcisovsky,[124] A. Marin,[21,ii] C. P. Marino,[168] F. Marroquim,[23a] R. Marshall,[81] Z. Marshall,[29] F. K. Martens,[157] S. Marti-Garcia,[166] A. J. Martin,[74] A. J. Martin,[174] B. Martin,[29] B. Martin,[87] F. F. Martin,[119] J. P. Martin,[92] Ph. Martin,[54] T. A. Martin,[17] V. J. Martin,[45] B. Martin dit Latour,[48] S. Martin-Haugh,[148] M. Martinez,[11] V. Martinez Outschoorn,[56] A. C. Martyniuk,[81] M. Marx,[81] F. Marzano,[131a] A. Marzin,[110] L. Masetti,[80] T. Mashimo,[154] R. Mashinistov,[93] J. Masik,[81] A. L. Maslennikov,[106] I. Massa,[19a,19b] G. Massaro,[104] N. Massol,[4] P. Mastrandrea,[131a,131b] A. Mastroberardino,[36a,36b] T. Masubuchi,[154] M. Mathes,[20] P. Matricon,[114] H. Matsumoto,[154] H. Matsunaga,[154] T. Matsushita,[66] C. Mattravers,[117,c] J. M. Maugain,[29] J. Maurer,[82] S. J. Maxfield,[72] D. A. Maximov,[106,f] E. N. May,[5] A. Mayne,[138] R. Mazini,[150] M. Mazur,[20] M. Mazzanti,[88a] E. Mazzoni,[121a,121b] S. P. Mc Kee,[86] A. McCarn,[164] R. L. McCarthy,[147] T. G. McCarthy,[28] N. A. McCubbin,[128] K. W. McFarlane,[55] J. A. Mcfayden,[138] H. McGlone,[52] G. Mchedlidze,[50b] R. A. McLaren,[29] T. Mclaughlan,[17] S. J. McMahon,[128] R. A. McPherson,[168,j] A. Meade,[83] J. Mechnich,[104] M. Mechtel,[173] M. Medinnis,[41] R. Meera-Lebbai,[110] T. Meguro,[115] R. Mehdiyev,[92] S. Mehlhase,[35] A. Mehta,[72] K. Meier,[57a] B. Meirose,[78] C. Melachrinos,[30] B. R. Mellado Garcia,[171] L. Mendoza Navas,[161] Z. Meng,[150,r] A. Mengarelli,[19a,19b] S. Menke,[98] C. Menot,[29] E. Meoni,[11] K. M. Mercurio,[56] P. Mermod,[117] L. Merola,[101a,101b] C. Meroni,[88a] F. S. Merritt,[30] A. Messina,[29] J. Metcalfe,[102] A. S. Mete,[63] C. Meyer,[80] C. Meyer,[30] J-P. Meyer,[135] J. Meyer,[172] J. Meyer,[53] T. C. Meyer,[29] W. T. Meyer,[63] J. Miao,[32d] S. Michal,[29] L. Micu,[25a] R. P. Middleton,[128] P. Miele,[29] S. Migas,[72] L. Mijović,[41] G. Mikenberg,[170] M. Mikestikova,[124] M. Mikuž,[73] D. W. Miller,[30] R. J. Miller,[87] W. J. Mills,[167] C. Mills,[56] A. Milov,[170] D. A. Milstead,[145a,145b] D. Milstein,[170] A. A. Minaenko,[127] M. Miñano Moya,[166] I. A. Minashvili,[64] A. I. Mincer,[107] B. Mindur,[37] M. Mineev,[64] Y. Ming,[129] L. M. Mir,[11] G. Mirabelli,[131a] L. Miralles Verge,[11] S. Misawa,[24] A. Misiejuk,[75] J. Mitrevski,[136] G. Y. Mitrofanov,[127] V. A. Mitsou,[166] S. Mitsui,[65] P. S. Miyagawa,[138] K. Miyazaki,[66] J. U. Mjörnmark,[78] T. Moa,[145a,145b] P. Mockett,[137] S. Moed,[56] V. Moeller,[27] K. Mönig,[41] N. Möser,[20] S. Mohapatra,[147] W. Mohr,[47] S. Mohrdieck-Möck,[98] A. M. Moisseev,[127,ii] R. Moles-Valls,[166] J. Molina-Perez,[29] J. Monk,[76] E. Monnier,[82] S. Montesano,[88a,88b] F. Monticelli,[69] S. Monzani,[19a,19b] R. W. Moore,[2] G. F. Moorhead,[85] C. Mora Herrera,[48] A. Moraes,[52] N. Morange,[135] J. Morel,[53] G. Morello,[36a,36b] D. Moreno,[80] M. Moreno Llácer,[166] P. Morettini,[49a] M. Morii,[56] J. Morin,[74] A. K. Morley,[29] G. Mornacchi,[29] S. V. Morozov,[95] J. D. Morris,[74] L. Morvaj,[100] H. G. Moser,[98] M. Mosidze,[50b] J. Moss,[108] R. Mount,[142] E. Mountricha,[135] S. V. Mouraviev,[93] E. J. W. Moyse,[83] M. Mudrinic,[12b] F. Mueller,[57a] J. Mueller,[122] K. Mueller,[20] T. A. Müller,[97] D. Muenstermann,[29] A. Muir,[167] Y. Munwes,[152] W. J. Murray,[128] I. Mussche,[104] E. Musto,[101a,101b] A. G. Myagkov,[127] M. Myska,[124] J. Nadal,[11] K. Nagai,[159] K. Nagano,[65] Y. Nagasaka,[59] A. M. Nairz,[29] Y. Nakahama,[29] K. Nakamura,[154] T. Nakamura,[154] I. Nakano,[109] G. Nanava,[20] A. Napier,[160] M. Nash,[76,c] N. R. Nation,[21] T. Nattermann,[20] T. Naumann,[41] G. Navarro,[161] H. A. Neal,[86] E. Nebot,[79] P. Yu. Nechaeva,[93] A. Negri,[118a,118b] G. Negri,[29] S. Nektarijevic,[48] A. Nelson,[162] S. Nelson,[142] T. K. Nelson,[142] S. Nemecek,[124] P. Nemethy,[107] A. A. Nepomuceno,[23a] M. Nessi,[29,v] M. S. Neubauer,[164] A. Neusiedl,[80] R. M. Neves,[107] P. Nevski,[24] P. R. Newman,[17] V. Nguyen Thi Hong,[135] R. B. Nickerson,[117] R. Nicolaidou,[135] L. Nicolas,[138] G. Nicoletti,[46] B. Nicquevert,[29] F. Niedercorn,[114] J. Nielsen,[136] T. Niinikoski,[29] N. Nikiforou,[34] A. Nikiforov,[15] V. Nikolaenko,[127] K. Nikolaev,[64] I. Nikolic-Audit,[77] K. Nikolics,[48] K. Nikolopoulos,[24] H. Nilsen,[47] P. Nilsson,[7] Y. Ninomiya,[154] A. Nisati,[131a] T. Nishiyama,[66] R. Nisius,[98] L. Nodulman,[5] M. Nomachi,[115] I. Nomidis,[153] M. Nordberg,[29] B. Nordkvist,[145a,145b] P. R. Norton,[128] J. Novakova,[125] M. Nozaki,[65] L. Nozka,[112] I. M. Nugent,[158a] A.-E. Nuncio-Quiroz,[20] G. Nunes Hanninger,[85] T. Nunnemann,[97] E. Nurse,[76] T. Nyman,[29] B. J. O'Brien,[45] S. W. O'Neale,[17,ii] D. C. O'Neil,[141] V. O'Shea,[52] F. G. Oakham,[28,d] H. Oberlack,[98] J. Ocariz,[77] A. Ochi,[66] S. Oda,[154] S. Odaka,[65] J. Odier,[82] H. Ogren,[60] A. Oh,[81] S. H. Oh,[44] C. C. Ohm,[145a,145b] T. Ohshima,[100] H. Ohshita,[139] T. Ohsugi,[58] S. Okada,[66] H. Okawa,[162] Y. Okumura,[100] T. Okuyama,[154] A. Olariu,[25a] M. Olcese,[49a] A. G. Olchevski,[64] M. Oliveira,[123a,h] D. Oliveira Damazio,[24] E. Oliver Garcia,[166] D. Olivito,[119] A. Olszewski,[38] J. Olszowska,[38]

C. Omachi,[66] A. Onofre,[123a,w] P. U. E. Onyisi,[30] C. J. Oram,[158a] M. J. Oreglia,[30] Y. Oren,[152] D. Orestano,[133a,133b] I. Orlov,[106] C. Oropeza Barrera,[52] R. S. Orr,[157] B. Osculati,[49a,49b] R. Ospanov,[119] C. Osuna,[11] G. Otero y Garzon,[26] J. P. Ottersbach,[104] M. Ouchrif,[134d] F. Ould-Saada,[116] A. Ouraou,[135] Q. Ouyang,[32a] M. Owen,[81] S. Owen,[138] V. E. Ozcan,[18a] N. Ozturk,[7] A. Pacheco Pages,[11] C. Padilla Aranda,[11] S. Pagan Griso,[14] E. Paganis,[138] F. Paige,[24] P. Pais,[83] K. Pajchel,[116] G. Palacino,[158b] C. P. Paleari,[6] S. Palestini,[29] D. Pallin,[33] A. Palma,[123a] J. D. Palmer,[17] Y. B. Pan,[171] E. Panagiotopoulou,[9] B. Panes,[31a] N. Panikashvili,[86] S. Panitkin,[24] D. Pantea,[25a] M. Panuskova,[124] V. Paolone,[122] A. Papadelis,[145a] Th. D. Papadopoulou,[9] A. Paramonov,[5] W. Park,[24,x] M. A. Parker,[27] F. Parodi,[49a,49b] J. A. Parsons,[34] U. Parzefall,[47] E. Pasqualucci,[131a] A. Passeri,[133a] F. Pastore,[133a,133b] Fr. Pastore,[75] G. Pásztor,[48,y] S. Pataraia,[173] N. Patel,[149] J. R. Pater,[81] S. Patricelli,[101a,101b] T. Pauly,[29] M. Pecsy,[143a] M. I. Pedraza Morales,[171] S. V. Peleganchuk,[106] H. Peng,[32b] R. Pengo,[29] A. Penson,[34] J. Penwell,[60] M. Perantoni,[23a] K. Perez,[34,z] T. Perez Cavalcanti,[41] E. Perez Codina,[11] M. T. Pérez García-Estañ,[166] V. Perez Reale,[34] L. Perini,[88a,88b] H. Pernegger,[29] R. Perrino,[71a] P. Perrodo,[4] S. Persembe,[3a] A. Perus,[114] V. D. Peshekhonov,[64] B. A. Petersen,[29] J. Petersen,[29] T. C. Petersen,[35] E. Petit,[82] A. Petridis,[153] C. Petridou,[153] E. Petrolo,[131a] F. Petrucci,[133a,133b] D. Petschull,[41] M. Petteni,[141] R. Pezoa,[31b] B. Pfeifer,[47] A. Phan,[85] P. W. Phillips,[128] G. Piacquadio,[29] E. Piccaro,[74] M. Piccinini,[19a,19b] S. M. Piec,[41] R. Piegaia,[26] J. E. Pilcher,[30] A. D. Pilkington,[81] J. Pina,[123a,b] M. Pinamonti,[163a,163c] A. Pinder,[117] J. L. Pinfold,[2] J. Ping,[32c] B. Pinto,[123a,b] O. Pirotte,[29] C. Pizio,[88a,88b] M. Plamondon,[168] M.-A. Pleier,[24] A. V. Pleskach,[127] A. Poblaguev,[24] S. Poddar,[57a] F. Podlyski,[33] L. Poggioli,[114] T. Poghosyan,[20] M. Pohl,[48] F. Polci,[54] G. Polesello,[118a] A. Policicchio,[36a,36b] A. Polini,[19a] J. Poll,[74] V. Polychronakos,[24] D. M. Pomarede,[135] D. Pomeroy,[22] K. Pommès,[29] L. Pontecorvo,[131a] B. G. Pope,[87] G. A. Popeneciu,[25a] D. S. Popovic,[12a] A. Poppleton,[29] X. Portell Bueso,[29] C. Posch,[21] G. E. Pospelov,[98] S. Pospisil,[126] M. Potekhin,[24] I. N. Potrap,[98] C. J. Potter,[148] C. T. Potter,[113] G. Poulard,[29] J. Poveda,[171] R. Prabhu,[76] P. Pralavorio,[82] A. Pranko,[14] S. Prasad,[56] R. Pravahan,[7] S. Prell,[63] K. Pretzl,[16] L. Pribyl,[29] D. Price,[60] L. E. Price,[5] M. J. Price,[29] D. Prieur,[122] M. Primavera,[71a] K. Prokofiev,[107] F. Prokoshin,[31b] S. Protopopescu,[24] J. Proudfoot,[5] X. Prudent,[43] H. Przysiezniak,[4] S. Psoroulas,[20] E. Ptacek,[113] E. Pueschel,[83] J. Purdham,[86] M. Purohit,[24,x] P. Puzo,[114] Y. Pylypchenko,[116] J. Qian,[86] Z. Qian,[82] Z. Qin,[41] A. Quadt,[53] D. R. Quarrie,[14] W. B. Quayle,[171] F. Quinonez,[31a] M. Raas,[103] V. Radeka,[24] V. Radescu,[57b] B. Radics,[20] T. Rador,[18a] F. Ragusa,[88a,88b] G. Rahal,[176] A. M. Rahimi,[108] D. Rahm,[24] S. Rajagopalan,[24] M. Rammensee,[47] M. Rammes,[140] M. Ramstedt,[145a,145b] A. S. Randle-Conde,[39] K. Randrianarivony,[28] P. N. Ratoff,[70] F. Rauscher,[97] M. Raymond,[29] A. L. Read,[116] D. M. Rebuzzi,[118a,118b] A. Redelbach,[172] G. Redlinger,[24] R. Reece,[119] K. Reeves,[40] A. Reichold,[104] E. Reinherz-Aronis,[152] A. Reinsch,[113] I. Reisinger,[42] D. Reljic,[12a] C. Rembser,[29] Z. L. Ren,[150] A. Renaud,[114] P. Renkel,[39] M. Rescigno,[131a] S. Resconi,[88a] B. Resende,[135] P. Reznicek,[97] R. Rezvani,[157] A. Richards,[76] R. Richter,[98] E. Richter-Was,[4,aa] M. Ridel,[77] M. Rijpstra,[104] M. Rijssenbeek,[147] A. Rimoldi,[118a,118b] L. Rinaldi,[19a] R. R. Rios,[39] I. Riu,[11] G. Rivoltella,[88a,88b] F. Rizatdinova,[111] E. Rizvi,[74] S. H. Robertson,[84,j] A. Robichaud-Veronneau,[117] D. Robinson,[27] J. E. M. Robinson,[76] M. Robinson,[113] A. Robson,[52] J. G. Rocha de Lima,[105] C. Roda,[121a,121b] D. Roda Dos Santos,[29] S. Rodier,[79] D. Rodriguez,[161] Y. Rodriguez Garcia,[161] A. Roe,[53] S. Roe,[29] O. Røhne,[116] V. Rojo,[1] S. Rolli,[160] A. Romaniouk,[95] M. Romano,[19a,19b] V. M. Romanov,[64] G. Romeo,[26] L. Roos,[77] E. Ros,[166] S. Rosati,[131a] K. Rosbach,[48] A. Rose,[148] M. Rose,[75] G. A. Rosenbaum,[157] E. I. Rosenberg,[63] P. L. Rosendahl,[13] O. Rosenthal,[140] L. Rosselet,[48] V. Rossetti,[11] E. Rossi,[131a,131b] L. P. Rossi,[49a] M. Rotaru,[25a] I. Roth,[170] J. Rothberg,[137] D. Rousseau,[114] C. R. Royon,[135] A. Rozanov,[82] Y. Rozen,[151] X. Ruan,[114,bb] I. Rubinskiy,[41] B. Ruckert,[97] N. Ruckstuhl,[104] V. I. Rud,[96] C. Rudolph,[43] G. Rudolph,[61] F. Rühr,[6] F. Ruggieri,[133a,133b] A. Ruiz-Martinez,[63] V. Rumiantsev,[90,ii] L. Rumyantsev,[64] K. Runge,[47] O. Runolfsson,[20] Z. Rurikova,[47] N. A. Rusakovich,[64] D. R. Rust,[60] J. P. Rutherfoord,[6] N. Ruthmann,[80] C. Ruwiedel,[14] P. Ruzicka,[124] Y. F. Ryabov,[120] V. Ryadovikov,[127] P. Ryan,[87] M. Rybar,[125] G. Rybkin,[114] N. C. Ryder,[117] S. Rzaeva,[10] A. F. Saavedra,[149] I. Sadeh,[152] H. F-W. Sadrozinski,[136] R. Sadykov,[64] F. Safai Tehrani,[131a] H. Sakamoto,[154] G. Salamanna,[74] A. Salamon,[132a] M. Saleem,[110] D. Salihagic,[98] A. Salnikov,[142] J. Salt,[166] B. M. Salvachua Ferrando,[5] D. Salvatore,[36a,36b] F. Salvatore,[148] A. Salvucci,[103] A. Salzburger,[29] D. Sampsonidis,[153] B. H. Samset,[116] A. Sanchez,[101a,101b] H. Sandaker,[13] H. G. Sander,[80] M. P. Sanders,[97] M. Sandhoff,[173] T. Sandoval,[27] C. Sandoval,[161] R. Sandstroem,[98] S. Sandvoss,[173] D. P. C. Sankey,[128] A. Sansoni,[46] C. Santamarina Rios,[84] C. Santoni,[33] R. Santonico,[132a,132b] H. Santos,[123a] J. G. Saraiva,[123a] T. Sarangi,[171] E. Sarkisyan-Grinbaum,[7] F. Sarri,[121a,121b] G. Sartisohn,[173] O. Sasaki,[65] N. Sasao,[67] I. Satsounkevitch,[89] G. Sauvage,[4] E. Sauvan,[4] J. B. Sauvan,[114] P. Savard,[157,d] V. Savinov,[122] D. O. Savu,[29] L. Sawyer,[24,l] D. H. Saxon,[52] L. P. Says,[33] C. Sbarra,[19a] A. Sbrizzi,[19a,19b] O. Scallon,[92] D. A. Scannicchio,[162] J. Schaarschmidt,[114] P. Schacht,[98] U. Schäfer,[80] S. Schaepe,[20]

S. Schaetzel,[57b] A. C. Schaffer,[114] D. Schaile,[97] R. D. Schamberger,[147] A. G. Schamov,[106] V. Scharf,[57a] V. A. Schegelsky,[120] D. Scheirich,[86] M. Schernau,[162] M. I. Scherzer,[14] C. Schiavi,[49a,49b] J. Schieck,[97] M. Schioppa,[36a,36b] S. Schlenker,[29] J. L. Schlereth,[5] E. Schmidt,[47] K. Schmieden,[20] C. Schmitt,[80] S. Schmitt,[57b] M. Schmitz,[20] A. Schöning,[57b] M. Schott,[29] D. Schouten,[158a] J. Schovancova,[124] M. Schram,[84] C. Schroeder,[80] N. Schroer,[57c] S. Schuh,[29] G. Schuler,[29] J. Schultes,[173] H.-C. Schultz-Coulon,[57a] H. Schulz,[15] J. W. Schumacher,[20] M. Schumacher,[47] B. A. Schumm,[136] Ph. Schune,[135] C. Schwanenberger,[81] A. Schwartzman,[142] Ph. Schwemling,[77] R. Schwienhorst,[87] R. Schwierz,[43] J. Schwindling,[135] T. Schwindt,[20] W. G. Scott,[128] J. Searcy,[113] G. Sedov,[41] E. Sedykh,[120] E. Segura,[11] S. C. Seidel,[102] A. Seiden,[136] F. Seifert,[43] J. M. Seixas,[23a] G. Sekhniaidze,[101a] D. M. Seliverstov,[120] B. Sellden,[145a] G. Sellers,[72] M. Seman,[143b] N. Semprini-Cesari,[19a,19b] C. Serfon,[97] L. Serin,[114] R. Seuster,[98] H. Severini,[110] M. E. Sevior,[85] A. Sfyrla,[29] E. Shabalina,[53] M. Shamim,[113] L. Y. Shan,[32a] J. T. Shank,[21] Q. T. Shao,[85] M. Shapiro,[14] P. B. Shatalov,[94] L. Shaver,[6] K. Shaw,[163a,163c] D. Sherman,[174] P. Sherwood,[76] A. Shibata,[107] H. Shichi,[100] S. Shimizu,[29] M. Shimojima,[99] T. Shin,[55] M. Shiyakova,[64] A. Shmeleva,[93] M. J. Shochet,[30] D. Short,[117] S. Shrestha,[63] M. A. Shupe,[6] P. Sicho,[124] A. Sidoti,[131a] A. Siebel,[173] F. Siegert,[47] Dj. Sijacki,[12a] O. Silbert,[170] J. Silva,[123a,b] Y. Silver,[152] D. Silverstein,[142] S. B. Silverstein,[145a] V. Simak,[126] O. Simard,[135] Lj. Simic,[12a] S. Simion,[114] B. Simmons,[76] M. Simonyan,[35] P. Sinervo,[157] N. B. Sinev,[113] V. Sipica,[140] G. Siragusa,[172] A. Sircar,[24] A. N. Sisakyan,[64] S. Yu. Sivoklokov,[96] J. Sjölin,[145a,145b] T. B. Sjursen,[13] L. A. Skinnari,[14] H. P. Skottowe,[56] K. Skovpen,[106] P. Skubic,[110] N. Skvorodnev,[22] M. Slater,[17] T. Slavicek,[126] K. Sliwa,[160] J. Sloper,[29] V. Smakhtin,[170] S. Yu. Smirnov,[95] Y. Smirnov,[24] L. N. Smirnova,[96] O. Smirnova,[78] B. C. Smith,[56] D. Smith,[142] K. M. Smith,[52] M. Smizanska,[70] K. Smolek,[126] A. A. Snesarev,[93] S. W. Snow,[81] J. Snow,[110] J. Snuverink,[104] S. Snyder,[24] M. Soares,[123a] R. Sobie,[168,j] J. Sodomka,[126] A. Soffer,[152] C. A. Solans,[166] M. Solar,[126] J. Solc,[126] E. Soldatov,[95] U. Soldevila,[166] E. Solfaroli Camillocci,[131a,131b] A. A. Solodkov,[127] O. V. Solovyanov,[127] J. Sondericker,[24] N. Soni,[2] V. Sopko,[126] B. Sopko,[126] M. Sosebee,[7] R. Soualah,[163a,163c] A. Soukharev,[106] S. Spagnolo,[71a,71b] F. Spanò,[75] R. Spighi,[19a] G. Spigo,[29] F. Spila,[131a,131b] R. Spiwoks,[29] M. Spousta,[125] T. Spreitzer,[157] B. Spurlock,[7] R. D. St. Denis,[52] T. Stahl,[140] J. Stahlman,[119] R. Stamen,[57a] E. Stanecka,[38] R. W. Stanek,[5] C. Stanescu,[133a] S. Stapnes,[116] E. A. Starchenko,[127] J. Stark,[54] P. Staroba,[124] P. Starovoitov,[90] A. Staude,[97] P. Stavina,[143a] G. Stavropoulos,[14] G. Steele,[52] P. Steinbach,[43] P. Steinberg,[24] I. Stekl,[126] B. Stelzer,[141] H. J. Stelzer,[87] O. Stelzer-Chilton,[158a] H. Stenzel,[51] K. Stevenson,[74] G. A. Stewart,[29] J. A. Stillings,[20] M. C. Stockton,[29] K. Stoerig,[47] G. Stoicea,[25a] S. Stonjek,[98] P. Strachota,[125] A. R. Stradling,[7] A. Straessner,[43] J. Strandberg,[146] S. Strandberg,[145a,145b] A. Strandlie,[116] M. Strang,[108] E. Strauss,[142] M. Strauss,[110] P. Strizenec,[143b] R. Ströhmer,[172] D. M. Strom,[113] J. A. Strong,[75,ii] R. Stroynowski,[39] J. Strube,[128] B. Stugu,[13] I. Stumer,[24,ii] J. Stupak,[147] P. Sturm,[173] D. A. Soh,[150,t] D. Su,[142] HS. Subramania,[2] A. Succurro,[11] Y. Sugaya,[115] T. Sugimoto,[100] C. Suhr,[105] K. Suita,[66] M. Suk,[125] V. V. Sulin,[93] S. Sultansoy,[3d] T. Sumida,[29] X. Sun,[54] J. E. Sundermann,[47] K. Suruliz,[138] S. Sushkov,[11] G. Susinno,[36a,36b] M. R. Sutton,[148] Y. Suzuki,[65] Y. Suzuki,[66] M. Svatos,[124] Yu. M. Sviridov,[127] S. Swedish,[167] I. Sykora,[143a] T. Sykora,[125] B. Szeless,[29] J. Sánchez,[166] D. Ta,[104] K. Tackmann,[41] A. Taffard,[162] R. Tafirout,[158a] N. Taiblum,[152] Y. Takahashi,[100] H. Takai,[24] R. Takashima,[68] H. Takeda,[66] T. Takeshita,[139] M. Talby,[82] A. Talyshev,[106,f] M. C. Tamsett,[24] J. Tanaka,[154] R. Tanaka,[114] S. Tanaka,[130] S. Tanaka,[65] Y. Tanaka,[99] K. Tani,[66] N. Tannoury,[82] G. P. Tappern,[29] S. Tapprogge,[80] D. Tardif,[157] S. Tarem,[151] F. Tarrade,[28] G. F. Tartarelli,[88a] P. Tas,[125] M. Tasevsky,[124] E. Tassi,[36a,36b] M. Tatarkhanov,[14] Y. Tayalati,[134d] C. Taylor,[76] F. E. Taylor,[91] G. N. Taylor,[85] W. Taylor,[158b] M. Teinturier,[114] M. Teixeira Dias Castanheira,[74] P. Teixeira-Dias,[75] K. K. Temming,[47] H. Ten Kate,[29] P. K. Teng,[150] S. Terada,[65] K. Terashi,[154] J. Terron,[79] M. Terwort,[41,p] M. Testa,[46] R. J. Teuscher,[157,j] J. Thadome,[173] J. Therhaag,[20] T. Theveneaux-Pelzer,[77] M. Thioye,[174] S. Thoma,[47] J. P. Thomas,[17] E. N. Thompson,[34] P. D. Thompson,[17] P. D. Thompson,[157] A. S. Thompson,[52] E. Thomson,[119] M. Thomson,[27] R. P. Thun,[86] F. Tian,[34] T. Tic,[124] V. O. Tikhomirov,[93] Y. A. Tikhonov,[106,f] P. Tipton,[174] F. J. Tique Aires Viegas,[29] S. Tisserant,[82] B. Toczek,[37] T. Todorov,[4] S. Todorova-Nova,[160] B. Toggerson,[162] J. Tojo,[65] S. Tokár,[143a] K. Tokunaga,[66] K. Tokushuku,[65] K. Tollefson,[87] M. Tomoto,[100] L. Tompkins,[30] K. Toms,[102] G. Tong,[32a] A. Tonoyan,[13] C. Topfel,[16] N. D. Topilin,[64] I. Torchiani,[29] E. Torrence,[113] H. Torres,[77] E. Torró Pastor,[166] J. Toth,[82,y] F. Touchard,[82] D. R. Tovey,[138] D. Traynor,[74] T. Trefzger,[172] L. Tremblet,[29] A. Tricoli,[29] I. M. Trigger,[158a] S. Trincaz-Duvoid,[77] T. N. Trinh,[77] M. F. Tripiana,[69] W. Trischuk,[157] A. Trivedi,[24,x] B. Trocmé,[54] C. Troncon,[88a] M. Trottier-McDonald,[141] M. Trzebinski,[38] A. Trzupek,[38] C. Tsarouchas,[29] J. C-L. Tseng,[117] M. Tsiakiris,[104] P. V. Tsiareshka,[89] D. Tsionou,[4,cc] G. Tsipolitis,[9] V. Tsiskaridze,[47] E. G. Tskhadadze,[50a] I. I. Tsukerman,[94] V. Tsulaia,[14] J.-W. Tsung,[20] S. Tsuno,[65] D. Tsybychev,[147] A. Tua,[138] A. Tudorache,[25a] V. Tudorache,[25a]

J. M. Tuggle,[30] M. Turala,[38] D. Turecek,[126] I. Turk Cakir,[3e] E. Turlay,[104] R. Turra,[88a,88b] P. M. Tuts,[34] A. Tykhonov,[73] M. Tylmad,[145a,145b] M. Tyndel,[128] H. Tyrvainen,[29] G. Tzanakos,[8] K. Uchida,[20] I. Ueda,[154] R. Ueno,[28] M. Ugland,[13] M. Uhlenbrock,[20] M. Uhrmacher,[53] F. Ukegawa,[159] G. Unal,[29] D. G. Underwood,[5] A. Undrus,[24] G. Unel,[162] Y. Unno,[65] D. Urbaniec,[34] E. Urkovsky,[152] G. Usai,[7] M. Uslenghi,[118a,118b] L. Vacavant,[82] V. Vacek,[126] B. Vachon,[84] S. Vahsen,[14] J. Valenta,[124] P. Valente,[131a] S. Valentinetti,[19a,19b] S. Valkar,[125] E. Valladolid Gallego,[166] S. Vallecorsa,[151] J. A. Valls Ferrer,[166] H. van der Graaf,[104] E. van der Kraaij,[104] R. Van Der Leeuw,[104] E. van der Poel,[104] D. van der Ster,[29] N. van Eldik,[83] P. van Gemmeren,[5] Z. van Kesteren,[104] I. van Vulpen,[104] M. Vanadia,[98] W. Vandelli,[29] G. Vandoni,[29] A. Vaniachine,[5] P. Vankov,[41] F. Vannucci,[77] F. Varela Rodriguez,[29] R. Vari,[131a] E. W. Varnes,[6] D. Varouchas,[14] A. Vartapetian,[7] K. E. Varvell,[149] V. I. Vassilakopoulos,[55] F. Vazeille,[33] G. Vegni,[88a,88b] J. J. Veillet,[114] C. Vellidis,[8] F. Veloso,[123a] R. Veness,[29] S. Veneziano,[131a] A. Ventura,[71a,71b] D. Ventura,[137] M. Venturi,[47] N. Venturi,[16] V. Vercesi,[118a] M. Verducci,[137] W. Verkerke,[104] J. C. Vermeulen,[104] A. Vest,[43] M. C. Vetterli,[141,d] I. Vichou,[164] T. Vickey,[144b,dd] O. E. Vickey Boeriu,[144b] G. H. A. Viehhauser,[117] S. Viel,[167] M. Villa,[19a,19b] M. Villaplana Perez,[166] E. Vilucchi,[46] M. G. Vincter,[28] E. Vinek,[29] V. B. Vinogradov,[64] M. Virchaux,[135,ii] J. Virzi,[14] O. Vitells,[170] M. Viti,[41] I. Vivarelli,[47] F. Vives Vaque,[2] S. Vlachos,[9] D. Vladoiu,[97] M. Vlasak,[126] N. Vlasov,[20] A. Vogel,[20] P. Vokac,[126] G. Volpi,[46] M. Volpi,[85] G. Volpini,[88a] H. von der Schmitt,[98] J. von Loeben,[98] H. von Radziewski,[47] E. von Toerne,[20] V. Vorobel,[125] A. P. Vorobiev,[127] V. Vorwerk,[11] M. Vos,[166] R. Voss,[29] T. T. Voss,[173] J. H. Vossebeld,[72] N. Vranjes,[12a] M. Vranjes Milosavljevic,[104] V. Vrba,[124] M. Vreeswijk,[104] T. Vu Anh,[80] R. Vuillermet,[29] I. Vukotic,[114] W. Wagner,[173] P. Wagner,[119] H. Wahlen,[173] J. Wakabayashi,[100] J. Walbersloh,[42] S. Walch,[86] J. Walder,[70] R. Walker,[97] W. Walkowiak,[140] R. Wall,[174] P. Waller,[72] C. Wang,[44] H. Wang,[171] H. Wang,[32b,ee] J. Wang,[150] J. Wang,[54] J. C. Wang,[137] R. Wang,[102] S. M. Wang,[150] A. Warburton,[84] C. P. Ward,[27] M. Warsinsky,[47] R. Wastie,[117] P. M. Watkins,[17] A. T. Watson,[17] M. F. Watson,[17] G. Watts,[137] S. Watts,[81] A. T. Waugh,[149] B. M. Waugh,[76] J. Weber,[42] M. Weber,[128] M. S. Weber,[16] P. Weber,[53] A. R. Weidberg,[117] P. Weigell,[98] J. Weingarten,[53] C. Weiser,[47] H. Wellenstein,[22] P. S. Wells,[29] M. Wen,[46] T. Wenaus,[24] S. Wendler,[122] Z. Weng,[150,t] T. Wengler,[29] S. Wenig,[29] N. Wermes,[20] M. Werner,[47] P. Werner,[29] M. Werth,[162] M. Wessels,[57a] C. Weydert,[54] K. Whalen,[28] S. J. Wheeler-Ellis,[162] S. P. Whitaker,[21] A. White,[7] M. J. White,[85] S. White,[121a,121b] S. R. Whitehead,[117] D. Whiteson,[162] D. Whittington,[60] F. Wicek,[114] D. Wicke,[173] F. J. Wickens,[128] W. Wiedenmann,[171] M. Wielers,[128] P. Wienemann,[20] C. Wiglesworth,[74] L. A. M. Wiik-Fuchs,[47] P. A. Wijeratne,[76] A. Wildauer,[166] M. A. Wildt,[41,p] I. Wilhelm,[125] H. G. Wilkens,[29] J. Z. Will,[97] E. Williams,[34] H. H. Williams,[119] W. Willis,[34] S. Willocq,[83] J. A. Wilson,[17] M. G. Wilson,[142] A. Wilson,[86] I. Wingerter-Seez,[4] S. Winkelmann,[47] F. Winklmeier,[29] M. Wittgen,[142] M. W. Wolter,[38] H. Wolters,[123a,h] W. C. Wong,[40] G. Wooden,[86] B. K. Wosiek,[38] J. Wotschack,[29] M. J. Woudstra,[83] K. W. Wozniak,[38] K. Wraight,[52] C. Wright,[52] D. Wright,[142] M. Wright,[52] B. Wrona,[72] S. L. Wu,[171] X. Wu,[48] Y. Wu,[32b,ff] E. Wulf,[34] R. Wunstorf,[42] B. M. Wynne,[45] S. Xella,[35] M. Xiao,[135] S. Xie,[47] Y. Xie,[32a] C. Xu,[32b,gg] D. Xu,[138] G. Xu,[32a] B. Yabsley,[149] S. Yacoob,[144b] M. Yamada,[65] H. Yamaguchi,[154] A. Yamamoto,[65] K. Yamamoto,[63] S. Yamamoto,[154] T. Yamamura,[154] T. Yamanaka,[154] J. Yamaoka,[44] T. Yamazaki,[154] Y. Yamazaki,[66] Z. Yan,[21] H. Yang,[86] U. K. Yang,[81] Y. Yang,[60] Y. Yang,[32a] Z. Yang,[145a,145b] S. Yanush,[90] Y. Yao,[14] Y. Yasu,[65] G. V. Ybeles Smit,[129] J. Ye,[39] S. Ye,[24] M. Yilmaz,[3c] R. Yoosoofmiya,[122] K. Yorita,[169] R. Yoshida,[5] C. Young,[142] S. Youssef,[21] D. Yu,[24] J. Yu,[7] J. Yu,[111] L. Yuan,[32a,hh] A. Yurkewicz,[105] B. Zabinski,[38] V. G. Zaets,[127] R. Zaidan,[62] A. M. Zaitsev,[127] Z. Zajacova,[29] Yo. K. Zalite,[120] L. Zanello,[131a,131b] P. Zarzhitsky,[39] A. Zaytsev,[106] C. Zeitnitz,[173] M. Zeller,[174] M. Zeman,[124] A. Zemla,[38] C. Zendler,[20] O. Zenin,[127] T. Ženiš,[143a] Z. Zinonos,[121a,121b] S. Zenz,[14] D. Zerwas,[114] G. Zevi della Porta,[56] Z. Zhan,[32d] D. Zhang,[32b,ee] H. Zhang,[87] J. Zhang,[5] Q. Zhang,[5] X. Zhang,[32d] Z. Zhang,[114] L. Zhao,[107] T. Zhao,[137] Z. Zhao,[32b] A. Zhemchugov,[64] S. Zheng,[32a] J. Zhong,[117] B. Zhou,[86] N. Zhou,[162] Y. Zhou,[150] C. G. Zhu,[32d] H. Zhu,[41] J. Zhu,[86] Y. Zhu,[32b] X. Zhuang,[97] V. Zhuravlov,[98] D. Zieminska,[60] R. Zimmermann,[20] S. Zimmermann,[20] S. Zimmermann,[47] M. Ziolkowski,[140] R. Zitoun,[4] L. Živković,[34] V. V. Zmouchko,[127,ii] G. Zobernig,[171] A. Zoccoli,[19a,19b] Y. Zolnierowski,[4] A. Zsenei,[29] M. zur Nedden,[15] V. Zutshi,[105] and L. Zwalinski[29]

(ATLAS Collaboration)

[1]*University at Albany, Albany, New York, USA*
[2]*Department of Physics, University of Alberta, Edmonton, Alberta, Canada*
[3a]*Department of Physics, Ankara University, Ankara, Turkey*
[3b]*Department of Physics, Dumlupinar University, Kutahya, Turkey*

[3c]Department of Physics, Gazi University, Ankara, Turkey
[3d]Division of Physics, TOBB University of Economics and Technology, Ankara, Turkey
[3e]Turkish Atomic Energy Authority, Ankara, Turkey
[4]LAPP, CNRS/IN2P3 and Université de Savoie, Annecy-le-Vieux, France
[5]High Energy Physics Division, Argonne National Laboratory, Argonne, Illinois, USA
[6]Department of Physics, University of Arizona, Tucson, Arizona, USA
[7]Department of Physics, The University of Texas at Arlington, Arlington, Texas, USA
[8]Physics Department, University of Athens, Athens, Greece
[9]Physics Department, National Technical University of Athens, Zografou, Greece
[10]Institute of Physics, Azerbaijan Academy of Sciences, Baku, Azerbaijan
[11]Institut de Física d'Altes Energies and Departament de Física de la Universitat Autònoma de Barcelona and ICREA, Barcelona, Spain
[12a]Institute of Physics, University of Belgrade, Belgrade, Serbia
[12b]Vinca Institute of Nuclear Sciences, University of Belgrade, Belgrade, Serbia
[13]Department for Physics and Technology, University of Bergen, Bergen, Norway
[14]Physics Division, Lawrence Berkeley National Laboratory and University of California, Berkeley, California, USA
[15]Department of Physics, Humboldt University, Berlin, Germany
[16]Albert Einstein Center for Fundamental Physics and Laboratory for High Energy Physics, University of Bern, Bern, Switzerland
[17]School of Physics and Astronomy, University of Birmingham, Birmingham, United Kingdom
[18a]Department of Physics, Bogazici University, Istanbul, Turkey
[18b]Division of Physics, Dogus University, Istanbul, Turkey
[18c]Department of Physics Engineering, Gaziantep University, Gaziantep, Turkey
[18d]Department of Physics, Istanbul Technical University, Istanbul, Turkey
[19a]INFN Sezione di Bologna, Italy
[19b]Dipartimento di Fisica, Università di Bologna, Bologna, Italy
[20]Physikalisches Institut, University of Bonn, Bonn, Germany
[21]Department of Physics, Boston University, Boston, Massachusetts, USA
[22]Department of Physics, Brandeis University, Waltham, Massachusetts, USA
[23a]Universidade Federal do Rio De Janeiro COPPE/EE/IF, Rio de Janeiro, Brazil
[23b]Federal University of Juiz de Fora (UFJF), Juiz de Fora, Brazil
[23c]Federal University of Sao Joao del Rei (UFSJ), Sao Joao del Rei, Brazil
[23d]Instituto de Fisica, Universidade de Sao Paulo, Sao Paulo, Brazil
[24]Physics Department, Brookhaven National Laboratory, Upton, New York, USA
[25a]National Institute of Physics and Nuclear Engineering, Bucharest, Romania
[25b]University Politehnica Bucharest, Bucharest, Romania
[25c]West University in Timisoara, Timisoara, Romania
[26]Departamento de Física, Universidad de Buenos Aires, Buenos Aires, Argentina
[27]Cavendish Laboratory, University of Cambridge, Cambridge, United Kingdom
[28]Department of Physics, Carleton University, Ottawa, Ontario, Canada
[29]CERN, Geneva, Switzerland
[30]Enrico Fermi Institute, University of Chicago, Chicago, Illinois, USA
[31a]Departamento de Fisica, Pontificia Universidad Católica de Chile, Santiago, Chile
[31b]Departamento de Física, Universidad Técnica Federico Santa María, Valparaíso, Chile
[32a]Institute of High Energy Physics, Chinese Academy of Sciences, Beijing, China
[32b]Department of Modern Physics, University of Science and Technology of China, Anhui, China
[32c]Department of Physics, Nanjing University, Jiangsu, China
[32d]School of Physics, Shandong University, Shandong, China
[33]Laboratoire de Physique Corpusculaire, Clermont Université and Université Blaise Pascal and CNRS/IN2P3, Aubiere Cedex, France
[34]Nevis Laboratory, Columbia University, Irvington, New York, USA
[35]Niels Bohr Institute, University of Copenhagen, Kobenhavn, Denmark
[36a]INFN Gruppo Collegato di Cosenza, Italy
[36b]Dipartimento di Fisica, Università della Calabria, Arcavata di Rende, Italy
[37]AGH University of Science and Technology, Faculty of Physics and Applied Computer Science, Krakow, Poland
[38]The Henryk Niewodniczanski Institute of Nuclear Physics, Polish Academy of Sciences, Krakow, Poland
[39]Physics Department, Southern Methodist University, Dallas, Texas, USA
[40]Physics Department, University of Texas at Dallas, Richardson, Texas, USA
[41]DESY, Hamburg and Zeuthen, Germany
[42]Institut für Experimentelle Physik IV, Technische Universität Dortmund, Dortmund, Germany
[43]Institut für Kern- und Teilchenphysik, Technical University Dresden, Dresden, Germany
[44]Department of Physics, Duke University, Durham, North Carolina, USA

[45]*SUPA - School of Physics and Astronomy, University of Edinburgh, Edinburgh, United Kingdom*
[46]*INFN Laboratori Nazionali di Frascati, Frascati, Italy*
[47]*Fakultät für Mathematik und Physik, Albert-Ludwigs-Universität, Freiburg i.Br., Germany*
[48]*Section de Physique, Université de Genève, Geneva, Switzerland*
[49a]*INFN Sezione di Genova, Italy*
[49b]*Dipartimento di Fisica, Università di Genova, Genova, Italy*
[50a]*E.Andronikashvili Institute of Physics, Tbilisi State University, Tbilisi, Georgia*
[50b]*High Energy Physics Institute, Tbilisi State University, Tbilisi, Georgia*
[51]*II Physikalisches Institut, Justus-Liebig-Universität Giessen, Giessen, Germany*
[52]*SUPA - School of Physics and Astronomy, University of Glasgow, Glasgow, United Kingdom*
[53]*II Physikalisches Institut, Georg-August-Universität, Göttingen, Germany*
[54]*Laboratoire de Physique Subatomique et de Cosmologie, Université Joseph Fourier and CNRS/IN2P3 and Institut National Polytechnique de Grenoble, Grenoble, France*
[55]*Department of Physics, Hampton University, Hampton, Virginia, USA*
[56]*Laboratory for Particle Physics and Cosmology, Harvard University, Cambridge, Massachusetts, USA*
[57a]*Kirchhoff-Institut für Physik, Ruprecht-Karls-Universität Heidelberg, Heidelberg, Germany*
[57b]*Physikalisches Institut, Ruprecht-Karls-Universität Heidelberg, Heidelberg, Germany*
[57c]*ZITI Institut für technische Informatik, Ruprecht-Karls-Universität Heidelberg, Mannheim, Germany*
[58]*Faculty of Science, Hiroshima University, Hiroshima, Japan*
[59]*Faculty of Applied Information Science, Hiroshima Institute of Technology, Hiroshima, Japan*
[60]*Department of Physics, Indiana University, Bloomington, Indiana, USA*
[61]*Institut für Astro- und Teilchenphysik, Leopold-Franzens-Universität, Innsbruck, Austria*
[62]*University of Iowa, Iowa City, Iowa, USA*
[63]*Department of Physics and Astronomy, Iowa State University, Ames, Iowa, USA*
[64]*Joint Institute for Nuclear Research, JINR Dubna, Dubna, Russia*
[65]*KEK, High Energy Accelerator Research Organization, Tsukuba, Japan*
[66]*Graduate School of Science, Kobe University, Kobe, Japan*
[67]*Faculty of Science, Kyoto University, Kyoto, Japan*
[68]*Kyoto University of Education, Kyoto, Japan*
[69]*Instituto de Física La Plata, Universidad Nacional de La Plata and CONICET, La Plata, Argentina*
[70]*Physics Department, Lancaster University, Lancaster, United Kingdom*
[71a]*INFN Sezione di Lecce, Italy*
[71b]*Dipartimento di Fisica, Università del Salento, Lecce, Italy*
[72]*Oliver Lodge Laboratory, University of Liverpool, Liverpool, United Kingdom*
[73]*Department of Physics, Jožef Stefan Institute and University of Ljubljana, Ljubljana, Slovenia*
[74]*School of Physics and Astronomy, Queen Mary University of London, London, United Kingdom*
[75]*Department of Physics, Royal Holloway University of London, Surrey, United Kingdom*
[76]*Department of Physics and Astronomy, University College London, London, United Kingdom*
[77]*Laboratoire de Physique Nucléaire et de Hautes Energies, UPMC and Université Paris-Diderot and CNRS/IN2P3, Paris, France*
[78]*Fysiska institutionen, Lunds universitet, Lund, Sweden*
[79]*Departamento de Fisica Teorica C-15, Universidad Autonoma de Madrid, Madrid, Spain*
[80]*Institut für Physik, Universität Mainz, Mainz, Germany*
[81]*School of Physics and Astronomy, University of Manchester, Manchester, United Kingdom*
[82]*CPPM, Aix-Marseille Université and CNRS/IN2P3, Marseille, France*
[83]*Department of Physics, University of Massachusetts, Amherst, Massachusetts, USA*
[84]*Department of Physics, McGill University, Montreal, Quebec, Canada*
[85]*School of Physics, University of Melbourne, Victoria, Australia*
[86]*Department of Physics, The University of Michigan, Ann Arbor, Michigan, USA*
[87]*Department of Physics and Astronomy, Michigan State University, East Lansing, Michigan, USA*
[88a]*INFN Sezione di Milano, Italy*
[88b]*Dipartimento di Fisica, Università di Milano, Milano, Italy*
[89]*B.I. Stepanov Institute of Physics, National Academy of Sciences of Belarus, Minsk, Republic of Belarus*
[90]*National Scientific and Educational Centre for Particle and High Energy Physics, Minsk, Republic of Belarus*
[91]*Department of Physics, Massachusetts Institute of Technology, Cambridge, Massachusetts, USA*
[92]*Group of Particle Physics, University of Montreal, Montreal, Quebec, Canada*
[93]*P.N. Lebedev Institute of Physics, Academy of Sciences, Moscow, Russia*
[94]*Institute for Theoretical and Experimental Physics (ITEP), Moscow, Russia*
[95]*Moscow Engineering and Physics Institute (MEPhI), Moscow, Russia*
[96]*Skobeltsyn Institute of Nuclear Physics, Lomonosov Moscow State University, Moscow, Russia*
[97]*Fakultät für Physik, Ludwig-Maximilians-Universität München, München, Germany*
[98]*Max-Planck-Institut für Physik (Werner-Heisenberg-Institut), München, Germany*

[99]Nagasaki Institute of Applied Science, Nagasaki, Japan
[100]Graduate School of Science, Nagoya University, Nagoya, Japan
[101a]INFN Sezione di Napoli, Italy
[101b]Dipartimento di Scienze Fisiche, Università di Napoli, Napoli, Italy
[102]Department of Physics and Astronomy, University of New Mexico, Albuquerque, New Mexico, USA
[103]Institute for Mathematics, Astrophysics and Particle Physics, Radboud University Nijmegen/Nikhef, Nijmegen, Netherlands
[104]Nikhef National Institute for Subatomic Physics and University of Amsterdam, Amsterdam, Netherlands
[105]Department of Physics, Northern Illinois University, DeKalb, Illinois, USA
[106]Budker Institute of Nuclear Physics, SB RAS, Novosibirsk, Russia
[107]Department of Physics, New York University, New York, New York, USA
[108]Ohio State University, Columbus, Ohio, USA
[109]Faculty of Science, Okayama University, Okayama, Japan
[110]Homer L. Dodge Department of Physics and Astronomy, University of Oklahoma, Norman, Oklahoma, USA
[111]Department of Physics, Oklahoma State University, Stillwater, Oklahoma, USA
[112]Palacký University, RCPTM, Olomouc, Czech Republic
[113]Center for High Energy Physics, University of Oregon, Eugene, Oregon, USA
[114]LAL, Univ. Paris-Sud and CNRS/IN2P3, Orsay, France
[115]Graduate School of Science, Osaka University, Osaka, Japan
[116]Department of Physics, University of Oslo, Oslo, Norway
[117]Department of Physics, Oxford University, Oxford, United Kingdom
[118a]INFN Sezione di Pavia, Italy
[118b]Dipartimento di Fisica, Università di Pavia, Pavia, Italy
[119]Department of Physics, University of Pennsylvania, Philadelphia, Pennsylvania, USA
[120]Petersburg Nuclear Physics Institute, Gatchina, Russia
[121a]INFN Sezione di Pisa, Italy
[121b]Dipartimento di Fisica E. Fermi, Università di Pisa, Pisa, Italy
[122]Department of Physics and Astronomy, University of Pittsburgh, Pittsburgh, Pennsylvania, USA
[123a]Laboratorio de Instrumentacao e Fisica Experimental de Particulas - LIP, Lisboa, Portugal
[123b]Departamento de Fisica Teorica y del Cosmos and CAFPE, Universidad de Granada, Granada, Spain
[124]Institute of Physics, Academy of Sciences of the Czech Republic, Praha, Czech Republic
[125]Faculty of Mathematics and Physics, Charles University in Prague, Praha, Czech Republic
[126]Czech Technical University in Prague, Praha, Czech Republic
[127]State Research Center Institute for High Energy Physics, Protvino, Russia
[128]Particle Physics Department, Rutherford Appleton Laboratory, Didcot, United Kingdom
[129]Physics Department, University of Regina, Regina, Saskatchewan, Canada
[130]Ritsumeikan University, Kusatsu, Shiga, Japan
[131a]INFN Sezione di Roma I, Italy
[131b]Dipartimento di Fisica, Università La Sapienza, Roma, Italy
[132a]INFN Sezione di Roma Tor Vergata, Italy
[132b]Dipartimento di Fisica, Università di Roma Tor Vergata, Roma, Italy
[133a]INFN Sezione di Roma Tre, Italy
[133b]Dipartimento di Fisica, Università Roma Tre, Roma, Italy
[134a]Faculté des Sciences Ain Chock, Réseau Universitaire de Physique des Hautes Energies - Université Hassan II, Casablanca, Morocco
[134b]Centre National de l'Energie des Sciences Techniques Nucleaires, Rabat, Morocco
[134c]Faculté des Sciences Semlalia, Université Cadi Ayyad, LPHEA-Marrakech, Morocco
[134d]Faculté des Sciences, Université Mohamed Premier and LPTPM, Oujda, Morocco
[134e]Faculté des Sciences, Université Mohammed V- Agdal, Rabat, Morocco
[135]DSM/IRFU (Institut de Recherches sur les Lois Fondamentales de l'Univers), CEA Saclay (Commissariat a l'Energie Atomique), Gif-sur-Yvette, France
[136]Santa Cruz Institute for Particle Physics, University of California Santa Cruz, Santa Cruz, California, USA
[137]Department of Physics, University of Washington, Seattle, Washington, USA
[138]Department of Physics and Astronomy, University of Sheffield, Sheffield, United Kingdom
[139]Department of Physics, Shinshu University, Nagano, Japan
[140]Fachbereich Physik, Universität Siegen, Siegen, Germany
[141]Department of Physics, Simon Fraser University, Burnaby, British Columbia, Canada
[142]SLAC National Accelerator Laboratory, Stanford, California, USA
[143a]Faculty of Mathematics, Physics & Informatics, Comenius University, Bratislava, Slovak Republic
[143b]Department of Subnuclear Physics, Institute of Experimental Physics of the Slovak Academy of Sciences, Kosice, Slovak Republic
[144a]Department of Physics, University of Johannesburg, Johannesburg, South Africa
[144b]School of Physics, University of the Witwatersrand, Johannesburg, South Africa

[145a]*Department of Physics, Stockholm University, Sweden*
[145b]*The Oskar Klein Centre, Stockholm, Sweden*
[146]*Physics Department, Royal Institute of Technology, Stockholm, Sweden*
[147]*Departments of Physics & Astronomy and Chemistry, Stony Brook University, Stony Brook, New York, USA*
[148]*Department of Physics and Astronomy, University of Sussex, Brighton, United Kingdom*
[149]*School of Physics, University of Sydney, Sydney, Australia*
[150]*Institute of Physics, Academia Sinica, Taipei, Taiwan*
[151]*Department of Physics, Technion: Israel Inst. of Technology, Haifa, Israel*
[152]*Raymond and Beverly Sackler School of Physics and Astronomy, Tel Aviv University, Tel Aviv, Israel*
[153]*Department of Physics, Aristotle University of Thessaloniki, Thessaloniki, Greece*
[154]*International Center for Elementary Particle Physics and Department of Physics, The University of Tokyo, Tokyo, Japan*
[155]*Graduate School of Science and Technology, Tokyo Metropolitan University, Tokyo, Japan*
[156]*Department of Physics, Tokyo Institute of Technology, Tokyo, Japan*
[157]*Department of Physics, University of Toronto, Toronto, Ontario, Canada*
[158a]*TRIUMF, Vancouver, British Columbia, Canada*
[158b]*Department of Physics and Astronomy, York University, Toronto, Ontario, Canada*
[159]*Institute of Pure and Applied Sciences, University of Tsukuba, 1-1-1 Tennodai,Tsukuba, Ibaraki 305-8571, Japan*
[160]*Science and Technology Center, Tufts University, Medford, Massachusetts, USA*
[161]*Centro de Investigaciones, Universidad Antonio Narino, Bogota, Colombia*
[162]*Department of Physics and Astronomy, University of California Irvine, Irvin,e California, USA*
[163a]*INFN Gruppo Collegato di Udine, Italy*
[163b]*ICTP, Trieste, Italy*
[163c]*Dipartimento di Chimica, Fisica e Ambiente, Università di Udine, Udine, Italy*
[164]*Department of Physics, University of Illinois, Urbana, Illinois, USA*
[165]*Department of Physics and Astronomy, University of Uppsala, Uppsala, Sweden*
[166]*Instituto de Física Corpuscular (IFIC) and Departamento de Física Atómica, Molecular y Nuclear and Departamento de Ingeniería Electrónica and Instituto de Microelectrónica de Barcelona (IMB-CNM), University of Valencia and CSIC, Valencia, Spain*
[167]*Department of Physics, University of British Columbia, Vancouver, British Columbia, Canada*
[168]*Department of Physics and Astronomy, University of Victoria, Victoria, British Columbia, Canada*
[169]*Waseda University, Tokyo, Japan*
[170]*Department of Particle Physics, The Weizmann Institute of Science, Rehovot, Israel*
[171]*Department of Physics, University of Wisconsin, Madison, Wisconsin, USA*
[172]*Fakultät für Physik und Astronomie, Julius-Maximilians-Universität, Würzburg, Germany*
[173]*Fachbereich C Physik, Bergische Universität Wuppertal, Wuppertal, Germany*
[174]*Department of Physics, Yale University, New Haven, Connecticut, USA*
[175]*Yerevan Physics Institute, Yerevan, Armenia*
[176]*Domaine scientifique de la Doua, Centre de Calcul CNRS/IN2P3, Villeurbanne Cedex, France*

[a]Also at Laboratorio de Instrumentacao e Fisica Experimental de Particulas - LIP, Lisboa, Portugal.
[b]Also at Faculdade de Ciencias and CFNUL, Universidade de Lisboa, Lisboa, Portugal.
[c]Also at Particle Physics Department, Rutherford Appleton Laboratory, Didcot, United Kingdom.
[d]Also at TRIUMF, Vancouver, BC, Canada.
[e]Also at Department of Physics, California State University, Fresno, CA, USA
[f]Also at Novosibirsk State University, Novosibirsk, Russia.
[g]Also at Fermilab, Batavia, IL, USA
[h]Also at Department of Physics, University of Coimbra, Coimbra, Portugal.
[i]Also at Università di Napoli Parthenope, Napoli, Italy.
[j]Also at Institute of Particle Physics (IPP), Canada.
[k]Also at Department of Physics, Middle East Technical University, Ankara, Turkey.
[l]Also at Louisiana Tech University, Ruston, LA, USA.
[m]Also at Department of Physics and Astronomy, University College London, London, United Kingdom.
[n]Also at Group of Particle Physics, University of Montreal, Montreal, QC, Canada.
[o]Also at Institute of Physics, Azerbaijan Academy of Sciences, Baku, Azerbaijan.
[p]Also at Institut für Experimentalphysik, Universität Hamburg, Hamburg, Germany.
[q]Also at Manhattan College, New York, NY, USA.
[r]Also at School of Physics, Shandong University, Shandong, China.
[s]Also at CPPM, Aix-Marseille Université and CNRS/IN2P3, Marseille, France.
[t]Also at School of Physics and Engineering, Sun Yat-sen University, Guanzhou, China.
[u]Also at Academia Sinica Grid Computing, Institute of Physics, Academia Sinica, Taipei, Taiwan.

[v]Also at Section de Physique, Université de Genève, Geneva, Switzerland.
[w]Also at Departamento de Fisica, Universidade de Minho, Braga, Portugal.
[x]Also at Department of Physics and Astronomy, University of South Carolina, Columbia, SC, USA.
[y]Also at Institute for Particle and Nuclear Physics, Wigner Research Centre for Physics, Budapest, Hungary.
[z]Also at California Institute of Technology, Pasadena, CA, USA.
[aa]Also at Institute of Physics, Jagiellonian University, Krakow, Poland.
[bb]Also at Institute of High Energy Physics, Chinese Academy of Sciences, Beijing, China.
[cc]Also at Department of Physics and Astronomy, University of Sheffield, Sheffield, United Kingdom.
[dd]Also at Department of Physics, Oxford University, Oxford, United Kingdom.
[ee]Also at Institute of Physics, Academia Sinica, Taipei, Taiwan.
[ff]Also at Department of Physics, The University of Michigan, Ann Arbor, MI, USA.
[gg]Also at DSM/IRFU (Institut de Recherches sur les Lois Fondamentales de l'Univers), CEA Saclay (Commissariat a l'Energie Atomique), Gif-sur-Yvette, France.
[hh]Also at Laboratoire de Physique Nucléaire et de Hautes Energies, UPMC and Université Paris-Diderot and CNRS/IN2P3, Paris, France.
[ii]Deceased.